STUDY ON WAVE PROPAGATION PHENOMENA IN LAYERED MEDIA

A thesis

submitted in fulfillment of the requirement
for the award of the degree of

DOCTOR OF PHILOSOPHY

in

MATHEMATICS

by

Richa Goyal

(Regd. No. 901611013)

under the supervision of

Dr. Satish Kumar

(Associate Professor)

School of Mathematics

Thapar Institute of Engineering and Technology
Patiala-147004, Punjab, India

October, 2021

DEDICATED

TO

THE ALMIGHTY

&

MY FAMILY

Certificate

This is to certify that the thesis entitled, "Study on Wave Propagation Phenomena in Layered media", submitted by Ms. Richa Goyal in the fulfillment of the requirement for the award of the Degree of Doctor of Philosophy in School of Mathematics, Thapar Institute of Engineering and Technology, Patiala, is a record of candidates own work carried out by her under my supervision and guidance.

The matter presented in this thesis has not been submitted in part or full for the award of any degree in any other University or Institute.

Attestation by supervisor

Dr. Satish Kumar
Associate Professor
School of Mathematics
Thapar Institute of Engineering and Technology
Patiala-147004
Punjab, India

Declaration

I hereby declare that the research work presented in this thesis entitled, "Study on Wave Propagation Phenomena in Layered media", submitted for the award of the degree of Doctor of Philosophy in School of Mathematics, Thapar Institute of Engineering and Technology, Patiala, is an authenticated record of my own research work carried out under the supervision of Dr. Satish Kumar (School of Mathematics) and refers other researcher's work are duly listed in the bibliography section.

The matter embodied in this thesis has not been submitted in part or full to any other university or institute for the award of any degree.

Richa Goyal

Richa Goyal

Attestation by supervisor

Dr. Satish Kumar

Associate Professor

School of Mathematics

Thapar Institute of Engineering and Technology

Patiala-147004

Punjab, India

Acknowledgements

This journey of Doctorate of Philosophy would not have been possible without the inspiration and support of several wonderful individuals who contribute in one way or the other to nurture me into a better person. After immense waiting, I got the opportunity to express my gratitude towards everyone who stood by me in this journey. First and foremost, I am deeply indebted to my supervisor Dr. Satish Kumar, Associate Professor, School of Mathematics, TIET, Patiala who has guided me through the ups and downs in this entire journey of never-ending learning. His deep understanding, motivation, and personal attention have provided a smooth base throughout the tenure of Ph.D. He, like a father, has always motivated me towards a better understanding of the concepts and problems. His noble thoughts and conviction have to lead me to perform well throughout my journey. It was really a fortunate experience to work under him. I could not have imagined having a better advisor and mentor for my Ph.D. study.

I also share my gratitude to the authorities of TIET for providing the necessary infrastructure and facilities to execute my research work. I would like to impart my sincere thanks to my IRB committee members: Dr. Ankush Pathania, Dr. Kavita, and Dr. Shruti Sharma for their helpful suggestions and comments during my progress presentations. I would like to express my gratitude to Dr. Arvind Kumar Lal, former Head of the Department for the support and providing their valuable suggestions regarding the project maintenance files. I am also thankful to all the faculty members and staff members of the School of Mathematics for their kind help, support, cooperation, love, and affection.

The track to my doctorate glazed with the financial assistance from the project under

Science & Engineering Research Board (SERB), a statutory body of the Department of Science & Technology, Government of India.

I feel privileged to communicate my earnest respects and appreciation to Dr. Vikas Sharma and Dr. Tanupreet Kaur (former Ph.D. students) for their persistent support, valuable recommendations, and advice throughout the research work. This journey would have been terrible without the unlimited support, valuable discussions, and suggestions of my friends and colleagues Kamal Kumar (who always helped in managing software), Rishu Arora (who helped in learning LATEX commands), Shruti Sharma (for valuable suggestions regarding effective paper writing) and Sukhveer Singh (for endless support), without their help this work could never be completed. I would like to extend my thanks to Vanita, Ashish, Madhu, Gagan, Dimple, Navjot, Jagbir, Prashu, Sonali, Deepika, Nancy, Vasudha, Arshpreet, Shahid Bhatt, Mohit, Vivek, Manpreet, Jaspreet, Rajinder, Harman, and all other research scholars for creating a friendly environment in the research lab. It is impossible to name everyone in the limited words, I humbly apologize for the same. I whole-heartedly thank every person who is not mentioned above but who contributed to my Ph.D. journey and I feel blessed to have you all.

I whole-heartedly with immense gratitude dedicate my thesis to my loving, caring, and supportive family without whom I could not reach this point in my life. I owe my sincere devotion to my father Sh. Sunil Kumar Goyal and my mother Smt. Sunita Rani who always lived with a dream of their daughter getting a degree of Doctorate. Their blessings had left no stone unturned in my path of research. Parents can never be thanked in words. The Love and support of my elder brother Sahil Goyal and my younger brother Shubham Goyal have always motivated me to keep on moving. Love and blessings of my grandmother-in-law Smt. Prem Lata has always enlightened my path of life. I also express my gratitude towards my father-in-law Sh. Sham Sunder Gupta, my mother-in-law Smt. Usha Gupta, my brother-in-law Tarun Gupta and my sister-in-law Bhanu Priya for all of their sacrifices they have made on my behalf.

I do not find enough words to express immense appreciation for my husband Varun Gupta, who devoted each day to me, taking care of me and the whole family. He has

always stood as a pillar by side, never letting me fall down, in the time of need. I want to apologize to my niece Janisha Gupta (my little Jinu) for missing few memorable moments of her life due to my constant engagement in this work. Besides this, several near and dear friends & relatives have helped me in the successful completion of this work in one or the other way. All above! I thank the Almighty beneath the blue sky, Who always empowered me with His heavenly blessings, and made me feel His presence every time I felt low!!!

Patiala **Richa Goyal**

Date:26-Oct-2021

Abstract

The wave propagation includes the situation where waves originate and propagate in the medium with different material properties and geometry. Studying the surface wave propagation in the layered structure has been of interest to researchers due to their extensive applications in the fields of geophysics, composite materials, acoustics as well as in nondestructive evaluation. The interactions among these layers depend on many factors such as mechanical properties, loading conditions, interfacial conditions, etc. Traditionally, the layered model involves a substrate based on the classical elastic model but this theory ignore the microstructure-related scale effects. To capture the size effects, two size-dependent models, i.e., 'Micropolar elastic model' and 'Couple stress elastic model' have been considered along with other different material layers such as smart material (piezoelectric material), viscoelastic material, orthotropic material, self-fiber reinforced material. The whole work of the thesis is structured into six chapters which are summarized as follow:

Chapter-1

This chapter involves the basic overview on continuum mechanics, classical theory of elasticity with brief summary on generalized Hooke's law. This chapter also involves the emergence of different microcontinuum theories, i.e., 'Micropolar theory' and 'Couple stress theory' of elasticity, basic governing equations together with constitutive equations are summarized. This also includes the brief overview on anisotropic materials like piezoelectric materials (also called 'Smart Materials') and viscoelastic materials.

Chapter-2

In this chapter, the propagation of Love wave have been investigated in a piezoelectric

ceramic bonded over a couple stress elastic half-space. The substrate is considered to have properties of a microstructure like granular macromorphic rock (Dionysos Marble). This study has been carried out by using two sets of piezoelectric medium, i.e., $PZT-5H$ and $BaTiO_3$. Closed-form expressions of the resulting dispersion relations are obtained analytically by applying feasible boundary conditions for both the cases of electrically open and electrically short conditions. The significant effects of the underlying microstructure of substrate, the thickness of piezoelectric layer along with the effects of piezoelectric constants and dielectric constants have been examined and demonstrated graphically on the phase velocity profiles of Love wave.

Chapter-3

In this chapter, Love-type surface waves have been explored in the size-dependent micropolar substrate with a finite layer of piezoelectric material. An analytical expression for the dispersion equations has been obtained for electrically open and short conditions and the results are shown graphically. For studying the impacts of underlying microstructure of the substrate, the layer thickness of piezoelectric material, piezoelectric and dielectric parameters, the dispersion curves have been plotted for non-dimensional phase velocity against non-dimensional wave number.

The main objectives of **Chapter 2** and **Chapter 3** is to identify a size-dependent models for studying Love-wave propagation in layered structure. It was observed that the couple stress model and micropolar elastic model may be used as substrate to overcome the shortcomings of classical theory of elasticity.

Chapter-4

This chapter is an extension of chapter 2 and chapter 3 in which study is extended to the double-layered model by considering another layer between the finite layer of piezoelectric material and the size-dependent substrate. The consideration of vertically heterogeneous viscoelastic material layer is more beneficial in the design process to achieve an explicit objective. In this context, this chapter contains two problems on the propagation of Love-type waves in two-layered structure comprising a piezoelectric material layer, viscoelastic layer along with the size-dependent substrate. Two materials of piezoelectric medium, i.e., $PZT-5H$ and $BaTiO_3$ materials are used to

carry out this study.

In first problem of this chapter, the couple stress elastic theory have been considered for analyzing the microstructural characteristics on Love wave propagation in double-layered structure. The dispersion equations are calculated for the real and damping case in closed form expression for open and short circuits. Numerical calculations have been done to examine the impact of different parameters by taking two distinct piezoelectric materials, i.e., $PZT-5H$ and $BaTiO_3$. The relevant particular cases are derived to validate the present study.

In second problem of this chapter, the micropolar model is considered for investigating the effects of micropolarity and their related parameters on the propagation of Love-type surface wave in double-layered structure. An analytical expression for the real and damping dispersion equations have been obtained in the compact-form under electrically open and electrically short conditions. The real and damping phase velocity profiles are affected significantly with the variation in associated parameter involved in the study. The influence of characteristic length and coupling number associated with substrate, the influence of heterogeneity and the internal friction parameter related to viscoelastic material along with the effects of piezoelectric materials have been demonstrated graphically. Particular cases are also deduced using relevant conditions.

Chapter-5

In this chapter, the propagation of Love-type wave have been studied considering the imperfect bonding between the substrate and the material layer. The strength of many engineering layered models rely on the bonding between the structural components. In chapter-2, 3 and 4, the problems are solved considering the perfect bonding between the material layer and substrate. But in reality, this condition is difficult to fulfil. Keeping this aspect in mind, Love-type surface wave have been studied in functionally graded orthotropic medium under initial stress bonded imperfectly over the size-dependent micropolar medium. The main focus of the study is to show the impact of imperfect bonding at the common interface of material layer and substrate. The compact-form of dispersion relations is accomplished to study Love-type wave

characteristics in a composite layered system. Numerical computations are performed and results are manifested through graphs to study the effect of various factors involved in the study.

Chapter-6

The purpose of this chapter is to explore the characteristics of Rayleigh-type surface wave propagation in a size-dependent couple stress substrate with a finite thickness self-fiber reinforced layer. The compact form of the secular equation is achieved by employing suitable boundary conditions for the model proposed. The phase velocity profiles of Rayleigh wave propagation in the size-dependent composite structures are illustrated which are extensively useful. The characteristic curves are plotted to manifest the effects of different affected parameters on the phase velocity of Rayleigh-type waves, namely the varying reinforced medium thickness, the parameter of material length representing the microstructural behavior of the substrate.

The findings of the above study may be utilized for the development of Love wave-based devices, in non-destructive evaluation, geophysics, civil engineering, rock mechanics, and can be an inspiration for engineering developments.

List of Papers

J1. **Richa Goyal**, Satish Kumar, Vikas Sharma. "Microstructural considerations on SH-Wave propagation in a piezoelectric layered structure." Journal of Theoretical and Applied Mechanics 56(4): 993–1004, 2018 **DOI: 10.15632/jtam-pl.56.4.993 and Impact factor: 0.831**.

J2. **Richa Goyal**, Satish Kumar, Vikas Sharma. "A size-dependent micropolar-piezoelectric layered structure for the analysis of Love wave." Waves in Random and Complex Media 30(3): 544–561, 2018 **DOI: 10.1080/17455030.2018.1542186 and Impact factor: 3.330**.

J3. **Richa Goyal**, Satish Kumar. "Quantifying viscoelastic, piezoelectric and couple stress effects on Love-type wave propagation." Smart Materials and Structures 28(10): 1050212019, 2019 **DOI: 10.1088/1361-665x/ab39bf and Impact factor: 3.543**.

J4. **Richa Goyal**, Satish Kumar. "Dispersion of Love waves in size-dependent substrate containing finite piezoelectric and viscoelastic layers." International Journal of Mechanics and Materials in Design volume 15: 767–790, 2019 **DOI: 10.1007/s10999-019-09441-5 and Impact factor: 3.480**.

J5. **Richa Goyal**, Satish Kumar. "Estimating the effects of imperfect bonding

and size-dependency on Love-type wave propagation in functionally graded orthotropic material under the influence of initial stress." Mechanics of Materials 155: 103772, 2021 **DOI: 10.1016/j.mechmat.2021.103772 and Impact factor: 2.993**.

J6. **Richa Goyal**, Satish Kumar. "Size-dependent investigation on the dispersion relation of Rayleigh-type wave propagation in fibre-reinforced layered medium." (Communicated).

Contents

1 Introduction **1**

1.1 Basic Introduction 1

1.2 Classical theory of elasticity 3

1.3 Generalized Hooke's law 4

1.4 Elastic waves 9

1.5 Application of elastic waves 13

1.6 Emergence of microcontinuum theories 14

1.6.1 Micropolar Theory 16

1.6.2 Couple Stress Theory 20

1.7 Piezoelectric Theory 23

1.8 Viscoelastic Theory 28

2 Microstructural considerations on Love wave propagation in a piezoelectric layered structure **33**

2.1 Introduction 33

2.2 Formulation of the problem 36

2.2.1 Dynamics of piezoelectric material layer 37

2.2.2 Dynamics of couple stress elastic half-space 39

2.3 Boundary conditions 41

2.4 Dispersion equations for electrically open condition 43

2.5 Dispersion equations for electrically short condition 44

2.6 Particular Cases and Validation of results 44

2.6.1 Case-1 44

2.6.2 Case-2 . . . 45
2.6.3 Case-3 . . . 45
2.7 Numerical results . . . 45
2.8 Conclusion . . . 53

3 A size-dependent micropolar- piezoelectric layered structure for the analysis of Love-type wave 55
3.1 Introduction . . . 55
3.2 Formulation of the problem . . . 56
3.2.1 Dynamics of semi-infinite micropolar substrate . . . 57
3.3 Boundary conditions . . . 61
3.4 Dispersion equations for electrically open condition . . . 63
3.5 Dispersion equations for electrically short condition . . . 63
3.6 Particular Cases . . . 64
3.6.1 Case-1 . . . 64
3.6.2 Case-2 . . . 65
3.6.3 Case-3 . . . 65
3.7 Numerical results and discussions . . . 65
3.8 Conclusion . . . 74

4 Analysis of Love-type wave propagation in double-layered structure 77
4.1 Introduction . . . 77
4.2 Dispersion of Love-type waves in size-dependent couple stress substrate containing finite piezoelectric and viscoelastic layers . . . 79
4.2.1 Formulation of the problem . . . 79
4.2.2 Solution for the vertically heterogeneous viscoelastic layer . . . 80
4.2.3 Boundary conditions . . . 83
4.2.4 Dispersion relations for electrically open conditions . . . 85
4.2.5 Dispersion relations for electrically short conditions . . . 86
4.2.6 Validation . . . 87
4.2.7 Numerical discussion . . . 90

4.2.8 Impact of microstructural parameter 90
4.2.9 Impact of heterogeneity of a viscoelastic layer 91
4.2.10 Impact of internal friction of viscoelastic layer 93
4.2.11 Impact of a piezoelectric layer material 98
4.2.12 Impact of Piezoelectric constant (e_{15}) 98
4.2.13 Impact of Dielectric constant (ϵ_{11}) 99
4.3 Dispersion of Love-type waves in size-dependent micropolar substrate containing finite piezoelectric and viscoelastic layers 102
4.3.1 Formulation of the problem 102
4.3.2 Boundary conditions 103
4.3.3 Dispersion equations for electrically open conditions 105
4.3.4 Dispersion equations for electrically short conditions 106
4.3.5 Validation 107
4.3.6 Numerical results 110
4.3.7 Effect of coupling constant (N) 110
4.3.8 Effect of characteristic length (l) 111
4.3.9 Effects of heterogeneity of a viscoelastic layer 113
4.3.10 Effects of internal friction of a viscoelastic layer 116
4.3.11 Effects of a piezoelectric layer material 119
4.4 Conclusion 125

5 The effects of imperfect bonding at the interface of layer and substrate on Love wave 129

5.1 Introduction 129
5.2 Formulation of the problem 132
5.2.1 Governing equations and solutions for FGOM L_1 133
5.2.2 Solutions for semi-infinite size-dependent medium L_2 135
5.3 Boundary conditions and Secular equations 137
5.4 Particular cases and Validation of results 139
5.4.1 Case-1 139

5.4.2 Case-2 . . . 140
5.4.3 Case-3 . . . 140
5.4.4 Case-4 . . . 140
5.4.5 Case-5 . . . 141
5.4.6 Case-6 . . . 141
5.4.7 Case-7 . . . 142
5.4.8 Case-8 . . . 142
5.5 Numerical results . . . 142
5.5.1 Effect of the imperfectness of stratum-substrate interface . . . 143
5.5.2 Effect of FGOM stratum . . . 144
5.5.3 Effect of micropolar elastic substrate . . . 145
5.6 Conclusion . . . 147

6 Size-dependent investigation on Rayleigh-type wave in fibre- reinforced layered medium 149

6.1 Introduction . . . 149
6.2 Problem formulation and Solutions . . . 151
6.2.1 For self-fiber reinforced layer at $-H < z < 0$ . . . 152
6.2.2 For couple stress substrate at $z > 0$ . . . 154
6.3 Boundary Conditions and Dispersion relations . . . 155
6.4 Particular Cases . . . 158
6.4.1 Case-1: . . . 158
6.4.2 Case-2: . . . 159
6.4.3 Case-3: . . . 159
6.5 Numerical Discussion . . . 159
6.5.1 Influence of self-fiber reinforced layer thickness H . . . 160
6.5.2 Influence of microstructural parameter l . . . 160
6.5.3 Influence of reinforcement parameter . . . 163
6.6 Conclusions . . . 163

List of Figures

1.1 Stress components (Ref: www.google/images.com) 4

1.2 Primary waves and secondary waves (Ref: www.google/images.com) . 11

1.3 Rayleigh waves and Love waves (Ref: www.google/images.com) . . . 13

2.1 Geometry of the problem. 36

2.2 Variation of non-dimensional phase velocity against non-dimensional wave number for different values of characteristic length l = 0.00001m, 0.0001m, 0.0004m, when H=0.002m in case of electrically open conditions. 47

2.3 Variation of non-dimensional phase velocity against non-dimensional wave number for different values of characteristic length l = 0.00001m, 0.0001m, 0.0004m, when H=0.002m in case of electrically short conditions. 48

2.4 Variation of non-dimensional phase velocity against non-dimensional wave number for classical elasticity and couple stress medium. 48

2.5 Variation of non-dimensional phase velocity against non-dimensional wave number for different values of the thickness of a piezoelectric layer H = 0.003m, 0.004m, 0.005m, when l = 0.0004m in case of electrically open conditions. 49

2.6 Variation of non-dimensional phase velocity against non-dimensional wave number for different values of the thickness of a piezoelectric layer H = 0.003m, 0.004m, 0.005m, when l = 0.0004m in case of electrically short conditions. 50

2.7 Variation of non-dimensional phase velocity against non-dimensional wave number for different values of piezoelectric constants e_{15} = 17, 21, 25 C/m^2 in 6(i) and e_{15} = 11, 15, 19 C/m^2 in 6(ii), for electrically open cases. 51

2.8 Variation of non-dimensional phase velocity against non-dimensional wave number for different values of piezoelectric constants e_{15} = 17, 21, 25 C/m^2 in (a) and e_{15} = 11, 15, 19 C/m^2 in (b), for electrically short cases. 51

2.9 Variation of non-dimensional phase velocity against non-dimensional wave number for different values of dielectric constants $\epsilon_{11} = 237 \times 10^{-10}$, 277×10^{-10}, 317×10^{-10} C^2/Nm^2 in (a), $\epsilon_{11} = 98 \times 10^{-10}$, 128×10^{-10}, 158×10^{-10} C^2/Nm^2 in (b), for electrically open cases. . 52

2.10 Variation of non-dimensional phase velocity against non-dimensional wave number for different values of dielectric constants $\epsilon_{11} = 237 \times 10^{-10}$, 277×10^{-10}, 317×10^{-10} C^2/Nm^2 in (a), $\epsilon_{11} = 98 \times 10^{-10}$, 128×10^{-10}, 158×10^{-10} C^2/Nm^2 in (b), for electrically short cases. . 52

3.1 Geometry of the problem. 57

3.2 Variation of non-dimensional phase velocity against non-dimensional wave number for different values of micropolar constants $N = 0.1, 0.7, 0.9$ in (a) and (b), when l=0.001m, H=0.3m in case of electrically open conditions. 67

3.3 Variation of non-dimensional phase velocity against non-dimensional wave number for different values of micropolar constants $N = 0.1, 0.7, 0.9$ in (a) and (b), when l=0.001m, H=0.3m in case of electrically short conditions. 67

3.4 Variation of non-dimensional phase velocity against non-dimensional wave number for different values of characteristic length $l = 0.001m, 0.002m, 0.003m$ in (a) and (b) in case of electrically open conditions. 68

3.5 Variation of non-dimensional phase velocity against non-dimensional wave number for different values of characteristic length $l = 0.001m, 0.004m, 0.007m$ in (a) and (b) in case of electrically short conditions. 69

3.6 Variation of non-dimensional phase velocity against non-dimensional wave number for classical elasticity and micropolar elasticity. 69

3.7 Variation of non-dimensional phase velocity against non-dimensional wave number for couple stress theory and micropolar elasticity. 70

3.8 Variation of non-dimensional phase velocity against non-dimensional wave number for different values of the thickness of piezoelectric layer $H = 0.003m, 0.004m, 0.005m$ in (a) and (b) in case of electrically open conditions. 70

3.9 Variation of non-dimensional phase velocity against non-dimensional wave number for different values of the thickness of piezoelectric layer $H = 0.003m, 0.004m, 0.005m$ in (a) and (b) in case of electrically short conditions. 71

3.10 Variation of non-dimensional phase velocity against non-dimensional wave number for different values of piezoelectric constants e_{15} = 17 C/m^2, 21 C/m^2, 25 C/m^2 in (a) and e_{15} = 11 C/m^2, 15 C/m^2, 19 C/m^2 in (b), when H=0.03m in case of electrically open conditions. . 72

3.11 Variation of non-dimensional phase velocity against non-dimensional wave number for different values of piezoelectric constants e_{15} = 17 C/m^2, 21 C/m^2, 25 C/m^2 in (a) and $e_{15} = 11C/m^2, 15C/m^2, 19C/m^2$ in (b), when H=0.03m in case of electrically short conditions. 72

3.12 Variation of non-dimensional phase velocity against non-dimensional wave number for different values of dielectric constants $\epsilon_{11} = 237\times10^{-10}$ C^2/Nm^2, 277×10^{-10} C^2/Nm^2, 317×10^{-10} C^2/Nm^2 in (a) and ϵ_{11} = 98×10^{-10} C^2/Nm^2, 128×10^{-10} C^2/Nm^2, 158×10^{-10} C^2/Nm^2 in (b), when H=0.03m in case of electrically open conditions. 73

3.13 Variation of non-dimensional phase velocity against non-dimensional wave number for different values of dielectric constants $\epsilon_{11} = 237\times10^{-10}$ C^2/Nm^2, 277×10^{-10} C^2/Nm^2, 317×10^{-10} C^2/Nm^2 in (a) and ϵ_{11} $= 98 \times 10^{-10}$ C^2/Nm^2, 128×10^{-10} C^2/Nm^2, 158×10^{-10} C^2/Nm^2 in (b), when H=0.03m in case of electrically short conditions. 74

4.1 Geometry 80

4.2 Variation of non-dimensional real phase velocity against non-dimensional wave number for distinct values of characteristic length in case of electrical open conditions. 91

4.3 Variation of non-dimensional damping phase velocity against non-dimensional wave number for distinct values of characteristic length in case of electrical open conditions. 92

4.4 Variation of non-dimensional real phase velocity against non-dimensional wave number for distinct values of characteristic length in case of electrical short conditions. 92

4.5 Variation of non-dimensional damping phase velocity against non-dimensional wave number for distinct values of characteristic length in case of electrical short conditions. 93

4.6 Variation of non-dimensional real phase velocity against non-dimensional wave number for distinct values of non-dimensional heterogeneity parameter in case of electrical open conditions. 94

4.7 Variation of non-dimensional damping phase velocity against non-dimensional wave number for distinct values of non-dimensional heterogeneity parameter in case of electrical open conditions. 94

4.8 Variation of non-dimensional real phase velocity against non-dimensional wave number for distinct values of non-dimensional heterogeneity parameter in case of electrical short conditions. 95

4.9 Variation of non-dimensional damping phase velocity against non-dimensional wave number for distinct values of non-dimensional heterogeneity parameter in case of electrical short conditions. 95

4.10 Variation of non-dimensional real phase velocity against non-dimensional wave number for distinct values of internal friction parameter in case of electrical open conditions. 96

4.11 Variation of non-dimensional damping phase velocity against non-dimensional wave number for distinct values of internal friction parameter in case of electrical open conditions. 96

4.12 Variation of non-dimensional real phase velocity against non-dimensional wave number for distinct values of internal friction parameter in case of electrical short conditions. 97

4.13 Variation of non-dimensional damping phase velocity against non-dimensional wave number for distinct values of internal friction parameter in case of electrical short conditions. 97

4.14 Real and damped phase speed versus wave number in case of electrically open conditions. 98

4.15 Real and damped phase speed versus wave number in case of electrically short conditions. 99

4.16 Variation of non-dimensional real phase velocity against non-dimensional wave number for different values of piezoelectric constant $e_{15} = 17C/m^2$, $21C/m^2$, $25C/m^2$ in (a) and $e_{15} = 11C/m^2$, $15C/m^2$, $19C/m^2$ in (b), when h_v=0.02m, h_p=0.02m, $l = 0.0001m$ in case of electrical open conditions. 100

4.17 Variation of non-dimensional real phase velocity against non-dimensional wave number for different values of piezoelectric constant $e_{15} = 17C/m^2$, $21C/m^2$, $25C/m^2$ in (a) and $e_{15} = 11C/m^2$, $15C/m^2$, $19C/m^2$ in (b), when h_v=0.02m, h_p=0.02m, $l = 0.0001m$ in case of electrical short conditions. 100

4.18 Variation of non-dimensional real phase velocity against non-dimensional wave number for different values of dielectric constant $\epsilon_{11} = 237 \times 10^{-10}C^2/Nm^2$, $277 \times 10^{-10}C^2/Nm^2$, $317 \times 10^{-10}C^2/Nm^2$ in (a) and $\epsilon_{11} = 98 \times 10^{-10}C^2/Nm^2$, $128 \times 10^{-10}C^2/Nm^2$, $158 \times 10^{-10}C^2/Nm^2$ in (b), when h_v=0.02m, h_p=0.02m, $l = 0.0001m$ in case of electrical open conditions. 101

4.19 Variation of non-dimensional real phase velocity against non-dimensional wave number for different values of dielectric constant $\epsilon_{11} = 237 \times 10^{-10}C^2/Nm^2$, $277 \times 10^{-10}C^2/Nm^2$, $317 \times 10^{-10}C^2/Nm^2$ in (a) and $\epsilon_{11} = 98 \times 10^{-10}C^2/Nm^2$, $128 \times 10^{-10}C^2/Nm^2$, $158 \times 10^{-10}C^2/Nm^2$ in (b), when h_v=0.02m, h_p=0.02m, $l = 0.0001m$ in case of electrical short conditions. 101

4.20 Geometry of the problem. 102

4.21 Variation of non-dimensional real phase velocity against non-dimensional wave number for different values of micropolar constant $N = 0.1, 0.6, 0.9$ when h_v=0.02m, h_p=0.02m in case of electrical open conditions. . . . 111

4.22 Variation of non-dimensional damping phase velocity against non-dimensional wave number for different values of micropolar constant $N = 0.1, 0.6, 0.9$ when h_v=0.02m, h_p=0.02m in case of electrical open conditions. . . . 112

4.23 Variation of non-dimensional real phase velocity against non-dimensional wave number for different values of micropolar constant $N = 0.1, 0.6, 0.9$ when h_v=0.02m, h_p=0.02m in case of electrical short conditions. . . . 112

4.24 Variation of non-dimensional damping phase velocity against non-dimensional wave number for different values of micropolar constant $N = 0.1, 0.6, 0.9$ when h_v=0.02m, h_p=0.02m in case of electrical short conditions. . . . 113

4.25 Variation of non-dimensional real phase velocity against non-dimensional wave number for different values of characteristic length l = 0.0001m, 0.0002m, 0.0003m when h_v=0.02m, h_p=0.02m in case of electrical open conditions. 114

4.26 Variation of non-dimensional damping phase velocity against non-dimensional wave number for different values of characteristic length $l = 0.0001$m, 0.0002m, 0.0003m when h_v=0.02m, h_p=0.02m in case of electrical open conditions. 114

4.27 Variation of non-dimensional real phase velocity against non-dimensional wave number for different values of characteristic length $l = 0.0001$m, 0.0002m, 0.0003m when h_v=0.02m, h_p=0.02m in case of electrical short conditions. 115

4.28 Variation of non-dimensional damping phase velocity against non-dimensional wave number for different values of characteristic length $l = 0.0001$m, 0.0002m, 0.0003m when h_v=0.02m, h_p=0.02m in case of electrical short conditions. 115

4.29 Variation of non-dimensional real phase velocity against non-dimensional wave number for couple stress theory and micropolar theory. 116

4.30 Variation of non-dimensional real phase velocity against non-dimensional wave number for different values of non-dimensional heterogeneity parameter $\alpha h_v = 0.08, 0.12, 0.16$, when h_v=0.02m, h_p=0.02m, $l = 0.0001m$ in case of electrical open conditions. 117

4.31 Variation of non-dimensional damping phase velocity against non-dimensional wave number for different values of non-dimensional heterogeneity parameter $\alpha h_v = 0.08, 0.12, 0.16$, when h_v=0.02m, h_p=0.02m, $l = 0.0001m$ in case of electrical open conditions. 117

4.32 Variation of non-dimensional real phase velocity against non-dimensional wave number for different values of non-dimensional heterogeneity parameter $\alpha h_v = 0.08, 0.12, 0.16$, when h_v=0.02m, h_p=0.02m, $l = 0.0001m$ in case of electrical short conditions. 118

4.33 Variation of non-dimensional damping phase velocity against non-dimensional wave number for different values of non-dimensional heterogeneity parameter $\alpha h_v = 0.08, 0.12, 0.16$, when h_v=0.02m, h_p=0.02m, $l = 0.0001m$ in case of electrical short conditions. 118

4.34 Variation of non-dimensional real phase velocity against non-dimensional wave number for different values of internal friction parameter $\frac{\mu_1}{\eta_1} = 6 \times 10^5$, 10×10^5, 20×10^5, when h_v=0.02m, h_p=0.02m, $l = 0.0001m$ in case of electrical open conditions. 119

4.35 Variation of non-dimensional damping phase velocity against non-dimensional wave number for different values of internal friction parameter $\frac{\mu_1}{\eta_1} = 6 \times 10^5$, 10×10^5, 20×10^5, when h_v=0.02m, h_p=0.02m, $l = 0.0001m$ in case of electrical open conditions. 120

4.36 Variation of non-dimensional real phase velocity against non-dimensional wave number for different values of internal friction parameter $\frac{\mu_1}{\eta_1} = 6 \times 10^5$, 10×10^5, 20×10^5, when h_v=0.02m, h_p=0.02m, $l = 0.0001m$ in case of electrical short conditions. 120

4.37 Variation of non-dimensional damping phase velocity against non-dimensional wave number for different values of internal friction parameter $\frac{\mu_1}{\eta_1} = 6 \times 10^5$, 10×10^5, 20×10^5, when h_v=0.02m, h_p=0.02m, $l = 0.0001m$ in case of electrical short conditions. 121

4.38 Variation of non-dimensional real and damped phase velocity against non-dimensional wave number when h_v=0.02m, h_p=0.02m, $l = 0.0001m$ in case of electrical open conditions. 122

4.39 Variation of non-dimensional real and damped phase velocity against non-dimensional wave number when h_v=0.02m, h_p=0.02m, $l = 0.0001m$ in case of electrical short conditions. 122

4.40 Variation of non-dimensional real phase velocity against non-dimensional wave number for different values of piezoelectric constant $e_{15} = 17C/m^2$, $21C/m^2$, $25C/m^2$ in (a) and $e_{15} = 11C/m^2$, $15C/m^2$, $19C/m^2$ in (b), when h_v=0.02m, h_p=0.02m, $l = 0.0001m$ in case of electrical open conditions. 123

4.41 Variation of non-dimensional real phase velocity against non-dimensional wave number for different values of piezoelectric constant $e_{15} = 17C/m^2$, $21C/m^2$, $25C/m^2$ in (a) and $e_{15} = 11C/m^2$, $15C/m^2$, $19C/m^2$ in (b), when h_v=0.02m, h_p=0.02m, $l = 0.0001m$ in case of electrical short conditions. 123

4.42 Variation of non-dimensional real phase velocity against non-dimensional wave number for different values of dielectric constant $\epsilon_{11} = 237 \times 10^{-10}C^2/Nm^2$, $277 \times 10^{-10}C^2/Nm^2$, $317 \times 10^{-10}C^2/Nm^2$ in (a) and $\epsilon_{11} = 98 \times 10^{-10}C^2/Nm^2$, $128 \times 10^{-10}C^2/Nm^2$, $158 \times 10^{-10}C^2/Nm^2$ in (b), when h_v=0.02m, h_p=0.02m, $l = 0.0001m$ in case of electrical open conditions. 124

4.43 Variation of non-dimensional real phase velocity against non-dimensional wave number for different values of dielectric constant $\epsilon_{11} = 237 \times 10^{-10}C^2/Nm^2$, $277 \times 10^{-10}C^2/Nm^2$, $317 \times 10^{-10}C^2/Nm^2$ in (a) and $\epsilon_{11} = 98 \times 10^{-10}C^2/Nm^2$, $128 \times 10^{-10}C^2/Nm^2$, $158 \times 10^{-10}C^2/Nm^2$ in (b), when h_v=0.02m, h_p=0.02m, $l = 0.0001m$ in case of electrical short conditions. 125

5.1 Physical model of the problem. 132

5.2 Characteristic curves ($\frac{c}{c_o}$ versus ξH) for variation of imperfectness of the interface on the Love-wave phase velocity. 144

5.3 Variation of $\frac{c}{c_o}$ versus ξH for different values of initial stress ($I = Po/2a_1$) on the Love-wave phase velocity. 145

5.4 Variation of $\frac{c}{c_o}$ versus ξH for different values of heterogeneity parameter (αH) on the Love-wave phase velocity. 146

5.5 Variation of $\frac{c}{c_o}$ versus ξH for different values of length scale parameter on the Love-wave phase velocity. 146

5.6 Variation of $\frac{c}{c_o}$ versus ξH for different values of coupling factor on the Love-wave phase velocity. 147

6.1 Physical model of the problem 151

6.2 Variation of phase velocity c/c_f verses wave number ξH for different values of layer thickness under reinforced medium. 161
6.3 Variation of phase velocity c/c_f verses wave number ξH for different values of layer thickness under reinforced-free medium. 161
6.4 Variation of phase velocity c/c_f verses wave number ξH for different values of intrinsic characteristic length parameter under reinforced medium. 162
6.5 Variation of phase velocity c/c_f verses wave number ξH for different values of intrinsic characteristic length parameter under reinforced-free medium. 162
6.6 Variation of phase velocity c/c_f verses wave number ξH for reinforced and reinforced free medium. 163

Chapter 1

Introduction

1.1 Basic Introduction

Modern physical theories consider that the matter is discontinuous on a microscopic scale whereas the hypothesis of continuum mechanics deal with the mechanical and kinematical behavior of solids and fluids on the macroscopic scale by modeling them as a continuous mass (i.e., the distance between two adjacent molecules is insignificant in comparison with the dimension of the entire body) instead of discrete particles. In this context, continuum mechanics deals with the bodies having large dimensions by neglecting the interatomic spacings in a crystal or mean free paths in gas on the microscopic scale, i.e., this theory can be applied to granular materials such as sand, provided that the dimensions of the region considered are large compared with those of individual grain.

Solid mechanics and *Fluid mechanics* are the important sectors of physics and applied mathematics, which constitute the foundation for civil and mechanical engineering in the field of continuum mechanics. The key emphasis of this coherent approach is the general mechanical concepts for all materials. Solid mechanics is one of the important branches of physical science that deals with the motion and deformation of continuous solid materials(such as steel, wood, geological and biological materials, concrete, and plastics) under externally applied loads such as forces that result in inertial force in

the body, chemical interactions, thermal changes, and electromagnetic forces [204]. In rigid-body mechanics, when an external force is applied to the rigid body, it can be translated or rotated as a whole body and it remains unchanged in size and shape. Continuum mechanics is more concerned with deformable bodies that are capable of changing their shape. For such bodies the relative motion of the particles is important, and this introduces the spatial derivatives of displacement, velocity, and so on as significant kinematic variables [189]. Any change from the normal configuration of the body in shape or size is called *deformation* and the forces that bring about deformation are called *deformation forces*. If the deformation forces don't exceed a certain elastic limit, then deformation disappears when the forces are removed. The point at which a material, if subjected to higher deforming force, will no longer return to its original shape is known as the elastic limit of the body.

Based on the properties of the material, they can be categorized as elastic and plastic bodies. Bodies that regain their original size and shape when deformation forces are removed are called perfectly elastic bodies (steel, quartz, aluminum, etc.). Some bodies have no gross tendency to recover their original shape and size upon the removal of applied forces and get permanently deformed are called plastic bodies (mud, putty, etc.). The elastic property of a continuum body depends on the strength of resistance to its deformation. The greater the resistance of a body to deform, the more elastic it is said to be.

The oldest theory developed at the beginning of the nineteenth century was the classical theory of elasticity. This theory provides a mathematical model for examining the mechanical conduct of a wide range of solid materials commonly used in many fields of science and engineering. In the analysis and designing of machine elements, the mechanical engineer uses elasticity. In the deflection analysis of structures such as beams, plates, and shells, civil technicians use elasticity to study the stress distribution. In crystalline solids, the material engineer uses elasticity around dislocations and in micro-structured materials. In modeling the conduct of the material with a complex microstructure, the concept of microcontinuum theory can be taken into considerations. There are several theories in existing literature based on the contin-

uum mechanics like the piezoelectric theory, orthotropic theory, viscoelastic theory, fiber-reinforced theory, and many more.

1.2 Classical theory of elasticity

Elasticity is the property of solids that recovers their original shape and size after removal of applied forces, i.e., when such solid bodies are loaded at sufficiently low temperature for a very short time, with sufficiently limited stress magnitude, its deformation can be fully recovered upon unloading. It deals with the evaluation of stress, strain, and displacement distribution in elastic solids under the influence of applied force. The elasticity of continuous materials is described through the stress-strain curve showing the relationship between stress and strain. Most metallic or crystalline materials exhibit a linear stress-strain response to the small deformation described by Hooke's law on neglecting higher-order terms. But the relationship is no longer linear for rubbery materials under larger deformation beyond elastic limits. For even higher stresses, the materials show plastic behavior, that is, they deform irreversibly and do not return to their original shape after no longer stress is applied. All engineering materials have a certain range of elasticity. The common materials of construction will remain elastic only for very small strains before they exhibit plastic stretching or brittle fracture. Therefore, it is necessary to understand the basics as well as mathematical aspects of elasticity.

Stress is defined as restoring force per unit area when deformed by the application of external force, and strain is defined as the measure of the degree of deformation, i.e. when the dimensions of the body get changed under the action of deforming forces (ratio of change in dimension of the body to its original dimension). Stress can further be classified as normal stress and shearing stress. The restoring force acting per unit area normal to the surface of the body is termed as normal stress whereas the restoring force acting per unit area tangential to the surface of the body is termed as shearing stress. Similarly, the strain can be categorized as normal strain and shear strain. Normal strain is defined as the ratio of change in length (ΔL) to its original

length (L) in a specific direction while a shear strain is defined as the change in angles with respect to two specific directions.

The state of strain at any point in the elastic body is characterized by nine quantities, called strain tensor e_{ij}. Similarly, the state of stress at any point in the material body is characterized by nine quantities, called stress tensors, σ_{ij}, where first subscript (i) indicates the direction of the normal to the plane and the second subscript (j) indicates the direction of the component of the stress vector. The components of the stress tensor acting on a small rectangular parallelepiped is shown in figure (1.1). Here $T^{(i)}$

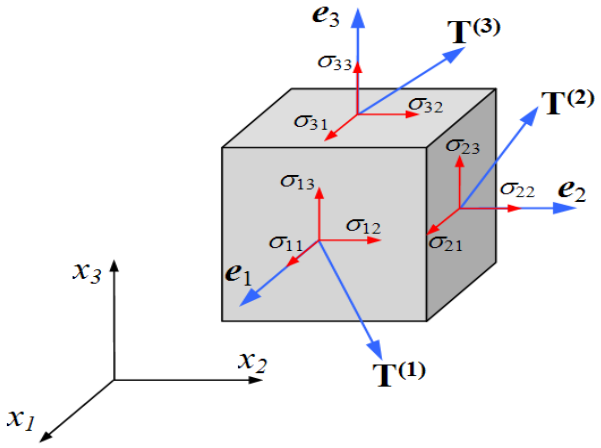

Figure 1.1: Stress components (Ref: www.google/images.com)

denotes the force traction vector acting on a face of the parallelepiped which can be defined in terms of symmetric stress tensor as:

$$T^{(i)} = \sigma_{ji} e_j, \quad i, j = 1, 2, 3.$$

1.3 Generalized Hooke's law

In 1822, Cauchy generalized Hooke's law for the deformation of an elastic medium. According to this, "Each component to stress at any point of an elastic solid body is the linear function of the components of strain at the point". The deformation of an elastic solid medium induces stresses within. Robert Hooke gave the relationship for an elastic medium that the stress is directly proportional to strain within the elastic

limit. The modified form of Hooke's law came into existence which states that the stress components are functions of strain components, i.e., $\sigma = \sigma(e)$, and used in the developments of the linear theory of elasticity [187].

$$\begin{aligned}
\sigma_{11} &= c_{1111}e_{11} + c_{1112}e_{12} + c_{1113}e_{13} + - - - + c_{1131}e_{31} + c_{1132}e_{32} + c_{1133}e_{33},\\
\sigma_{12} &= c_{1211}e_{11} + c_{1212}e_{12} + c_{1213}e_{13} + - - - + c_{1231}e_{31} + c_{1232}e_{32} + c_{1233}e_{33},\\
\sigma_{13} &= c_{1311}e_{11} + c_{1312}e_{12} + c_{1313}e_{13} + - - - + c_{1331}e_{31} + c_{1332}e_{32} + c_{1333}e_{33},\\
\sigma_{21} &= c_{2111}e_{11} + c_{2112}e_{12} + c_{2113}e_{13} + - - - + c_{2131}e_{31} + c_{2132}e_{32} + c_{2133}e_{33},\\
\sigma_{22} &= c_{2211}e_{11} + c_{2212}e_{12} + c_{2213}e_{13} + - - - + c_{2231}e_{31} + c_{2232}e_{32} + c_{2233}e_{33},\\
\sigma_{23} &= c_{2311}e_{11} + c_{2312}e_{12} + c_{2313}e_{13} + - - - + c_{2331}e_{31} + c_{2332}e_{32} + c_{2333}e_{33},\\
\sigma_{31} &= c_{3111}e_{11} + c_{3112}e_{12} + c_{3113}e_{13} + - - - + c_{3131}e_{31} + c_{3132}e_{32} + c_{3133}e_{33},\\
\sigma_{32} &= c_{3211}e_{11} + c_{3212}e_{12} + c_{3213}e_{13} + - - - + c_{3231}e_{31} + c_{3232}e_{32} + c_{3233}e_{33},\\
\sigma_{33} &= c_{3311}e_{11} + c_{3312}e_{12} + c_{3313}e_{13} + - - - + c_{3331}e_{31} + c_{3332}e_{32} + c_{3333}e_{33}.
\end{aligned} \tag{1.1}$$

The compact form of equation (1.1) is:

$$\sigma_{ij} = c_{ijkl}e_{kl}, \qquad (i,j,k,l = 1,2,3), \tag{1.2}$$

where

$$e_{kl} = \frac{1}{2}\left(\frac{\partial u_k}{\partial x_l} + \frac{\partial u_l}{\partial x_k}\right) = \frac{1}{2}(u_{k,l} + u_{l,k}), \quad i,j = (1,2,3).$$

Here, c_{ijkl} represents the stiffness tensor (or elasticity tensor) of fourth-order having $3 \times 3 \times 3 \times 3 = 81$ constants in number, which characterize the elastic properties of a solid medium. Usually, these elastic material constants depend on the physical properties of the elastic medium and are independent of strain tensor e_{ij}.

When all the components of the strain tensor are zero, i.e., $e_{kl} = 0$, which implies that all the components of the stress tensor are also zero, i.e., $\sigma_{ij} = 0$. This means the initially unstrained state of a body is unstressed. As the strain tensors are dimensionless quantities which implies that the elastic constants have the same dimension as that of stress tensors.

The majority of structural materials are crystalline substances and thus very small

quantities of them cannot be considered isotropic. However, assumptions of isotropy and homogeneity do not produce serious differences between experimental and theoretical findings, when applied to an entire body. It is because of the fact that most crystals are of small dimensions relative to the entire body and are chaotically distributed so that the behavior of the material is generally isotropic. The rolling process also creates a certain orientation of crystals, so that many rolling metals are anisotropic. If c_{ijkl} is independent of the position of points, i.e., elastic constants are the same for all points in the medium, then the medium is called elastically homogeneous. If c_{ijkl} varies from point to point in the body, then the medium is called elastically non-homogeneous or inhomogeneous.

Since the stress and strain tensor are symmetric, i.e., $\sigma_{ij} = \sigma_{ji}$ and $e_{kl} = e_{lk}$, using this condition in equation (1.1), here are 6 independent stress equations and each equation contains 6 independent material elastic constants. So, the number of elastic constants further reduces from 81 to 36 material constants. In the absence of material symmetries and if these 36 elastic constants are independent, then the material is said to be a generalized anisotropic medium known as triclinic medium. For simplicity, one can replace pair of indices ij or kl by single index p or q, where i, j, k and l take the values $1, 2, 3$; p and q take the values $1, 2, 3, 4, 5, 6$ provided in Table 1.1.

The generalized Hooke's law may be written in matrix form as:

Table 1.1: Voigt notation

ij or kl	11	22	33	23 or 32	13 or 31	12 or 21
p or q	1	2	3	4	5	6

$$\begin{bmatrix} \sigma_{11} \\ \sigma_{22} \\ \sigma_{33} \\ \sigma_{23} \\ \sigma_{31} \\ \sigma_{12} \end{bmatrix} = \begin{bmatrix} c_{11} & c_{12} & c_{13} & c_{14} & c_{15} & c_{16} \\ c_{21} & c_{22} & c_{23} & c_{24} & c_{25} & c_{26} \\ c_{31} & c_{32} & c_{33} & c_{34} & c_{35} & c_{36} \\ c_{41} & c_{42} & c_{43} & c_{44} & c_{45} & c_{46} \\ c_{51} & c_{52} & c_{53} & c_{54} & c_{55} & c_{56} \\ c_{61} & c_{62} & c_{63} & c_{64} & c_{65} & c_{66} \end{bmatrix} \begin{bmatrix} e_{11} \\ e_{22} \\ e_{33} \\ 2e_{23} \\ 2e_{31} \\ 2e_{12} \end{bmatrix}. \tag{1.3}$$

The elastic constants are symmetric, i.e., $c_{ij} = c_{ji}$, following energy density function for the isothermal or adiabatic system. In this case, the number of elastic constants is reduced from 36 to 21. Generally, the internal structure of the material possesses certain symmetries. For a material having one plane of elastic symmetry, the number of independent elastic constant reduces from 21 to 13 constants. The material with 13 elastic constants is known as a monoclinic medium. Using $c_{14} = c_{15} = c_{24} = c_{25} = c_{34} = c_{35} = c_{46} = c_{56} = 0$, equation (1.3) reduces to

$$\begin{bmatrix} \sigma_{11} \\ \sigma_{22} \\ \sigma_{33} \\ \sigma_{23} \\ \sigma_{31} \\ \sigma_{12} \end{bmatrix} = \begin{bmatrix} c_{11} & c_{12} & c_{13} & 0 & 0 & c_{16} \\ c_{12} & c_{22} & c_{23} & 0 & 0 & c_{26} \\ c_{13} & c_{23} & c_{33} & 0 & 0 & c_{36} \\ 0 & 0 & 0 & c_{44} & c_{45} & 0 \\ 0 & 0 & 0 & c_{45} & c_{55} & 0 \\ c_{16} & c_{26} & c_{36} & 0 & 0 & c_{66} \end{bmatrix} \begin{bmatrix} e_{11} \\ e_{22} \\ e_{33} \\ 2e_{23} \\ 2e_{31} \\ 2e_{12} \end{bmatrix}. \tag{1.4}$$

The orthotropic material shows the symmetry of its elastic properties with respect to three orthogonal planes, due to which the elastic constant reduces from 13 to 9. Certain types of wood, ceramics, metal sheets, heavy rollers, and bones exemplify orthotropic material. Using $c_{16} = c_{26} = c_{36} = c_{45} = 0$ in equation (1.4), the stress-strain relation for orthotropic medium is:

$$\begin{bmatrix} \sigma_{11} \\ \sigma_{22} \\ \sigma_{33} \\ \sigma_{23} \\ \sigma_{31} \\ \sigma_{12} \end{bmatrix} = \begin{bmatrix} c_{11} & c_{12} & c_{13} & 0 & 0 & 0 \\ c_{12} & c_{22} & c_{23} & 0 & 0 & 0 \\ c_{13} & c_{23} & c_{33} & 0 & 0 & 0 \\ 0 & 0 & 0 & c_{44} & 0 & 0 \\ 0 & 0 & 0 & 0 & c_{55} & 0 \\ 0 & 0 & 0 & 0 & 0 & c_{66} \end{bmatrix} \begin{bmatrix} e_{11} \\ e_{22} \\ e_{33} \\ 2e_{23} \\ 2e_{31} \\ 2e_{12} \end{bmatrix}. \tag{1.5}$$

The transversely isotropic material possesses the axis of symmetry having 5 independent elastic constants. The stress-strain components for transversely isotropic

medium is:

$$\begin{bmatrix}\sigma_{11}\\ \sigma_{22}\\ \sigma_{33}\\ \sigma_{23}\\ \sigma_{31}\\ \sigma_{12}\end{bmatrix} = \begin{bmatrix} c_{11} & c_{12} & c_{13} & 0 & 0 & 0 \\ c_{12} & c_{11} & c_{13} & 0 & 0 & 0 \\ c_{13} & c_{13} & c_{33} & 0 & 0 & 0 \\ 0 & 0 & 0 & c_{44} & 0 & 0 \\ 0 & 0 & 0 & 0 & c_{44} & 0 \\ 0 & 0 & 0 & 0 & 0 & \frac{1}{2}(c_{11}-c_{12}) \end{bmatrix} \begin{bmatrix} e_{11}\\ e_{22}\\ e_{33}\\ 2e_{23}\\ 2e_{31}\\ 2e_{12}\end{bmatrix}. \tag{1.6}$$

In view of the fact that isotropic materials are not dependent on the orientation of the axes of coordinates but possess rotational symmetry with respect to two perpendicular axes. These isotropic materials have the same properties in all directions. In this case, the elastic constant reduces to 2, i.e., λ and μ which are known as Cauchy Lame's constants. The stress-strain relation for an isotropic medium is:

$$\begin{bmatrix}\sigma_{11}\\ \sigma_{22}\\ \sigma_{33}\\ \sigma_{23}\\ \sigma_{31}\\ \sigma_{12}\end{bmatrix} = \begin{bmatrix} c_{12}+2c_{44} & c_{12} & c_{12} & 0 & 0 & 0 \\ c_{12} & c_{12}+2c_{44} & c_{12} & 0 & 0 & 0 \\ c_{12} & c_{12} & c_{12}+2c_{44} & 0 & 0 & 0 \\ 0 & 0 & 0 & c_{44} & 0 & 0 \\ 0 & 0 & 0 & 0 & c_{44} & 0 \\ 0 & 0 & 0 & 0 & 0 & c_{44} \end{bmatrix} \begin{bmatrix} e_{11}\\ e_{22}\\ e_{33}\\ 2e_{23}\\ 2e_{31}\\ 2e_{12}\end{bmatrix}. \tag{1.7}$$

where $c_{12} = \lambda$ and $c_{44} = \mu$ are called Lame's constants in the theory of elasticity. The compact tensor form of the constitutive equation which defines the relationship between the components of stress and strain tensor [187] is:-

$$\sigma_{ij} = \lambda\delta_{ij}e_{kk} + 2\mu e_{ij}, \qquad (i,j,k = 1,2,3). \tag{1.8}$$

where $e_{kk} = \triangle = e_{11} + e_{22} + e_{33}$ represents the cubic dilatation defined as change in volume per unit volume and $\delta_{ij} = \begin{cases} 1, & \text{if } i = j, \\ 0, & \text{if } i \neq j. \end{cases}$ is called Kronecker's delta.

Equation of equilibrium: Consider a continuous body in equilibrium having volume V which is bounded by closed surface S. For equilibrium, the resultant forces acting on the medium within volume V must vanish. In that case, the equation of equilibrium for classical elasticity is given as:

$$\sigma_{ji,j} + F_i = 0, \quad i,j = 1,2,3. \tag{1.9}$$

where F_i represents the components of body forces per unit volume and comma $(,)$ represents the differentiation w.r.t coordinate x_j. If ρ is the density of continuous medium, then the components of force of inertia (i.e., mass $\times$ acceleration) per unit volume are $\rho\frac{\partial^2 u_i}{\partial t^2}$. The dynamical equation for continuous medium is

$$\sigma_{ji,j} + F_i = \rho\frac{\partial^2 u_i}{\partial t^2}, \quad i,j = 1,2,3. \tag{1.10}$$

By substituting the stress-strain relation (1.8) into the dynamical equation (1.10) for an isotropic medium is

$$(\lambda+\mu)u_{j,ji} + \mu u_{i,jj} + F_i = \rho\ddot{u}_i, \quad i,j = 1,2,3. \tag{1.11}$$

where dot (.) represents differentiation w.r.t. time t.
The vector form of the equation of motion in terms of displacement components for an isotropic medium is

$$(\lambda+\mu)\nabla(\nabla.\overrightarrow{u}) + \mu\nabla^2\overrightarrow{u} + \overrightarrow{F} = \rho\frac{\partial^2\overrightarrow{u}}{\partial t^2}. \tag{1.12}$$

1.4 Elastic waves

A **wave** is defined as a periodical disturbance or variation which gradually transfers energy in a medium from one point to another point. All waves require a source and medium of propagation. The medium through which the wave travels may experience some local oscillations as the wave passes, but the particles in the medium do not

travel with the wave.

Elastic waves are mechanical disturbances that propagate through a material and cause oscillations to its material particles about their equilibrium positions. The properties of elastic waves depend on the elastic properties of the material in which they propagate. These waves are physically no different from seismic, sound, or ultrasound waves, other than in their respective ranges of frequencies. The roots of such waves lie in seismic waves. The waves generated by an explosion, earthquakes, volcanic eruptions, magma movement, large landslides are known as seismic waves. The velocity of seismic wave propagation depends on the density and elasticity of the medium as well as the type of wave that propagates in a medium. Velocity tends to increase with depth through the earth's crust and mantle but drops sharply going from the mantle to the outer core.

The propagation of seismic waves forms the foundation of seismology. Seismology is a good way to develop and improve various techniques for modeling regional and global-scale geophysical processes and the determination of the internal structure of the earth. Seismologists use seismographs to record the amount of time it takes for the seismic waves to travel through different layers of the earth. As the waves travel through in a medium having different densities and stiffness, the waves can be refracted and reflected. Because of the different behavior of waves in different materials, seismologists can deduce the type of material through which the waves are traveling. Seismographs record the amplitude and frequency of seismic waves and yield information about the earth and its subsurface structure. Artificially generated seismic waves recorded during seismic surveys are used to collect data in oil and gas prospecting and engineering. Most of the literature on the studies of the elastic waves may found in text [45, 17, 3, 4]. Liao [111] developed a computing procedure for calculating the unknown coefficients by using boundary measures. Liao et al. [112] developed a compact and efficient method for solving the wave equations.

The wave propagation phenomena in solids can be broadly divided into two categories which are defined as

1. **Body waves:** The seismic waves which travel through the interior of the earth's

surface are called body waves. Acoustic waves in the air and electromagnetic waves in the vacuum are an example of body waves. These waves are further divided into two parts:

(i) **Primary waves (P-waves):** These waves are also known as longitudinal waves or compressional waves. These waves can move through solid and fluid mediums, like water or the liquid layers of the earth. It pushes and pulls the rock as it moves through just like sound waves push and pull the air. The motion of the particle of P-waves is in the same direction of wave propagation. The vibration caused by P-waves is a volume change, alternating from compression to expansion in the direction that the wave is traveling. These waves are the fastest waves and consequently, the first to 'arrive' at a seismic station.

(ii) **Secondary waves (S-waves):** S-waves are also named shear waves, or transverse waves, or rotational waves because they don't change the volume of the material through which they propagate. These waves are slower than P-waves. The particle movement of these waves is perpendicular or normal to the direction of wave propagation and the particle oscillates up and down about their equilibrium position. S-waves can travel only through solids, as fluids (liquids and gases) do not support shear stresses.

2. **Surface waves:** Seismic surface waves can travel along the earth's surface. They

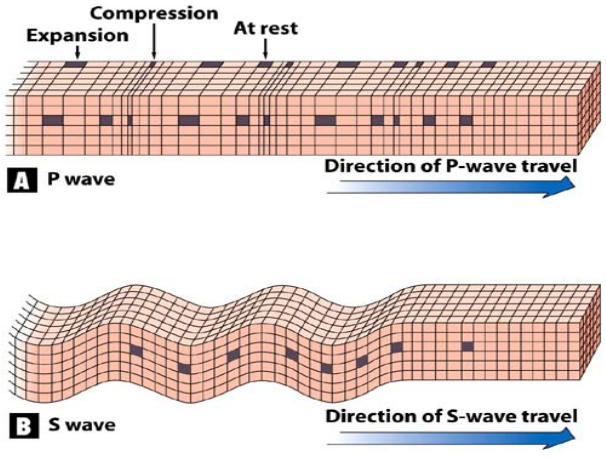

Figure 1.2: Primary waves and secondary waves (Ref: www.google/images.com)

can be classified as a form of mechanical surface waves. They travel more slowly than

seismic body waves (P-waves and S-waves). In large earthquakes, surface waves can have an amplitude of several centimeters. Waves in the ocean and ripples in a cup of water are an example of surface waves. Further, surface waves can be categorized as:
(i) **Love waves:** British seismologist A.E.H. Love [121] predicted the existence of Love-type surface waves which are horizontally polarized shear surface waves and a result of interference of multiple shear waves (SH-waves), exists only when a finite thickness layer is deposited on semi-infinite substrate and shear wave velocity in the layer is less than that of the substrate. The motion of a particle is transverse to the direction of wave propagation and occurs in the horizontal plane only. In seismology, these waves cause horizontal shifting of the earth during an earthquake. Love waves travel with a lower velocity than P or S waves.
(ii) **Rayleigh waves:** Rayleigh waves are also known as 'ground roll' because these waves roll along the ground similar to waves that roll across an ocean or lake. In 1885, Lord Rayleigh [151] mathematically showed the existence of Rayleigh-type waves. Most of the shaking felt from an earthquake is due to the Rayleigh wave, which can be much larger than the other waves. These waves have both longitudinal and transverse motions. The amplitude of the displacement of such waves in the medium dies exponentially with the increasing distance from the surface. The particle motion of these waves is always in a vertical plane and moves in an elliptical path. With the increasing depth, the elliptic motion changes from retrograde (counterclockwise) at the surface to prograde passing through a node at which there is no horizontal motion. Love wave travels slightly faster than Rayleigh-type surface waves. The velocity of the Rayleigh wave is approximately 0.9 times the velocity of the Love wave. The major difference between the characteristics of the Love wave and Rayleigh wave is that Love wave (do not propagate through water) can affect surface water only insofar as the sides of lakes and ocean bays push water sideways like the sides of a vibrating tank, whereas Rayleigh waves because of the vertical component of their motion can affect the bodies of water such as lakes. In a layered medium (like the crust and upper mantle), the velocity of the Rayleigh waves depends on their frequency and wavelength and this phenomenon is called dispersion. A homogeneous, isotropic elastic medium,

Rayleigh waves exhibit non-dispersive characteristics. However, if the properties of the elastic medium vary with the depth, then Rayleigh waves become dispersive. Many authors gave different mathematical techniques to solve non-linear dispersion equations considering different material properties and geometries [84, 9, 87, 96].

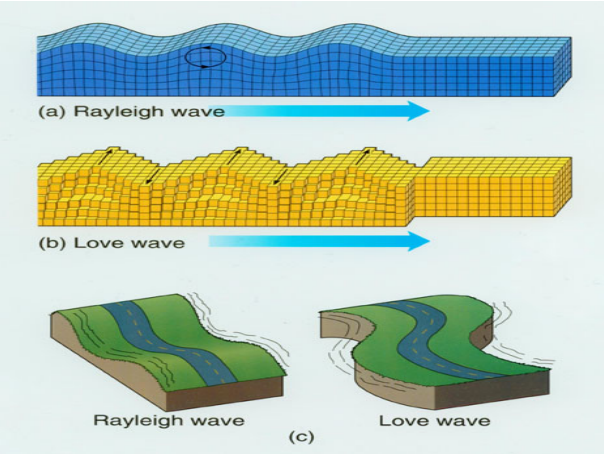

Figure 1.3: Rayleigh waves and Love waves (Ref: www.google/images.com)

1.5 Application of elastic waves

Geologists use the phenomenon of elastic wave propagation (generated from earthquakes) by considering the earth as an elastic solid for gathering information about the internal construction of the earth. Another aspect of these waves is their use for the characterization of oil or gas exploration, minerals, crystals, and hydrocarbons buried within the layers of the earth. In the field of construction, the main emphasis is on the response to impact or loads. Elastic wave theory also finds applications to predict all aspects of the response and to determine the strength of structures under loading conditions. Ultrasonic waves are used widely in the field of non-destructive testing for materials characterization, to determine the structural and mechanical properties of the material, to detect cracks, corrosion, and other material defects. With the introduction of a pulse into a solid, defects may be detected with the pulse energy reflections from the defect. These detection applications make use of longi-

tudinal waves, transverse waves, or surface waves. The phenomenon of propagation of waves in thin strips and bulk solids is used to construct delay lines. The pulse velocity of electrical signals is delayed by converting it into a mechanical pulse by using a transducer. These signals are made to propagate in some solid media and are recovered after a specified time through another transducer. These waves have many applications in the field of mining, where explosions are used to produce stress waves in rocks. These shock waves are used to remove fractures and heavy rocks. The Literature on wave propagation and their related phenomena is given in the book by Graff [62].

1.6 Emergence of microcontinuum theories

In classical continuum mechanics, the molecular structure of the matter is not taken into account because materials are considered to be continuous and homogeneous in the mathematical sense which means that each material particle of an elastic body is treated as a geometric point irrespective of its orientation. In this theory, the deformation of an elastic body is described by displacement vector and the transfer of load on the surface element through the force vector called the stress vector. This theory is consistent with the experiments performed on structural materials like aluminum, concrete, steel, etc. under elastic limitations but is not able to describe the sized impact of materials relative to the inner length of their microstructure due to the absence of scaling parameters. Notable inconsistencies between theoretical and experimental findings were found in some materials, such as polymers, cell solids, asphalts, bones, fibrous, etc [41]. These discrepancies mainly occur in the dynamic problems of elastic vibrations with high-frequency and low-wavelength, i.e., for ultrasonic waves. The classical principle of elasticity inevitably fails in the case of vibration in granular and multimolecular bodies. The failure of this theory lies in the fact that the microstructure of the granular bodies affects significantly the transmission of waves at higher frequencies or shorter wavelengths. The range of possible materials to be modeled by microstructure theories is very wide.

According to Eringen [41, 43], the micropolar theory can model composites with rigid chopped fibers, elastic solids with rigid granular inclusions, and other elastic materials such as liquid crystals. The application of micropolar theory to solids with periodic microstructure is extensive and successful [144]. It ranges from natural materials with lattice structures (crystals) to man-made composite materials and engineering structures such as infinite-fiber composites, sandwich structures, grid structures, trusses, and honeycombs. In biomechanics, Bone is a heterogeneous material with microstructural features.

The investigation of microstructural characteristics of materials with structural features is important for engineers and material scientists. The shortcomings of the classical theory of elasticity have led to the development of size-dependent continuum mechanics that describes the behavior of the material at the micro-scale as well as at the macro-scale. New measures of deformation related to length scale are needed in the desired continuum theory for explaining the microstructural characteristics of the material. In this context, various size-dependent models have been proposed for capturing the material's microstructural impacts and these size effects can be captured by introducing an additional length scale parameter, called "characteristic length".

Initially, Voigt [200] introduced the concept of couple stresses theory by considering couple stresses, in addition, to force stresses to remove the shortcomings of the classical theory of elasticity. However, Cosserat and Cosserat [32] brothers were the first to develop the complete theory of non-symmetric elasticity by taking the assumption that every material particle is associated with the rigid triad. In this model, the deformation of the medium is characterized by the displacement vector along with the independent rotation vector. Displacements and rotations are associated with non-symmetric stresses and couple stresses respectively through constitutive relations. This was contrary to the classical elasticity which described stress as a symmetric tensor. This theory didn't get the attention it deserves at their time and then almost after 50 years, the field was further explored by several analysts such as Mindlin and Tiersten [134], Toupin [193], Koiter [94], Toupin [194], Eringen [41, 43, 42, 44], Hadjesfandiari and Dargush [67] by considering distinct microcontin-

uum theories. Many researchers applied these microstructural theories to study the dispersive characteristic of surface wave propagation phenomenon in different layered structures [161, 210, 197, 143, 58, 173, 164, 99, 162, 61].

In this thesis, the two different microcontinuum theories have been considered, i.e., micropolar theory of elasticity proposed by Eringen [41] and consistent couple stress theory proposed by Hadjesfandiari and Dargush [67].

1.6.1 Micropolar Theory

Eringen [41] proposed a micropolar model of elasticity which admits independent microrotation degree of freedom which represents the local rotation of the material points and is completely independent of the classical displacement. This model employs four micropolar elastic constants α, β, γ, and κ in addition to two classical elastic constants λ and μ called Lame's constants.

The constitutive relations for the micropolar theory of elasticity [41] are:

$$\sigma_{il}^{(m)} = \lambda_m u_{k,k}\delta_{il} + \mu_m(u_{i,l} + u_{l,i}) + \kappa_m(u_{l,i} - \epsilon_{ilk}\phi_k^{(m)}), \tag{1.13}$$

$$m_{il}^{(m)} = \alpha_m \phi_{k,k}^{(m)}\delta_{il} + \beta_m \phi_{i,l}^{(m)} + \gamma_m \phi_{l,i}^{(m)}. \tag{1.14}$$

The equation of motion for a micropolar elastic model in the absence of body force are:

$$(\lambda_m + \mu_m)\nabla(\nabla.\overrightarrow{u}) + (\mu_m + \kappa_m)\nabla^2\overrightarrow{u} + \kappa_m(\nabla \times \vec{\phi}^{(m)}) = \rho_m \frac{\partial^2 \overrightarrow{u}}{\partial t^2}, \tag{1.15}$$

$$(\alpha_m + \beta_m + \gamma_m)\nabla(\nabla.\vec{\phi}^{(m)}) - \gamma_m \nabla \times (\nabla \times \phi^{(m)}) + \kappa_m(\nabla \times \overrightarrow{u}) - 2\kappa_m\vec{\phi}^{(m)} = j\rho_m \frac{\partial \vec{\phi}^{(m)}}{\partial t^2}. \tag{1.16}$$

where i, k, $l = 1, 2, 3$; ρ_m is the mass density of the micropolar elastic model, σ_{il} and m_{il} are the force stress tensor and couple stress tensor respectively, $\overrightarrow{u} = (u_1, u_2, u_3)$ and $\vec{\phi}^{(m)}$ denotes the mechanical displacement and microrotation function respectively, λ_m, μ_m are Lame's constant, α_m, β_m, γ_m, κ_m are micropolar material param-

eters which can be expressed in terms of two another specialized constants called the characteristic length (l) and coupling factor (N), j is micro inertia.

This theory is preferred for capturing the microstructural effects by considering material length-parameter. These micropolar material parameters can be expressed in terms of two specialized constants called characteristic length (l) and coupling factor (N) [53] as:

$$\gamma = 4l^2\left(\mu + \frac{\kappa}{2}\right), \quad \kappa = \frac{2N^2\mu}{1-2N^2}.$$

where the coupling number ($0 \leq N < 1$) determines the degree of micropolarity exhibited by the materials, $N = 0$ corresponds to the classical theory of elasticity. The characteristic length (l) quantifies the related length scale parameter of the material. Most researchers use the size-dependent hypothesis, to identify the material's microstructural characteristics and their related mechanical problems [43]. Iesan [74] used micropolar continuum theory to study some earthquake-related problems. The experimental investigation on the micropolar theory was carried out by Gauthier [57]. Yang and Lakes [210] examined the size-effects in quasistatic bending of compact bones and these effects were consistent with micropolar theory. Park and Lakes [147] showed that strain distribution in wet bones follows the prediction of cosserat elasticity, whereas strain distribution in dry bones behaves nearly classically. Thus, micropolar elastic theories were proposed to explain microstructural size effects on bones. Fatemi et al. [53] investigated the generalized continuum mechanics theories which account for the influence of microstructure-related scale effects on the macroscopic properties of bone.

Pabst [144] outlines the applications of micropolar theory for modeling solid composites (fiber, platelet, or particulate), porous media (solids with microcrack), and suspension (containing isomeric or anisomeric particles). He showed non-linear and linear constitutive equations for anisotropic and isotropic solids and fluids. He also presented the physical significance of the material parameters and discussed the reduction of their number due to symmetry. McGregor and Wheel [127] determined the micropolar constitutive parameters for two material variants that differ only in

their matrix topology from both experimental tests and finite-element analysis. They claimed that the degree of micropolarity is determined by the coupling number (N) and the intrinsic lattice size scale is reflected by the parameter, characteristic length (l). Eremeyev et al. [40] applied micropolar theory to analyze the stress concentration problems near notches and holes of various sizes for bone reconstruction. A domain-independent interaction integral for linear elastic fracture mechanics of micropolar materials was studied by Yu et al. [212]. Leonetti et al. [106] and Fantuzzi et al. [51] highlighted the anisotropic effects accounting for the micropolar moduli related to the variation of microstructure internal sizes.

These theories magnetized the attention of many researchers to apply it in the field of wave propagation phenomenon under distinct conditions to describe the behavior of different physical objects such as cellular solids, granular media, bones, chopped fibers, platelet composite materials, aluminum epoxy, solid suspension, and foaming, rigid cellular animal blood, porous objects, foams. Kennedy and Kim [93] applied a finite element method to study dynamic stress concentrations in micropolar elastic materials when subjected to suddenly applied load under plane strain problem. Strong micropolar material properties were found to cause a significant reduction in the dynamic stress concentration caused by the diffraction of a plane dilatational wave by a circular or elliptical cavity. Erbay et al. [39] studied the nonlinear modulation of transverse waves propagating in an infinite micropolar elastic medium. Tomar and Kumar [192] examined the reflection and refraction of longitudinal displacement wave impinge obliquely at the interface between homogeneous liquid half-space and micropolar elastic solid half-space. Nath et al. [137] derived the general frequency equation for the propagation of magneto-thermoelastic surface waves in a homogeneous, isotropic micropolar medium in the presence of a constant magnetic field. Erbay [38] used the asymptotic technique to obtain the two-dimensional dynamic equations of thin micropolar elastic plates from the three-dimensional dynamic equations of micropolar elasticity theory.

Midya [130] demonstrated the Love-type wave propagating in a homogeneous isotropic micropolar layered structure. Song et al. [188] examined the propagation of plane

harmonic at the interface between two micropolar viscoelastic media under generalized magneto-thermoviscoelastic theory. Midya et al. [131] discussed the problem of diffraction of plane harmonic SH-waves incident normally on a line crack in a micropolar elastic medium. Sharma and Kumar [163] studied the Lamb wave phenomenon in micropolar thermoelastic solid plates submerged in the liquid with varying temperatures. They showed the significant effect of fluid loading on the phase velocity, attenuation coefficient, and specific loss factor of symmetric and asymmetric modes of wave propagation in micropolar thermoelastic plates. Kumar and Gupta [98] investigated the propagation of waves in a transversely isotropic micropolar medium possessing thermoelastic properties based on Lord and Shulaman theory, Green and Lindsay theory, and coupled thermoelasticity theory. Using Stroh formalism, Chirita and Ghiba [29] obtained the solution for the propagation of Rayleigh waves in Cosserat elastic materials. The reflection and transmission of plane harmonic waves at the interface between liquid and micropolar viscoelastic solid with stretch were studied by Singh [180]. An enhanced micropolar model was proposed by Merkel and Luding [128] which involves the minimum number of elastic constants to consistently predict the dispersion relations in the long-wavelength limit. Kundu et al. [101] studied the propagation of a Love-type surface wave in a heterogeneous micropolar medium lying over an elastic inhomogeneous half-space when both density and rigidity was assumed to vary linearly with depth.

Singh et al. [175] investigated the surface wave propagation in the presence of irregularities at the common interface of a distinct micropolar elastic medium. Othman and Abd-Elaziz [142] studied the influence of the rotation and gravitational field on the plane waves of a linearly magneto-micropolar thermoelastic medium using the dual-phase-lag model (DPL). Hilal et al. [71] showed the influence of gravitational field in a rotating micropolar thermoelastic medium with micro temperatures. The impact of imperfect interfacial bonding on Love-type wave propagation in a vertically heterogeneous fiber-reinforced material layer lying over a micropolar elastic substrate was examined by Kaur et al. [88]. Lianngenga and Singh [110] obtained the dispersive frequency equation for symmetric and anti-symmetric vibrations in the microp-

olar thermoelastic plate with voids. Singh et al. [181] examined the reflection and transmission phenomenon of plane waves at an interface between two different transversely isotropic micropolar piezoelectric half-spaces. Gupta et al. [65] demonstrated the influence of periodic corrugated boundary surfaces on the propagation of plane SH-waves in fiber-reinforced medium lying over semi-infinite micropolar medium under the action of the magnetic field. Zhou et al. [214] demonstrated the dispersion of elastic wave propagation in micropolar metamaterial plates with periodical arranged resonators. He et al. [69] did an experimental investigation on the scale effect of mechanical properties of heterogeneous micropolar materials.

1.6.2 Couple Stress Theory

Hadjesfandiari and Dargush [67] demonstrated consistent couple stress theory which consists of three material parameters for isotropic case, i.e., Cauchy Lame's constant λ, μ, and characteristic length l. The characteristic length describes the effects of the inner microstructure of material which is negligible as compared to the dimensions of the body and is of the order of the average cell size or internal microstructure of the material. In this proposed study it was shown that the couple stress tensor is skew-symmetric and the skew-symmetric part of the gradient of the rotation tensor is the consistent curvature tensor. Hadjesfandiari and Dargush [68] developed the basic solutions for linear isotropic two-dimensional and three-dimensional stress elasticity depending on the composition of displacement fields into dilatational and solenoid components. Fakhrabadi [48] investigated the size effects on nanomechanical behaviors of nanoelectronics devices using consistent couple-stress theory.

Sharma and Kumar [165] employed the consistent couple stress theory to capture the size effects on the propagation of Lamb waves in an elastic plate with microstructure. The impact of the scaling parameter was outlined by Fathalilou and Rezazadeh [54] on the thermoelastic damping of a microbeam using the couple stress theory with microstructure. The influence of microstructure, heterogeneity, and internal friction on the propagation of the shear wave in the viscoelastic layer bonded with

the couple stress substrate was studied by Sharma and Kumar [166]. Wang et al. [201] presented the transmission and reflection of elastic waves having a couple stress layers sandwiched between semi-infinite couple stress half-spaces. Sharma and Kumar [167] investigated the shear wave propagation in a viscoelastic layer structure bonded imperfectly to the couple stress substrate. They showed the impact of inner microstructures and heterogeneity of the considered layered structure.

Ghodrati et al. [59] investigated the propagation characteristics of Lamb waves in non-classical micro/nano-plates to extract the dispersion equations utilizing three size-dependent models namely indeterminate, modified, and consistent couple stress theories. They plotted the dispersion curves for the phase and group velocities to illustrate the microstructural effects in very high frequencies. Sharma and Kumar [169] obtained the secular equations for the propagation of leaky Rayleigh wave in the couple stress substrate loaded with inviscid liquid layer to study the impacts of microstructures of the material. Kumar et al. [97] investigated the propagation features of Rayleigh waves at the boundary surface of couple stress elastic solids with mass diffusion in the context of Lord-Shulman and Green-Lindsay theories of generalized thermoelastic. Under the influence of gravity, Sharma and Kumar [168] studied the dispersive characteristics of Rayleigh wave in couple stress half-space loaded with an inviscid liquid layer of finite thickness or a liquid half-space. Fan and Xu [49] studied Love wave propagation in elastic half-space covered with the finite layer of couple stress medium. Sharma and Kumar [170] obtained the frequency equations for magnetically open and short conditions to unfold the veiled features of the propagation of Love-type wave through piezomagnetic material overlying couple stress substrate, under the influence of viscous liquid loading. Jouneghani et al. [81] examined the micro and nano-mechanical behavior of orthotropic doubly-curved shells based on the couple stress theory of elasticity.

Singhal et al. [185] examined the transmission of a Love-type wave through compressive stressed orthotropic material welded imperfectly on the couple stress half-space. They graphically demonstrated the remarkable effects of the initial stress parameter, imperfect interface parameter, friction parameter, phase, and group velocity on the

Love-type waves. Based on the thermoelastic Green-Naghdi theory, Li et al. [109] examined the characteristics of the reflection and transmission of thermoelastic waves at the interface of two couple stress elastic solids. Singh et al. [179] analytically examined the propagation of G-type wave in functionally graded transversely isotropic substrate beneath a stratum considering couple stress. They outlined the substantial effects of characteristic length, anisotropy, and functional gradedness on the phase velocity profiles of G-type waves. Alavi et al. [5] studied a linear size-dependent Timoshenko beam model based on the consistent couple stress theory for capturing the microstructural effects. To explicate the influence of imperfectness at the interfacial surface, Sharma and Sharma [171] obtained the dispersion and damping equations for the propagation of Love wave in fiber-reinforced layer bonded imperfectly over the couple stress half-space having internal microstructures. They showed that the proposed model should be the nearest approximation of the Earth because it exhibits many heterogeneities in the form of microstructures. Under transverse mechanical loading, Alinaghizadeh and Shariati [6] developed a non-classical model to study the nonlinear behavior of annular sector microplates using couple stress theory. They showed the effects of nonlinearity, foundation parameters, length scale parameters, and geometric parameters on the deflections of the annular sector and square microplates.

The constitutive relations for couple stress theory [67] are

$$\sigma_{ji}^{(c)} = \lambda_c u_{k,k}\delta_{ij} + \mu_c(u_{i,j} + u_{j,i}) - \eta_c\nabla^2(u_{i,j} - u_{j,i}), \tag{1.17}$$

$$\mu_{ji}^{(c)} = 4\eta_c(\omega_{i,j} - \omega_{j,i}), \tag{1.18}$$

where

$$\omega_i = \frac{1}{2}\epsilon_{ijk}u_{k,j}.$$

The equation of motion for couple stress model in the absence of body force is:

$$(\lambda_c + \mu_c + \eta_c\nabla^2)u_{k,ki} + (\mu_c - \eta_c\nabla^2)u_{i,kk} = \rho_c\frac{\partial^2 u_i}{\partial t^2}. \tag{1.19}$$

The vector form of equation (1.19) is:

$$(\lambda_c + \mu_c + \eta_c \nabla^2)\nabla(\nabla . \overrightarrow{u}) + (\mu_c - \eta_c \nabla^2)\nabla^2 \overrightarrow{u} = \rho_c \frac{\partial^2 \overrightarrow{u}}{\partial t^2}. \tag{1.20}$$

where $i, j, k = 1, 2, 3$; λ_c, μ_c are Lame constants, $\eta_c = \mu_c l^2$ is the couple stress coefficient, l is the characteristic length, ρ_c is the mass density of the couple stress model, δ_{ij} is Kronecker delta and ϵ_{ijk} is the alternating tensor, $\overrightarrow{u}$ is the mechanical displacement component, $\sigma_{ji}^{(c)}$ is non-symmetric force-stress tensor and $\mu_{ji}^{(c)}$ is skew-symmetric couple stress tensor.

1.7 Piezoelectric Theory

The phenomenon of piezoelectricity was discovered in the late 19th century. Piezoelectricity means electricity generated from pressure. In 1880, Pierre and Jacques Curie [34] experimentally discovered the direct piezoelectric effects in various naturally occurring substances, including Rochelle salt and quartz. In 1881, Lippmann [113] used the term piezoelectricity, derived from the Greek word "piezein" meaning "to press". It was mathematically hypothesized and then experimentally proven that a material exhibiting the direct effect of piezoelectricity would also exhibit the inverse effect. The piezoelectricity phenomenon was developed and applied in sonar and quartz crystals. In 1921, Walter Cady [18] invented the quartz-crystal-controlled oscillator and narrow-band quartz crystal filter used in the communication system. World war II spurred the growth of this field, especially with the urgent needs by the military to detect submarines.

The theory of piezoelectricity grabbed great attention because of the 'smart structural' properties of its material. These materials have the ability to produce an electric charge when subjected to mechanical stress called the direct piezoelectric effect and show deformation when subjected to an electric field called the inverse piezoelectric effect. These materials are highly anisotropic and strongly orientation-dependent.

These materials need to be poled in a particular direction to provide strong piezoelectric effects, although some materials exhibit natural or spontaneous polarization. As an indicator of the magnitude of the piezoelectric effects, a field of 1000 volt/meter applied between the ends of the quartz rod, produces a strain of 10^7. Conversely, a small strain can generate an enormous field. In 1981, Auld [11] demonstrated the two basic physical phenomena involved in all piezoelectric devices, i.e., wave propagation and resonance. He was the first to present the connection between piezoelectricity and crystal symmetry. Irino and Shimizu [76] investigated the propagation characteristics of the Stoneley waves across the interface between the piezoelectric material and isotropic material. Iesan [75] studied the plane strain problems and their existence in the static theory of linear piezoelectricity. Pak [145] developed a conservation law that leads to a path-independent integral of fracture mechanics along with the governing equations and boundary conditions for the linear piezoelectric materials. Lesan [107] gave some general theorems for the quasi-static and the dynamic piezoelectricity by establishing a reciprocity relation which implies new uniqueness results and minimum principles. Honein et al. [72] proposed a systematic methodology based on a matrix formalism and the concept of the surface impedance tensor to study the wave propagation characteristics in a piezoelectric layered structure. They also studied the subsonic interfacial waves when the plate is in contact with a nonconducting acoustic fluid. Lakhtakia [102] investigated the analytical solutions for the propagation of waves in a piezoelectric, continuously twisted, structurally chiral medium along the axis of spirality. Mawassy et al. [126] gave a variational approach of homogenization of piezoelectric composites towards piezoelectric and flexoelectric effective media.

Various investigations have been undertaken for the characteristic analysis of surface wave propagation in the layered piezoelectric structure due to its significant applications in the field of navigation, electronics, communication, micro-system technology as well as in the surface acoustic wave (SAW) devices like sensors, transducer, resonators, filters, amplifiers, oscillators, delay lines, etc. [37]. Curtis and Redwood [35] discussed a solution for the dispersion characteristics of the transverse surface waves in a piezoelectric material carrying a metal layer of finite thickness and gave the con-

ditions for the existence of various modes. The properties of the Love wave and its applications to sensor devices were outlined by Jakoby and Vellekoop [77]. In these kinds of sensors, a thin layer of the piezoelectric material is deposited on a substrate to enhance the performance of SAW-devices.

Wang [205] examined shear horizontal (SH) wave propagation in a semi-infinite solid medium surface bonded by a layer of piezoelectric material abutting the vacuum. Zakharenko [213] examined Love-type waves in layered systems consisting of two cubic piezoelectric crystals. Huang and Li [73] examined the propagation of shear waves along with a weak interface of two dissimilar piezoelectric cubic crystals with an imperfect bonding. Wang and Zhao [203] studied the propagation of Love wave in two-layered piezoelectric/elastic composite plates under the influence of the interfacial defect based on the shear spring model. Arani et al. [8] studied the size-dependent wave propagation of double-piezoelectric nanobeam-systems, based on the Euler-Bernoulli beam model. Gaur and Rana [56] studied the propagation of SH-waves in a porous piezoelectric composite structure. Li and Jin [108] observed the excitation and propagation of the shear horizontal waves in a piezoelectric layer imperfectly bonded to a metal or an elastic substrate. Kong et al. [95] examined the propagation characteristic of SH wave in an mm2 piezoelectric layer on an elastic substrate. The evolution of the electro-mechanical impedance of the piezoelectricity sensor was investigated to determine the setting time of the cement paste by Lee et al. [105]. Yang et al. [211] studied the effect of Love wave propagating in structure with a nanoscale piezoelectric layer lying on an elastic substrate. Singh et al. [178] examined the propagation of the Love wave in an irregular piezoelectric layer bonded on an isotropic elastic substrate to display the impacts of the rectangular and parabolic irregularities.

Nie et al. [139] investigated the propagation behavior of two transverse surface waves, i.e., Love waves and Bleustein-Gulyaev waves in the composite structure having piezoelectric and piezomagnetic layers bonded on the elastic substrate. Gaur [55] examined the effects of initial stress on the propagation of SH-waves in the piezoelectric layered structure. Ninh and Bich [140] examined the nonlinear electro-thermo-mechanical vi-

bration of nanocomposite cylindrical shells with piezoelectric actuators. Chaudhary et al. [27] investigated the influence of the interfacial imperfectness on SH waves propagation in initially stressed and rotating piezoelectric composite structure. Baroi et al. [13] investigated the propagation of shear waves in a porous piezoelectric substrate loaded with a viscous liquid to study the dynamic response of the affecting parameters. Kazemi et al. [92] examined the free vibration, static deflection, and pull-in instability of a fully-clamped functionally graded micro-plate subjected to electrostatic and piezoelectric excitations. Cao et al. [19] examined the dispersion curves and the attenuation tendency of the generalized Rayleigh waves for real wave number cases in a transversely isotropic piezoelectric semiconductor half-space. Chaudhary et al. [28] studied the impact of the interfacial imperfection on the propagation of Love waves in the piezoelectric gradient layer over the elastic substrate. Jiaoa et al. [79] studied the wave propagation phenomenon in a piezoelectric semiconductor slab sandwiched between two transversely isotropic piezoelectric half-spaces. Nirwal et al. [141] demonstrated the analysis of different boundary types on the propagation of the surface wave in bedded piezo-structure with flexoelectric effect. Heydarpour et al. [70] used the thermoelastic approach based on Lord-Shulman and Maxwell's formulations to study the wave propagation in functionally graded cylindrical panels with piezoelectric layers under a thermal shock loading. Jam and Shodja[78] studied the interfacial influence on the electromagnetic radiation emanating from an embedded piezoelectric nanofiber incident upon by SH-waves.

The constitutive relations for a piezoelectric medium [20] are

$$\sigma_{ij} = c_{ijkl} S_{kl} - e_{kij} E_k, \tag{1.21}$$

$$D_j = e_{jkl} S_{kl} + \epsilon_{jk} E_k. \tag{1.22}$$

The equation of motion and the electric displacement equilibrium equation of the piezoelectric medium are

$$\sigma_{ji,j} = \rho_p \frac{\partial^2 u_i}{\partial t^2}, \tag{1.23}$$

$$D_{i,i} = 0, \tag{1.24}$$

where i, j, k, $l = 1, 2, 3$; σ_{ij} and S_{kl} are the stress and the strain tensors respectively, c_{ijkl} , e_{kij} and ϵ_{jk} are the elastic, the piezoelectric and the dielectric coefficients respectively, u_i and D_j denotes the mechanical and the electric displacement respectively, ρ_p is the mass density of the piezoelectric medium, E_k is the electrical field intensity.

The constitutive equations (1.21) and (1.22) can be written in compact matrix notation by replacing pair of indices ij or kl by single index p or q, where i, j, k and l take the values $1, 2, 3$; p and q take the values $1, 2, 3, 4, 5, 6$. Normal stress components of piezoelectric materials are denoted by subscripts $1, 2, 3$ respectively and the shear stress components denoted by subscripts $4, 5, 6$ respectively. By using $\sigma_{ij} \to \sigma_p$, $c_{ijkl} \to c_{pq}$, $e_{kij} \to e_{kp}$ and $S_{kl} \to S_q$, one may obtain

$$\sigma_p = c_{pq} S_q - e_{kp} E_k, \tag{1.25}$$

$$D_j = e_{jq} S_q + \epsilon_{jk} E_k. \tag{1.26}$$

The equations (1.25) and (1.26) can be written in matrix form as:

$$\begin{bmatrix} \sigma_1 \\ \sigma_2 \\ \sigma_3 \\ \sigma_4 \\ \sigma_5 \\ \sigma_6 \end{bmatrix} = \begin{bmatrix} c_{11} & c_{12} & c_{13} & c_{14} & c_{15} & c_{16} \\ c_{21} & c_{22} & c_{23} & c_{24} & c_{25} & c_{26} \\ c_{31} & c_{32} & c_{33} & c_{34} & c_{35} & c_{36} \\ c_{41} & c_{42} & c_{43} & c_{44} & c_{45} & c_{46} \\ c_{51} & c_{52} & c_{53} & c_{54} & c_{55} & c_{56} \\ c_{61} & c_{62} & c_{63} & c_{64} & c_{65} & c_{66} \end{bmatrix} \begin{bmatrix} S_1 \\ S_2 \\ S_3 \\ S_4 \\ S_5 \\ S_6 \end{bmatrix} - \begin{bmatrix} e_{11} & e_{21} & e_{31} \\ e_{12} & e_{22} & e_{32} \\ e_{13} & e_{23} & e_{33} \\ e_{14} & e_{24} & e_{34} \\ e_{15} & e_{25} & e_{35} \\ e_{16} & e_{26} & e_{36} \end{bmatrix} \begin{bmatrix} E_1 \\ E_2 \\ E_3 \end{bmatrix}. \tag{1.27}$$

$$\begin{bmatrix} D_1 \\ D_2 \\ D_3 \end{bmatrix} = \begin{bmatrix} e_{11} & e_{12} & e_{13} & e_{14} & e_{15} & e_{16} \\ e_{21} & e_{22} & e_{23} & e_{24} & e_{25} & e_{26} \\ e_{31} & e_{32} & e_{33} & e_{34} & e_{35} & e_{36} \end{bmatrix} \begin{bmatrix} S_1 \\ S_2 \\ S_3 \\ S_4 \\ S_5 \\ S_6 \end{bmatrix} + \begin{bmatrix} \epsilon_{11} & \epsilon_{12} & \epsilon_{13} \\ \epsilon_{21} & \epsilon_{22} & \epsilon_{23} \\ \epsilon_{31} & \epsilon_{32} & \epsilon_{33} \end{bmatrix} \begin{bmatrix} E_1 \\ E_2 \\ E_3 \end{bmatrix}. \tag{1.28}$$

where

$$\sigma_1 = \sigma_{11}, \quad \sigma_2 = \sigma_{22}, \quad \sigma_3 = \sigma_{33}, \quad \sigma_4 = \sigma_{23} \text{ or } \sigma_{32}, \quad \sigma_5 = \sigma_{31} \text{ or } \sigma_{13}, \quad \sigma_6 = \sigma_{12} \text{ or } \sigma_{21},$$
$$S_1 = S_{11}, \quad S_2 = S_{22}, \quad S_3 = S_{33}, \quad S_4 = 2S_{23}, \quad S_5 = 2S_{31}, \quad S_6 = 2S_{12}.$$

The relation between the strain components and the mechanical displacement components is given by:

$$S_{ij} = \frac{1}{2}(u_{i,j} + u_{j,i}), \quad i, j = 1, 2, 3.$$

$$\begin{gathered} S_x = \frac{\partial u_1}{\partial x}, \ S_y = \frac{\partial u_2}{\partial y}, \ S_z = \frac{\partial u_3}{\partial z}, \ S_{yz} = \frac{1}{2}\left(\frac{\partial u_3}{\partial y} + \frac{\partial u_2}{\partial z}\right), \\ S_{zx} = \frac{1}{2}\left(\frac{\partial u_1}{\partial z} + \frac{\partial u_3}{\partial x}\right), \ S_{xy} = \frac{1}{2}\left(\frac{\partial u_1}{\partial y} + \frac{\partial u_2}{\partial x}\right). \end{gathered} \tag{1.29}$$

The relation between the electric potential field and the electric potential function is:

$$E_k = -\phi^{(p)}_{,k}.$$

$$E_x = -\frac{\partial \phi^{(p)}}{\partial x}, \ E_y = -\frac{\partial \phi^{(p)}}{\partial y}, \ E_z = -\frac{\partial \phi^{(p)}}{\partial z}. \tag{1.30}$$

1.8 Viscoelastic Theory

Viscoelasticity is the behavior of materials which at the same time exhibit elastic and viscous characteristics under deformation. As viscoelastic materials have a factor of viscosity, they have a time-dependent strain rate. When an applied load is removed, elastic materials do not dissipate energy, however, viscoelastic material does. Some materials like wood, synthetic polymers, metals as well as human tissue at high tem-

peratures show noteworthy viscoelastic impacts. In some applications, even a small viscoelastic response can be significant. Many engineering structural materials exhibit viscoelastic behavior which has great impacts on the performance of that material. The problem of studying surface wave propagation in a viscoelastic medium has been of great interest in several contexts because it finds application in the design process. Many authors investigated surface wave propagation in viscoelastic layered structure [153, 174].

Cooper [31] examined the reflection and the transmission of the plane waves at an interface between two viscoelastic materials. Shaw and Bugl [172] and Schoenberg [160] discussed the transmission and the reflection of plane waves through layered linear viscoelastic media. Borcherdt [15] investigated Rayleigh-type surface wave in a linear viscoelastic half-space and discussed results theoretically about the velocity, absorption coefficients, and displacement. Szabo and Wu [190] examined longitudinal and shear wave propagation in the viscoelastic medium by considering a model based on a time-domain statement of causality that describes the observed power-law behavior of many viscoelastic materials. Cerveny and Psencik [21] outlined the effects of the plane wave under the consideration of homogeneous and inhomogeneous viscoelastic half-space. Kaur et al. [86] studied reflection and refraction of SH-waves at a corrugated interface between two laterally and vertically heterogeneous viscoelastic solid half-spaces. Tomar and Kaur [191] examined the shear wave propagation at a corrugated interface between anisotropic elastic and the viscoelastic solid half-spaces. Liu and He [117] presented an analytical investigation of Love wave propagation in a structure with a piezoelectric substrate covered by multiple elastic, isotropic, and non-piezoelectric layers. The results showed that a Love wave sensor with such a two-layer structure can achieve better performances than with only one viscoelastic or elastic guiding layer. Cui et al. [33] determined SH-wave propagation in piezoelectric structure, where a viscoelastic thin layer is imperfectly bonded to a semi-infinite piezoelectric substrate. Liu et al. [118] and Liu [116] provided a theoretical model for the analysis of Love waves in a structure with multiple guiding viscoelastic layers deposited on piezoelectric half-space.

Sahu et al. [155] contemplated SH-waves in viscoelastic layer place on an elastic half-space with self-weight to display the impact of heterogeneity, internal friction, and gravity. Kaur et al. [90, 91] studied the influence of perfectly and imperfectly bonded micropolar elastic half-space with a non-homogeneous viscoelastic layer on the propagation behavior of the shear wave. Chatterjee et al. [22] studied the shear wave propagation in viscoelastic heterogeneous layers lying over an initially stressed half-space. Kakar and Kakar [83] illustrated the impact of a point source on the propagation behavior of Love waves in a viscoelastic heterogeneous layer lying over a viscoelastic substrate. Liu et al. [119] investigated seismic wave propagation in a viscoelastic medium with an irregular free surface. They showed that for interpreting the characteristics of seismic wave propagation in areas with rugged or rapidly varying topography, viscoelastic media can better represent the properties of the earth than acoustic/elastic media. Negin and Yahnioglu [138] examined the attenuation of the seismic Rayleigh waves propagating in an elastic crustal layer of the earth over the viscoelastic mantle because the deep layers of the earth are viscoelastic, causing seismic waves to dissipate as they propagate through the material. As a result, the study of seismic waves must be able to accurately explain the effects of attenuation and dispersion of the propagated waves. Yan et al. [209] used the experimental and simulation methods to study the noise reduction performance of cylindrical shells with different acoustic covering with viscoelastic material layers in the mid-low frequency range. Amirinezhad et al. [7] studied the propagation of acoustic waves through polymeric form plate by considering a mathematical model of functionally graded viscoelastic material.

The constitutive relation for viscoelastic solid of Voigt-type [150] is

$$\sigma_{ij}^{(v)} = \left(\lambda_v + \lambda_v^{'}\frac{\partial}{\partial t}\right)\delta_{ij}u_{k,k} + \left(\mu_v + \eta_v\frac{\partial}{\partial t}\right)(u_{i,j} + u_{j,i}). \tag{1.31}$$

The equation of motion for viscoelastic material in the absence of body forces is:

$$\sigma_{ji,j} = \rho_v \frac{\partial^2 u_i}{\partial t^2}. \tag{1.32}$$

where $i, j, k = 1, 2, 3$; λ_v, μ_v are Lame's constants, $\lambda_v^{'}, \eta_v$ are internal friction parameter of a viscoelastic layer, ρ_v is the mass density of viscoelastic material, δ_{ij} is kronecker delta, u_i is the mechanical displacement component, σ_{ij} is symmetric force-stress tensor for viscoelastic material.

Chapter 2

Microstructural considerations on Love wave propagation in a piezoelectric layered structure

2.1 Introduction

The understanding of the behavior of elastic surface waves in a layered system plays a vital role because of their widespread applications ranging from earthquake engineering to the designing of surface acoustic wave devices (SAW). In view of the modes of propagation characteristics, SAW devices are comprehensively partitioned into Love wave and Rayleigh wave devices. Due to the concentration of acoustic energy within the guiding layer and near to the surface of the substrate, the Love-type wave offers high sensitivity, which would be helpful for the fabrication of Love wave-based sensors. For the designing of these sensors, a thin film of piezoelectric material is deposited onto a non-piezoelectric substrate such as elastic, isotropic, viscoelastic, dielectric substrate, etc. In piezoelectric material, the electrical charges are gener-

The content of this chapter is published in the journal *'Journal of Theoretical and Applied Mechanics'*, 56(4):993–1004, 2018, *(SCI, Impact factor:0.831)*

ated and electricity is induced due to the mechanical stress applied. On account of their unique features, these materials are utilized to fabricate acoustic gadgets, sensors, transducers, actuators, and so on [183]. Many researchers have done astonishing work to demonstrate the conduct of Love-type wave propagation in a composite layered structure involving piezoelectric material under different boundary conditions. Liu et al. [115] showed the characteristics of a Love-type wave using initial stress in a layered system involving a piezoelectric layer of finite thickness, which is perfectly bonded to the elastic substrate. Jin et al. [80] examined the propagation of Love waves in a piezoelectric layered structure consisting of a piezoelectric layer overlying an elastic half-space with inhomogeneous initial stress. Wang et al. [206] examined the dispersion behaviors of SH waves propagating in a layered structure consisting of a piezoelectric layer and an elastic cylinder with an imperfect bonding. Singh et al. [177] investigated the propagation of a Love-type wave in an irregular piezoelectric layer lying over a piezoelectric half-space. Gupta and Vashishth [66] studied bulk wave propagation in a monoclinic porous piezoelectric material. Ezzin et al. [46] examined the propagation of Love waves in a transversely isotropic piezoelectric layer on a piezomagnetic half-space. Wei et al. [207] and Ezzin et al. [47] examined the propagation of SH-guided waves in the piezoelectric/piezomagnetic layered plates. Chaudhary et al. [25] highlighted the effect of normal and shear stresses, dielectric and electric potential produced due to moving load in a prestressed piezoelectric substrate.

Borges et al. [16] studied the effect of isotropic hardening parameter based on the plastic crack tip opening displacement to predict the fatigue crack growth rate. The interaction size amongst the micro-cracks in the particular neighborhood depends on the microstructural feature of the material and is linked to the length scale supporting the need to present micro-level information in the constitutive models. On this ground, it is relevant to consider microcontinuum theories. Many analysts successively proposed different microcontinuum theories viz. couple stress theory [200, 32, 134, 193], micropolar theory [43], microstretch (non-linear) [44] theory , micromorphic theory [42], the strain gradient theory [132, 133, 36, 10], to capture the size-effects of materials

like polymers, foams, cellular solids, grain-size particles, etc. These theories have the potential to incorporate micro-size effects by introducing additional size-dependent parameters. Many experiments have indeed been performed with a microstructural analysis to validate the justification of the material length scale parameter of the nonlocal approach [148, 129]. Being one of the generalized continuum theories, the consistent couple stress theory was given by Hadjesfandiari and Dargush [67] has been employed to study more about the microstructural characteristics of Love wave propagation in the composite piezoelectric layered structure.

Though Love wave propagation has been examined in detail for a piezoelectric layer overlying solid substrate but the role of the microstructure of the substrate has not been investigated to the full extent. Due to the continuous development in nano-electromechanical systems (NEMS) and micro-electromechanical system (MEMS), Love wave-based sensors with the microstructural exhibiting substrate are more efficient in this current age of NEMS and MEMS. In recent years, electromechanical devices with characteristic scales in the 1nm to 100nm range are being investigated to explore the scaling effect beyond that of traditional MEMS. Such devices and systems are referred to as NEMS systems [114, 208]. Farokhi and Ghayesh [52] derived the nonlinear equation of motion by employing the size-dependent modified couple stress theory while studying the behavior of MEMS.

To enhance the domain of Love wave propagation, the present chapter aims to investigate the microstructural considerations on Love wave propagation in a piezoelectric layered structure consisting of a finite thickness piezoelectric material layer lying over the semi-infinite couple stress substrate. The substrate is considered to have the properties of microstructure like granular macromorphic rock (Dionysos Marble). Two sets of a piezoelectric layer, i.e., $PZT-5H$ and $BaTiO_3$ materials are considered over a solid substrate. Closed-form expressions of the dispersion equation for both the cases of electrically open and electrically short conditions for the propagation of Love-wave are obtained. Numerical computations are performed and the results are manifested through graphs to examine the influence of the underlying microstructure of the substrate, thickness of the layer, piezoelectric and dielectric constants on the

phase velocity profiles of the Love-type wave. Particular cases are deduced to validate the present study.

2.2 Formulation of the problem

Consider a piezoelectric layer of thickness H (where $-H \leq x \leq 0$) lying over a couple stress elastic half-space. The Cartesian coordinate system is considered in such a way that the Love wave is propagating along the y-axis and the x-axis is pointing positive vertically downward as shown in figure 2.1. Conventionally, the poling direction is assumed along the z-axis. Let $u_i^{(p)} = (u_p, v_p, w_p)$ and $u_i^{(c)} = (u_c, v_c, w_c)$ are the

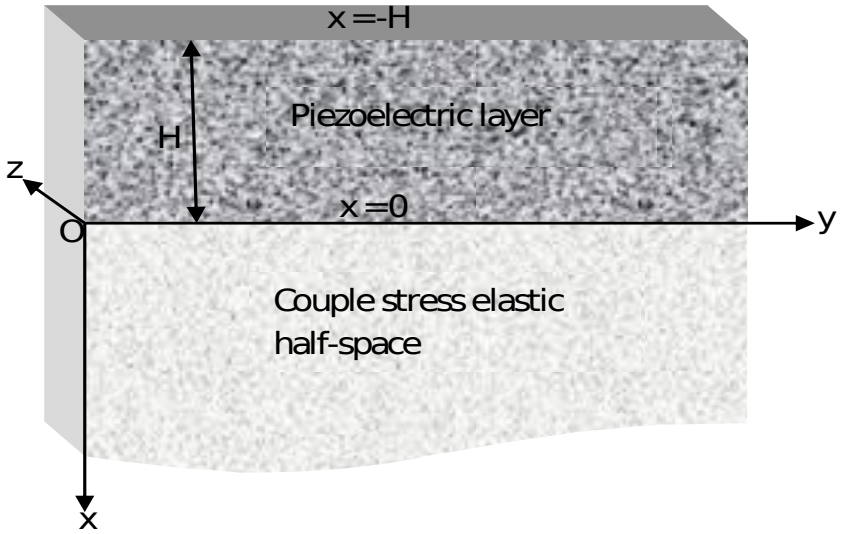

Figure 2.1: Geometry of the problem.

mechanical displacement components due to the propagation of the Love wave in the upper piezoelectric layer and the lower couple stress elastic half-space respectively. As the Love wave is propagating along the direction of the y-axis and it causes displacement in the z-direction only. For Love wave propagation:

$$\begin{aligned} u_p = 0,\ v_p = 0,\ w_p = w_p(x, y, t), \\ u_c = 0,\ v_c = 0,\ w_c = w_c(x, y, t). \end{aligned} \tag{2.1}$$

Suppose that the electric potential function of the upper piezoelectric layer is:

$$\phi^{(p)} = \phi^{(p)}(x, y, t). \tag{2.2}$$

2.2.1 Dynamics of piezoelectric material layer

The constitutive relations and the equation of motion for a piezoelectric material layer in the absence of body forces are given through equations (1.21)–(1.24) in Chapter-1. For the transversely isotropic piezoelectric material, equations (1.27) and (1.28) can be expressed in the component form with z-axis being a symmetric axis of material as [115]:

$$\begin{bmatrix} \sigma_x^{(p)} \\ \sigma_y^{(p)} \\ \sigma_z^{(p)} \\ \sigma_{yz}^{(p)} \\ \sigma_{zx}^{(p)} \\ \sigma_{xy}^{(p)} \end{bmatrix} = \begin{bmatrix} c_{11} & c_{12} & c_{13} & 0 & 0 & 0 \\ c_{12} & c_{11} & c_{13} & 0 & 0 & 0 \\ c_{13} & c_{13} & c_{33} & 0 & 0 & 0 \\ 0 & 0 & 0 & c_{44} & 0 & 0 \\ 0 & 0 & 0 & 0 & c_{44} & 0 \\ 0 & 0 & 0 & 0 & 0 & \frac{1}{2}(c_{11} - c_{12}) \end{bmatrix} \begin{bmatrix} S_x \\ S_y \\ S_z \\ 2S_{yz} \\ 2S_{zx} \\ 2S_{xy} \end{bmatrix} - \begin{bmatrix} 0 & 0 & e_{31} \\ 0 & 0 & e_{31} \\ 0 & 0 & e_{33} \\ 0 & e_{15} & 0 \\ e_{15} & 0 & 0 \\ 0 & 0 & 0 \end{bmatrix} \begin{bmatrix} E_x \\ E_y \\ E_z \end{bmatrix},$$

$$\begin{bmatrix} D_x \\ D_y \\ D_z \end{bmatrix} = \begin{bmatrix} 0 & 0 & 0 & 0 & e_{15} & 0 \\ 0 & 0 & 0 & e_{15} & 0 & 0 \\ e_{31} & e_{31} & e_{33} & 0 & 0 & 0 \end{bmatrix} \begin{bmatrix} S_x \\ S_y \\ S_z \\ 2S_{yz} \\ 2S_{zx} \\ 2S_{xy} \end{bmatrix} + \begin{bmatrix} \epsilon_{11} & 0 & 0 \\ 0 & \epsilon_{11} & 0 \\ 0 & 0 & \epsilon_{33} \end{bmatrix} \begin{bmatrix} E_x \\ E_y \\ E_z \end{bmatrix}, \tag{2.3}$$

where $c_{11}, c_{12}, c_{13}, c_{33}, c_{44}$ are the elastic constants, e_{15}, e_{31}, e_{33} are the piezoelectric constants and $\epsilon_{11}, \epsilon_{33}$ are the dielectric constants.

On using equation (2.1) into equation (1.29), the components for strain tensor are:

$$\begin{gathered} S_x = 0,\ S_y = 0,\ S_z = 0,\ S_{xy} = 0, \\ S_{yz} = \frac{1}{2}\frac{\partial w_p}{\partial y},\ S_{zx} = \frac{1}{2}\frac{\partial w_p}{\partial x}. \end{gathered} \tag{2.4}$$

Using equation (2.1) into equation (1.30), the components of the electrical potential field are

$$E_x = -\frac{\partial \phi^{(p)}}{\partial x},\ E_y = -\frac{\partial \phi^{(p)}}{\partial y},\ E_z = 0. \tag{2.5}$$

Invoking equations (2.4) and (2.5) into equation (2.3), the components of the stress tensor and electrical displacement reduce to

$$\begin{aligned} \sigma_x^{(p)} = 0,\ \sigma_y^{(p)} = 0,\ \sigma_z^{(p)} = 0,\ \sigma_{xy}^{(p)} = 0, \\ \sigma_{yz}^{(p)} = c_{44}\frac{\partial w_p}{\partial y} + e_{15}\frac{\partial \phi^{(p)}}{\partial y}, \\ \sigma_{zx}^{(p)} = c_{44}\frac{\partial w_p}{\partial x} + e_{15}\frac{\partial \phi^{(p)}}{\partial x}, \\ D_x = e_{15}\frac{\partial w_p}{\partial x} - \epsilon_{11}\frac{\partial \phi^{(p)}}{\partial x}, \\ D_y = e_{15}\frac{\partial w_p}{\partial y} - \epsilon_{11}\frac{\partial \phi^{(p)}}{\partial y}, \\ D_z = 0. \end{aligned} \tag{2.6}$$

Now, by substituting equation (2.6) into equations (1.23) and (1.24), one may obtain the following governing equations for the piezoelectric layer.

$$c_{44}\nabla^2 w_p + e_{15}\nabla^2 \phi^{(p)} = \rho_p \ddot{w}_p, \tag{2.7}$$

$$e_{15}\nabla^2 w_p - \epsilon_{11}\nabla^2 \phi^{(p)} = 0. \tag{2.8}$$

On solving equations (2.7) and (2.8), one may get

$$\frac{\partial^2 w_p}{\partial x^2} + \frac{\partial^2 w_p}{\partial y^2} = \frac{1}{c_p^2}\frac{\partial^2 w_p}{\partial t^2}, \tag{2.9}$$

$$\frac{\partial^2 \phi^{(p)}}{\partial x^2} + \frac{\partial^2 \phi^{(p)}}{\partial y^2} = \frac{1}{c_p^2}\left(\frac{e_{15}}{\epsilon_{11}}\right)\frac{\partial^2 w_p}{\partial t^2}, \tag{2.10}$$

where

$$c_p = \sqrt{\frac{c_{44}^*}{\rho_p}} \quad and \quad c_{44}^* = \left(c_{44} + \frac{e_{15}^2}{\epsilon_{11}}\right).$$

Here, c_p is the shear wave velocity in the piezoelectric layer.

Assume the solutions of the equations (2.9) and (2.10) as

$$w_p = W_p(x)e^{\iota\xi(y-ct)}, \tag{2.11}$$

$$\phi^{(p)} = \varphi^{(p)}(x)e^{\iota\xi(y-ct)}, \tag{2.12}$$

where ξ is the wave number and c is the phase velocity.

On using equations (2.11) and (2.12), equations (2.9) and (2.10) reduce to

$$\frac{d^2W_p(x)}{dx^2} + a^2\xi^2 W_p(x) = 0, \tag{2.13}$$

$$\frac{d^2\varphi^{(p)}(x)}{dx^2} - \xi^2\varphi^{(p)}(x) + \frac{\xi^2c^2}{c_p^2}\left(\frac{e_{15}}{\epsilon_{11}}\right)[A_1\sin(a\xi x) + A_2\cos(a\xi x)] = 0, \tag{2.14}$$

where

$$a^2 = \left(\frac{c^2}{c_p^2} - 1\right).$$

On solving the differential equations (2.13) and (2.14), one may get the following mechanical displacement and electric potential function as:

$$w_p(x, y, t) = [A_1\sin(\xi ax) + A_2\cos(\xi ax)]e^{\iota\xi(y-ct)}, \tag{2.15}$$

$$\phi^{(p)}(x, y, t) = \left[\frac{e_{15}}{\epsilon_{11}}[A_1\sin(\xi ax) + A_2\cos(\xi ax)] + A_3e^{-\xi x} + A_4e^{\xi x}\right]e^{\iota\xi(y-ct)}, \tag{2.16}$$

where A_1, A_2, A_3, A_4 are arbitrary constants.

2.2.2 Dynamics of couple stress elastic half-space

The constitutive relations and the equation of motion for a couple stress medium in the absence of body forces are given through equations (1.17)–(1.20) in Chapter-1.

On substituting equation (2.1) into (1.20); the following governing equation for couple

stress medium is obtained:

$$\left(\frac{\partial^2 w_c}{\partial x^2}+\frac{\partial^2 w_c}{\partial y^2}\right)-l^2\left(\frac{\partial^4 w_c}{\partial x^4}+2\frac{\partial^4 w_c}{\partial x^2\partial y^2}+\frac{\partial^4 w_c}{\partial y^4}\right)=\frac{1}{c_{cs}^2}\frac{\partial^2 w_c}{\partial t^2}, \tag{2.17}$$

where

$$c_{cs}=\sqrt{\frac{\mu_c}{\rho_c}}.$$

Here, c_{cs} is the shear wave velocity in couple stress substrate.

The solution of the equation (2.17) is considered as

$$w_c=W_c(x)e^{\iota\xi(y-ct)}. \tag{2.18}$$

Using equation (2.18), equation (2.17) reduces to

$$\frac{d^4W_c(x)}{dx^4}-P\frac{d^2W_c(x)}{dx^2}+QW_c(x)=0, \tag{2.19}$$

where

$$P=2\xi^2+\frac{1}{l^2},$$

$$Q=\xi^2\left(\xi^2+\frac{1}{l^2}\left(1-\frac{c^2}{c_{cs}^2}\right)\right).$$

On solving the differential equation (2.19), one may have

$$W_c(x)=(A_1^{'}e^{-px}+A_2^{'}e^{-qx}+A_3^{'}e^{px}+A_4^{'}e^{qx}), \tag{2.20}$$

where $A_1^{'}, A_2^{'}, A_3^{'}, A_4^{'}$ are arbitrary constants.

With the increase in depth, the amplitude of waves decreases in a couple stress elastic medium. So, using the feasible condition $W_c(x)\to 0$ as $x\to\infty$ in the general solution of differential equation (2.20), one can obtain the following displacement component associated with couple stress medium

$$w_c(x,y,t)=(A_1^{'}e^{-px}+A_2^{'}e^{-qx})e^{\iota\xi(y-ct)}, \tag{2.21}$$

where

$$p = \sqrt{\frac{P + \sqrt{P^2 - 4Q}}{2}},$$

$$q = \sqrt{\frac{P - \sqrt{P^2 - 4Q}}{2}}.$$

2.3 Boundary conditions

For the propagation of Love wave in a piezoelectric layer lying over a couple stress elastic half-space, the following boundary conditions are to be satisfied:

(A) Boundary conditions for the traction-free surface of the piezoelectric layer

(i) The mechanical stress-free condition is:

$$\sigma_{zx}^{(p)} = 0 \quad at \quad x = -H. \tag{2.22}$$

(ii) The electrical boundary condition on traction-free surface is

(a) Electrically open condition

$$D_x = 0 \quad at \quad x = -H. \tag{2.23}$$

(b) Electrically short condition

$$\phi^{(p)} = 0 \quad at \quad x = -H. \tag{2.24}$$

(B) Boundary conditions at the common interface of a piezoelectric layer and a couple stress elastic half-space are

(iii) Stresses are continuous at the common interface of the layer and half-space

$$\sigma_{zx}^{(p)} = \sigma_{zx}^{(c)} \quad at \quad x = 0. \tag{2.25}$$

(iv) Displacement fields are continuous at the common interface of the layer

and half-space

$$w_p = w_c \quad at \quad x = 0. \tag{2.26}$$

(v) Electric potential function should vanish at the common interface of the layer and half-space

$$\phi^{(p)} = 0 \quad at \quad x = 0. \tag{2.27}$$

(vi) Couple stress tensor should vanish at the common interface of the layer and half-space

$$\mu_{xy}^{(c)} = 0 \quad at \quad x = 0. \tag{2.28}$$

Using equations (2.15) and (2.16), the constitutive equation (2.6) reduce to

$$\sigma_{zx}^{(p)} = \left[\xi a c_{44}^{*} \cos(\xi a x) A_1 - \xi a c_{44}^{*} \sin(\xi a x) A_2 - \xi e_{15} e^{-\xi x} A_3 + \xi e_{15} e^{\xi x} A_4\right] e^{\iota\xi(y-ct)}, \tag{2.29}$$

$$D_x = \left[\xi \epsilon_{11} e^{-\xi x} A_3 - \xi \epsilon_{11} e^{\xi x} A_4\right] e^{\iota\xi(y-ct)}. \tag{2.30}$$

Using equation (2.1) into the equations (1.17) and (1.18), one may get the constitutive relations in terms of the displacement components as

$$\sigma_{zx}^{(c)} = \mu_c \frac{\partial w_c}{\partial x} + \eta_c \left(\frac{\partial^3 w_c}{\partial y^2 \partial x} + \frac{\partial^3 w_c}{\partial x^3}\right), \tag{2.31}$$

$$\mu_{xy}^{(c)} = -2\eta_c \left(\frac{\partial^2 w_c}{\partial x^2} + \frac{\partial^2 w_c}{\partial y^2}\right). \tag{2.32}$$

Using equation (2.21), equations (2.31) and (2.32) reduce to

$$\sigma_{zx}^{(c)} = [P_1 e^{-px} A_1^{'} + Q_1 e^{-qx} A_2^{'}] e^{\iota\xi(y-ct)}, \tag{2.33}$$

$$\mu_{xy}^{(c)} = 2\eta_c [k_p e^{-px} A_1^{'} + k_q e^{-qx} A_2^{'}] e^{\iota\xi(y-ct)}, \tag{2.34}$$

where

$$k_p = \xi^2 - p^2 \quad and \quad k_q = \xi^2 - q^2.$$

$$P_1 = \mu_c p(l^2 k_p - 1) \quad and \quad Q_1 = \mu_c q(l^2 k_q - 1).$$

Using equations (2.15)–(2.16), (2.29)–(2.30), (2.21), (2.33)–(2.34) into the boundary conditions (2.22)–(2.28), one may obtain the following algebraic equations in terms of unknown coefficients A_1, A_2, A_3, A_4, $A_1^{'}$ and $A_2^{'}$.

$$ac_{44}^{*}\cos(a\xi H)A_1 + ac_{44}^{*}\sin(a\xi H)A_2 - e_{15}e^{\xi H}A_3 + e_{15}e^{-\xi H}A_4 = 0, \tag{2.35}$$

$$e^{\xi H}A_3 - e^{-\xi H}A_4 = 0, \tag{2.36}$$

$$-\frac{e_{15}}{\epsilon_{11}}\sin(a\xi H)A_1 + \frac{e_{15}}{\epsilon_{11}}\cos(a\xi H)A_2 + e^{\xi H}A_3 + e^{-\xi H}A_4 = 0, \tag{2.37}$$

$$a\xi c_{44}^{*}A_1 - \xi e_{15}A_3 + \xi e_{15}A_4 - P_1A_1^{'} - Q_1A_2^{'} = 0, \tag{2.38}$$

$$A_2 - A_1^{'} - A_2^{'} = 0, \tag{2.39}$$

$$\frac{e_{15}}{\epsilon_{11}}A_2 + A_3 + A_4 = 0, \tag{2.40}$$

$$k_pA_1^{'} + k_qA_2^{'} = 0. \tag{2.41}$$

2.4 Dispersion equations for electrically open condition

The conditions mentioned in equations (2.35)–(2.36) and (2.38)–(2.41) constitute six boundary conditions for this case. To obtain non-trivial solution, determinant of the coefficients of the unknowns A_1, A_2, A_3, A_4, $A_1^{'}$ and $A_2^{'}$ must vanish. The frequency equation for the Love wave propagation in case of electrically open conditions is obtained as:

$$\xi(k_p - k_q)\left[\frac{e_{15}^2}{\epsilon_{11}}\tanh(\xi H) + ac_{44}^{*}\tan(a\xi H)\right] - (P_1k_q - Q_1k_p) = 0. \tag{2.42}$$

Equation (2.42) represents the dispersion relations of Love wave in an electrically open circuit for a piezoelectric layer lying over a couple stress elastic half-space.

2.5 Dispersion equations for electrically short condition

The conditions mentioned in equations (2.35) and (2.37)–(2.41) constitute six boundary conditions for this case. To obtain non-trivial solution, determinant of the coefficients of the unknowns A_1, A_2, A_3, A_4, $A_1^{'}$ and $A_2^{'}$ must vanish. The frequency equation for the Love wave propagation in case of electrically short conditions is obtained as:

$$\begin{aligned}\xi(k_p-k_q)\left[\left(a^2c_{44}^{*2}-\frac{e_{15}^4}{\epsilon_{11}^2}\right)\tan(a\xi H)\tanh(\xi H)+2ac_{44}^*\frac{e_{15}^2}{\epsilon_{11}}\left(1-\frac{\sec(a\xi H)}{\cosh(\xi H)}\right)\right]\\ -(P_1k_q-Q_1k_p)\left[ac_{44}^*\tanh(\xi H)-\frac{e_{15}^2}{\epsilon_{11}}\tan(a\xi H)\right]=0.\end{aligned} \tag{2.43}$$

Equation (2.43) represents the dispersion relations of Love wave in an electrically short circuit for a piezoelectric layer lying over a couple stress elastic half-space.

2.6 Particular Cases and Validation of results

2.6.1 Case-1

In the absence of the scaling parameter, i.e., $l \to 0$, the couple stress substrate reduces to an isotropic elastic substrate and $\frac{P_1k_q-Q_1k_p}{k_p-k_q} \to \xi\mu_c\sqrt{1-\frac{c^2}{c_{cs}^2}}$, equations (2.42)–(2.43) reduce to the propagation of Love wave in a piezoelectric material layer lying over the elastic substrate.

$$\frac{e_{15}^2}{\epsilon_{11}}\tanh(\xi H)+ac_{44}^*\tan(a\xi H)=\mu_c\sqrt{1-\frac{c^2}{c_{cs}^2}}. \tag{2.44}$$

$$\frac{\left[\left(a^2{c_{44}^*}^2-\frac{e_{15}^4}{\epsilon_{11}^2}\right)\tan(a\xi H)\tanh(\xi H)+2ac_{44}^*\frac{e_{15}^2}{\epsilon_{11}}\left(1-\frac{\sec(a\xi H)}{\cosh(\xi H)}\right)\right]}{\left[ac_{44}^*\tanh(\xi H)-\frac{e_{15}^2}{\epsilon_{11}}\tan(a\xi H)\right]}=\mu_c\sqrt{1-\frac{c^2}{c_{cs}^2}}. \tag{2.45}$$

Equations (2.44) and (2.45) represent the dispersion relations for the propagation of the Love wave in a piezoelectric layer lying over an isotropic elastic half-space in case of electrically open and short conditions respectively.

2.6.2 Case-2

In the absence of piezoelectric parameter, i.e., $e_{15} = 0$ and $c_{44}^{*} \to c_{44}$, equations (2.42)–(2.43) reduce to the propagation of Love wave in an isotropic elastic layer lying over the couple stress elastic half-space.

$$\xi c_{44}\sqrt{\frac{c^2}{\overline{c_p^2}} - 1}\tan\left(\xi H\sqrt{\frac{c^2}{\overline{c_p^2}} - 1}\right) = \frac{P_1 k_q - Q_1 k_p}{k_p - k_q}, \tag{2.46}$$

where

$$\overline{c_p} = \sqrt{\frac{c_{44}}{\rho_p}}.$$

2.6.3 Case-3

Pondering the previous case and taking $l \to 0$, i.e., couple stress half-space reduces to isotropic elastic half-space and equation (2.46) reduces to:

$$\tan\left(\xi H\sqrt{\frac{c^2}{\overline{c_p^2}} - 1}\right) = \frac{\mu_c\sqrt{1 - \frac{c^2}{\overline{c_{cs}^2}}}}{c_{44}\sqrt{\frac{c^2}{\overline{c_p^2}} - 1}}, \tag{2.47}$$

where $\overline{c_p^2} < c^2 < c_{cs}^2$.

Equation (2.47) represents the dispersion relation for Love wave propagation in isotropic elastic layer lying over the isotropic elastic substrate in this limiting case. This equation matches with the well-known classical Love wave dispersion equation [122].

2.7 Numerical results

To illustrate the results graphically, the semi-infinite couple stress substrate has been considered which is made of Dionysos Marble having microstructural properties [197]

as shown in Table 2.1.

Table 2.1: Material constants for a couple stress elastic substrate.

$\rho_c = 2717kg/m^3$
$\mu_c = 30.5 \times 10^9 N/m^2$
$c_{cs} = 3350m/s$

The piezoelectric layer of $PZT-5H$ or $BaTiO_3$ material are considered [115] having properties as shown in Table 2.2.

Table 2.2: Material constants for piezoelectric layer.

Materials	$PZT-5H$ ceramic	$BaTiO_3$ ceramic
Elastic constants c_{44} $(10^{10}\ N/m^2)$	2.30	4.40
Mass density ρ_p $(10^3\ kg/m^3)$	7.50	7.28
Piezoelectric constant e_{15} (C/m^2)	17.0	11.0
Dielectric constant ϵ_{11} $(10^{-10}\ C^2/Nm^2)$	277.0	128.0

Dispersion curves of the Love-type waves propagating in a piezoelectric layer overlying a couple stress mediums have been demonstrated in Figures 2.2–2.10. Figures 2.2, 2.5, 2.7, 2.9 correspond to electrically open conditions and Figures 2.3, 2.6, 2.8, 2.10 correspond to electrically short conditions. One of the common features observed in all these characteristic curves is that the non-dimensional phase velocity (c/c_p) decreases with an increase in non-dimensional wave number (ξH). Throughout the Chapters, only the zeroth mode of the Love wave propagation has been considered in the piezoelectric layered structure. This mode appears at different wave number range for different materials and it is also affected with electrically open and short conditions.

Effects of the microstructure of the substrate

Figures 2.2 and 2.3 show the variation of non-dimensional phase speed (c/c_p) with

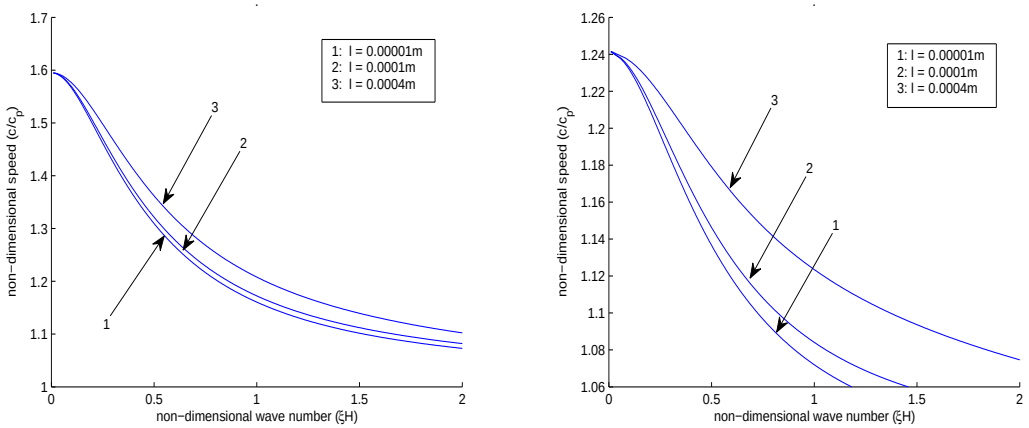

(a) For $PZT-5H$ ceramic (b) For $BaTiO_3$ ceramic

Figure 2.2: Variation of non-dimensional phase velocity against non-dimensional wave number for different values of characteristic length l = 0.00001m, 0.0001m, 0.0004m, when H=0.002m in case of electrically open conditions.

respect to non-dimensional wave number (ξH) for different values of the characteristic length parameter $l = 0.00001m, 0.0001m, 0.0004m$. The thickness of the piezoelectric material layer is taken as $H = 0.002m$. It can be observed that the microstructure of the substrate affects the phase velocity profiles significantly. It can be seen from the profiles that with the increase in characteristic length, phase velocity increases for both the considered materials of piezoelectric material layer. For $PZT-5H$ material, the plots are shown in Figures 2.2(a) and 2.3(a) and for $BaTiO_3$ material, the plots are shown in Figure 2.2(b) and 2.3(b). Profiles under electrically open conditions are shown in figure 2.2 and under electrically short conditions is shown in figure 2.3. Furthermore, the dispersion curves are plotted together for electrically open and short cases in Figure 2.4 to compare the size-dependent couple stress theory with classical theory for both the considered materials of the piezoelectric medium. The characteristic curves demonstrate the microstructural effects of the semi-infinite solid substrate that remains ignored in the classical elastic model.

Effects of the thickness of a piezoelectric layer

Figures 2.5 and 2.6 demonstrate the impact of the layer thickness of piezoelectric

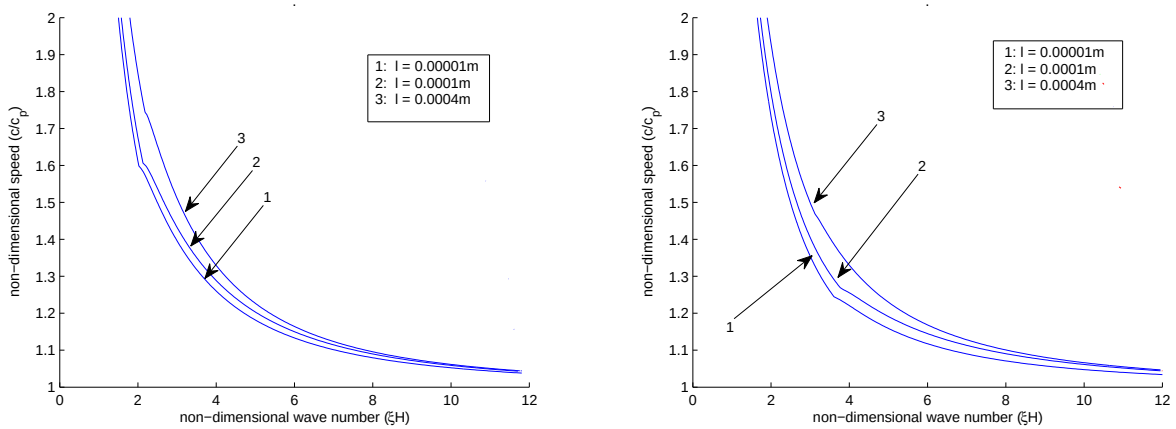

(a) For $PZT-5H$ ceramic (b) For $BaTiO_3$ ceramic

Figure 2.3: Variation of non-dimensional phase velocity against non-dimensional wave number for different values of characteristic length l = 0.00001m, 0.0001m, 0.0004m, when H=0.002m in case of electrically short conditions.

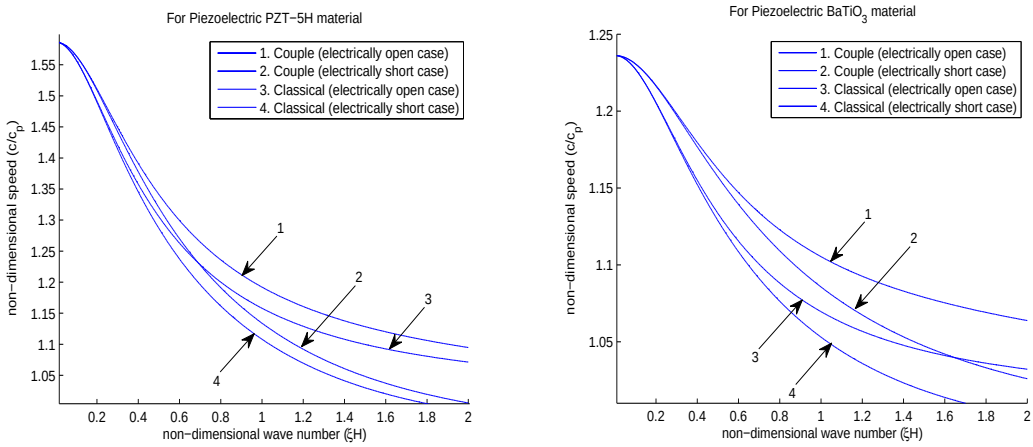

(a) For $PZT-5H$ ceramic (b) For $BaTiO_3$ ceramic

Figure 2.4: Variation of non-dimensional phase velocity against non-dimensional wave number for classical elasticity and couple stress medium.

medium on the phase velocity profiles of Love wave propagating in a layered structure. To elucidate this effect, the different values for the thickness of the piezoelectric material layer are considered, i.e., $H = 0.003m, 0.004m, 0.005m$, and the characteristic length parameter $l = 0.0004m$ is kept constant. It is observed that the thickness of the piezoelectric material layer exhibits adverse effects on the phase velocity of the Love wave which means the phase velocity profiles decrease with the increase in the thickness of the piezoelectric material layer. Characteristic profiles for the electrically open conditions are shown in Figure 2.5 and for electrically short conditions is shown in Figure 2.6. Figures 2.5(a) and 2.6(a) are plotted for $PZT - 5H$ material and Figures 2.5(b) and 2.6(b) are plotted for $BaTiO_3$ material.

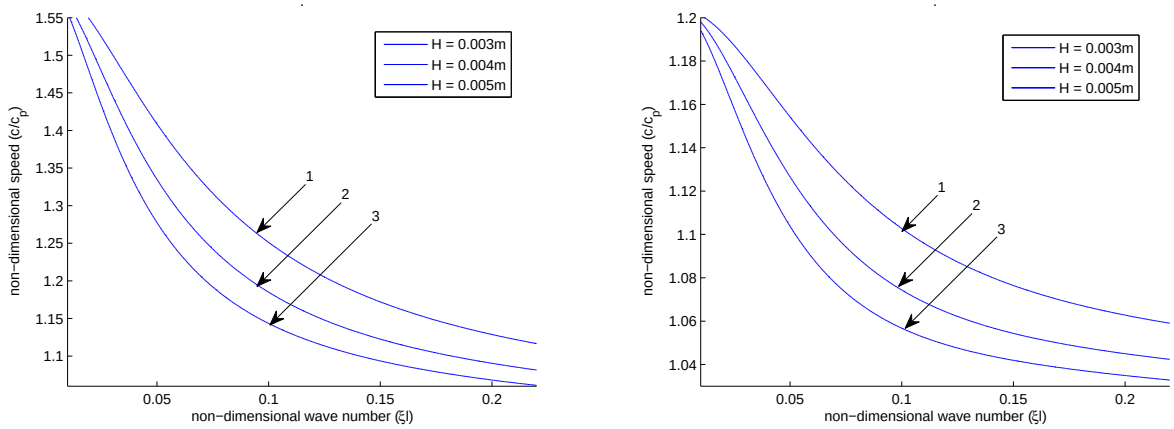

(a) For $PZT - 5H$ ceramic

(b) For $BaTiO_3$ ceramic

Figure 2.5: Variation of non-dimensional phase velocity against non-dimensional wave number for different values of the thickness of a piezoelectric layer H = 0.003m, 0.004m, 0.005m, when l = 0.0004m in case of electrically open conditions.

Effects of piezoelectric constants

Figures 2.7 and 2.8 show the variation of non-dimensional speed (c/c_p) against non-dimensional wave number (ξH) for the Love wave propagation. The characteristic curves are plotted for three different values of piezoelectric parameter $e_{15} = 17\ C/m^2$, $21\ C/m^2$, $25\ C/m^2$ for $PZT - 5H$ material shown in Figures 2.7(a) and 2.8(a) and $e_{15} = 11\ C/m^2$, $15\ C/m^2$, $19\ C/m^2$ for $BaTiO_3$ material shown in Figures 2.7(b) and 2.8(b) under both the cases of an electrically open and short conditions respectively.

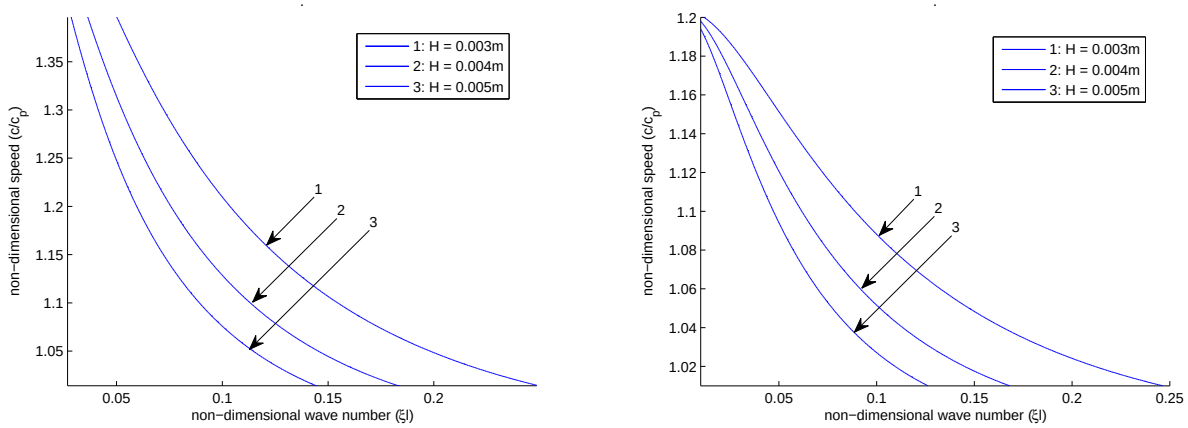

(a) For $PZT-5H$ ceramic

(b) For $BaTiO_3$ ceramic

Figure 2.6: Variation of non-dimensional phase velocity against non-dimensional wave number for different values of the thickness of a piezoelectric layer H = 0.003m, 0.004m, 0.005m, when l = 0.0004m in case of electrically short conditions.

The thickness of a piezoelectric material layer $H = 0.002m$ and the characteristic length parameter $l = 0.0001m$ associated with the couple stress substrate are kept constant. The piezoelectric material parameter does not favor the phase velocity profiles of Love waves. It is observed that the increase in piezoelectric material parameter leads to the decrease in phase velocity profiles for both the cases of an electrically open and short conditions.

Effects of dielectric material parameter

The influence of the dielectric parameter associated with the piezoelectric medium are displayed in Figures 2.9 and 2.10 for two different materials of the piezoelectric medium, i.e., for $PZT-5H$ material and $BaTiO_3$ material on the propagation of the Love wave in the considered structure. For $PZT-5H$ material, the different values of dielectric parameter are considered as $\epsilon_{11} = 237 \times 10^{-10}\ C^2/Nm^2$, $277 \times 10^{-10}\ C^2/Nm^2$, $317 \times 10^{-10}\ C^2/Nm^2$ and for $BaTiO_3$ material, the distinct values of dielectric parameter are considered as $\epsilon_{11} = 98 \times 10^{-10}\ C^2/Nm^2$, $128 \times 10^{-10}\ C^2/Nm^2$, $158 \times 10^{-10}\ C^2/Nm^2$. The characteristic curves for $PZT-5H$ material are shown in Figures 2.9(a) and 2.10(a) and for $BaTiO_3$ material, the plots are shown in

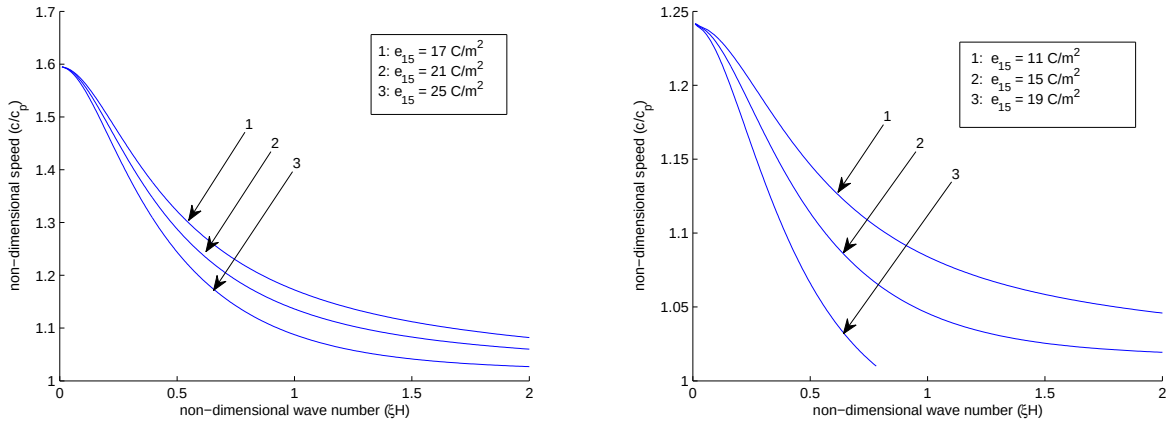

(a) For $PZT-5H$ ceramic (b) For $BaTiO_3$ ceramic

Figure 2.7: Variation of non-dimensional phase velocity against non-dimensional wave number for different values of piezoelectric constants e_{15} = 17, 21, 25 C/m^2 in 6(i) and e_{15} = 11, 15, 19 C/m^2 in 6(ii), for electrically open cases.

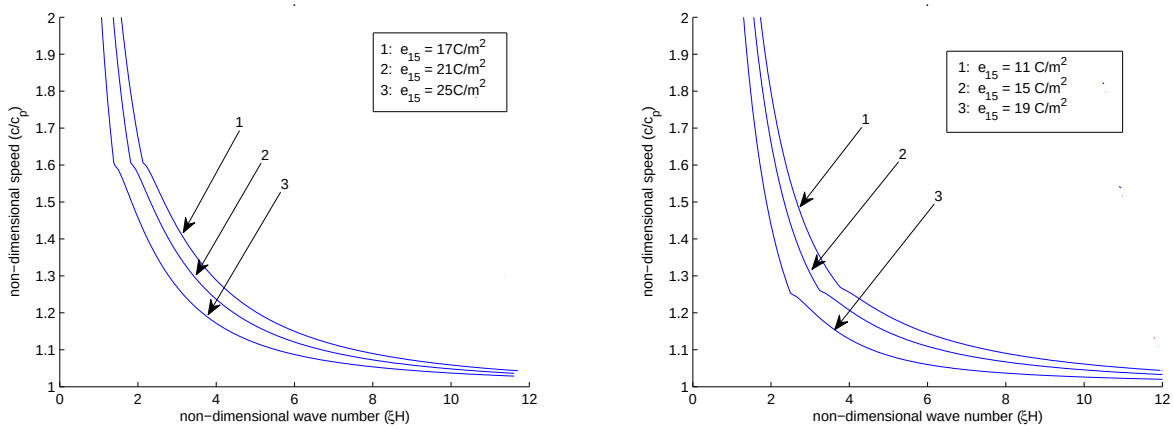

(a) For $PZT-5H$ ceramic (b) For $BaTiO_3$ ceramic

Figure 2.8: Variation of non-dimensional phase velocity against non-dimensional wave number for different values of piezoelectric constants e_{15} = 17, 21, 25 C/m^2 in (a) and e_{15} = 11, 15, 19 C/m^2 in (b), for electrically short cases.

Figures 2.9(b) and 2.10(b). The material characteristic length parameter is taken as $l = 0.0001m$ and the thickness of a piezoelectric medium layer is taken as $H = 0.002m$. The dielectric material parameter associated with the piezoelectric medium affects the phase velocity profiles significantly. It is observed that the phase velocity of the Love wave increases with the increase in the dielectric material parameter for both

the considered materials of a piezoelectric material layer under both the cases of an electrically open and short conditions.

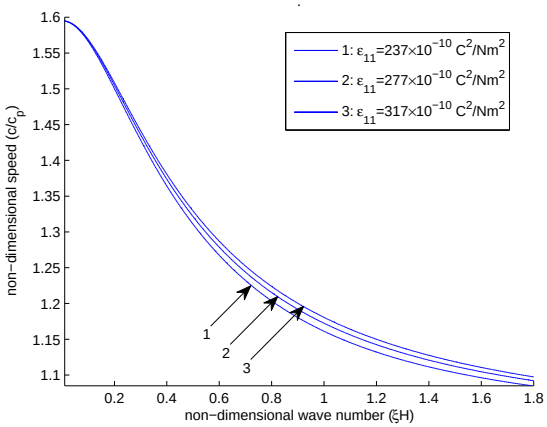

(a) For $PZT-5H$ ceramic

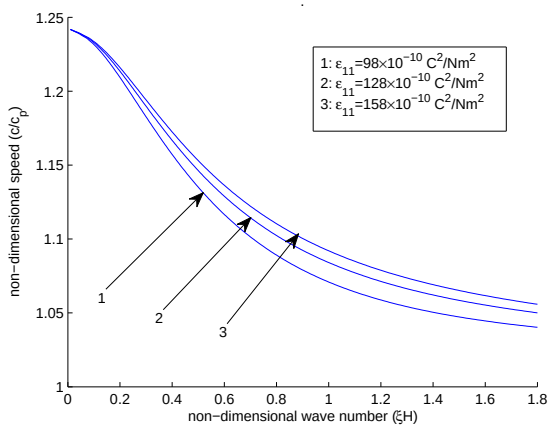

(b) For $BaTiO_3$ ceramic

Figure 2.9: Variation of non-dimensional phase velocity against non-dimensional wave number for different values of dielectric constants $\epsilon_{11} = 237 \times 10^{-10}$, 277×10^{-10}, 317×10^{-10} C^2/Nm^2 in (a), $\epsilon_{11} = 98 \times 10^{-10}$, 128×10^{-10}, 158×10^{-10} C^2/Nm^2 in (b), for electrically open cases.

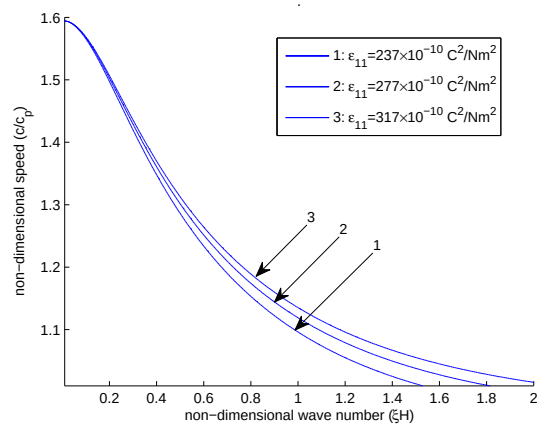

(a) For $PZT-5H$ ceramic

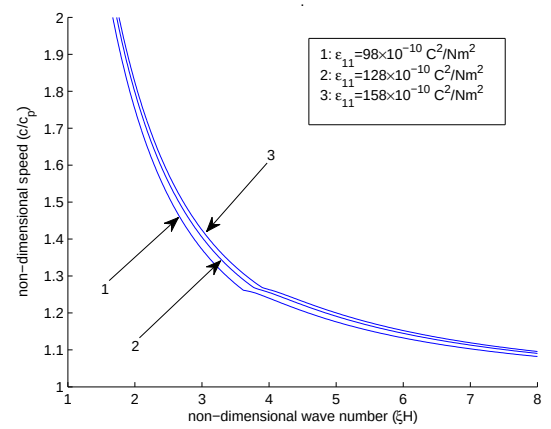

(b) For $BaTiO_3$ ceramic

Figure 2.10: Variation of non-dimensional phase velocity against non-dimensional wave number for different values of dielectric constants $\epsilon_{11} = 237 \times 10^{-10}$, 277×10^{-10}, 317×10^{-10} C^2/Nm^2 in (a), $\epsilon_{11} = 98 \times 10^{-10}$, 128×10^{-10}, 158×10^{-10} C^2/Nm^2 in (b), for electrically short cases.

2.8 Conclusion

The dispersion equations (2.42) and (2.43) provide an implicit relation between the phase velocity of the Love wave and the different characteristic parameters associated with the layer and the substrate. The phase velocity profiles are affected with the variation in associated parameters of the considered layered structure. The major conclusions of the study may be pointed out as follow:

(i) Wave number affects the phase velocity profiles of the Love wave significantly. The non-dimensional phase velocity decreases with an increase in non-dimensional wave number in each case of electrically open and short circuits for both the considered materials of a piezoelectric medium.

(ii) The material characteristic length of the couple stress material exhibits favoring effects on the phase velocity profiles of the Love wave, i.e., with the increase in the characteristic length, the phase velocity of the Love wave also increases.

(iii) The thickness of the piezoelectric material layer shows an adverse effect on the phase velocity profiles of Love waves. It is observed that the phase velocity of the Love wave decreases with the increase in the thickness parameter associated with a piezoelectric layer.

(iv) Piezoelectric parameter affects the phase velocity profiles of the Love wave substantially. Specifically, the increase in piezoelectric parameters leads to a decrease in the phase velocity of the Love wave propagation in the piezoelectric layer overlying the couple stress elastic half-space.

(v) Dielectric parameter associated with the piezoelectric layer favors the phase velocity profiles of Love waves. It is observed that with an increase in dielectric parameters, the phase velocity of the layered structure increases.

(vi) The significant effects have been observed while comparing the dispersion curves of size-dependent couple stress theory with the classical theory of elasticity for

both the considered materials of a piezoelectric medium under electrically open and short conditions.

Chapter 3

A size-dependent micropolar-piezoelectric layered structure for the analysis of Love-type wave

3.1 Introduction

As already mentioned in chapter-2, it is important to investigate the influence of size-dependency on the phase velocity profiles of Love wave propagation in the composite layered structure. The dispersion equation obtained in the Love wave propagation plays an important role in the designing of Love wave-based sensors. However, the dispersion relation involving an elastic substrate-piezoelectric layered structure is always supposed to have certain shortcomings. These shortcomings are due to the lack of any material length scale parameter in the constitutive relation of the classical elasticity. Thus, to enhance the domain of the applicability of Love wave-based devices and to authenticate, another microcontinuum theory is considered, i.e., the micropolar theory proposed by Eringen [41] for analyzing the microstructural effects

The content of this chapter is published in the journal *'Waves in Random and Complex Media'*, 30(3):544–561, 2018, *(SCI, Impact factor:2.930)*

of structurally sensitive materials incorporating granular media, microcracking, microporosity, cellular solids, bones, platelets.

In this chapter, the propagation of Love-type waves has been investigated in a layered structure consisting of a piezoelectric material layer lying over a semi-infinite size-dependent micropolar substrate exhibiting microstructural characteristics. By employing appropriate boundary conditions for the layer and substrate, the secular equations are obtained analytically in the compact form for both the cases of electrically open and electrically short conditions. Two sets of the piezoelectric material layer, namely, $PZT-5H$ and $BaTiO_3$ material are considered to manifest the results graphically. The effects of internal microstructures of the size-dependent substrate, the thickness of a piezoelectric material layer, the piezoelectric constants, and the dielectric constants are illustrated graphically on the phase velocity profiles of the Love-type wave for both the considered materials of the piezoelectric layer under electrically open and short conditions. Some particular cases are also obtained using the relevant conditions and the Classical Love wave equation is also deduced to validate the outcome of the present study.

3.2 Formulation of the problem

Consider a micropolar elastic half-space covered with a transversely isotropic piezoelectric layer of thickness H where $-H \leq x \leq 0$. The Cartesian frame of reference is considered in such a way that the Love wave is propagating along the y-axis and the x-axis is pointing positive vertically downward as shown in Figure 3.1. Conventionally, the direction of polarization is assumed along the z-axis. Let $u_i^{(p)} = (u_p, v_p, w_p)$ and $u_i^{(m)} = (u_m, v_m, w_m)$ are the mechanical displacement components in the upper piezoelectric layer and the lower micropolar elastic half-space respectively, obtained due to the propagation of the Love wave. As the Love wave is propagating along the direction of the y-axis, it causes displacement in the z-direction only. For Love wave propagation, one may suppose that

$$u_p = 0,\ v_p = 0,\ w_p = w_p(x, y, t),$$

$$u_m = 0,\ v_m = 0,\ w_m = w_m(x, y, t). \tag{3.1}$$

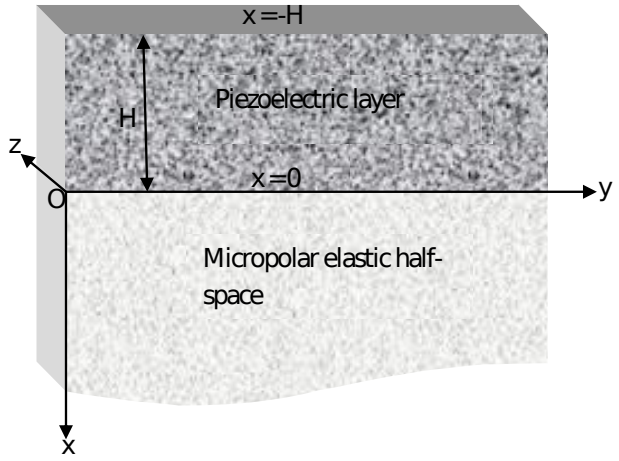

Figure 3.1: Geometry of the problem.

By following the procedure adopted in sections 2.2.1 and 2.3 of Chapter-2, the mechanical displacement and the electric potential component for a piezoelectric material layer are obtained as

$$\begin{aligned}
w_p(x, y, t) &= [A_1 \sin(\xi a x) + A_2 \cos(\xi a x)] e^{\iota\xi(y-ct)}, \\
\phi^{(p)}(x, y, t) &= \left[\frac{e_{15}}{\epsilon_{11}}[A_1 \sin(\xi a x) + A_2 \cos(\xi a x)] + A_3 e^{-\xi x} + A_4 e^{\xi x}\right] e^{\iota\xi(y-ct)}, \\
\sigma_{zx}^{(p)} &= \left[\xi a c_{44}^* \cos(\xi a x) A_1 - \xi a c_{44}^* \sin(\xi a x) A_2 - \xi e_{15} e^{-\xi x} A_3 + \xi e_{15} e^{\xi x} A_4\right] e^{\iota\xi(y-ct)}, \\
D_x &= \left[\xi \epsilon_{11} e^{-\xi x} A_3 - \xi \epsilon_{11} e^{\xi x} A_4\right] e^{\iota\xi(y-ct)}.
\end{aligned} \tag{3.2}$$

The notations and symbols are same as used in sections 2.2.1 and 2.3 of Chapter-2

3.2.1 Dynamics of semi-infinite micropolar substrate

The constitutive relations and the equations of motion for a micropolar elastic half-space in the absence of body forces are given through equations (1.13)–(1.16) in Chapter-1.

To explicate the size-dependency effects in micropolar medium, the parametric rela-

tion given by Fatemi et al. [53] having the parameter coupling constant 'N' and the characteristic length parameter 'l' are used.

$$\gamma_m = 4l^2\left(\mu_m + \frac{\kappa_m}{2}\right) \quad and \quad \kappa_m = \frac{2N^2\mu_m}{1-2N^2}, \tag{3.3}$$

where the micropolarity of substrate is characterized by coupling factor N with $0 < N < 1$ and characteristic length l which quantifies the size-effect of material and is of the order of the average cell size of the material; $N = 0$ represents the classical elasticity.

By using Helmholtz decomposition for microrotation vectors $\vec{\phi}^{(m)}$ in terms of potential function φ_m and ψ_m, one may get

$$\vec{\phi}^{(m)} = \nabla\varphi_m + \nabla \times \vec{\psi_m}, \quad \nabla.\vec{\psi_m} = 0, \tag{3.4}$$

where $\overrightarrow{\psi_m} = (0, 0, -\psi_m)$ and $\overrightarrow{\phi^{(m)}} = (\phi_1^{(m)}, \phi_2^{(m)}, \phi_3^{(m)})$.

The microrotation vector in the component form can be written from equation (3.4) as:

$$\phi_1^{(m)} = \frac{\partial\varphi_m}{\partial x} - \frac{\partial\psi_m}{\partial y},\ \phi_2^{(m)} = \frac{\partial\varphi_m}{\partial y} + \frac{\partial\psi_m}{\partial x}\ and\ \phi_3^{(m)} = 0. \tag{3.5}$$

Utilizing equations (3.1) and (3.5), equations (1.15)–(1.16) reduce to

$$\nabla^2 w_m + \theta_1^2\nabla^2\psi_m = \frac{1}{\theta_2^2}\frac{\partial^2 w_m}{\partial t^2}, \tag{3.6}$$

$$\nabla^2\varphi_m - \frac{2\theta_5^2}{\theta_3^2+\theta_4^2}\varphi_m = \frac{1}{\theta_3^2+\theta_4^2}\frac{\partial^2\varphi_m}{\partial t^2}, \tag{3.7}$$

$$\nabla^2\psi_m - \frac{2\theta_5^2}{\theta_3^2}\psi_m - \frac{\theta_5^2}{\theta_3^2}w_m = \frac{1}{\theta_3^2}\frac{\partial^2\psi_m}{\partial t^2}, \tag{3.8}$$

where

$$\begin{cases} \theta_1 = \sqrt{\frac{\kappa_m}{\mu_m+\kappa_m}},\ \theta_2 = \sqrt{\frac{\mu_m+\kappa_m}{\rho_m}},\ \theta_3 = \sqrt{\frac{\gamma_m}{j\rho_m}}, \\ \theta_4 = \sqrt{\frac{\alpha_m+\beta_m}{j\rho_m}},\ \theta_5 = \sqrt{\frac{\kappa_m}{j\rho_m}}. \end{cases}$$

Assuming the solution of equations (3.6)–(3.8) of the form

$$(\varphi_m, \psi_m, w_m)(x, y, t) = (\Phi_m, \Psi_m, W_m)(x)e^{\iota\xi(y-ct)}, \tag{3.9}$$

where ξ is the wave number and c is the phase velocity.

Employing the solution given in equation (3.9) into the equations (3.6)–(3.8), one may get the following differential equations:

$$(D^2 - r^2)\Phi_m = 0, \tag{3.10}$$

$$\left(D^2 + \frac{\xi^2 c^2}{\theta_2^2} - \xi^2\right)W_m + \theta_1^2(D^2 - \xi^2)\Psi_m = 0, \tag{3.11}$$

$$\left(D^2 + \frac{\xi^2 c^2}{\theta_3^2} - 2\frac{\theta_5^2}{\theta_3^2} - \xi^2\right)\Psi_m - \left(\frac{\theta_5^2}{\theta_3^2}\right)W_m = 0, \tag{3.12}$$

where $D \equiv \frac{d}{dx}$,

$$r = \sqrt{\left(\xi^2 - \frac{\xi^2 c^2}{\theta_3^2 + \theta_4^2} + \frac{2\theta_5^2}{\theta_3^2 + \theta_4^2}\right)}.$$

On solving equations (3.11) and (3.12) simultaneously, one may get

$$\left(\frac{d^4}{dx^4} - S\frac{d}{dx^2} + T\right)\Psi_m = 0, \tag{3.13}$$

where

$$S = 2\xi^2 - \frac{\theta_5^2}{\theta_3^2}(\theta_1^2 - 2) - \xi^2 c^2\left(\frac{1}{\theta_2^2} + \frac{1}{\theta_3^2}\right),$$

$$T = \left(\frac{\xi^2 c^2}{\theta_3^2} - \frac{2\theta_5^2}{\theta_3^2} - \xi^2\right)\left(\frac{\xi^2 c^2}{\theta_2^2} - \xi^2\right) - \frac{\theta_1^2\theta_5^2\xi^2}{\theta_3^2}.$$

The equation (3.13) can be rewritten as:

$$(D^2 - s^2)(D^2 - t^2)\Psi_m = 0, \tag{3.14}$$

where

$$s^2, t^2 = \frac{S \pm \sqrt{S^2 - 4T}}{2}.$$

On solving equations (3.10) and (3.14) and using the feasible conditions that $\Phi_m(x)$ and $\Psi_m(x) \to 0$ as $x \to \infty$ in the general solution of the differential equations, one may obtain

$$\varphi_m(x, y, t) = e^{-rx} B_1 e^{\iota\xi(y-ct)}, \tag{3.15}$$

$$\psi_m(x, y, t) = (e^{-sx} B_2 + e^{-tx} B_3) e^{\iota\xi(y-ct)}, \tag{3.16}$$

where B_1, B_2, B_3 are the arbitrary constants.

On substituting the value of $\Psi_m(x)$ from equation (3.16) into (3.12) and using the feasible condition that $W_m(x) \to 0$ as $x \to \infty$, the mechanical displacement component in micropolar elastic half-space is obtained as

$$w_m(x, y, t) = (\wp_1 e^{-sx} B_2 + \wp_2 e^{-tx} B_3) e^{\iota\xi(y-ct)}, \tag{3.17}$$

where

$$\wp_1 = \frac{\theta_3^2}{\theta_5^2}\left(s^2 + \frac{\xi^2 c^2}{\theta_3^2} - \frac{2\theta_5^2}{\theta_3^2} - \xi^2\right),$$

$$\wp_2 = \frac{\theta_3^2}{\theta_5^2}\left(t^2 + \frac{\xi^2 c^2}{\theta_3^2} - \frac{2\theta_5^2}{\theta_3^2} - \xi^2\right).$$

Using equations (3.15) and (3.16) in (3.5), the components of the microrotation vector associated with the semi-infinite micropolar substrate are obtained as

$$\phi_1^{(m)} = (-re^{-rx} B_1 - \iota\xi e^{-sx} B_2 - \iota\xi e^{-tx} B_3) e^{\iota\xi(y-ct)}. \tag{3.18}$$

$$\phi_2^{(m)} = (\iota\xi e^{-rx} B_1 - se^{-sx} B_2 - te^{-tx} B_3) e^{\iota\xi(y-ct)}. \tag{3.19}$$

3.3 Boundary conditions

The following boundary conditions are to be satisfied for the propagation of the Love wave in a piezoelectric layer overlying a micropolar elastic half-space.

(A) Boundary conditions for the traction-free surface of the piezoelectric layer

(i) The mechanical traction-free condition is:

$$\sigma_{zx}^{(p)} = 0 \quad at \quad x = -H. \tag{3.20}$$

(ii) The electrical boundary condition on traction-free surface is

(a) Electrically open condition

$$D_x = 0 \quad at \quad x = -H. \tag{3.21}$$

(b) Electrically short condition

$$\phi^{(p)} = 0 \quad at \quad x = -H. \tag{3.22}$$

(B) Boundary conditions at the common interface of a piezoelectric layer and a micropolar elastic half-space are

(iii) Displacement fields are continuous at the common interface of layer and half-space

$$w_p = w_m \quad at \quad x = 0. \tag{3.23}$$

(iv) Stresses are continuous at the common interface of layer and half-space

$$\sigma_{zx}^{(p)} = \sigma_{zx}^{(m)} \quad at \quad x = 0. \tag{3.24}$$

(v) Electric potential function should vanish at the common interface of layer and half-space

$$\phi^{(p)} = 0 \quad at \quad x = 0. \tag{3.25}$$

(vi) Couple stress tractions should vanish at the common interface of layer and half-space

$$m_{xy}^{(m)} = 0 \quad at \quad x = 0. \tag{3.26}$$

$$m_{xx}^{(m)} = 0 \quad at \quad x = 0. \tag{3.27}$$

Invoking equations (3.17)–(3.19) into equations (1.13)–(1.14) of the constitutive relations, the following components of the stresses in micropolar medium are obtained as:

$$\sigma_{zx}^{(m)} = (-\iota\xi\kappa_m e^{-rx}B_1 - \wp_3 e^{-sx}B_2 - \wp_4 e^{-tx}B_3)e^{\iota\xi(y-ct)}, \tag{3.28}$$

$$m_{xy}^{(m)} = (-\iota\xi\wp_5 e^{-rx}B_1 + \wp_6 e^{-sx}B_2 + \wp_7 e^{-tx}B_3)e^{\iota\xi(y-ct)}, \tag{3.29}$$

$$m_{xx}^{(m)} = (\wp_8 e^{-rx}B_1 + \iota\wp_9 e^{-sx}B_2 + \iota\wp_{10} e^{-tx}B_3)e^{\iota\xi(y-ct)}, \tag{3.30}$$

where

$\wp_3 = s(\mu_m\wp_1 - \kappa_m), \quad \wp_4 = t(\mu_m\wp_2 - \kappa_m), \quad \wp_5 = -\xi r(\beta_m + \gamma_m),$

$\wp_6 = (\beta_m\xi^2 + \gamma_m s^2), \quad \wp_7 = (\beta_m\xi^2 + \gamma_m t^2), \quad \wp_8 = r^2(\alpha_m + \beta_m + \gamma_m) - \alpha_m\xi^2,$

$\wp_9 = \xi s(\beta_m + \gamma_m), \quad \wp_{10} = \xi t(\beta_m + \gamma_m).$

Using equations (3.2), (3.17)–(3.19) and (3.28)–(3.30) into the boundary equations (3.20)-(3.27), one may obtain the following algebraic equations with respect to unknown coefficients A_1, A_2, A_3, A_4, B_1, B_2 and B_3.

$$ac_{44}^{*}\cos(a\xi H)A_1 + ac_{44}^{*}\sin(a\xi H)A_2 - e_{15}e^{\xi H}A_3 + e_{15}e^{-\xi H}A_4 = 0, \tag{3.31}$$

$$e^{\xi H}A_3 - e^{-\xi H}A_4 = 0, \tag{3.32}$$

$$-\frac{e_{15}}{\epsilon_{11}}\sin(a\xi H)A_1 + \frac{e_{15}}{\epsilon_{11}}\cos(a\xi H)A_2 + e^{\xi H}A_3 + e^{-\xi H}A_4 = 0, \tag{3.33}$$

$$A_2 - \wp_1 B_2 - \wp_2 B_3 = 0, \tag{3.34}$$

$$a\xi c_{44}^{*}A_1 - \xi e_{15}A_3 + \xi e_{15}A_4 + \iota\xi\kappa_m B_1 + \wp_3 B_2 + \wp_4 B_3 = 0, \tag{3.35}$$

$$\frac{e_{15}}{\epsilon_{11}}A_2 + A_3 + A_4 = 0, \tag{3.36}$$

$$\iota\wp_5 B_1 + \wp_6 B_2 + \wp_7 B_3 = 0, \tag{3.37}$$

$$\wp_8 B_1 + \iota\wp_9 B_2 + \iota\wp_{10} B_3 = 0. \tag{3.38}$$

3.4 Dispersion equations for electrically open condition

The conditions mentioned in equations (3.31)–(3.32) and (3.34)–(3.38) constitute seven boundary conditions for this case. To obtain a non-trivial solution, the determinant of the unknown coefficients of the system, A_1, A_2, A_3, A_4, B_1, B_2 and B_3 vanish. The frequency equation for the propagation of the Love-type wave in case of an electrically open conditions is obtained as

$$\xi a c_{44}^{*} \wp_{15} \tan(\xi a H) + \xi \wp_{15} \frac{e_{15}^2}{\epsilon_{11}} \tanh(\xi H) + \wp_{14} = 0, \tag{3.39}$$

where $\wp_{11} = \wp_6\wp_{10} - \wp_7\wp_9$, $\wp_{12} = \wp_5\wp_{10} + \wp_7\wp_8$, $\wp_{13} = \wp_5\wp_9 + \wp_6\wp_8$,
$\wp_{14} = \xi\kappa_m\wp_{11} - \wp_3\wp_{12} + \wp_4\wp_{13}$, $\wp_{15} = \wp_1\wp_{12} - \wp_2\wp_{13}$.
Equation (3.39) represents the dispersion relations of Love-type wave for an electrically open conditions for a piezoelectric layer lying over the micropolar elastic half-space.

3.5 Dispersion equations for electrically short condition

The conditions mentioned in equations (3.31) and (3.33)-(3.38) constitute seven boundary conditions for this case. To obtain a non-trivial solution, the determinant of the unknown coefficients of the system, A_1, A_2, A_3, A_4, B_1, B_2 and B_3 vanish. The frequency equation for the propagation of the Love wave in case of an electrically short

conditions is obtained as

$$\left(ac_{44}^{*}\tanh(\xi H)-\frac{e_{15}^{2}}{\epsilon_{11}}\tan(\xi aH)\right)\wp_{14}+2\xi ac_{44}^{*}\wp_{15}\frac{e_{15}^{2}}{\epsilon_{11}}\left(1-\frac{\sec(\xi aH)}{\cosh(\xi H)}\right)+ \xi\wp_{15}\wp_{16}\tan(\xi aH)\tanh(\xi H)=0, \tag{3.40}$$

where $\wp_{16}=a^{2}c_{44}^{*2}-\frac{e_{15}^{4}}{\epsilon_{11}^{2}}$.

Equation (3.40) represents the dispersion relations of the Love wave in electrically short conditions for a piezoelectric layer lying over a micropolar elastic half-space.

3.6 Particular Cases

3.6.1 Case-1

In the absence of micropolarity, i.e., α_m, β_m, γ_m and $\kappa_m \to 0$, the micropolar elastic half-space reduces to an isotropic elastic half-space, $\theta_2 \to c_m$ and $\frac{\wp_{14}}{\wp_{15}} \to -\xi\mu_m\sqrt{1-\frac{c^2}{c_m^2}}$; equations (3.39)–(3.40) reduce to Love-type wave propagation in a piezoelectric material layer lying over an isotropic elastic half-space.

$$ac_{44}^{*}\tan(a\xi H)+\frac{e_{15}^{2}}{\epsilon_{11}}\tanh(\xi H)=\mu_m\sqrt{1-\frac{c^2}{c_m^2}}, \tag{3.41}$$

$$\frac{\left[2ac_{44}^{*}\frac{e_{15}^{2}}{\epsilon_{11}}\left(1-\frac{\sec(a\xi H)}{\cosh(\xi H)}\right)+\wp_{16}\tan(a\xi H)\tanh(\xi H)\right]}{\left[ac_{44}^{*}\tanh(\xi H)-\frac{e_{15}^{2}}{\epsilon_{11}}\tan(a\xi H)\right]}=\mu_m\sqrt{1-\frac{c^2}{c_m^2}}, \tag{3.42}$$

where

$$c_m=\sqrt{\frac{\mu_m}{\rho_m}}.$$

Equations (3.41) and (3.42) represent the dispersion relations for the propagation of the Love wave in a piezoelectric layer lying over an isotropic elastic half-space in case of electrically open and short conditions respectively.

3.6.2 Case-2

In the absence of piezoelectric parameter, i.e., $e_{15} = 0$ and $c_{44}^{*} \to c_{44}$, equations (3.39)–(3.40) reduce to Love-type wave propagation in an isotropic elastic layer lying over a micropolar elastic half-space.

$$\xi c_{44}\sqrt{\frac{c^2}{\overline{c_p^2}} - 1}\tan\left(\xi H\sqrt{\frac{c^2}{\overline{c_p^2}} - 1}\right) = -\frac{\wp_{14}}{\wp_{15}}, \tag{3.43}$$

where

$$\overline{c_p} = \sqrt{\frac{c_{44}}{\rho_p}}.$$

Equation (3.43) represents the dispersion relation for Love-type wave propagation in an isotropic elastic layer lying over the micropolar elastic substrate.

3.6.3 Case-3

Pondering the previous case and α_m, β_m, γ_m and $\kappa_m \to 0$, i.e., micropolar elastic half-space reduces to isotropic elastic half-space; equation (3.43) reduces to

$$\tan\left(\xi H\sqrt{\frac{c^2}{\overline{c_p^2}} - 1}\right) = \frac{\mu_m\sqrt{1 - \frac{c^2}{c_m^2}}}{c_{44}\sqrt{\frac{c^2}{\overline{c_p^2}} - 1}}, \tag{3.44}$$

where $\overline{c_p^2} < c^2 < c_m^2$.

Equation (3.44) represents the dispersion relation for Love-type wave propagation in an isotropic elastic layer lying over the isotropic elastic substrate which matches with the well-known Classical Love wave [122] equation which validates the outcome of the present problem.

3.7 Numerical results and discussions

For illustrating the results, the piezoelectric layer of $PZT - 5H$ or $BaTiO_3$ materials are considered [115] having properties as shown in Table 2.2 taken from section 2.7

of Chapter-2. For the semi-infinite micropolar elastic substrate, the following data of aluminium-epoxy material [90] have been considered which is shown in Table 3.1.

Table 3.1: Material constants for micropolar elastic substrate.

$\rho_m = 2.19 \times 10^3 kg/m^3$
$\lambda_m = 7.59 \times 10^{10} N/m^2$
$\mu_m = 1.89 \times 10^{10} N/m^2$
$j = 0.196 \times 10^{-4} m^2$
$\alpha_m = 0.01 \times 10^6 N$
$\beta_m = 0.015 \times 10^6 N$

The characteristic curves have been examined in Figures 3.2–3.13 for the propagation of the Love type waves in the layered piezoelectric structure. All the curves are plotted for the non-dimensional phase velocity (c/c_p) against non-dimensional wave number (ξH) for two different materials of piezoelectric layer, i.e., $PZT-5H$ and $BaTiO_3$ material. There is one common feature observed in all these figures that the phase velocity show dispersion and it decreases with the increase in non-dimensional wave number. Figures 3.2, 3.4, 3.8, 3.10, 3.12 are associated with the electrically open conditions and Figures 3.3, 3.5, 3.9, 3.11, 3.13 are associated with the electrically short conditions.

Effect of coupling constant (N)

Figures 3.2 and 3.3 demonstrate the effect of coupling constants that quantifies the degree of micropolarity in a micropolar media on the phase velocity profiles of the Love wave propagating in a piezoelectric layer lying over a micropolar elastic half-space. The dispersion curves are plotted for different values of micropolar coupling parameter, i.e., $N = 0.1, 0.7, 0.9$ to show the microstructural effects of the semi-infinite substrate under both the cases of electrically open and short conditions. Here, the characteristic length of material and the thickness of a layer is taken as $l = 0.001m$ and $H = 0.3m$ respectively. It is observed that the micropolarity of the substrate

affects the phase velocity profiles significantly. As the degree of micropolarity (N) increases, the phase velocity of the Love wave increases for both the considered materials of a piezoelectric layer, i.e., $PZT-5H$ and $BaTiO_3$ material under both the cases of electrically open and short conditions.

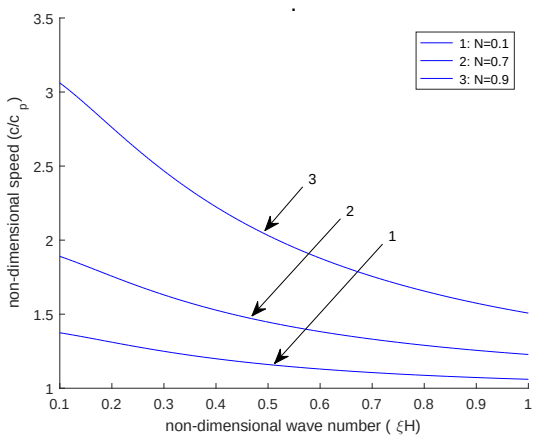

(a) For $PZT-5H$ ceramic

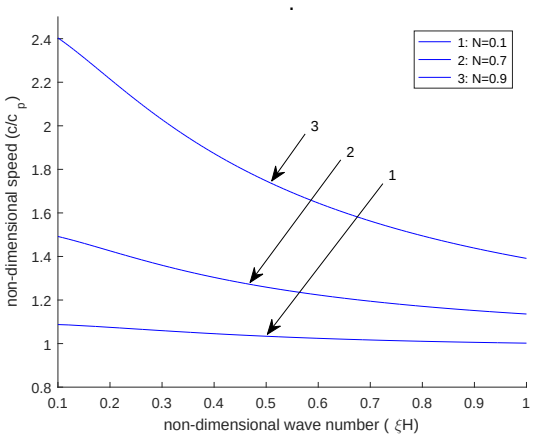

(b) For $BaTiO_3$ ceramic

Figure 3.2: Variation of non-dimensional phase velocity against non-dimensional wave number for different values of micropolar constants $N = 0.1, 0.7, 0.9$ in (a) and (b), when l=0.001m, H=0.3m in case of electrically open conditions.

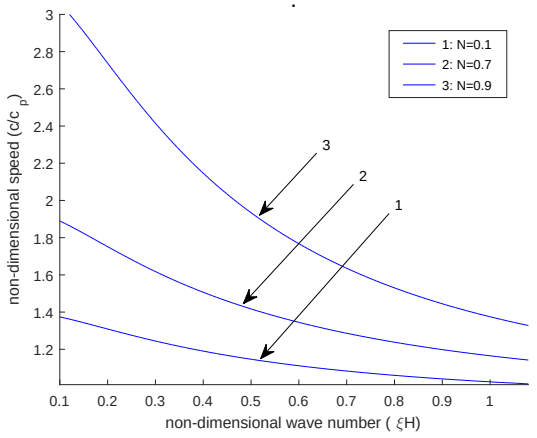

(a) For $PZT-5H$ ceramic

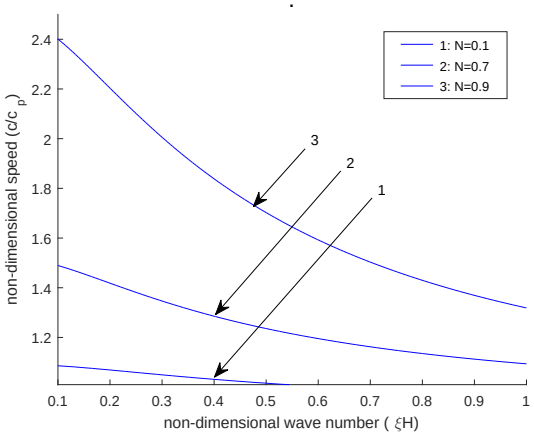

(b) For $BaTiO_3$ ceramic

Figure 3.3: Variation of non-dimensional phase velocity against non-dimensional wave number for different values of micropolar constants $N = 0.1, 0.7, 0.9$ in (a) and (b), when l=0.001m, H=0.3m in case of electrically short conditions.

Effect of the characteristic length (l)

Figures 3.4 and 3.5 show the characteristic profiles of non-dimensional phase velocity (c/c_p) against non-dimensional wave number (ξH) for different values of the intrinsic characteristic length of the micropolar media, i.e., $l = 0.001m, 0.002m, 0.003m$. The significant effects of the material characteristic length on the phase velocity profiles of the Love wave are observed. It is observed that the phase velocity profiles of the Love wave increase with an increase in the characteristic length. The characteristic curves clearly indicate the size-effects observed in the propagation of the Love wave in a piezoelectric layered structure. Figures 3.4(a) and 3.5(a) are associated with the $PZT-5H$ piezoelectric material and Figures 3.4(b) and 3.5(b) are associated with the $BaTiO_3$ piezoelectric material under both the cases of an electrically open and electrically short conditions. The phase velocity profiles in Figure 3.6 and 3.7 demonstrate the comparison of micropolar elasticity with the classical theory of elasticity and micropolar elasticity with couple stress theory for electrically open and short conditions. Figure 3.6(a) and 3.7(a) are plotted for piezoelectric $PZT-5H$ material whereas Figure 3.6(b) and 3.7(b) are plotted for piezoelectric $BaTiO_3$ material. The trends of phase velocity profiles for each theory are the same, i.e., with the increase in non-dimensional wave number, phase velocity decreases.

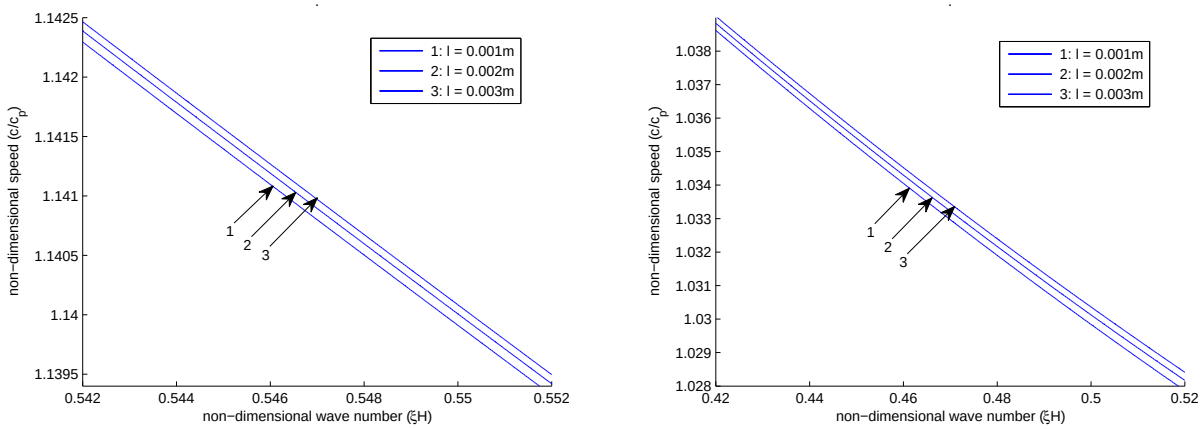

(a) For $PZT-5H$ ceramic

(b) For $BaTiO_3$ ceramic

Figure 3.4: Variation of non-dimensional phase velocity against non-dimensional wave number for different values of characteristic length $l = 0.001m, 0.002m, 0.003m$ in (a) and (b) in case of electrically open conditions.

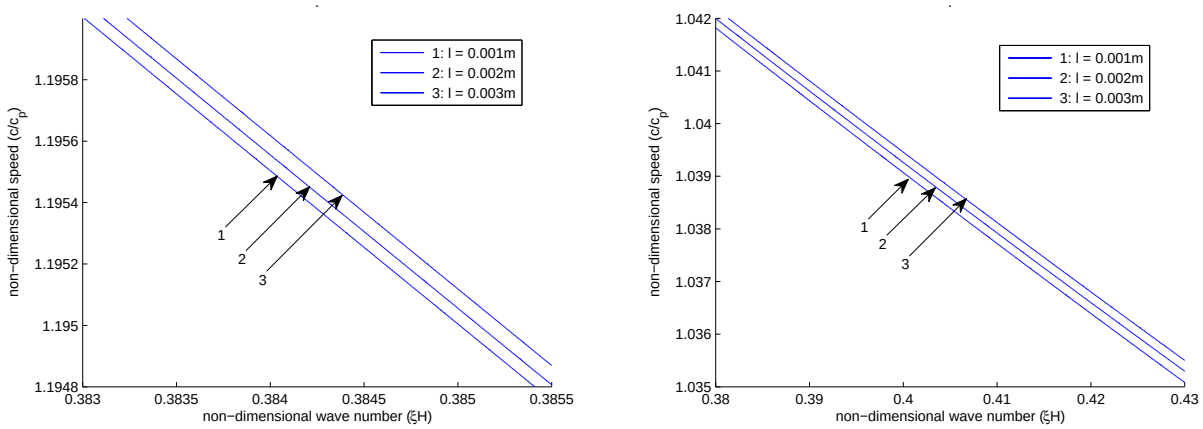

(a) For $PZT-5H$ ceramic (b) For $BaTiO_3$ ceramic

Figure 3.5: Variation of non-dimensional phase velocity against non-dimensional wave number for different values of characteristic length $l = 0.001m, 0.004m, 0.007m$ in (a) and (b) in case of electrically short conditions.

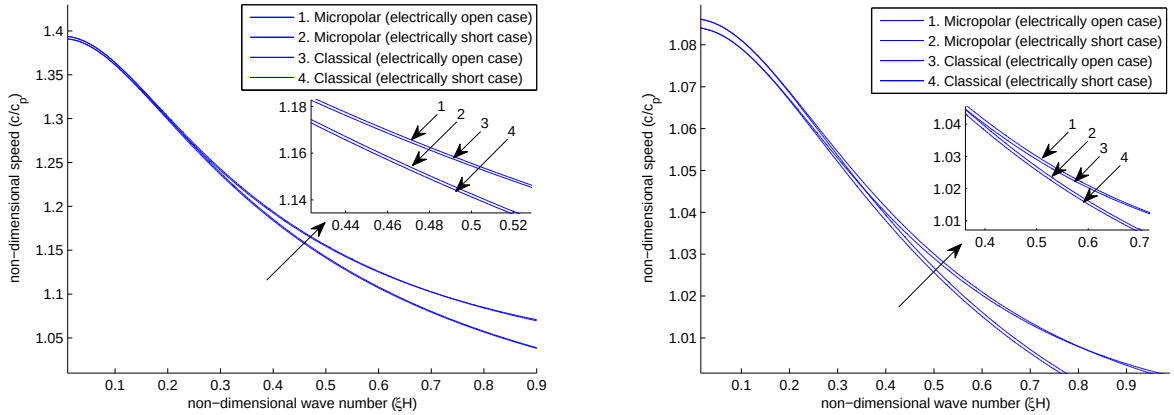

(a) For $PZT-5H$ ceramic (b) For $BaTiO_3$ ceramic

Figure 3.6: Variation of non-dimensional phase velocity against non-dimensional wave number for classical elasticity and micropolar elasticity.

Effects of the thickness of a layer

Figures 3.8 and 3.9 show the variation of non-dimensional phase velocity (c/c_p) against non-dimensional wave number (ξl) for different values of the thickness of a piezoelectric material layer, i.e., $H = 0.003m, 0.004m, 0.005m$. Here, the characteristic length is $l = 0.005m$ and the coupling factor N is 0.033. It is observed that the thickness of a piezoelectric layer lying over a micropolar elastic half-space does not favors the

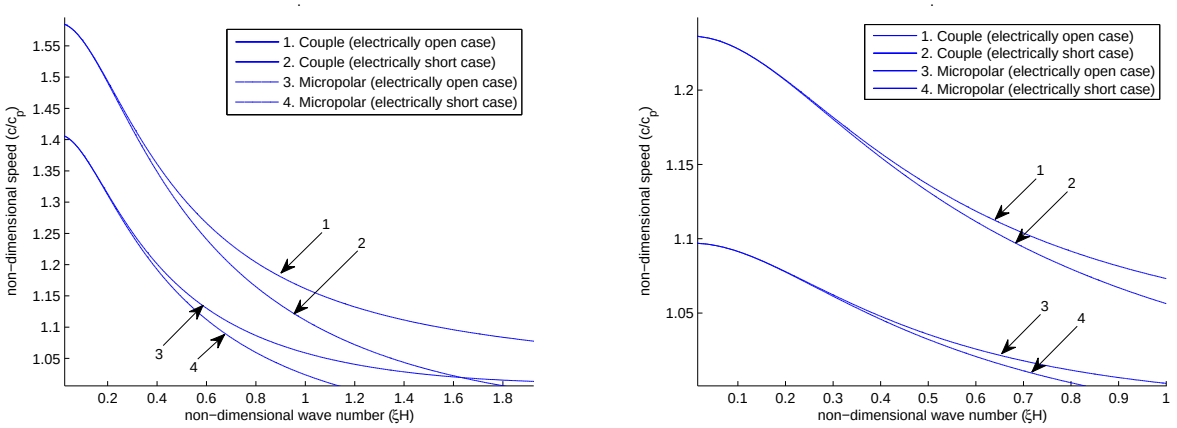

(a) For $PZT-5H$ ceramic (b) For $BaTiO_3$ ceramic

Figure 3.7: Variation of non-dimensional phase velocity against non-dimensional wave number for couple stress theory and micropolar elasticity.

phase velocity profiles, i.e., with the increase in the thickness of a piezoelectric layer, the phase velocity of the Love wave decreases. Figures 3.8(a) and 3.9(a) correspond to the piezoelectric material $PZT-5H$ and Figures 3.8(b) and 3.9(b) correspond to the piezoelectric material $BaTiO_3$ under both the cases of an electrically open and electrically short conditions.

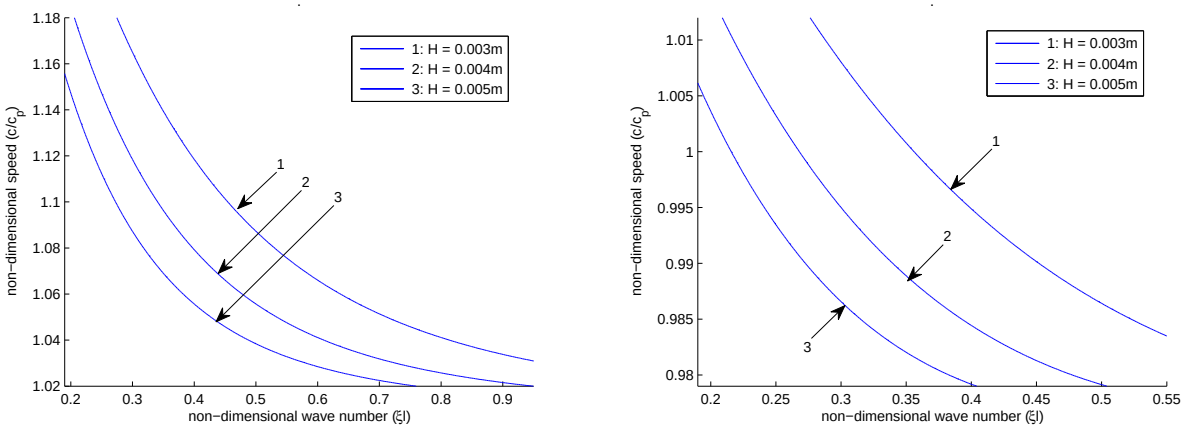

(a) For $PZT-5H$ ceramic (b) For $BaTiO_3$ ceramic

Figure 3.8: Variation of non-dimensional phase velocity against non-dimensional wave number for different values of the thickness of piezoelectric layer $H = 0.003m, 0.004m, 0.005m$ in (a) and (b) in case of electrically open conditions.

Effects of the piezoelectric constants

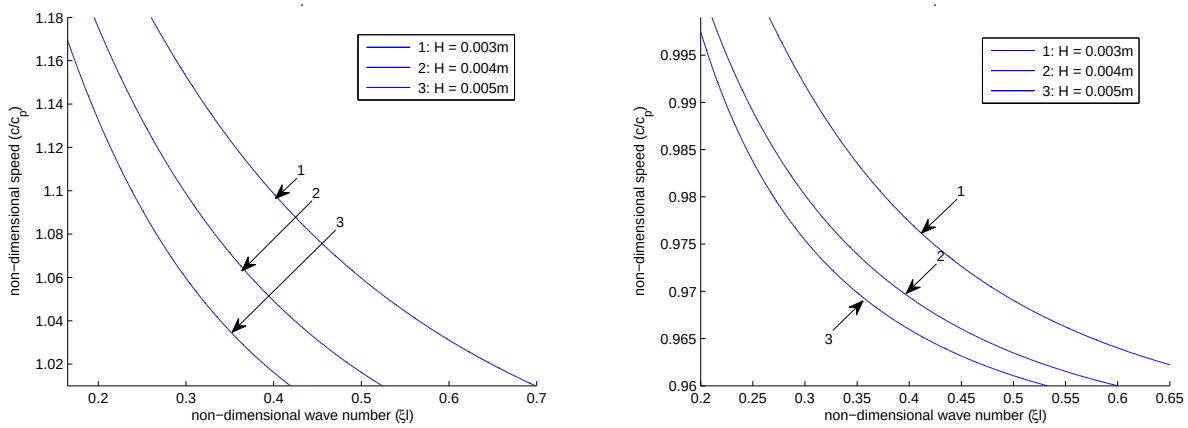

(a) For $PZT-5H$ ceramic

(b) For $BaTiO_3$ ceramic

Figure 3.9: Variation of non-dimensional phase velocity against non-dimensional wave number for different values of the thickness of piezoelectric layer $H = 0.003m, 0.004m, 0.005m$ in (a) and (b) in case of electrically short conditions.

Figures 3.10 and 3.11 show the trend of non-dimensional speed (c/c_p) with respect to non-dimensional wave number (ξH) for the Love wave propagation. The dispersion curves are plotted for three different values of the piezoelectric parameter $e_{15} = 17$ C/m^2, 21 C/m^2, 25 C/m^2, for the piezoelectric material $PZT-5H$, as shown in Figures 3.10(a) and 3.11(a) and $e_{15} = 11$ C/m^2, 15 C/m^2, 19 C/m^2, for $BaTiO_3$ material, shown in Figures 3.10(b) and 3.11(b) in each case of an electrically open and short conditions. The thickness of a piezoelectric material layer is taken as $H = 0.03m$ associated with the micropolar elastic half-space. It is observed that the phase velocity profiles of the Love wave decreases with the increase in the piezoelectric constant associated with a piezoelectric ceramic under both the cases of an electrically open and short conditions.

Effects of the dielectric constants

Figures 3.12 and 3.13 illustrate the effects of dielectric constants on the Love wave propagation in a piezoelectric layered structure. Here, the different values of dielectric constants are considered as $\epsilon_{11} = 237 \times 10^{-10}$ C^2/Nm^2, 277×10^{-10} C^2/Nm^2, 317×10^{-10} C^2/Nm^2 for $PZT-5H$ material, shown in Figures 3.12(a) and 3.13(a) and $\epsilon_{11} = 98 \times 10^{-10}$ C^2/Nm^2, 128×10^{-10} C^2/Nm^2, 158×10^{-10} C^2/Nm^2 for $BaTiO_3$

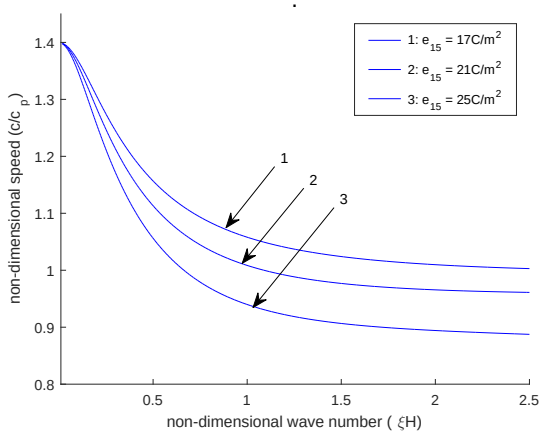

(a) For $PZT-5H$ ceramic

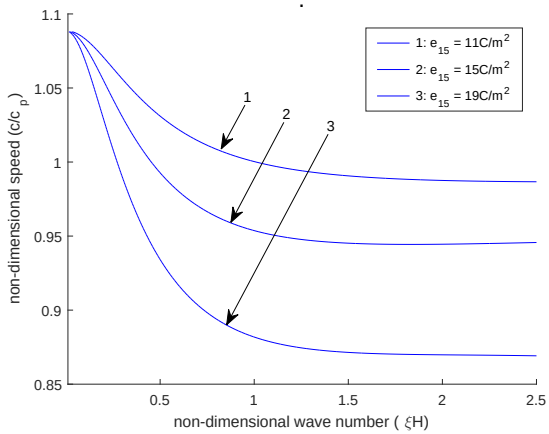

(b) For $BaTiO_3$ ceramic

Figure 3.10: Variation of non-dimensional phase velocity against non-dimensional wave number for different values of piezoelectric constants $e_{15} = 17\ C/m^2$, $21\ C/m^2$, $25\ C/m^2$ in (a) and $e_{15} = 11\ C/m^2$, $15\ C/m^2$, $19\ C/m^2$ in (b), when H=0.03m in case of electrically open conditions.

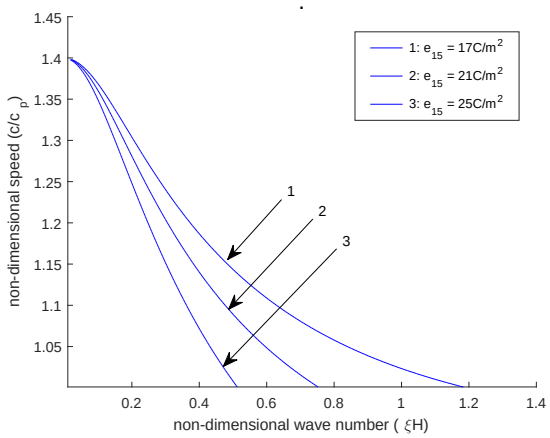

(a) For $PZT-5H$ ceramic

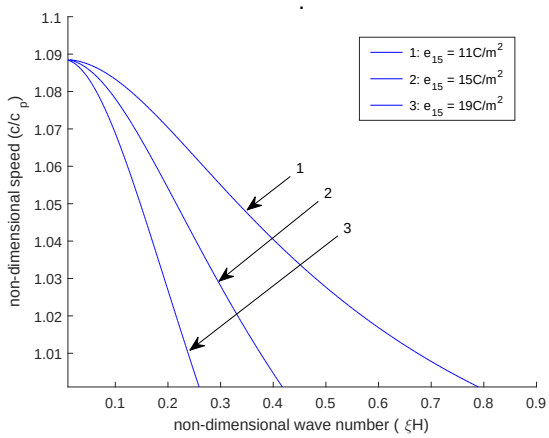

(b) For $BaTiO_3$ ceramic

Figure 3.11: Variation of non-dimensional phase velocity against non-dimensional wave number for different values of piezoelectric constants $e_{15} = 17\ C/m^2$, $21\ C/m^2$, $25\ C/m^2$ in (a) and $e_{15} = 11C/m^2, 15C/m^2, 19C/m^2$ in (b), when H=0.03m in case of electrically short conditions.

material, shown in Figures 3.12(b) and 3.13(b), for both cases of electrically open and short conditions. Here, the thickness of a piezoelectric layer is taken as $H = 0.03m$. The phase velocity profiles are affected significantly with the change in the dielectric parameter associated with a piezoelectric ceramic. It is observed that with

the increase in the dielectric constant, the phase velocity characteristics of the Love wave also increases for both the considered materials of the piezoelectric material layer under both the cases of electrically open and short conditions.

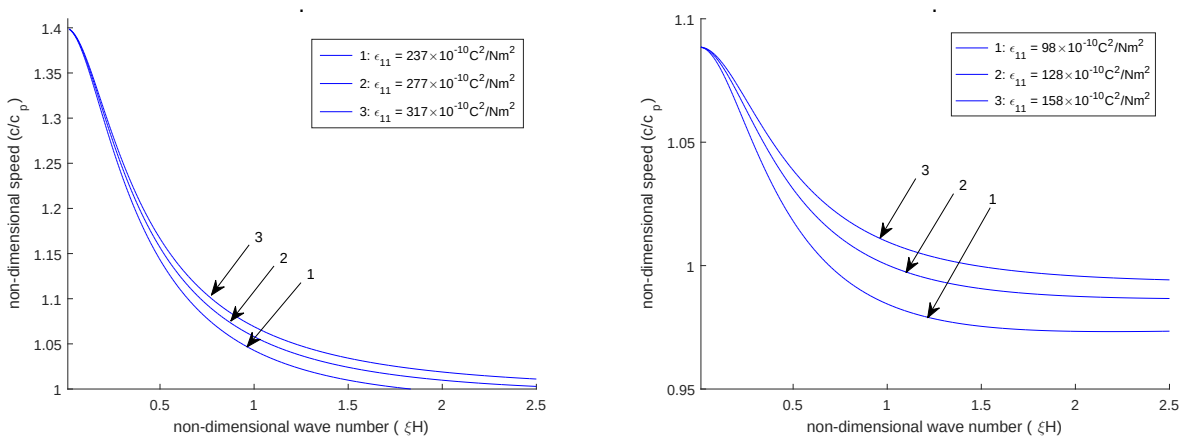

(a) For $PZT-5H$ ceramic

(b) For $BaTiO_3$ ceramic

Figure 3.12: Variation of non-dimensional phase velocity against non-dimensional wave number for different values of dielectric constants $\epsilon_{11} = 237 \times 10^{-10}\ C^2/Nm^2$, $277 \times 10^{-10}\ C^2/Nm^2$, $317 \times 10^{-10}\ C^2/Nm^2$ in (a) and $\epsilon_{11} = 98 \times 10^{-10}\ C^2/Nm^2$, $128 \times 10^{-10}\ C^2/Nm^2$, $158 \times 10^{-10}\ C^2/Nm^2$ in (b), when H=0.03m in case of electrically open conditions.

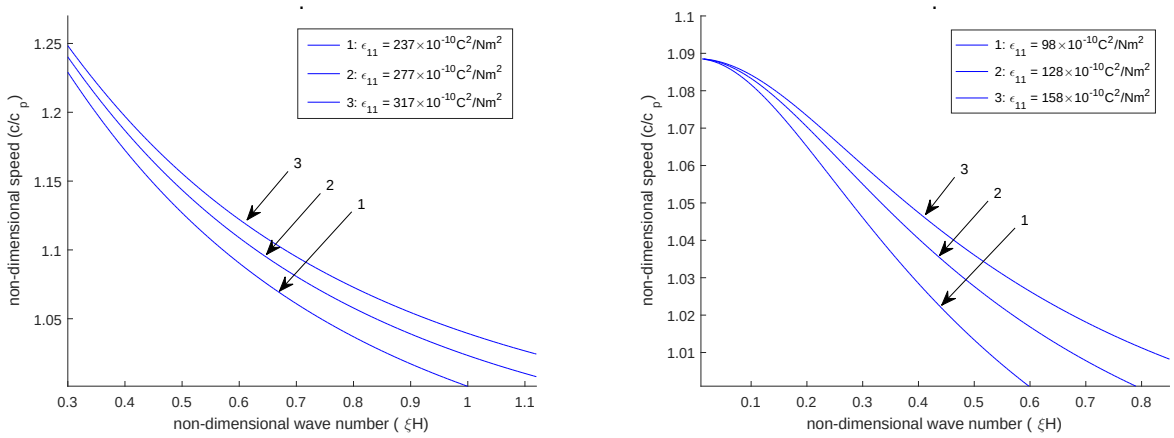

(a) For $PZT-5H$ ceramic

(b) For $BaTiO_3$ ceramic

Figure 3.13: Variation of non-dimensional phase velocity against non-dimensional wave number for different values of dielectric constants $\epsilon_{11} = 237 \times 10^{-10}\ C^2/Nm^2$, $277 \times 10^{-10}\ C^2/Nm^2$, $317 \times 10^{-10}\ C^2/Nm^2$ in (a) and $\epsilon_{11} = 98 \times 10^{-10}\ C^2/Nm^2$, $128 \times 10^{-10}\ C^2/Nm^2$, $158 \times 10^{-10}\ C^2/Nm^2$ in (b), when H=0.03m in case of electrically short conditions.

3.8 Conclusion

The effects of the microstructure of the substrate have been studied on the propagation of the Love wave by considering the micropolar piezoelectric structure. An analytical expression for the dispersion equations has been obtained and the results are shown graphically. The following conclusions are made based on obtained results.

(i) In the considered layered model, the phase velocity profiles show dispersion. Generally, in all graphs, the phase velocity decreases with an increase in non-dimensional wave number under both the cases of electrically open and short conditions for both the considered materials of a piezoelectric medium.

(ii) The effects of the coupling factor are significant in the short wave number range or the long-wavelength region. It is observed that with the increase in the degree of micropolarity of the micropolar medium, the phase velocity of the Love wave also increases.

(iii) The characteristic length of the micropolar material favors the phase velocity characteristics of the Love wave, i.e., with an increase in characteristic length,

the phase velocity of the Love wave increases. This effect justifies the consideration of microstructural properties of the semi-infinite substrate.

(iv) The thickness of the piezoelectric material layer does not exhibit favoring effects on the phase velocity profiles of Love waves, i.e., with the increase in the thickness of a piezoelectric layer, the phase velocity of the Love wave decreases.

(v) Piezoelectric parameter associated with the piezoelectric medium affects the phase velocity profiles of the Love wave. Specifically, the increase in piezoelectric parameters leads to a decrease in phase velocity of the Love wave propagation in the piezoelectric layered structure.

(vi) Dielectric constants associated with the piezoelectric layer show the favoring effects with the phase velocity profiles of the Love wave for both the considered materials of the piezoelectric medium. It is observed that with an increase in dielectric parameters the phase velocity of the layered system increases.

(vii) The influence of micropolarity on the phase velocity profiles of the Love wave is shown by plotting the characteristic curves for micropolar elasticity with the classical theory of elasticity as well as with the couple stress theory.

It is observed that both couple-piezoelectric and micropolar-piezoelectric layered models can be used for studying the effects of the microstructural substrate on the Love-type wave propagation in a piezoelectric layered medium. Almost similar trends are observed for these size-dependent models. The major outcome of these two chapters is the selection of the appropriate model for studying the size-dependency effects in the layered media.

Chapter 4

Analysis of Love-type wave propagation in double-layered structure

4.1 Introduction

The surface wave propagation in a hybrid structure exhibits significant effects because of its extensive applications running from seismic tremors to the structuring of surface acoustic wave (SAW) sensors. Many authors have presented the behavior of the Love-type wave using multi guiding layers of various materials. Salah et al. [158] demonstrated the influence of a soft middle layer on Love wave propagation in a layered piezoelectric system. Jiaoa et al. [79] examined the wave propagation through a piezoelectric semiconductor slab sandwiched between two piezoelectric half-spaces. Using Wentzel-Kramers-Brillouin (WKB) technique, Sahu et al. [157] investigated the transference of Love-type waves in functionally graded piezoelectric material (FGPM)

The content of this chapter are published in following journals:
1. The contents of section 3.2 are published in the journal *'Smart Materials and Structures'*, 28:105021(12pp), 2019, *(SCI, Impact factor:3.543)*.
2. The contents of section 3.3 are published in the journal *'International Journal of Mechanics and Materials in Design'*, 15:767–790, 2019, *(SCI, Impact factor:2.993)*.

layer bonded between viscous liquid and pre-stressed piezoelectric half-space. They showed that this study provides a theoretical foundation for optimization of SAW devices and obtained results are useful in the development of liquid viscosity sensors. Singhal et al. [184] and Singh et al. [182] delineated the propagation behavior of Love-type surface wave in a structure comprising of FGPM layer sandwiched between two dissimilar piezomagnetic/piezoelectric layers and substrate respectively.

Looking at the merits of the hybrid model, the consideration of another layer between a thin film of piezoelectric ceramic and size-dependent substrate will be more fruitful in the design process to accomplish an explicit objective. Some materials like wood, synthetic polymers, metals as well as human tissue at high temperatures show noteworthy viscoelastic impacts. The problem of studying a Love wave propagation in a viscoelastic medium has been of great interest in several contexts because it finds application in the design process by using certain viscoelastic material. Many authors investigated surface wave propagation in viscoelastic layered structure [153, 174, 172, 160, 117]. The variations in rigidity, density, or continuous change in the material's elastic properties in a vertical direction lead to heterogeneities in an elastic medium. Therefore, it is important to consider the heterogeneity or gradedness in these materials which have drawn the interest of scientists and engineers because the components of such materials exhibit the properties like high thermal or corrosion resistivity that can be helpful in improving the bonding strength of adhesives in metallic ceramic composites. These materials are inhomogeneous and can cause mild variability in design and structure to account for similar changes in material properties. Different functionalities and functions can be accomplished with these materials. Linear, quadratic, harmonic, or exponential modes of inhomogeneity in the medium may be considered. In this chapter, the harmonic mode of inhomogeneity has been employed in the viscoelastic material layer for the development of more efficient and high-performance Love wave-based devices.

The objective of this chapter is to investigate the microstructural considerations on the Love-type wave propagation in double-layered structures. In section 4.2 of this chapter, a theoretical model consisting of a heterogeneous viscoelastic layer sandwiched

between a finite layer of piezoelectric material and size-dependent couple stress substrate is considered, and in section 4.3, the propagation of Love wave is considered in a double-layered structure consisting of finite layers of viscoelastic and piezoelectric material lying over the semi-infinite size-dependent micropolar substrate. In both problems, the traction-free surface is considered at the top layer of the considered problem. The real and damping dispersion relations are obtained analytically in closed-form for both the cases of electrically open and short conditions. The impacts of heterogeneity, internal friction related to the viscoelastic material layer, together with the internal microstructures of the substrate are demonstrated graphically. The effects of the piezoelectric medium are displayed by taking $PZT-5H$ or $BaTiO_3$ materials of the piezoelectric layer. Particular cases are deduced and the classical Love wave equation is also obtained to validate the study.

4.2 Dispersion of Love-type waves in size-dependent couple stress substrate containing finite piezoelectric and viscoelastic layers

4.2.1 Formulation of the problem

Assume a piezoelectric layer having thickness h_p, a heterogeneous viscoelastic layer having thickness h_v, lying over the couple stress substrate. A rectangular frame of reference is considered in which the direction of the Love wave propagation is considered along the y-axis, which causes particle displacement along the z-axis and the x-axis is taken toward the downward direction which has been shown in figure 4.1. The direction of poling of a piezoelectric layer is taken toward the z-axis.

Let $u_i^{(p)} = (u_p, v_p, w_p)$, $u_i^{(v)} = (u_v, v_v, w_v)$ and $u_i^{(c)} = (u_c, v_c, w_c)$ are the mechanical displacement components in the upper piezoelectric layer, the middle viscoelastic layer and the lower couple stress elastic half-space respectively, obtained due to the propagation of the Love wave. As the Love wave is propagating along the direction

of the y-axis, it causes displacement in the z-direction only. One may suppose that

$$\begin{aligned} u_p = 0,\ v_p = 0,\ w_p = w_p(x, y, t), \\ u_v = 0,\ v_v = 0,\ w_v = w_v(x, y, t), \\ u_c = 0,\ v_c = 0,\ w_c = w_c(x, y, t). \end{aligned} \tag{4.1}$$

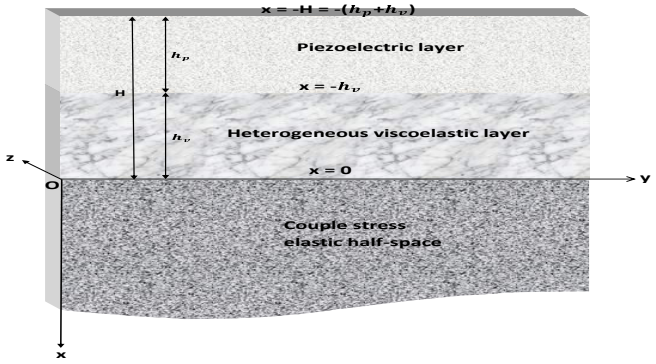

Figure 4.1: Geometry

By following the procedure adopted in sections 2.2.1 and 2.2.2 of Chapter-2, the mechanical displacement component for piezoelectric material layer and for the couple stress medium are obtained as

$$w_p(x, y, t) = [A_1 \sin(\xi a x) + A_2 \cos(\xi a x)] e^{\iota\xi(y-ct)}, \tag{4.2}$$

$$\phi^{(p)}(x, y, t) = \left[\frac{e_{15}}{\epsilon_{11}}[A_1 \sin(\xi a x) + A_2 \cos(\xi a x)] + A_3 e^{-\xi x} + A_4 e^{\xi x}\right] e^{\iota\xi(y-ct)}, \tag{4.3}$$

$$w_c(x, y, t) = (A_1^{'} e^{-px} + A_2^{'} e^{-qx}) e^{\iota\xi(y-ct)}. \tag{4.4}$$

The notations and symbols are same as used in sections 2.2.1 and 2.2.2 of Chapter-2.

4.2.2 Solution for the vertically heterogeneous viscoelastic layer

By using equation (4.1) in equations (1.31) and (1.32), the non-vanishing equation of motion for the viscoelastic layer [155, 150] for the Love wave propagation in the

xy-plane is obtained as

$$\frac{\partial}{\partial x}\tau_{zx}^{(v)} + \frac{\partial}{\partial y}\tau_{zy}^{(v)} = \rho_v \frac{\partial^2 w_v}{\partial t^2}, \tag{4.5}$$

where

$$\begin{aligned} \tau_{zx}^{(v)} &= \left(\mu_v + \eta_v \frac{\partial}{\partial t}\right)\frac{\partial w_v}{\partial x}, \\ \tau_{zy}^{(v)} &= \left(\mu_v + \eta_v \frac{\partial}{\partial t}\right)\frac{\partial w_v}{\partial y}. \end{aligned} \tag{4.6}$$

Here, a heterogeneity is considered in the viscoelastic layer. So, μ_v, η_v, ρ_v can be composed as a function of the depth which is given as

$$\begin{aligned} \mu_v &= \mu_1(1 - \sin \alpha x), \\ \eta_v &= \eta_1(1 - \sin \alpha x), \\ \rho_v &= \rho_V(1 - \sin \alpha x), \end{aligned} \tag{4.7}$$

where α is the heterogeneity parameter and dimension is the inverse of the length, ρ_V is the mass density, μ_1 is the modulus of rigidity, η_1 is the internal friction parameter. Using equations (4.6) and (4.7) into equation (4.5), the equation of motion for vertically heterogeneous viscoelastic layer is obtained as

$$\frac{\partial}{\partial x}\left[\left(\mu_v + \eta_v \frac{\partial}{\partial t}\right)\frac{\partial w_v}{\partial x}\right] + \left(\mu_v + \eta_v \frac{\partial}{\partial t}\right)\frac{\partial^2 w_v}{\partial y^2} = \rho_v \frac{\partial^2 w_v}{\partial t^2}. \tag{4.8}$$

The solution of equation (4.8) is considered as

$$w_v = W_v(x) e^{\iota\xi(y-ct)}. \tag{4.9}$$

On substituting equations (4.7) and (4.9) in equation (4.8), one may obtain

$$\frac{d^2 W_v}{dx^2} + \frac{(\overline{\mu_v'})}{(\overline{\mu_v})}\frac{dW_v}{dx} + \left(\frac{\omega^2 \rho_v}{\overline{\mu_v}} - \xi^2\right) W_v = 0, \tag{4.10}$$

where

$$\begin{aligned} \overline{\mu_v} &= \mu_v - \iota\omega\eta_v, \\ \overline{\mu_v}' &= \frac{d\overline{\mu_v}}{dx}. \end{aligned} \tag{4.11}$$

The following transformation is used to solve equation (4.10)

$$W_v(x) = \frac{Y(x)}{\sqrt{\overline{\mu_v}}}. \tag{4.12}$$

Using equation (4.12) in equation (4.10), one may obtain the following differential equation

$$\frac{d^2Y}{dx^2} + m^2 Y = 0, \tag{4.13}$$

where

$$\begin{aligned} m^2 &= \frac{\alpha^2}{4} + \frac{\omega^2 \rho_V}{\overline{\mu_1}} - \xi^2, \\ \overline{\mu_1} &= \mu_1 - \iota\omega\eta_1. \end{aligned} \tag{4.14}$$

The value of m can be written as:

$$\begin{cases} m = m_1 + \iota m_2,\ m_1 = \sqrt{r}\cos\frac{\theta}{2},\ m_2 = \sqrt{r}\sin\frac{\theta}{2}, \\ r = \sqrt{F_1^2 + F_2^2},\ \tan\theta = \frac{F_1}{F_2}, \\ F_1 = \frac{\omega^3\rho_V\eta_1}{\mu_1^2+\omega^2\eta_1^2},\ F_2 = \frac{\alpha^2}{4} - \xi^2 + \frac{\omega^2\rho_V\mu_1}{\mu_1^2+\omega^2\eta_1^2},\ c_v = \sqrt{\frac{\mu_1}{\rho_V}}. \end{cases}$$

Here c_v represents the shear wave velocity in the viscoelastic layer.

The general solution of the differential equation (4.13) can be written as

$$Y(x) = D_1 \cos mx + D_2 \sin mx, \tag{4.15}$$

where D_1 *and* D_2 are the arbitrary constants.

Substituting equations (4.15) and (4.12) into equation (4.9); the displacement component for the viscoelastic material layer is obtained as

$$w_v(x, y, t) = \frac{1}{\sqrt{\overline{\mu_1}}\sqrt{1 - \sin\alpha x}}(D_1 \cos mx + D_2 \sin mx)e^{\iota\xi(y-ct)}. \tag{4.16}$$

Using equations (4.16) and (4.7) into equation (4.6), the required constitutive relation for the viscoelastic material layer is obtained as:

$$\tau_{zx}^{(v)} = \frac{\sqrt{\overline{\mu_1}}}{2\sqrt{1-\sin\alpha x}}\Big[\Big(\alpha\cos\alpha x\cos mx - 2m(1-\sin\alpha x)\sin mx\Big)D_1 + \Big(\alpha\cos\alpha x\sin mx + 2m(1-\sin\alpha x)\cos mx\Big)D_2\Big]e^{\iota\xi(y-ct)}. \tag{4.17}$$

4.2.3 Boundary conditions

The following boundary conditions are to be satisfied for the propagation of the Love-type wave propagation in the considered hybrid model.

(A) For the traction-free surface at $x = -H = -(h_v + h_p)$:

$$\tau_{zx}^{(p)} = 0, \tag{4.18}$$

$$D_x = 0 \quad (for \quad electrically \quad open \quad case), \tag{4.19}$$

$$\phi^{(p)} = 0 \quad (for \quad electrically \quad short \quad case). \tag{4.20}$$

(B) For the common interface of piezoelectric and viscoelastic layer at $x = -h_v$:

$$\tau_{zx}^{(p)} = \tau_{zx}^{(v)}, \tag{4.21}$$

$$w_p = w_v, \tag{4.22}$$

$$\phi^{(p)} = 0. \tag{4.23}$$

(C) For the common interface of couple stress half-space and viscoelastic layer $x = 0$:

$$\tau_{zx}^{(v)} = \tau_{zx}^{(c)}, \tag{4.24}$$

$$w_v = w_c, \tag{4.25}$$

$$\mu_{xy}^{(c)} = 0. \tag{4.26}$$

Using equations (4.18)–(4.26), the following equations can be obtained in terms of unknown coefficients A_1, A_2, A_3, A_4, $A_1^{'}$, $A_2^{'}$, D_1 and D_2.

$$ac_{44}^{*}\cos(\xi aH)A_1 + ac_{44}^{*}\sin(\xi aH)A_2 - e_{15}e^{\xi H}A_3 + e_{15}e^{-\xi H}A_4 = 0, \tag{4.27}$$

$$e^{\xi H}A_3 - e^{-\xi H}A_4 = 0, \tag{4.28}$$

$$-\frac{e_{15}}{\epsilon_{11}}\sin(\xi aH)A_1 + \frac{e_{15}}{\epsilon_{11}}\cos(\xi aH)A_2 + e^{\xi H}A_3 + e^{-\xi H}A_4 = 0, \tag{4.29}$$

$$\begin{aligned}\xi a c_{44}^{*}\cos(\xi a h_v)A_1 + \xi a c_{44}^{*}\sin(\xi a h_v)A_2 - \xi e_{15}e^{\xi h_v}A_3 \\ +\xi e_{15}e^{-\xi h_v}A_4 - \frac{\sqrt{\overline{\mu_1}}}{2\sqrt{1+\sin\alpha h_v}}T_1 D_1 - \frac{\sqrt{\overline{\mu_1}}}{2\sqrt{1+\sin\alpha h_v}}T_2 D_2 = 0,\end{aligned} \tag{4.30}$$

$$\sin(\xi a h_v)A_1 - \cos(\xi a h_v)A_2 + \frac{\cos(m h_v)}{\sqrt{\overline{\mu_1}}\sqrt{1+\sin\alpha h_v}}D_1 - \frac{\sin(m h_v)}{\sqrt{\overline{\mu_1}}\sqrt{1+\sin\alpha h_v}}D_2 = 0, \tag{4.31}$$

$$-\frac{e_{15}}{\epsilon_{11}}\sin(\xi a h_v)A_1 + \frac{e_{15}}{\epsilon_{11}}\cos(\xi a h_v)A_2 + e^{\xi h_v}A_3 + e^{-\xi h_v}A_4 = 0, \tag{4.32}$$

$$\frac{\alpha\sqrt{\overline{\mu_1}}}{2}D_1 + m\sqrt{\overline{\mu_1}}D_2 - P_1 A_1^{'} - Q_1 A_2^{'} = 0, \tag{4.33}$$

$$\frac{1}{\sqrt{\overline{\mu_1}}}D_1 - A_1^{'} - A_2^{'} = 0, \tag{4.34}$$

$$k_p A_1^{'} + k_q A_2^{'} = 0, \tag{4.35}$$

where

$$T_1 = 2m(1+\sin\alpha h_v)\sin(m h_v) + \alpha\cos(\alpha h_v)\cos(m h_v) = J_1 + \iota I_1,$$

$$J_1 = 2(1+\sin\alpha h_v)(m_1 S_1 - m_2 S_2) + \alpha E_1\cos\alpha h_v,$$

$$I_1 = 2(1+\sin\alpha h_v)(m_1 S_2 + m_2 S_1) - \alpha E_2\cos\alpha h_v,$$

$$T_2 = 2m(1+\sin\alpha h_v)\cos(m h_v) - \alpha\cos(\alpha h_v)\sin(m h_v) = J_2 + \iota I_2,$$

$$J_2 = 2(1+\sin\alpha h_v)(m_1 E_1 + m_2 E_2) - \alpha S_1\cos\alpha h_v,$$

$$I_2 = 2(1+\sin\alpha h_v)(m_2 E_1 - m_1 E_2) - \alpha S_2\cos\alpha h_v,$$

$$S_1 = \sin(m_1 h_v)\cosh(m_2 h_v),\ \ S_2 = \cos(m_1 h_v)\sinh(m_2 h_v),$$

$$E_1 = \cos(m_1 h_v)\cosh(m_2 h_v),\ \ E_2 = \sin(m_1 h_v)\sinh(m_2 h_v),$$

$$k_p = \xi^2 - p^2,\ \ k_q = \xi^2 - q^2, P_1 = \mu_c p(l^2 k_p - 1),\ \ Q_1 = \mu_c q(l^2 k_q - 1).$$

4.2.4 Dispersion relations for electrically open conditions

The equations (4.27)–(4.28) and (4.30)–(4.35) constitute eight boundary conditions. The determinant of square matrix must vanish to obtain the non-trivial solution of unknown coefficients A_1, A_2, A_3, A_4, $A_1^{'}$, $A_2^{'}$, D_1 and D_2. The dispersion equation in case of open circuit is

$$\begin{aligned}\xi a c_{44}^{*} R_1 \sin(\xi aH - \xi a h_v)\cosh(\xi H - \xi h_v) + \xi \frac{e_{15}^2}{\epsilon_{11}} R_1 \cos(\xi aH - \xi a h_v)\times \\ \sinh(\xi H - \xi h_v) - R_2 \cos(\xi aH - \xi a h_v)\cosh(\xi H - \xi h_v) = 0,\end{aligned} \tag{4.36}$$

where

$$R_1 = L_1 + \iota L_2,\ R_2 = N_1 + \iota N_2,$$

$$L_1 = \frac{(k_p Q_1 - k_q P_1)(\mu_1 S_1 - \omega \eta_1 S_2)}{{\mu_1}^2 + \omega^2 {\eta_1}^2} - \frac{\alpha(k_p - k_q)S_1}{2} - (k_p - k_q)(m_1 E_1 + m_2 E_2),$$

$$L_2 = \frac{(k_p Q_1 - k_q P_1)(\mu_1 S_2 + \omega \eta_1 S_1)}{{\mu_1}^2 + \omega^2 {\eta_1}^2} - \frac{\alpha(k_p - k_q)S_2}{2} - (k_p - k_q)(m_2 E_1 - m_1 E_2),$$

$$N_1 = \frac{1}{2}(k_p Q_1 - k_q P_1)J_2 - \frac{1}{4}\alpha(k_p - k_q)(\mu_1 J_2 + \omega \eta_1 I_2) + \frac{1}{2}(k_p - k_q)K_1,$$

$$N_2 = \frac{1}{2}(k_p Q_1 - k_q P_1)I_2 - \frac{1}{4}\alpha(k_p - k_q)(\mu_1 I_2 - \omega \eta_1 J_2) + \frac{1}{2}(k_p - k_q)K_2,$$

$$K_1 = (m_1 \mu_1 + \omega \eta_1 m_2)J_1 - (m_2 \mu_1 - \omega \eta_1 m_1)I_1,$$

$$K_2 = (m_1 \mu_1 + \omega \eta_1 m_2)I_1 + (m_2 \mu_1 - \omega \eta_1 m_1)J_1.$$

On comparing the real and imaginary parts of equation (4.36),one may have

$$\begin{aligned}\xi a c_{44}^{*} L_1 \sin(\xi aH - \xi a h_v)\cosh(\xi H - \xi h_v) + \xi \frac{e_{15}^2}{\epsilon_{11}} L_1 \cos(\xi aH - \xi a h_v)\times \\ \sinh(\xi H - \xi h_v) - N_1 \cos(\xi aH - \xi a h_v)\cosh(\xi H - \xi h_v) = 0,\end{aligned} \tag{4.37}$$

and

$$\begin{aligned}\xi a c_{44}^{*} L_2 \sin(\xi aH - \xi a h_v)\cosh(\xi H - \xi h_v) + \xi \frac{e_{15}^2}{\epsilon_{11}} L_2 \cos(\xi aH - \xi a h_v)\times \\ \sinh(\xi H - \xi h_v) - N_2 \cos(\xi aH - \xi a h_v)\cosh(\xi H - \xi h_v) = 0.\end{aligned} \tag{4.38}$$

The dispersion relations obtained in equation (4.37) and (4.38) correspond to the real and damping equation, respectively for the Love wave propagation in the considered model.

4.2.5 Dispersion relations for electrically short conditions

The equations (4.27) and (4.29)–(4.35) constitute eight boundary conditions. The determinant of square matrix must vanish to obtain the non-trivial solution of unknown coefficients A_1, A_2, A_3, A_4, A_1', A_2', D_1 and D_2. The dispersion equation in case of short circuit is:

$$\begin{aligned}&\Bigg[2\xi ac_{44}^{*}\frac{e_{15}^{2}}{\epsilon_{11}}-2\xi ac_{44}^{*}\frac{e_{15}^{2}}{\epsilon_{11}}\cos(\xi aH-\xi ah_v)\cosh(\xi H-\xi h_v)\\&\quad+\xi\left(\frac{e_{15}^{4}}{\epsilon_{11}^{2}}-a^{2}{c_{44}^{*}}^{2}\right)\sin(\xi aH-\xi ah_v)\sinh(\xi H-\xi h_v)\Bigg]R_1\\&+\Bigg[ac_{44}^{*}\cos(\xi aH-\xi ah_v)\sinh(\xi H-\xi h_v)-\frac{e_{15}^{2}}{\epsilon_{11}}\sin(\xi aH-\\&\qquad\xi ah_v)\cosh(\xi H-\xi h_v)\Bigg]R_2=0.\end{aligned}\tag{4.39}$$

On comparing the real and the imaginary parts of equation (4.39), one may obtain

$$\begin{aligned}&\Bigg[2\xi ac_{44}^{*}\frac{e_{15}^{2}}{\epsilon_{11}}-2\xi ac_{44}^{*}\frac{e_{15}^{2}}{\epsilon_{11}}\cos(\xi aH-\xi ah_v)\cosh(\xi H-\xi h_v)\\&\quad+\xi\left(\frac{e_{15}^{4}}{\epsilon_{11}^{2}}-a^{2}{c_{44}^{*}}^{2}\right)\sin(\xi aH-\xi ah_v)\sinh(\xi H-\xi h_v)\Bigg]L_1\\&+\Bigg[ac_{44}^{*}\cos(\xi aH-\xi ah_v)\sinh(\xi H-\xi h_v)-\frac{e_{15}^{2}}{\epsilon_{11}}\sin(\xi aH-\\&\qquad\xi ah_v)\cosh(\xi H-\xi h_v)\Bigg]N_1=0,\end{aligned}\tag{4.40}$$

and

$$\begin{aligned}\Bigg[2\xi ac_{44}^{*}\frac{e_{15}^{2}}{\epsilon_{11}}-2\xi ac_{44}^{*}\frac{e_{15}^{2}}{\epsilon_{11}}\cos(\xi aH-\xi ah_v)\cosh(\xi H-\xi h_v)\\ +\xi\left(\frac{e_{15}^{4}}{\epsilon_{11}^{2}}-a^{2}{c_{44}^{*}}^{2}\right)\sin(\xi aH-\xi ah_v)\sinh(\xi H-\xi h_v)\Bigg]L_2\\ +\Bigg[ac_{44}^{*}\cos(\xi aH-\xi ah_v)\sinh(\xi H-\xi h_v)-\frac{e_{15}^{2}}{\epsilon_{11}}\sin(\xi aH-\\ \xi ah_v)\cosh(\xi H-\xi h_v)\Bigg]N_2=0.\end{aligned} \tag{4.41}$$

The dispersion relations obtained in equations (4.40) and (4.41) correspond to the real and damping equation for the Love-type wave propagation in the considered hybrid model.

4.2.6 Validation

Case-1 By considering thickness of piezoelectric medium $h_p = 0$, the equation (4.36) reduces to

$$R_2 = 0. \tag{4.42}$$

On solving equation (4.42), one may get the dispersion relation for Love-type wave in viscoelastic layer perfectly bonded to couple stress substrate.

$$\begin{aligned}2J_1(\mu_1 m_1+\omega\eta_1 m_2)(p^2-q^2)+2I_1(\omega\eta_1 m_1-\mu_1 m_2)(p^2-q^2)\\ +2J_2A+\alpha(\mu_1 J_2+\omega\eta_1 I_2)(q^2-p^2)=0,\end{aligned} \tag{4.43}$$

and

$$\begin{aligned}2J_1(\mu_1 m_2-\omega\eta_1 m_1)(p^2-q^2)+2I_1(\omega\eta_1 m_2+\mu_1 m_1)(p^2-q^2)\\ +2I_2A+\alpha(\mu_1 I_2-\omega\eta_1 J_2)(q^2-p^2)=0,\end{aligned} \tag{4.44}$$

where $A=\mu l^2(\xi^2-p^2)(\xi^2-q^2)(p-q)+\mu q(\xi^2-p^2)-\mu p(\xi^2-q^2)$.

The dispersion relations obtained in equation (4.43) and (4.44) are the real and damping equations for the propagation of a Love wave in a viscoelastic heterogeneous layer overlying couple stress substrate. It is the same as obtained from Sharma and Kumar [166].

Case-2 On pondering previous case and in the absence of heterogeneity parameter,

i.e., $\alpha = 0$ associated with viscoelastic layer, equation (4.42) reduces to

$$2J_1^{'}(\mu_1 m_1^{'} + \omega\eta_1 m_2^{'})(p^2 - q^2) + 2I_1^{'}(\omega\eta_1 m_1^{'} - \mu_1 m_2^{'})(p^2 - q^2) + 2J_2^{'}A = 0, \quad (4.45)$$

$$2J_1^{'}(\mu_1 m_2^{'} - \omega\eta_1 m_1^{'})(p^2 - q^2) + 2I_1^{'}(\omega\eta_1 m_2^{'} + \mu_1 m_1^{'})(p^2 - q^2) + 2I_2^{'}A = 0, \quad (4.46)$$

where

$$m^{'} = m_1^{'} + \iota m_2^{'},\ m_1^{'} = \sqrt{r^{'}}\cos\frac{\theta}{2},\ m_2^{'} = \sqrt{r^{'}}\sin\frac{\theta}{2},$$
$$r^{'} = \sqrt{{F_1^{'}}^2 + {F_2^{'}}^2},\ \tan\theta = \frac{F_1^{'}}{F_2^{'}},$$
$$F_1^{'} = \frac{\omega^3\rho_1\eta_1}{{\mu_1}^2 + \omega^2{\eta_1}^2},\ F_2^{'} = \frac{\omega^2\rho_1\eta_1}{{\mu_1}^2 + \omega^2{\eta_1}^2} - \xi^2.$$

$$T_1^{'} = 2m^{'}\sin(m^{'}h_v) = J_1^{'} + \iota I_1^{'},$$
$$J_1^{'} = 2(m_1^{'}S_1^{'} - m_2^{'}S_2^{'}),\ I_1^{'} = 2(m_1^{'}S_2^{'} + m_2^{'}S_1^{'}).$$

$$T_2^{'} = 2m^{'}\cos(m^{'}h_v) = J_2^{'} + \iota I_2^{'},$$
$$J_2^{'} = 2(m_1^{'}E_1^{'} + m_2^{'}E_2^{'}),\ I_2^{'} = 2(m_2^{'}E_1^{'} - m_1^{'}E_2^{'}).$$

$$S_1^{'} = \sin(m_1^{'}h_v)\cosh(m_2^{'}h_v),\ S_2^{'} = \cos(m_1^{'}h_v)\sinh(m_2^{'}h_v).$$

$$E_1^{'} = \cos(m_1^{'}h_v)\cosh(m_2^{'}h_v),\ E_2^{'} = \sin(m_1^{'}h_v)\sinh(m_2^{'}h_v).$$

$$R_1^{'} = L_1^{'} + \iota L_2^{'},\ R_2^{'} = N_1^{'} + \iota N_2^{'}.$$

$$L_1^{'} = \frac{(k_pQ_1 - k_qP_1)(\mu_1 S_1^{'} - \omega\eta_1 S_2^{'})}{{\mu_1}^2 + \omega^2{\eta_1}^2} - (k_p - k_q)(m_1^{'}E_1^{'} + m_2^{'}E_2^{'}),$$
$$L_2^{'} = \frac{(k_pQ_1 - k_qP_1)(\mu_1 S_2^{'} + \omega\eta_1 S_1^{'})}{{\mu_1}^2 + \omega^2{\eta_1}^2} - (k_p - k_q)(m_2^{'}E_1^{'} - m_1^{'}E_2^{'}).$$

$$N_1^{'} = \frac{1}{2}(k_pQ_1 - k_qP_1)J_2^{'} + \frac{1}{2}(k_p - k_q)K_1^{'},$$
$$N_2^{'} = \frac{1}{2}(k_pQ_1 - k_qP_1)I_2^{'} + \frac{1}{2}(k_p - k_q)K_2^{'}.$$

$$K_1^{'} = (m_1^{'}\mu_1 + \omega\eta_1 m_2^{'})J_1^{'} - (m_2^{'}\mu_1 - \omega\eta_1 m_1^{'})I_1^{'},$$
$$K_2^{'} = (m_1^{'}\mu_1 + \omega\eta_1 m_2^{'})I_1^{'} + (m_2^{'}\mu_1 - \omega\eta_1 m_1^{'})J_1^{'}.$$

Equation (4.45) and (4.46) are the dispersion equations for real and damping phase

speed in the layered system involving homogeneous viscoelastic layer lying over couple stress elastic half-space.

Case-3 In the absence of viscoelasticity, i.e., $\alpha = 0$ and $\eta_1 = 0$, the equations (4.36) and (4.39) reduce to

$$\xi(k_p - k_q)\left[\frac{e_{15}^2}{\epsilon_{11}}\tanh(\xi h_p) + ac_{44}^*\tan(a\xi h_p)\right] + [\mu p(1 - l^2k_p)k_q - \mu q(1 - l^2k_q)k_p] = 0, \tag{4.47}$$

and

$$\xi(k_p - k_q)\left[\left(a^2{c_{44}^*}^2 - \frac{e_{15}^4}{\epsilon_{11}^2}\right)\tan(\xi a h_p)\tanh(\xi h_p) + 2ac_{44}^*\frac{e_{15}^2}{\epsilon_{11}}\left(1 - \frac{\sec(\xi a h_p)}{\cosh(\xi h_p)}\right)\right] + [\mu p(1 - l^2k_p)k_q - \mu q(1 - l^2k_q)k_p]\left[ac_{44}^*\tanh(\xi h_p) - \frac{e_{15}^2}{\epsilon_{11}}\tan(\xi a h_p)\right] = 0. \tag{4.48}$$

Equation (4.47) and (4.48) are the dispersion equations for Love wave propagation in piezoelectric medium overlying semi-infinite couple stress substrate for electrically open and short conditions, respectively. It is same as obtained in sections 2.4 and 2.5 in Chapter 2.

Case-4 In the absence of piezoelectric parameter, i.e., $e_{15} = 0$ and $c_{44}^* \to c_{44}$, equations (4.47) and (4.48) reduce to Love-type wave propagation in isotropic elastic layer lying over couple stress elastic half-space.

$$\xi c_{44}\sqrt{\frac{c^2}{\overline{c_p^2}} - 1}\tan\left(\xi H\sqrt{\frac{c^2}{\overline{c_p^2}} - 1}\right) = \frac{P_1k_q - Q_1k_p}{k_p - k_q}, \tag{4.49}$$

where

$$\overline{c_p} = \sqrt{\frac{c_{44}}{\rho_p}}.$$

where equation (4.49) matches with the equation (2.46) of section 2.6 in Chapter 2.

Case-5 Pondering the previous case and taking $l \to 0$, i.e., couple stress half-space reduces to isotropic elastic half-space and $\frac{P_1k_q - Q_1k_p}{k_p - k_q} \to \xi\mu_c\sqrt{1 - \frac{c^2}{c_{cs}^2}}$, equation (4.49)

reduces to:

$$\tan\left(\xi H\sqrt{\frac{c^2}{\overline{\overline{c_p^2}}}-1}\right)=\frac{\mu_c\sqrt{1-\frac{c^2}{\overline{\overline{c_{cs}^2}}}}}{c_{44}\sqrt{\frac{c^2}{\overline{\overline{c_p^2}}}-1}}. \tag{4.50}$$

Equation (4.50) represents the dispersion relation for Love-wave propagation in isotropic elastic layer lying over the isotropic elastic substrate which matches with the well-known Classical Love wave [122] equation which also validates the outcome of the present problem.

4.2.7 Numerical discussion

For illustrating the numerical results, the couple stress substrate is considered which is made up of Dionysos Marble having microstructural properties as provided in Table 2.1 and the material parameters for piezoelectric layers of $PZT-5H$ or $BaTiO_3$ are provided in Table 2.2 in section 2.7 of Chapter-2. The material parameters for viscoelastic layer [63] are provided in Table 4.1

Table 4.1: Material constants for viscoelastic layer

ρ_V	4705	kg/m^3
μ_1	1.987×10^{10}	N/m^2
$\frac{\mu_1}{\eta_1}$	10^6	s^{-1}

Equations (4.36) and (4.39) represent the dispersion relation under electrically open and short circuit, respectively. Here, all the graphs are plotted for dimensionless real and damping phase speed versus dimensionless wave number. One common phenomenon observed in all figures is, that with an increment in dimensionless wave number, the real as well as damping phase velocity decreases. Figures - 4.2, 4.3, 4.6, 4.7, 4.10, 4.11, 4.14 correspond to electrically open conditions and figures - 4.4, 4.5, 4.8, 4.9, 4.12, 4.13, 4.15 correspond to electrically short conditions.

4.2.8 Impact of microstructural parameter

The influence of microstructure of the substrate is shown by considering distinct values of characteristic length $l=0.00001m$, $0.0001m$, $0.0004m$. The thickness of viscoelastic

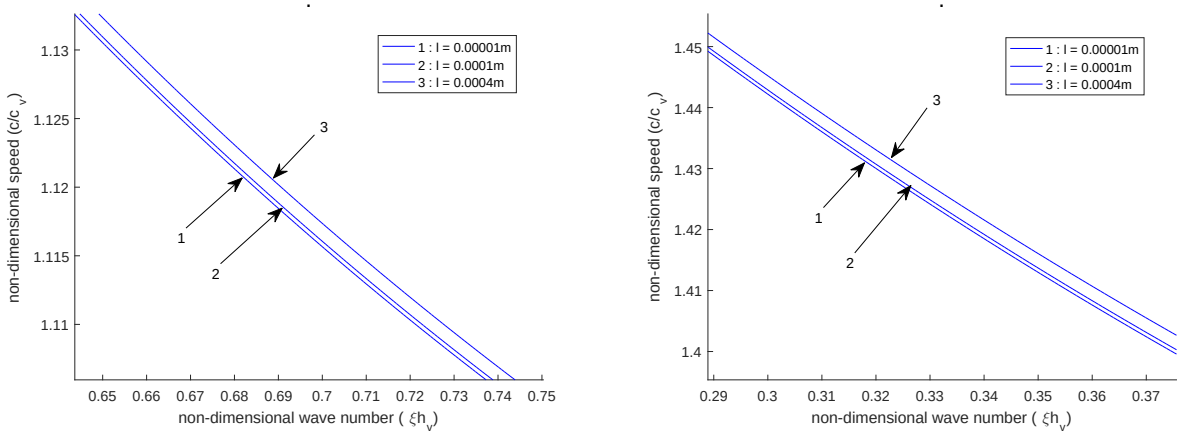

(a) For $PZT-5H$ ceramic

(b) For $BaTiO_3$ ceramic

Figure 4.2: Variation of non-dimensional real phase velocity against non-dimensional wave number for distinct values of characteristic length in case of electrical open conditions.

and piezoelectric medium is taken as $h_v = 0.02m$ and $h_p = 0.02m$, respectively. In these figures, the microstructure of substrate exhibits the favoring effect on the phase velocity profiles of Love wave, i.e., with an increment in characteristic length, the real and damping phase speed also increases. Figures-4.2 and 4.4 correspond to real phase velocity and figures-4.3 and 4.5 correspond to damped phase velocity under electrically open and short conditions respectively. Graphs 4.2(a), 4.3(a), 4.4(a), 4.5(a) are plotted for $PZT-5H$ material and 4.2(b), 4.3(b), 4.4(b), 4.5(b) are plotted for $BaTiO_3$ material.

4.2.9 Impact of heterogeneity of a viscoelastic layer

The influence of the heterogeneity parameter associated with viscoelastic medium is displayed in figures 4.6–4.9. These figures are plotted for distinct values of heterogeneity parameter $\alpha h_v = 0.08$, 0.12 and 0.16. The thickness of both the layers are considered as $h_v = 0.02m$, $h_p = 0.02m$ and characteristic length as $l = 0.0004m$. The characteristic profiles are affected significantly with the change in value of heterogeneity parameter. Here, it is noticed that with the increase in heterogeneity, the phase velocity of Love wave decreases. Figure 4.6 and 4.7 correspond to electrically

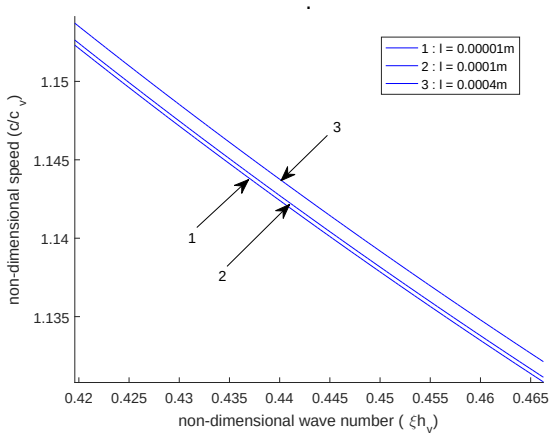

(a) For $PZT-5H$ ceramic

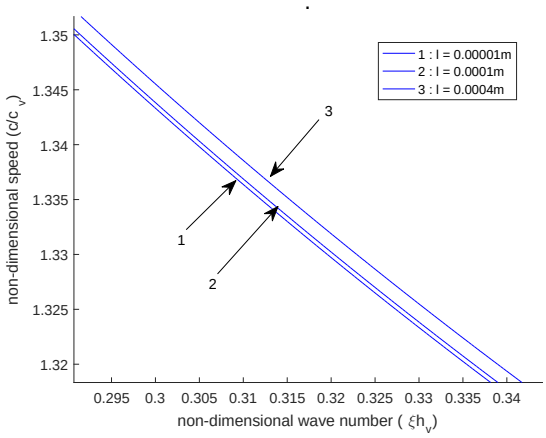

(b) For $BaTiO_3$ ceramic

Figure 4.3: Variation of non-dimensional damping phase velocity against non-dimensional wave number for distinct values of characteristic length in case of electrical open conditions.

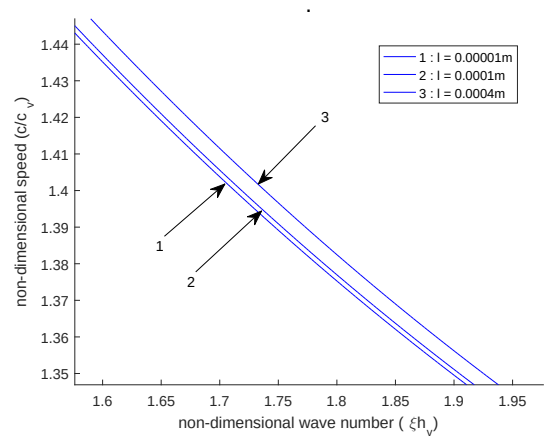

(a) For $PZT-5H$ ceramic

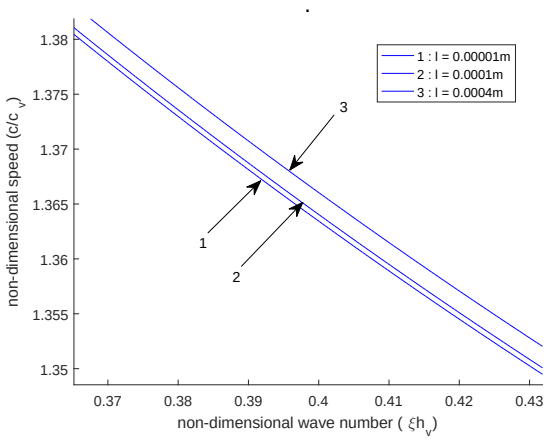

(b) For $BaTiO_3$ ceramic

Figure 4.4: Variation of non-dimensional real phase velocity against non-dimensional wave number for distinct values of characteristic length in case of electrical short conditions.

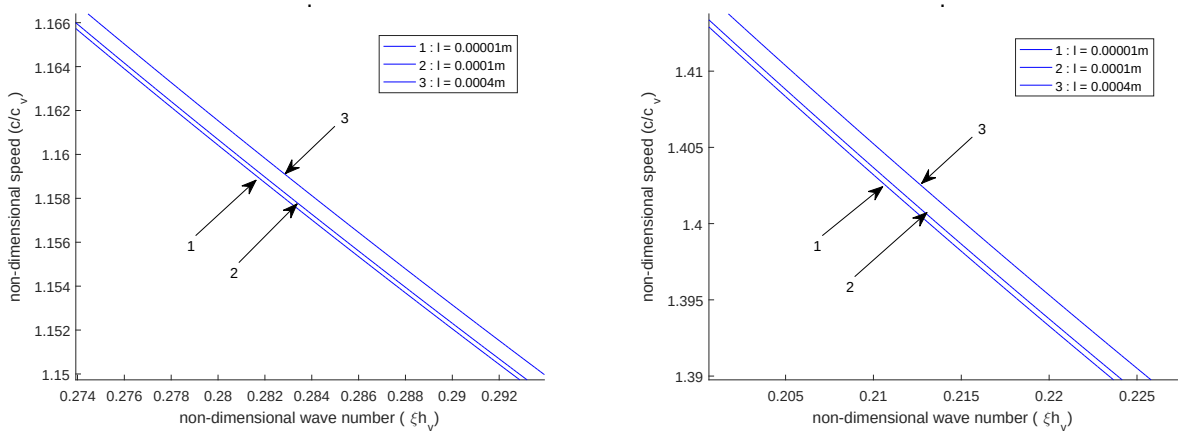

(a) For $PZT-5H$ ceramic (b) For $BaTiO_3$ ceramic

Figure 4.5: Variation of non-dimensional damping phase velocity against non-dimensional wave number for distinct values of characteristic length in case of electrical short conditions.

open conditions and figures 4.8 and 4.9 correspond to electrically short conditions, whereas figures 4.6(a), 4.7(a), 4.8(a), 4.9(a) are plotted for $PZT-5H$ material and 4.6(b), 4.7(b), 4.8(b), 4.9(b) are plotted for $BaTiO_3$ material.

4.2.10 Impact of internal friction of viscoelastic layer

Figures 4.10–4.13 demonstrate the effects of the internal friction parameter associated with viscoelastic layer sandwiched between a finite layer of piezoelectric medium and couple stress substrate. Here, figures are plotted by taking distinct values of internal friction parameter $\frac{\mu_1}{\eta_1} = 6\times10^5,\ 10\times10^5,\ 20\times10^5$ where $h_v = 0.02m$, $h_p = 0.02m$ and $l = 0.0004m$. The phase velocity profiles do not exhibit the favoring effect with the variation in friction parameter. Here, the real and damping phase speed of Love wave decreases with an increment in internal friction parameter. Figures 4.10, 4.11 and 4.12, 4.13 are plotted for electrically open and short conditions respectively.

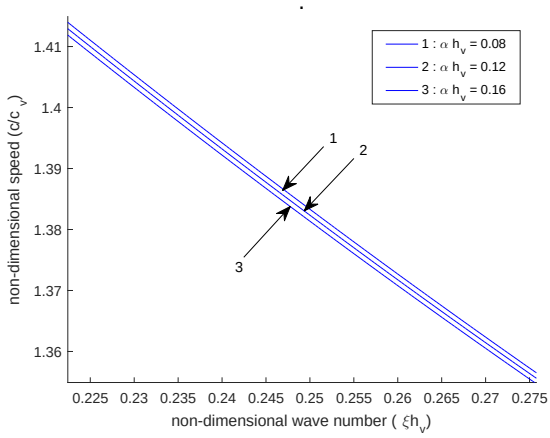

(a) For $PZT-5H$ ceramic

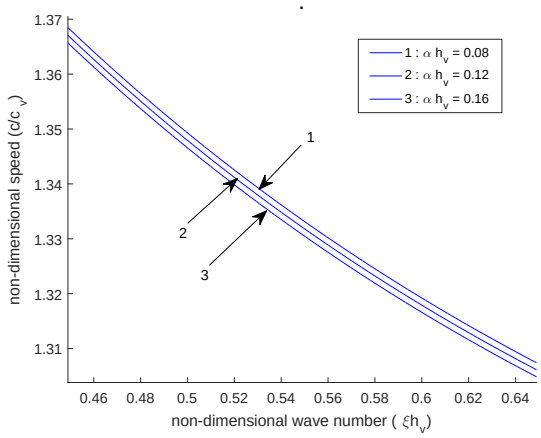

(b) For $BaTiO_3$ ceramic

Figure 4.6: Variation of non-dimensional real phase velocity against non-dimensional wave number for distinct values of non-dimensional heterogeneity parameter in case of electrical open conditions.

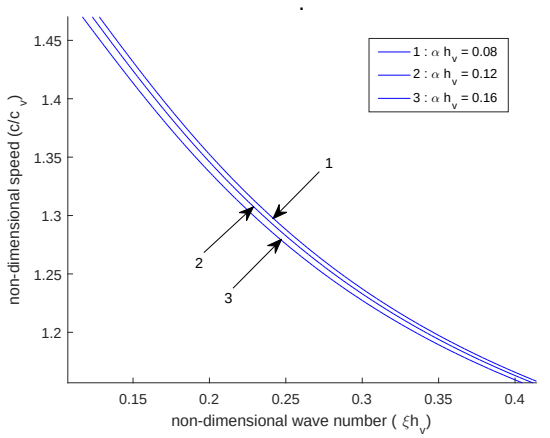

(a) For $PZT-5H$ ceramic

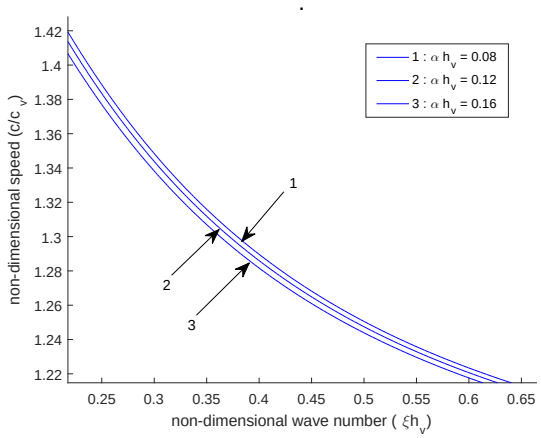

(b) For $BaTiO_3$ ceramic

Figure 4.7: Variation of non-dimensional damping phase velocity against non-dimensional wave number for distinct values of non-dimensional heterogeneity parameter in case of electrical open conditions.

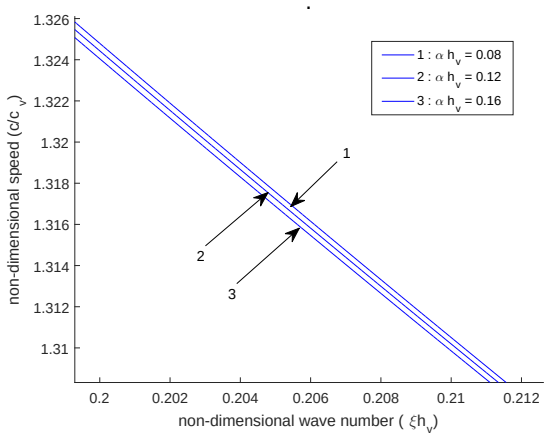

(a) For $PZT-5H$ ceramic

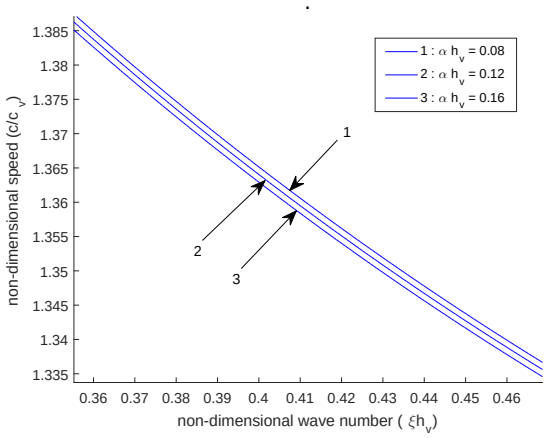

(b) For $BaTiO_3$ ceramic

Figure 4.8: Variation of non-dimensional real phase velocity against non-dimensional wave number for distinct values of non-dimensional heterogeneity parameter in case of electrical short conditions.

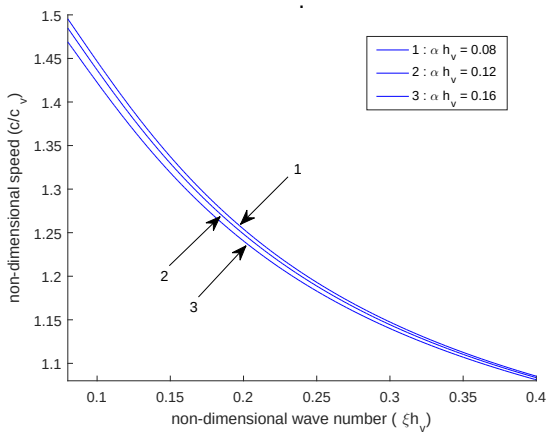

(a) For $PZT-5H$ ceramic

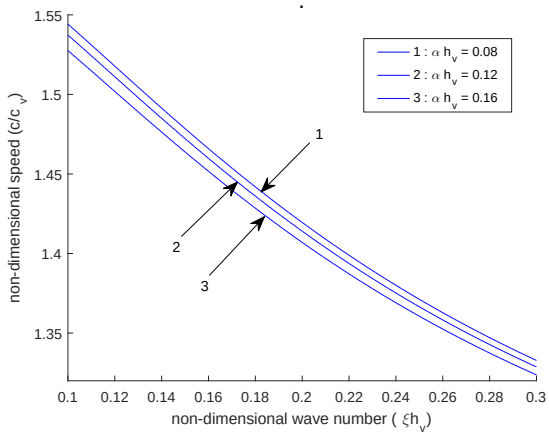

(b) For $BaTiO_3$ ceramic

Figure 4.9: Variation of non-dimensional damping phase velocity against non-dimensional wave number for distinct values of non-dimensional heterogeneity parameter in case of electrical short conditions.

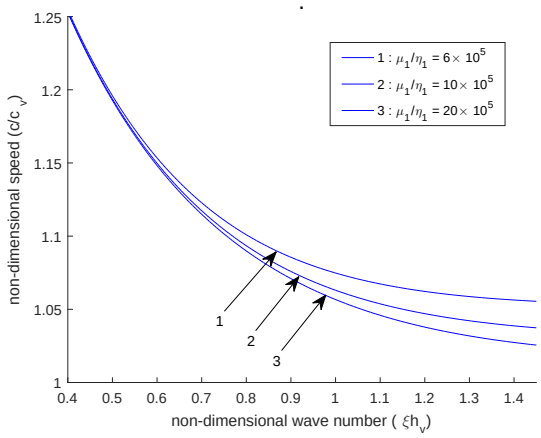

(a) For $PZT-5H$ ceramic

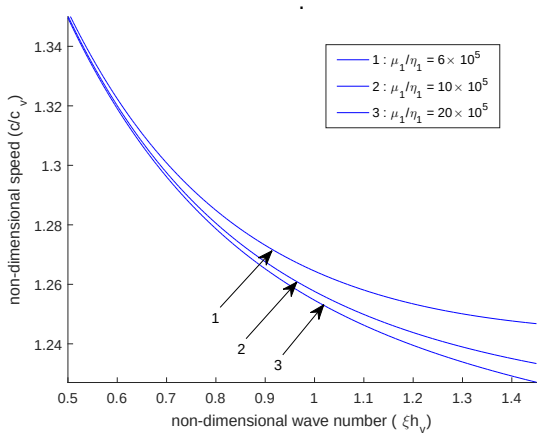

(b) For $BaTiO_3$ ceramic

Figure 4.10: Variation of non-dimensional real phase velocity against non-dimensional wave number for distinct values of internal friction parameter in case of electrical open conditions.

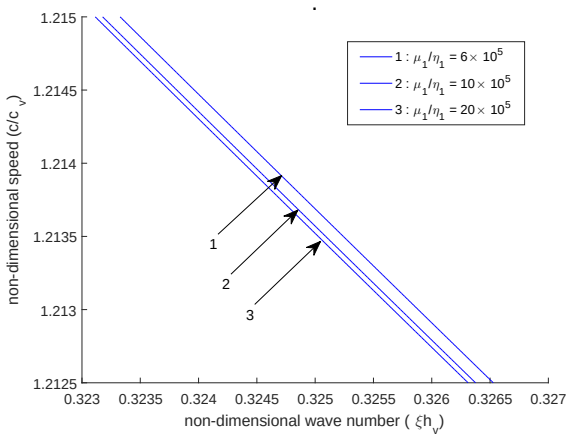

(a) For $PZT-5H$ ceramic

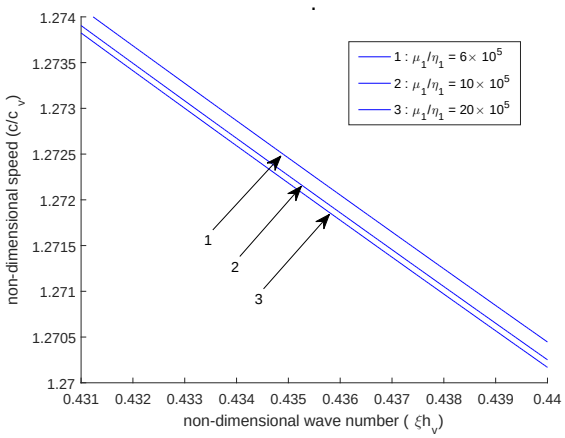

(b) For $BaTiO_3$ ceramic

Figure 4.11: Variation of non-dimensional damping phase velocity against non-dimensional wave number for distinct values of internal friction parameter in case of electrical open conditions.

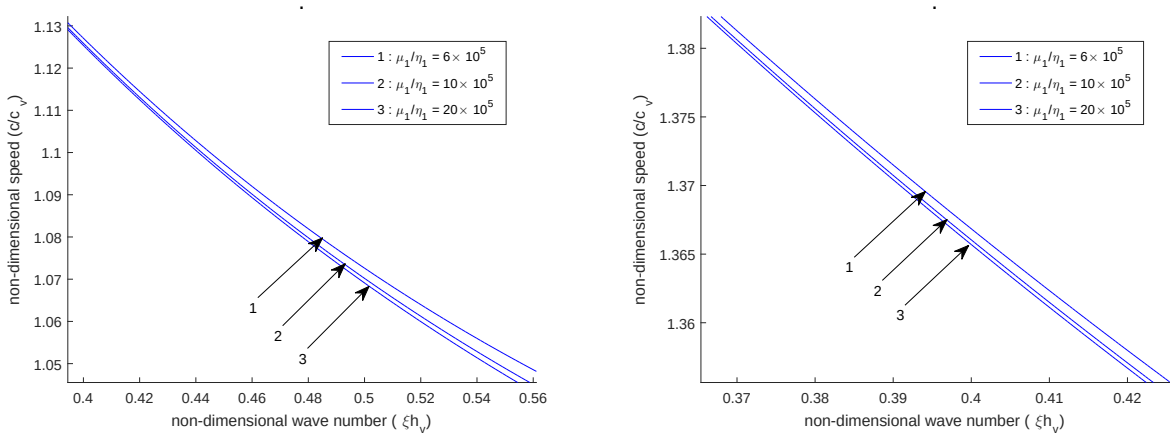

(a) For $PZT-5H$ ceramic (b) For $BaTiO_3$ ceramic

Figure 4.12: Variation of non-dimensional real phase velocity against non-dimensional wave number for distinct values of internal friction parameter in case of electrical short conditions.

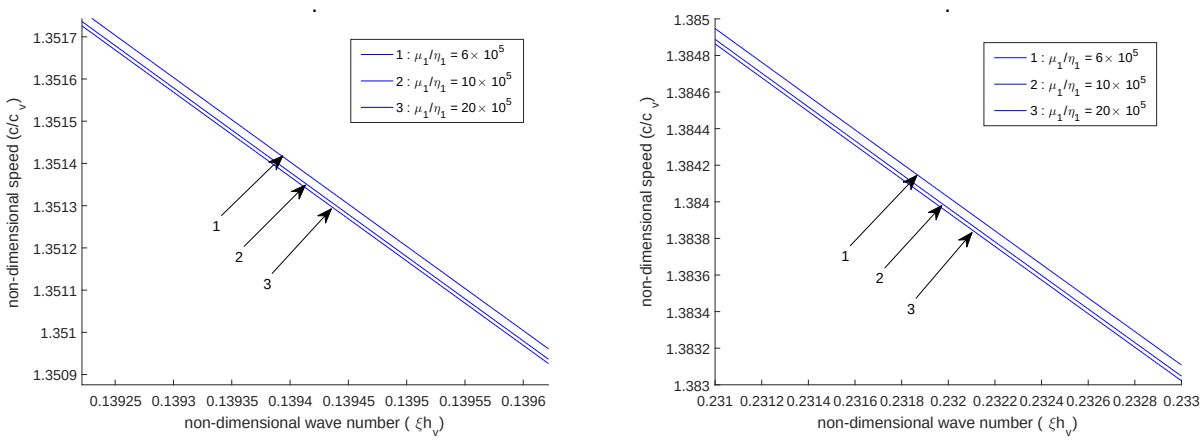

(a) For $PZT-5H$ ceramic (b) For $BaTiO_3$ ceramic

Figure 4.13: Variation of non-dimensional damping phase velocity against non-dimensional wave number for distinct values of internal friction parameter in case of electrical short conditions.

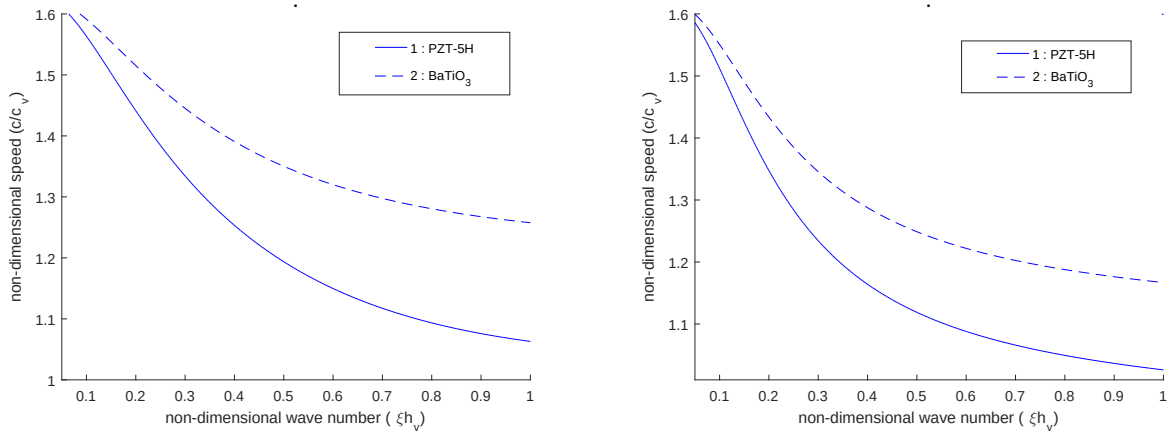

(a) For real (b) For damping

Figure 4.14: Real and damped phase speed versus wave number in case of electrically open conditions.

4.2.11 Impact of a piezoelectric layer material

In figures 4.14 and 4.15, the impact of piezoelectric medium is shown by considering two piezoelectric material, i.e., $PZT-5H$ and $BaTiO_3$ material. It can be observed that the phase speed for $PZT-5H$ material is less in comparison with $BaTiO_3$ piezoelectric material. Figures-4.14(a) and 4.15(a) correspond to real phase velocity and figures-4.14(b) and 4.15(b) correspond to damping phase velocity for both the taken materials of a piezoelectric layer.

4.2.12 Impact of Piezoelectric constant (e_{15})

Figures 4.16 and 4.17 elucidate the effects of piezoelectric constant on the real phase velocity profiles of Love-type wave propagation in composite double-layered structure. To address this effect, the dispersion curves are plotted by considering different values of piezoelectric parameter $e_{15} = 17C/m^2$, $21C/m^2$, $25C/m^2$ for piezoelectric $PZT-5H$ material and $e_{15} = 11C/m^2$, $15C/m^2$, $19C/m^2$ for piezoelectric $BaTiO_3$ material. The characteristic length is taken as $l = 0.0001m$; the thicknesses of the piezoelectric layer and the viscoelastic layer as $h_p = 0.02m$ and $h_v = 0.02m$ respectively. It can be observed from figures 4.16 and 4.17 that the piezoelectric parameter exhibits a

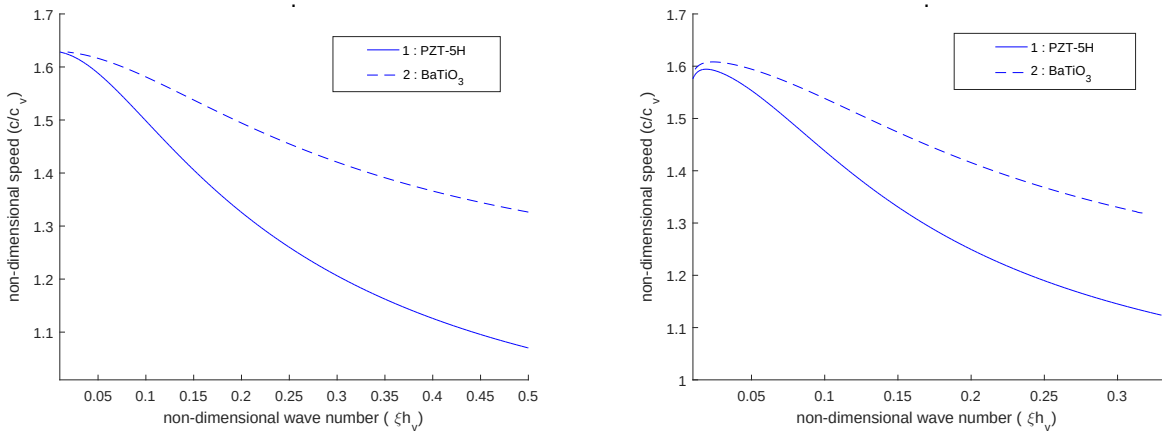

(a) For real (b) For damping

Figure 4.15: Real and damped phase speed versus wave number in case of electrically short conditions.

discouraging impact on the real phase velocity profiles of a Love-type wave for both the considered material of piezoelectric material under both cases of electrically open and short conditions.

4.2.13 Impact of Dielectric constant (ϵ_{11})

The effect of dielectric constant on the real phase velocity profiles of Love-type surface wave propagation in hybrid layered structure is shown in figures 4.18 and 4.19. To document this dielectric effect associated with piezoelectric medium, the distinct values of dielectric constant are considered as $277 \times 10^{-10} C^2/Nm^2$, $317 \times 10^{-10} C^2/Nm^2$ for $PZT - 5H$ material and $\epsilon_{11} = 98 \times 10^{-10} C^2/Nm^2$, $128 \times 10^{-10} C^2/Nm^2$, $158 \times 10^{-10} C^2/Nm^2$ for $BaTiO_3$ material. Here, the value of the characteristic length is taken as $l = 0.0001m$; the thicknesses of the piezoelectric layer and the viscoelastic layer as $h_p = 0.02m$ and $h_v = 0.02m$ respectively. It can be perceived from both the figures that the real phase velocity profiles increase with the increase in dielectric constant under both the cases of electrically open and short conditions.

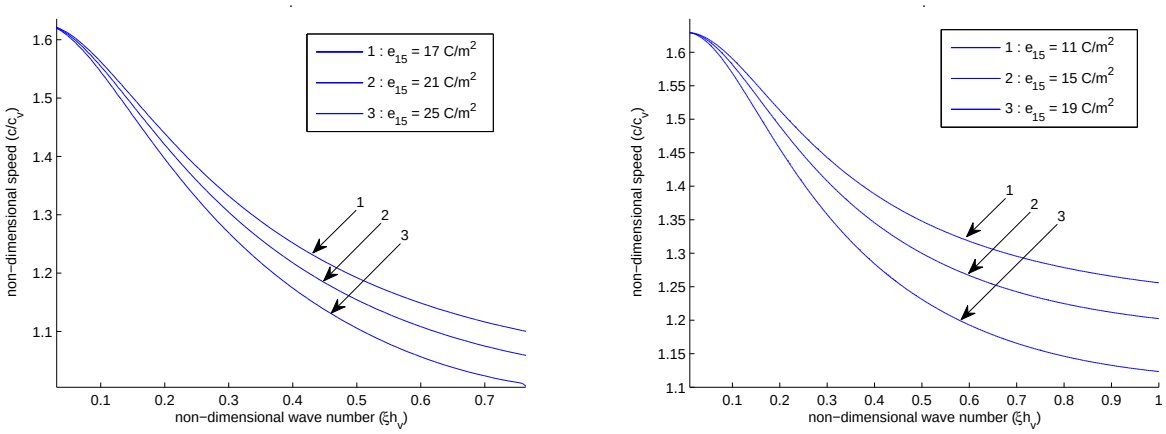

(a) For $PZT-5H$ ceramic (b) For $BaTiO_3$ ceramic

Figure 4.16: Variation of non-dimensional real phase velocity against non-dimensional wave number for different values of piezoelectric constant $e_{15} = 17C/m^2$, $21C/m^2$, $25C/m^2$ in (a) and $e_{15} = 11C/m^2$, $15C/m^2$, $19C/m^2$ in (b), when h_v=0.02m, h_p=0.02m, $l = 0.0001m$ in case of electrical open conditions.

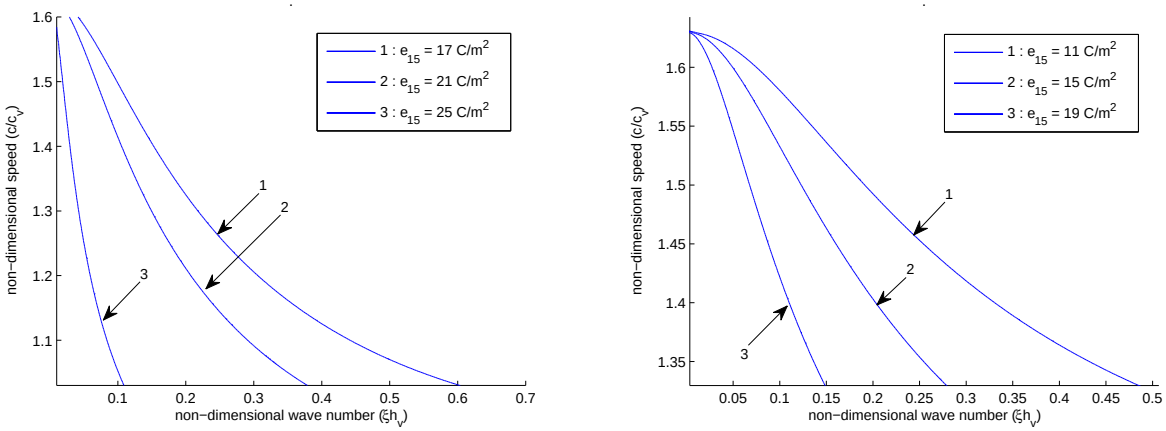

(a) For $PZT-5H$ ceramic (b) For $BaTiO_3$ ceramic

Figure 4.17: Variation of non-dimensional real phase velocity against non-dimensional wave number for different values of piezoelectric constant $e_{15} = 17C/m^2$, $21C/m^2$, $25C/m^2$ in (a) and $e_{15} = 11C/m^2$, $15C/m^2$, $19C/m^2$ in (b), when h_v=0.02m, h_p=0.02m, $l = 0.0001m$ in case of electrical short conditions.

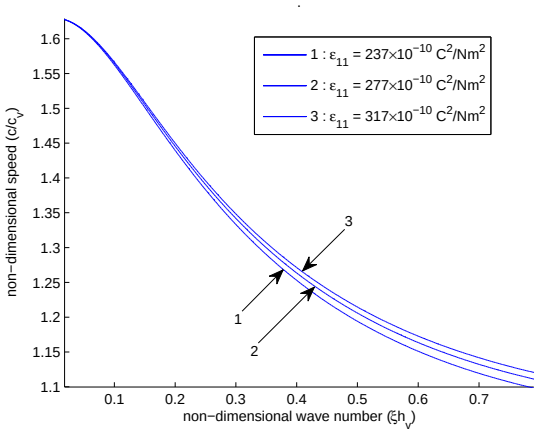

(a) For $PZT-5H$ ceramic

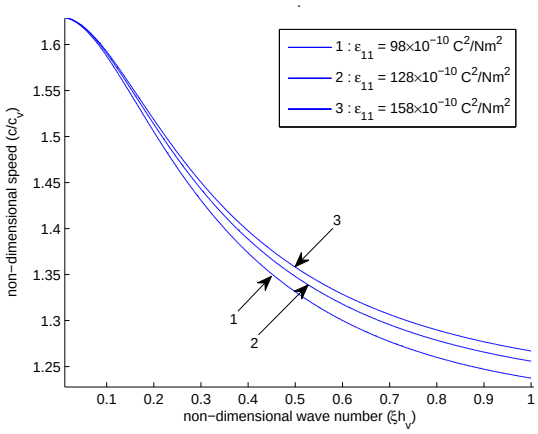

(b) For $BaTiO_3$ ceramic

Figure 4.18: Variation of non-dimensional real phase velocity against non-dimensional wave number for different values of dielectric constant $\epsilon_{11} = 237 \times 10^{-10}C^2/Nm^2$, $277 \times 10^{-10}C^2/Nm^2$, $317 \times 10^{-10}C^2/Nm^2$ in (a) and $\epsilon_{11} = 98 \times 10^{-10}C^2/Nm^2$, $128 \times 10^{-10}C^2/Nm^2$, $158 \times 10^{-10}C^2/Nm^2$ in (b), when h_v=0.02m, h_p=0.02m, $l = 0.0001m$ in case of electrical open conditions.

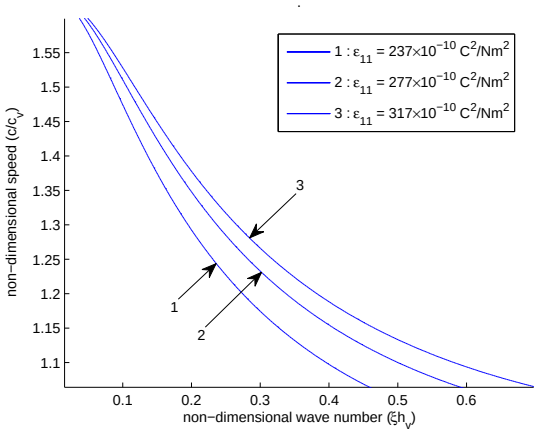

(a) For $PZT-5H$ ceramic

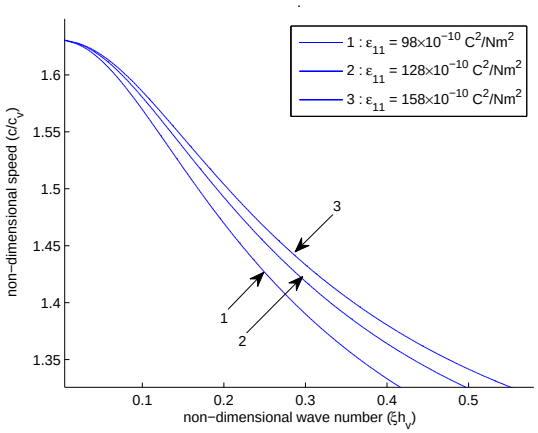

(b) For $BaTiO_3$ ceramic

Figure 4.19: Variation of non-dimensional real phase velocity against non-dimensional wave number for different values of dielectric constant $\epsilon_{11} = 237 \times 10^{-10}C^2/Nm^2$, $277 \times 10^{-10}C^2/Nm^2$, $317 \times 10^{-10}C^2/Nm^2$ in (a) and $\epsilon_{11} = 98 \times 10^{-10}C^2/Nm^2$, $128 \times 10^{-10}C^2/Nm^2$, $158 \times 10^{-10}C^2/Nm^2$ in (b), when h_v=0.02m, h_p=0.02m, $l = 0.0001m$ in case of electrical short conditions.

4.3 Dispersion of Love-type waves in size-dependent micropolar substrate containing finite piezoelectric and viscoelastic layers

4.3.1 Formulation of the problem

Consider a double-layered structure consisting of a viscoelastic layer and a piezoelectric layer lying over a semi-infinite micropolar substrate. The rectangular Cartesian coordinate system is considered in such a way that the Love wave is propagating along the y-axis and x-axis is pointing positive vertically downward as shown in figure 4.20. The common interface is chosen between a viscoelastic layer and a micropolar elastic half-space in the direction of y-axis; The thickness of a piezoelectric layer and a viscoelastic layer is h_p and h_v respectively. The poling direction of the piezoelectric layer is considered along the z-axis. Let $u_i^{(p)}=(u_p, v_p, w_p)$; $u_i^{(v)}=(u_v, v_v, w_v)$ and

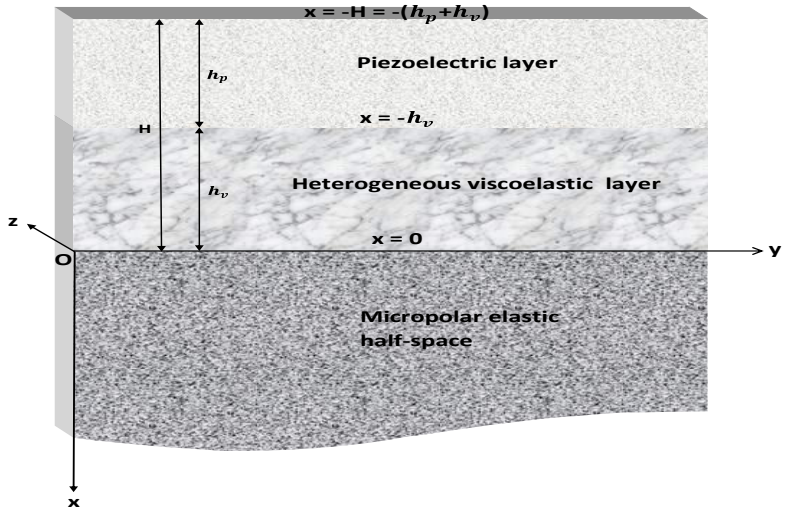

Figure 4.20: Geometry of the problem.

$u_i^{(m)}=(u_m, v_m, w_m)$ are the mechanical displacement components in the upper piezoelectric layer; the middle viscoelastic layer and the lower semi-infinite micropolar substrate respectively, due to the propagation of Love wave.

As Love type wave is propagating along the direction of y-axis, it causes displacement in z-direction only. One may suppose that

$$\begin{aligned} u_p = 0,\ v_p = 0,\ w_p = w_p(x, y, t), \\ u_v = 0,\ v_v = 0,\ w_v = w_v(x, y, t), \\ u_m = 0,\ v_m = 0,\ w_m = w_m(x, y, t). \end{aligned} \tag{4.51}$$

By following the procedure adopted in section 2.2.1 of Chapter-2, in section 3.2.1 of Chapter-3 and in section 4.2.2 of Chapter-4 the mechanical displacement component for piezoelectric material layer, for the micropolar medium and for viscoelastic medium are

$$w_p(x, y, t) = [A_1 \sin(\xi a x) + A_2 \cos(\xi a x)] e^{\iota\xi(y-ct)}, \tag{4.52}$$

$$\phi^{(p)}(x, y, t) = \left[\frac{e_{15}}{\epsilon_{11}}[A_1 \sin(\xi a x) + A_2 \cos(\xi a x)] + A_3 e^{-\xi x} + A_4 e^{\xi x}\right] e^{\iota\xi(y-ct)}, \tag{4.53}$$

$$w_v = \frac{1}{\sqrt{\overline{\mu_1}}\sqrt{1 - \sin \alpha x}} (D_1 \cos mx + D_2 \sin mx) e^{\iota\xi(y-ct)}, \tag{4.54}$$

$$w_m(x, y, t) = (\wp_1 e^{-sx} B_2 + \wp_2 e^{-tx} B_3) e^{\iota\xi(y-ct)}, \tag{4.55}$$

$$\phi_1^{(m)} = (-re^{-rx} B_1 - \iota\xi e^{-sx} B_2 - \iota\xi e^{-tx} B_3) e^{\iota\xi(y-ct)}, \tag{4.56}$$

$$\phi_2^{(m)} = (\iota\xi e^{-rx} B_1 - se^{-sx} B_2 - te^{-tx} B_3) e^{\iota\xi(y-ct)}. \tag{4.57}$$

The notations and symbols are same as used in sections 2.2.1, 3.2.1, 4.2.2 of Chapter-2, 3 and 4, respectively.

4.3.2 Boundary conditions

The following boundary conditions are to be satisfied for the propagation of Love-type wave in the considered hybrid model.

(A) For the traction-free surface of the piezoelectric layer at $x = -H = -(h_v + h_p)$:

$$\sigma_{zx}^{(p)} = 0, \tag{4.58}$$

$$D_x = 0 \quad (\textit{electrically open condition}), \tag{4.59}$$

$$\phi^{(p)} = 0 \quad (\textit{electrically short condition}). \tag{4.60}$$

(B) For the common interface of viscoelastic layer and piezoelectric layer at $x = -h_v$:

$$\sigma_{zx}^{(p)} = \sigma_{zx}^{(v)}, \tag{4.61}$$

$$w_p = w_v, \tag{4.62}$$

$$\phi^{(p)} = 0. \tag{4.63}$$

(C) For the common interface of viscoelastic layer and micropolar elastic substrate at $x = 0$:

$$\sigma_{zx}^{(v)} = \sigma_{zx}^{(m)}, \tag{4.64}$$

$$w_v = w_m, \tag{4.65}$$

$$m_{xy} = 0, \tag{4.66}$$

$$m_{xx} = 0. \tag{4.67}$$

Using the mechanical displacement components, electrical displacement components and their corresponding stresses into the boundary equations (4.58)-(4.67), one can obtain the following algebraic equations in terms of unknown coefficients A_1, A_2, A_3, A_4, D_1, D_2, B_1, B_2 and B_3.

$$ac_{44}^{*}\cos(\xi aH)A_1 + ac_{44}^{*}\sin(\xi aH)A_2 - e_{15}e^{(\xi H)}A_3 + e_{15}e^{(-\xi H)}A_4 = 0, \tag{4.68}$$

$$e^{(\xi H)}A_3 - e^{(-\xi H)}A_4 = 0, \tag{4.69}$$

$$-\frac{e_{15}}{\epsilon_{11}}\sin(\xi aH)A_1 + \frac{e_{15}}{\epsilon_{11}}\cos(\xi aH)A_2 + e^{(\xi H)}A_3 + e^{(-\xi H)}A_4 = 0, \tag{4.70}$$

$$\begin{aligned}\xi ac_{44}^{*}\cos(\xi ah_v)A_1 + \xi ac_{44}^{*}\sin(\xi ah_v)A_2 - \xi e_{15}e^{(\xi h_v)}A_3 + \xi e_{15}e^{(-\xi h_v)}A_4 \\ -\frac{\sqrt{\mu_1}}{2\sqrt{1+\sin\alpha h_v}}T_1D_1 - \frac{\sqrt{\mu_1}}{2\sqrt{1+\sin\alpha h_v}}T_2D_2 = 0,\end{aligned} \tag{4.71}$$

$$\sin(\xi a h_v)A_1 - \cos(\xi a h_v)A_2 + \frac{\cos(m h_v)}{\sqrt{\overline{\mu_1}}\sqrt{1+\sin\alpha h_v}}D_1 - \frac{\sin(m h_v)}{\sqrt{\overline{\mu_1}}\sqrt{1+\sin\alpha h_v}}D_2 = 0, \quad (4.72)$$

$$-\frac{e_{15}}{\epsilon_{11}}\sin(\xi a h_v)A_1 + \frac{e_{15}}{\epsilon_{11}}\cos(\xi a h_v)A_2 + e^{(\xi h_v)}A_3 + e^{(-\xi h_v)}A_4 = 0, \quad (4.73)$$

$$\frac{\alpha\sqrt{\overline{\mu_1}}}{2}D_1 + m\sqrt{\overline{\mu_1}}D_2 + \iota\xi\kappa_m B_1 + \wp_3 B_2 + \wp_4 B_3 = 0, \quad (4.74)$$

$$\frac{1}{\sqrt{\overline{\mu_1}}}D_1 - \wp_1 B_2 - \wp_2 B_3 = 0, \quad (4.75)$$

$$\iota\wp_5 B_1 + \wp_6 B_2 + \wp_7 B_3 = 0, \quad (4.76)$$

$$\wp_8 B_1 + \iota\wp_9 B_2 + \iota\wp_{10} B_3 = 0. \quad (4.77)$$

The notations and symbols are same as used in Chapter-2, 3 and 4, respectively.

4.3.3 Dispersion equations for electrically open conditions

The conditions mentioned in equations (4.68)–(4.69) and (4.71)–(4.77) constitute nine boundary conditions for this case. To obtain a non-trivial solution, determinant of the coefficients of the unknowns A_1, A_2, A_3, A_4, D_1, D_2, B_1, B_2 and B_3 should vanish. The frequency equation for Love-wave in case of electrically open conditions is obtained as:

$$\xi\left[\frac{e_{15}^2}{\epsilon_{11}}\cos(\xi a h_p)\sinh(\xi h_p) + a c_{44}^{*}\sin(\xi a h_p)\cosh(\xi h_p)\right]M_1 + \left[\cos(\xi a h_p)\cosh(\xi h_p)\right]M_2 = 0, \quad (4.78)$$

where

$$M_1 = \frac{1}{\sqrt{1+\sin(\alpha h_v)}}\left(\frac{1}{\overline{\mu_1}}\wp_{14}\sin(m h_v) - \frac{1}{2}\alpha\wp_{15}\sin(m h_v) - m\wp_{15}\cos(m h_v)\right) = G_1 + \iota G_2,$$

$$M_2 = \frac{1}{4\sqrt{1+\sin(\alpha h_v)}}\left(-2m\overline{\mu_1}\wp_{15}T_1 + \alpha\overline{\mu_1}\wp_{15}T_2 - 2\wp_{14}T_2\right) = G_5 + \iota G_6.$$

$$G_1 = \frac{1}{\sqrt{1+\sin(\alpha h_v)}}\left(-\wp_{15}(m_1 E_1 + m_2 E_2) - \frac{1}{2}\alpha\wp_{15}S_1 + \wp_{14}\frac{(\mu_1 S_1 - \omega\eta_1 S_2)}{\mu_1^2 + \omega^2\eta_1^2}\right),$$

$$G_2 = \frac{1}{\sqrt{1+\sin(\alpha h_v)}}\bigg(- \wp_{15}(m_2E_1 - m_1E_2) - \frac{1}{2}\alpha\wp_{15}S_2 + \wp_{14}\frac{(\mu_1 S_2 + \omega\eta_1 S_1)}{\mu_1^2+\omega^2\eta_1^2}\bigg).$$

$$G_3 = (m_1\mu_1 + m_2\omega\eta_1)J_1 - (m_2\mu_1 - m_1\omega\eta_1)I_1,$$

$$G_4 = (m_2\mu_1 - m_1\omega\eta_1)J_1 + (m_1\mu_1 + m_2\omega\eta_1)I_1.$$

$$G_5 = \frac{1}{\sqrt{1+\sin(\alpha h_v)}}\bigg(\frac{1}{4}\alpha\wp_{15}(\mu_1 J_2 + \omega\eta_1 I_2) - \frac{1}{2}\wp_{15}G_3 - \frac{1}{2}\wp_{14}J_2\bigg),$$

$$G_6 = \frac{1}{\sqrt{1+\sin(\alpha h_v)}}\bigg(\frac{1}{4}\alpha\wp_{15}(\mu_1 I_2 - \omega\eta_1 J_2) - \frac{1}{2}\wp_{15}G_4 - \frac{1}{2}\wp_{14}I_2\bigg).$$

Now, comparing real and imaginary parts on both sides of equation (4.78), one may have

$$\begin{aligned}\xi\bigg[\frac{e_{15}^2}{\epsilon_{11}}\cos(\xi a h_p)\sinh(\xi h_p) + ac_{44}^*\sin(\xi a h_p)\cosh(\xi h_p)\bigg]G_1 \\ +\bigg[\cos(\xi a h_p)\cosh(\xi h_p)\bigg]G_5 = 0,\end{aligned} \tag{4.79}$$

and

$$\begin{aligned}\xi\bigg[\frac{e_{15}^2}{\epsilon_{11}}\cos(\xi a h_p)\sinh(\xi h_p) + ac_{44}^*\sin(\xi a h_p)\cosh(\xi h_p)\bigg]G_2 \\ +\bigg[\cos(\xi a h_p)\cosh(\xi h_p)\bigg]G_6 = 0.\end{aligned} \tag{4.80}$$

Equations (4.79) and (4.80) represent the dispersion relations for the real and damped phase velocity equation of Love wave in an electrical open circuit for a viscoelastic layer and a piezoelectric layer lying over micropolar elastic half-space.

4.3.4 Dispersion equations for electrically short conditions

The conditions mentioned in equations (4.58) and (4.60)–(4.67) constitute nine boundary conditions for this case. To obtain a non-trivial solution, the determinant of the coefficients of the unknowns A_1, A_2, A_3, A_4, D_1, D_2, B_1, B_2 and B_3 should vanish. The frequency equation for Love wave in case of electrically short conditions is

obtained as:

$$\left[2ac_{44}^{*}\frac{e_{15}^{2}}{\epsilon_{11}}\left(1-\cos(\xi ah_p)\cosh(\xi h_p)\right)-\left(a^2{c_{44}^{*}}^2-\frac{e_{15}^{4}}{\epsilon_{11}^{2}}\right)\sin(\xi ah_p)\sinh(\xi h_p)\right]\xi M_1$$
$$-\left[ac_{44}^{*}\cos(\xi ah_p)\sinh(\xi h_p)-\frac{e_{15}^{2}}{\epsilon_{11}}\sin(\xi ah_p)\cosh(\xi h_p)\right]M_2=0. \quad (4.81)$$

Now, comparing real and imaginary parts on both sides of equation (4.81), one may have

$$\left[2ac_{44}^{*}\frac{e_{15}^{2}}{\epsilon_{11}}\left(1-\cos(\xi ah_p)\cosh(\xi h_p)\right)-\left(a^2{c_{44}^{*}}^2-\frac{e_{15}^{4}}{\epsilon_{11}^{2}}\right)\sin(\xi ah_p)\sinh(\xi h_p)\right]\xi G_1$$
$$-\left[ac_{44}^{*}\cos(\xi ah_p)\sinh(\xi h_p)-\frac{e_{15}^{2}}{\epsilon_{11}}\sin(\xi ah_p)\cosh(\xi h_p)\right]G_5=0, \quad (4.82)$$

and

$$\left[2ac_{44}^{*}\frac{e_{15}^{2}}{\epsilon_{11}}\left(1-\cos(\xi ah_p)\cosh(\xi h_p)\right)-\left(a^2{c_{44}^{*}}^2-\frac{e_{15}^{4}}{\epsilon_{11}^{2}}\right)\sin(\xi ah_p)\sinh(\xi h_p)\right]\xi G_2$$
$$-\left[ac_{44}^{*}\cos(\xi ah_p)\sinh(\xi h_p)-\frac{e_{15}^{2}}{\epsilon_{11}}\sin(\xi ah_p)\cosh(\xi h_p)\right]G_6=0. \quad (4.83)$$

Equations (4.82) and (4.83) represent the dispersion relations for the real and damped velocity equation of Love wave in case of electrically short conditions for a viscoelastic layer and a piezoelectric layer overlying micropolar elastic half-space.

4.3.5 Validation

Case-1: Considering the thickness of piezoelectric layer to be zero, i.e., $h_p = 0$, the dispersion equation (4.78) reduces to

$$M_2 = 0. \quad (4.84)$$

On solving equation (4.84), one may obtain the dispersion relation for Love wave in heterogeneous viscoelastic layer bonded perfectly to semi-infinite micropolar elastic

substrate.

$$\tan(m_1 h_v) = \frac{\wp_{26} + \wp_{29}\tanh(m_2 h_v)}{\wp_{28} + \wp_{27}\tanh(m_2 h_v)}, \tag{4.85}$$

and

$$\tan(m_1 h_v) = \frac{-\wp_{27} - \wp_{28}\tanh(m_2 h_v)}{\wp_{29} + \wp_{26}\tanh(m_2 h_v)}, \tag{4.86}$$

where

$$\wp_{16} = m_1\mu_1 + m_2\omega\eta_1, \quad \wp_{17} = m_2\mu_1 - m_1\omega\eta_1, \quad \wp_{18} = \alpha\mu_1\wp_{15} - 2\wp_{14},$$

$$\wp_{19} = \alpha\omega\eta_1\wp_{15}, \quad \wp_{20} = -2\wp_{15}\wp_{16}, \quad \wp_{21} = 2\wp_{15}\wp_{17},$$

$$\wp_{22} = m_1\wp_{18} + m_2\wp_{19}, \quad \wp_{23} = m_2\wp_{18} - m_1\wp_{19}, \quad \wp_{24} = m_1\wp_{20} + m_2\wp_{21},$$

$$\wp_{25} = m_1\wp_{21} - m_2\wp_{20}, \quad \wp_{26} = -(\alpha\wp_{20} + \widetilde{A}\wp_{22}), \quad \wp_{27} = \widetilde{A}\wp_{23} - \alpha\wp_{21},$$

$$\wp_{28} = \widetilde{A}\wp_{24} - \alpha\wp_{18}, \quad \wp_{29} = \alpha\wp_{19} - \widetilde{A}\wp_{25}, \quad \widetilde{A} = 2(1 + \csc(\alpha h_v))\tan(\alpha h_v).$$

Equations (4.85) and (4.86) represent the real and damping phase velocity dispersion equations for Love wave propagation in vertically heterogeneous viscoelastic layer lying over the semi-infinite micropolar substrate. These equations are the same as obtained and discussed by Kaur et al. [91].

Case-2: On pondering previous case and considering heterogeneity parameter to be zero, i.e., $\alpha = 0$ in equation (4.84), the dispersion relation for Love wave in a homogeneous viscoelastic layer lying over micropolar elastic half-space is obtained as:

$$\left[(m_1\mu_1 + m_2\omega\eta_1)J_1^{'} - (m_2\mu_1 - m_1\omega\eta_1)I_1^{'}\right]\wp_{15} + J_2^{'}\wp_{14} = 0, \tag{4.87}$$

and

$$\left[(m_2\mu_1 - m_1\omega\eta_1)J_1^{'} + (m_1\mu_1 + m_2\omega\eta_1)I_1^{'}\right]\wp_{15} + I_2^{'}\wp_{14} = 0. \tag{4.88}$$

Equations (4.87) and (4.88) represent the dispersion relations for the real and damping phase velocity equations in homogeneous viscoelastic layered structure.

Case-3: On considering the thickness of viscoelastic medium layer, heterogeneity

parameter and internal friction parameter to be zero, i.e., $h_v = 0$, $\alpha = 0$, $\eta_1 = 0$ respectively, the dispersion equations (4.78) and (4.81) reduce to

$$\left[\xi\frac{e_{15}^2}{\epsilon_{11}}\tanh(\xi h_p) + \xi a c_{44}^* \tan(\xi a h_p)\right]\wp_{15} + \wp_{14} = 0, \tag{4.89}$$

and

$$\begin{aligned}\left[a c_{44}^* \tanh(\xi h_p) - \frac{e_{15}^2}{\epsilon_{11}}\tan(\xi a h_p)\right]\wp_{14} + 2\xi a\left[1 - \frac{\sec(\xi a h_p)}{\cosh(\xi h_p)}\right]c_{44}^*\wp_{15}\frac{e_{15}^2}{\epsilon_{11}} \\ +\xi\left[a^2 {c_{44}^*}^2 - \frac{e_{15}^4}{\epsilon_{11}^2}\right]\tan(\xi a h_p)\tanh(\xi h_p)\wp_{15} = 0.\end{aligned} \tag{4.90}$$

Equations (4.89) and (4.90) represent the dispersion relations for Love wave propagation in piezoelectric layer lying over micropolar elastic half-space for both the cases of electrically open and short conditions respectively. It is same as obtained in sections 3.4 and 3.5 in Chapter-3.

Case-4: On considering the previous case and in the absence of piezoelectric parameter, i.e., $e_{15} = 0$ and $c_{44}^* \to c_{44}$, equations (4.89)–(4.90) reduce to Love-type wave propagation in isotropic elastic layer lying over the micropolar elastic half-space.

$$\xi c_{44}\sqrt{\frac{c^2}{\overline{c_p^2}} - 1}\tan\left(\xi H\sqrt{\frac{c^2}{\overline{c_p^2}} - 1}\right) = -\frac{\wp_{14}}{\wp_{15}}, \tag{4.91}$$

where

$$\overline{c_p} = \sqrt{\frac{c_{44}}{\rho_p}}.$$

where equation (4.91) matches with the equation (3.43) of section 3.6 in Chapter-3.

Case-5: Pondering the previous case and α_m, β_m, γ_m and $\kappa_m \to 0$, i.e., the micropolar elastic half-space reduces to isotropic elastic half-space $\theta_2 \to c_m$ and $\frac{\wp_{14}}{\wp_{15}} \to -\xi\mu_m\sqrt{1 - \frac{c^2}{c_m^2}}$; equation (4.91) reduces to

$$\tan\left(\xi H\sqrt{\frac{c^2}{\overline{c_p^2}} - 1}\right) = \frac{\mu_m\sqrt{1 - \frac{c^2}{c_m^2}}}{c_{44}\sqrt{\frac{c^2}{\overline{c_p^2}} - 1}}. \tag{4.92}$$

Equation (4.92) represents the dispersion relation for Love-type wave propagation in isotropic elastic layer lying over the isotropic elastic substrate which matches with the well-known Classical Love wave [122] equation which validates the outcome of the present problem.

4.3.6 Numerical results

The values of the material parameters for piezoelectric medium, micropolar medium and viscoelastic medium are taken from Tables 2.2, 3.1, 4.1 which is provided in Chapter-2, 3 and 4, respectively. Equations (4.78) and (4.81) represent the dispersion relations which provides an implicit relation between the real ((4.79), (4.82)) and the damping ((4.80), (4.83)) phase velocity of Love wave in the layered structure consisting of a viscoelastic layer and a piezoelectric layer lying over a semi-infinite micropolar substrate. The characteristic curves are plotted for non-dimensional real and damping phase velocity (c/c_v) against non-dimensional wave number (ξh_v) by considering two different materials of piezoelectric media, i.e., $PZT-5H$ and $BaTiO_3$ materials. In all the figures 4.21–4.43, it is observed that the real and the damping phase velocity decreases with the increase in wave number in both the cases of electrically open and short conditions. The profiles of an electrically open conditions are shown in figures 4.21, 4.22, 4.25, 4.26, 4.30, 4.31, 4.34, 4.35, 4.38, 4.40, 4.42 and the profiles of the electrically short conditions are shown in figures 4.23, 4.24, 4.27, 4.28, 4.32, 4.33, 4.36, 4.37, 4.39, 4.41, 4.43.

4.3.7 Effect of coupling constant (N)

The effect of the coupling constant that quantifies the degree of micropolarity in micropolar media is shown in figures 4.21–4.24. The dispersion curves are plotted by considering different values of micropolar constant, i.e., $N = 0.1, 0.6, 0.9$ to show the microstructural effect of the semi-infinite substrate for both the cases of electrically open and short conditions. Here, the characteristic length of material is considered as $l = 0.0001m$, and the thickness of viscoelastic and piezoelectric medium is taken

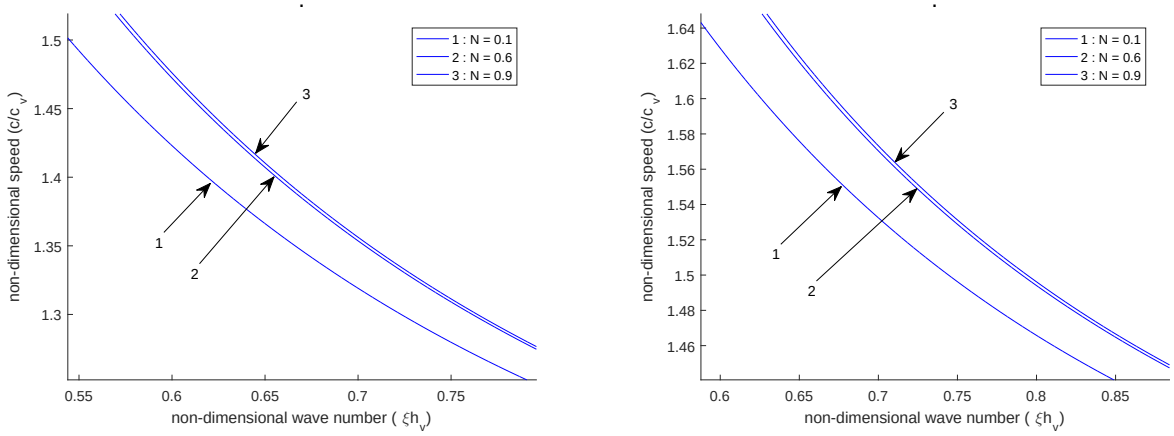

(a) For $PZT-5H$ ceramic

(b) For $BaTiO_3$ ceramic

Figure 4.21: Variation of non-dimensional real phase velocity against non-dimensional wave number for different values of micropolar constant $N = 0.1, 0.6, 0.9$ when h_v=0.02m, h_p=0.02m in case of electrical open conditions.

as $h_v = 0.02m$ and $h_p = 0.02m$ respectively. It is observed that the micropolarity of the substrate affects the phase velocity profiles significantly. As the degree of micropolarity (N) increases, the phase velocity profiles of the Love wave increases for both the considered materials of piezoelectric materials. Figures 4.21 and 4.22 show the phase velocity profiles for electrically open conditions and figures 4.23 and 4.24 show the phase velocity profiles for the electrical short conditions.

4.3.8 Effect of characteristic length (l)

To study the effect of intrinsic characteristic length associated with micropolar media, the different values of characteristic length are considered as $l = 0.0001m$, $0.0002m$, $0.0003m$. Here, the thickness of a piezoelectric layer and a viscoelastic layer is taken as $h_p = 0.02m$ and $h_v = 0.02m$ respectively. The real and damping phase velocity profiles are affected significantly with the variation in characteristic length. From figures 4.25–4.28, it is observed that the real and damping phase velocity profiles of the Love wave increase with an increase in characteristic length. The dispersion in characteristic profiles clearly indicates the size effects observed for the propagation of Love wave in a double-layered structure with the microstructural substrate. The

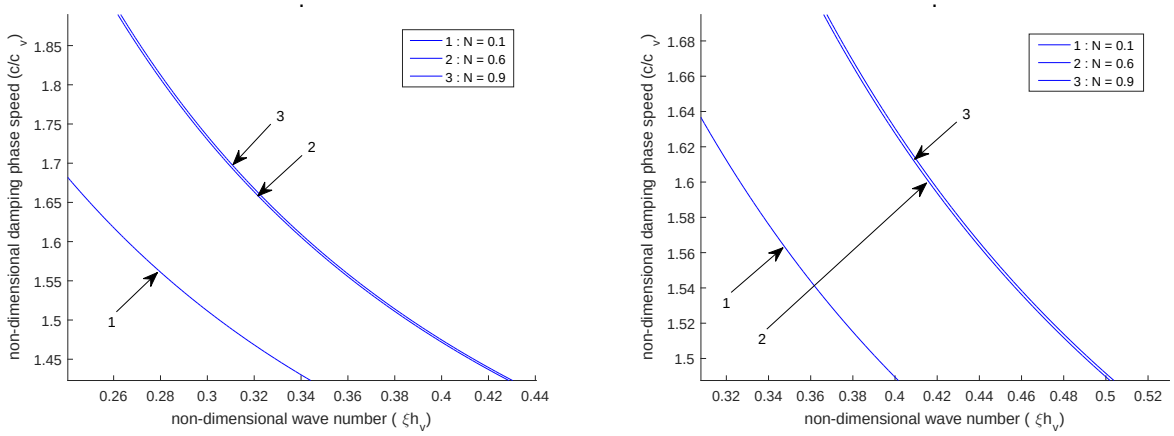

(a) For $PZT-5H$ ceramic (b) For $BaTiO_3$ ceramic

Figure 4.22: Variation of non-dimensional damping phase velocity against non-dimensional wave number for different values of micropolar constant $N = 0.1, 0.6, 0.9$ when h_v=0.02m, h_p=0.02m in case of electrical open conditions.

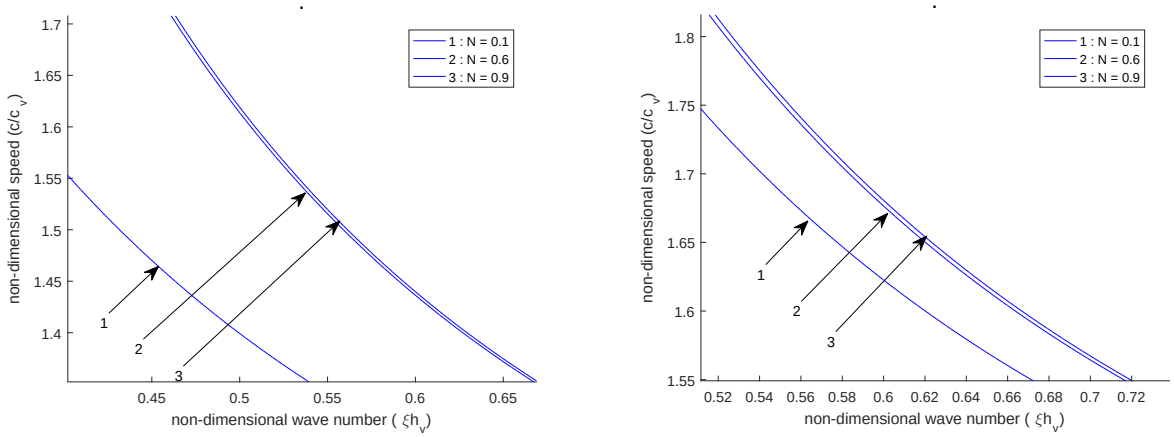

(a) For $PZT-5H$ ceramic (b) For $BaTiO_3$ ceramic

Figure 4.23: Variation of non-dimensional real phase velocity against non-dimensional wave number for different values of micropolar constant $N = 0.1, 0.6, 0.9$ when h_v=0.02m, h_p=0.02m in case of electrical short conditions.

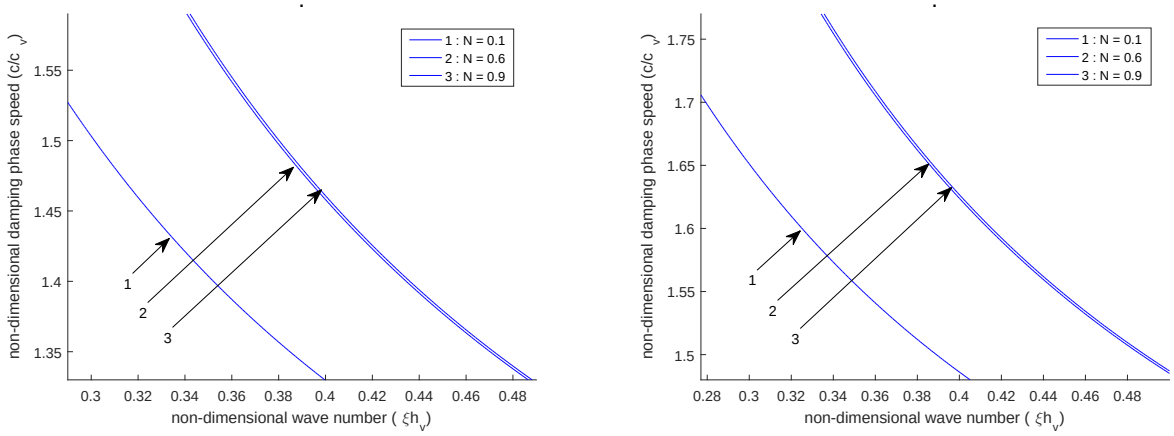

(a) For $PZT-5H$ ceramic

(b) For $BaTiO_3$ ceramic

Figure 4.24: Variation of non-dimensional damping phase velocity against non-dimensional wave number for different values of micropolar constant $N = 0.1, 0.6, 0.9$ when h_v=0.02m, h_p=0.02m in case of electrical short conditions.

characteristic profiles for the corresponding electrically open and short conditions are shown in figures 4.25, 4.26 and figures 4.27, 4.28 respectively, whereas figures-4.25(a), 4.26(a), 4.27(a), 4.28(a) correspond to $PZT-5H$ material and figures-4.25(b), 4.26(b), 4.27(b), 4.28(b) correspond to $BaTiO_3$ material. The dispersive curves are also plotted for real phase velocity in Figure 4.29 to show the comparison of couple stress theory and micropolar theory for both the materials of the piezoelectric medium under electrically open and short conditions. Almost similar trends are observed in characteristic profiles for both the size-dependent microcontinuum theories.

4.3.9 Effects of heterogeneity of a viscoelastic layer

The effects of heterogeneity parameter associated with viscoelastic media on the real and damping phase velocity profiles of Love wave are displayed in figures 4.30–4.33. The characteristic curves are plotted for different values of a heterogeneity parameter $\alpha h_v = 0.08$, 0.12 and 0.16. Here, characteristic length of material is fixed i.e. $l = 0.0001m$ and thickness of a piezoelectric layer and a viscoelastic layer are taken

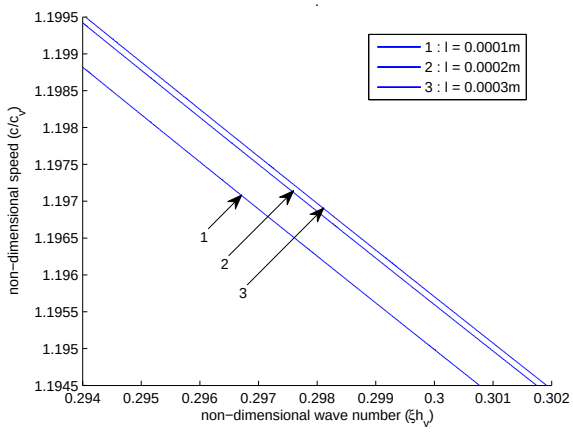

(a) For $PZT-5H$ ceramic

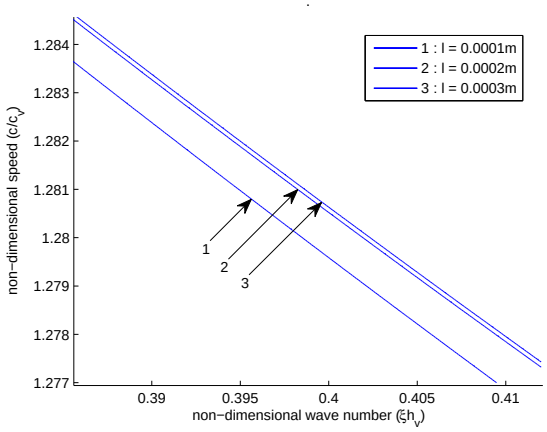

(b) For $BaTiO_3$ ceramic

Figure 4.25: Variation of non-dimensional real phase velocity against non-dimensional wave number for different values of characteristic length l = 0.0001m, 0.0002m, 0.0003m when h_v=0.02m, h_p=0.02m in case of electrical open conditions.

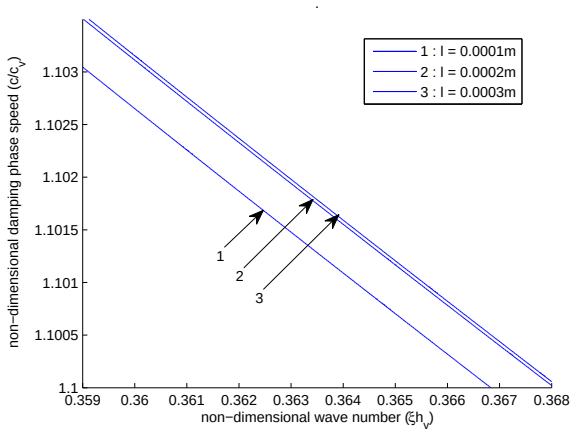

(a) For $PZT-5H$ ceramic

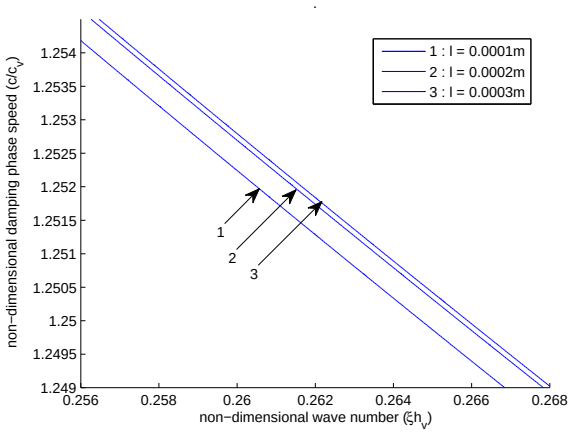

(b) For $BaTiO_3$ ceramic

Figure 4.26: Variation of non-dimensional damping phase velocity against non-dimensional wave number for different values of characteristic length l = 0.0001m, 0.0002m, 0.0003m when h_v=0.02m, h_p=0.02m in case of electrical open conditions.

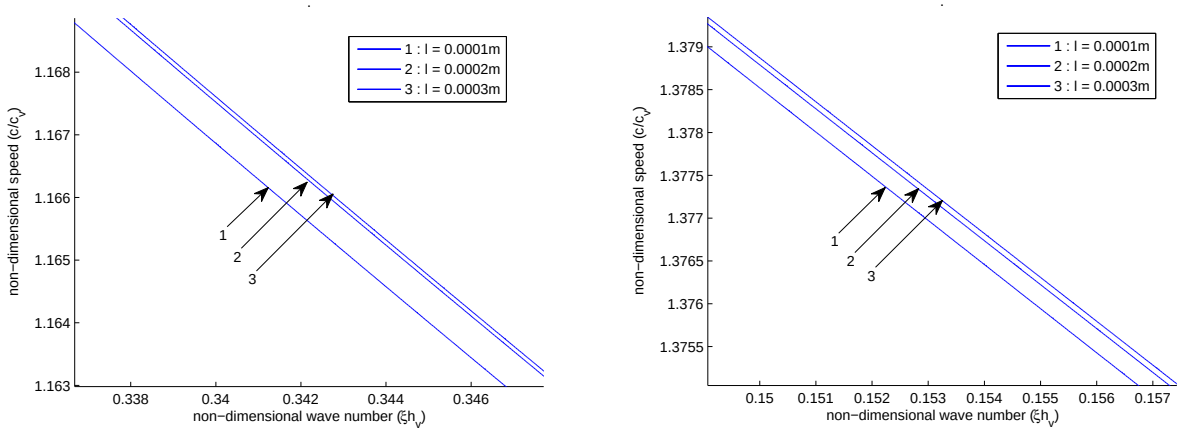

(a) For $PZT-5H$ ceramic (b) For $BaTiO_3$ ceramic

Figure 4.27: Variation of non-dimensional real phase velocity against non-dimensional wave number for different values of characteristic length l = 0.0001m, 0.0002m, 0.0003m when h_v=0.02m, h_p=0.02m in case of electrical short conditions.

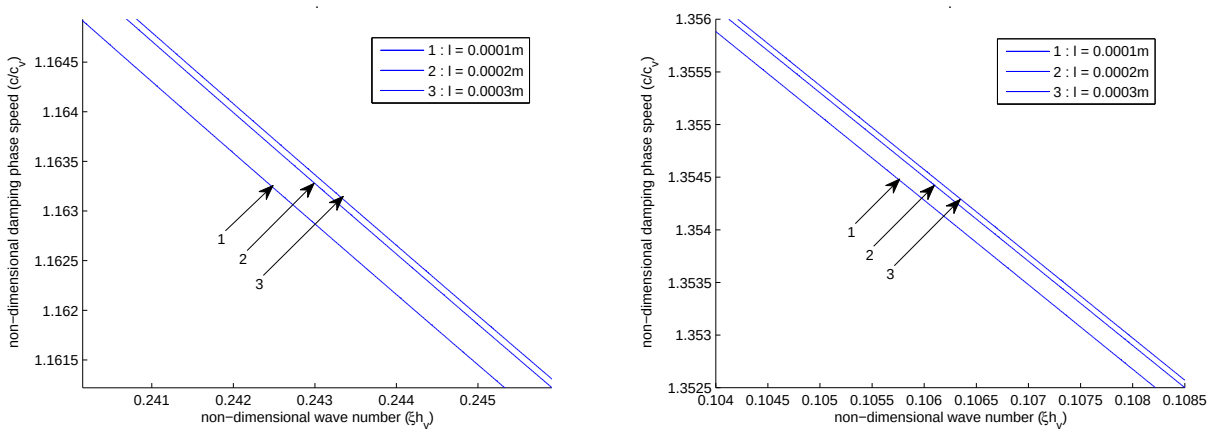

(a) For $PZT-5H$ ceramic (b) For $BaTiO_3$ ceramic

Figure 4.28: Variation of non-dimensional damping phase velocity against non-dimensional wave number for different values of characteristic length l = 0.0001m, 0.0002m, 0.0003m when h_v=0.02m, h_p=0.02m in case of electrical short conditions.

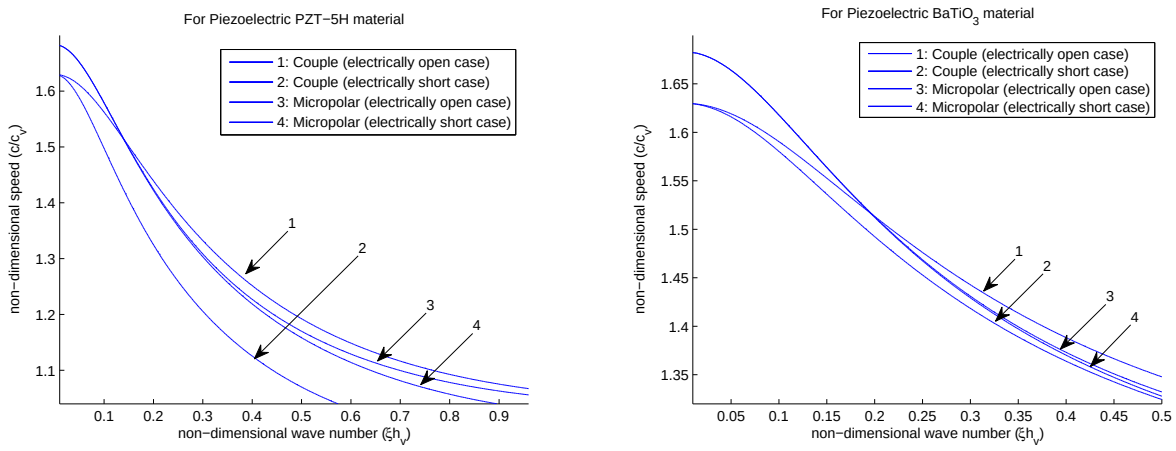

Figure 4.29: Variation of non-dimensional real phase velocity against non-dimensional wave number for couple stress theory and micropolar theory.

as $h_v = 0.02m$ and $h_p = 0.02m$ respectively. It is observed that heterogeneity of a viscoelastic layer affects the phase velocity profiles significantly. The phase velocity profiles of Love wave decreases with the increase in heterogeneity parameter (αh_v) associated with a viscoelastic medium for both the considered materials of the piezoelectric materials. Figures-4.30 and 4.31 correspond to electrically open conditions and figures-4.32 and 4.33 correspond to an electrical short conditions. The characteristic profiles for $PZT-5H$ and $BaTiO_3$ material are shown in figures 4.30(a), 4.31(a), 4.32(a), 4.33(a) and figures- 4.30(b), 4.31(b), 4.32(b), 4.33(b) respectively.

4.3.10 Effects of internal friction of a viscoelastic layer

Figures 4.34–4.37 show the effects of internal friction associated with viscoelastic media in Love wave propagation in a hybrid structure with micropolar half-space. Here, the different values are considered to study the effect of internal friction parameter as $\frac{\mu_1}{\eta_1} = 6 \times 10^5,\ 10 \times 10^5,\ 20 \times 10^5$ for two different piezoelectric materials. The material characteristic length parameter is taken as $l = 0.0001m$ and the thickness of a piezoelectric layer and a viscoelastic layer as $h_p = 0.02m$ and $h_v = 0.02m$ respectively. Significant effects have been observed on the phase velocity profiles of Love wave in double-layered structure with the change in internal friction parameter associated with a viscoelastic layer. It is observed that the real and damping phase

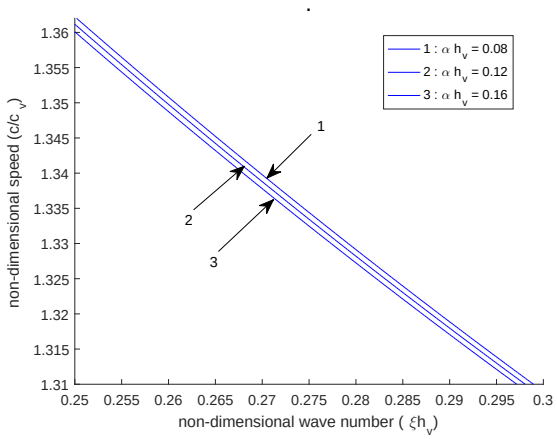

(a) For $PZT-5H$ ceramic

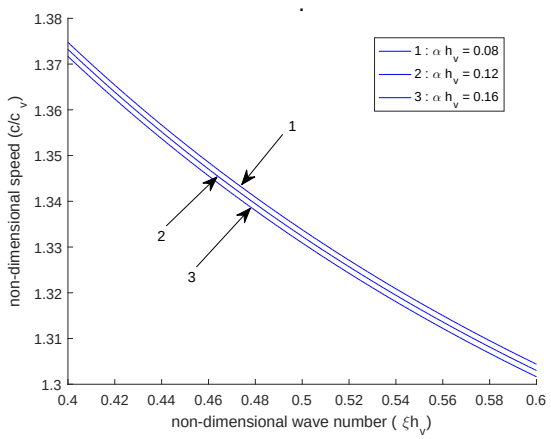

(b) For $BaTiO_3$ ceramic

Figure 4.30: Variation of non-dimensional real phase velocity against non-dimensional wave number for different values of non-dimensional heterogeneity parameter αh_v = 0.08, 0.12, 0.16, when h_v=0.02m, h_p=0.02m, $l = 0.0001m$ in case of electrical open conditions.

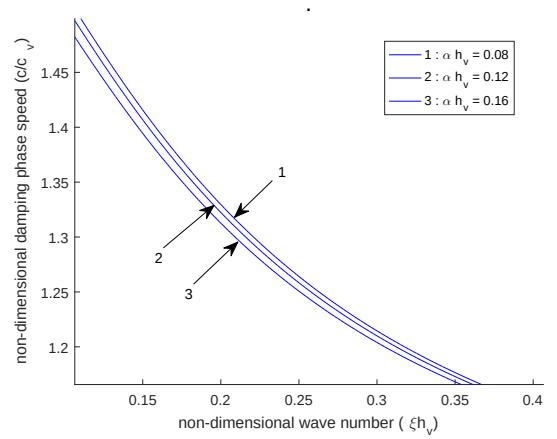

(a) For $PZT-5H$ ceramic

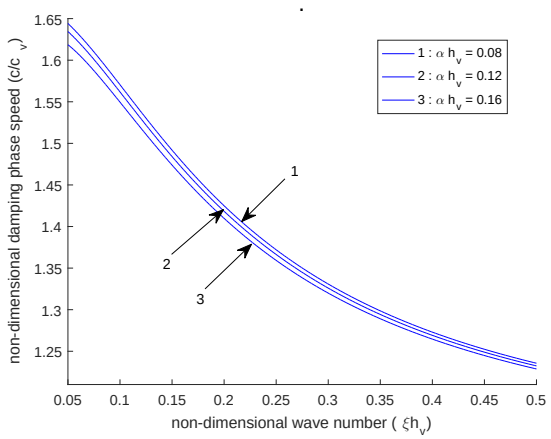

(b) For $BaTiO_3$ ceramic

Figure 4.31: Variation of non-dimensional damping phase velocity against non-dimensional wave number for different values of non-dimensional heterogeneity parameter αh_v = 0.08, 0.12, 0.16, when h_v=0.02m, h_p=0.02m, $l = 0.0001m$ in case of electrical open conditions.

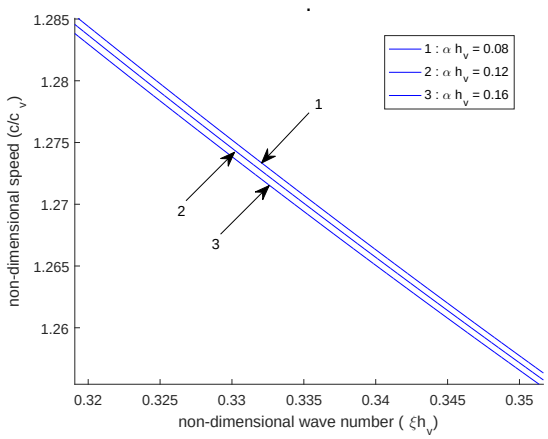

(a) For $PZT-5H$ ceramic

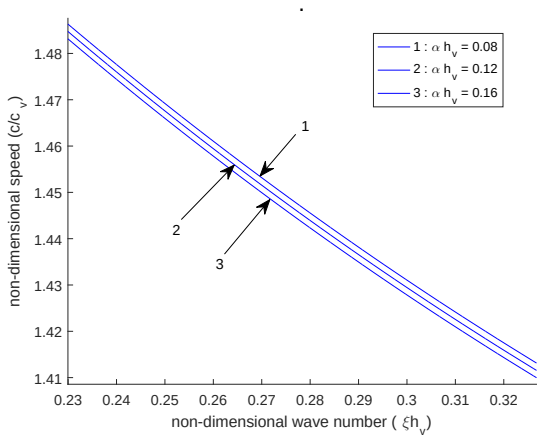

(b) For $BaTiO_3$ ceramic

Figure 4.32: Variation of non-dimensional real phase velocity against non-dimensional wave number for different values of non-dimensional heterogeneity parameter αh_v = 0.08, 0.12, 0.16, when h_v=0.02m, h_p=0.02m, $l = 0.0001m$ in case of electrical short conditions.

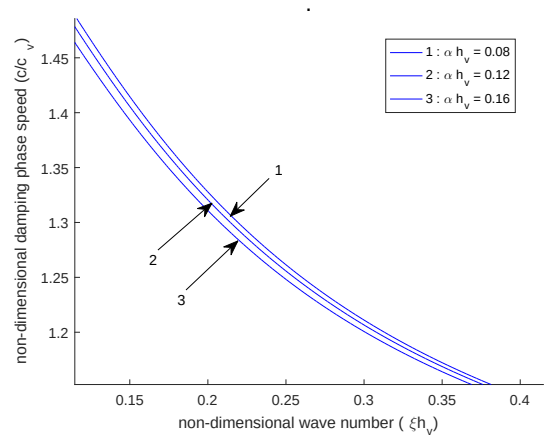

(a) For $PZT-5H$ ceramic

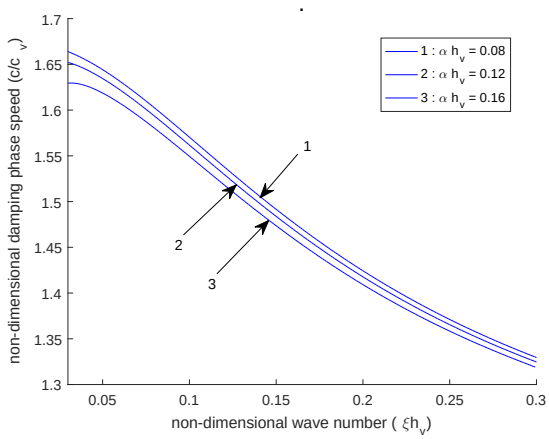

(b) For $BaTiO_3$ ceramic

Figure 4.33: Variation of non-dimensional damping phase velocity against non-dimensional wave number for different values of non-dimensional heterogeneity parameter αh_v = 0.08, 0.12, 0.16, when h_v=0.02m, h_p=0.02m, $l = 0.0001m$ in case of electrical short conditions.

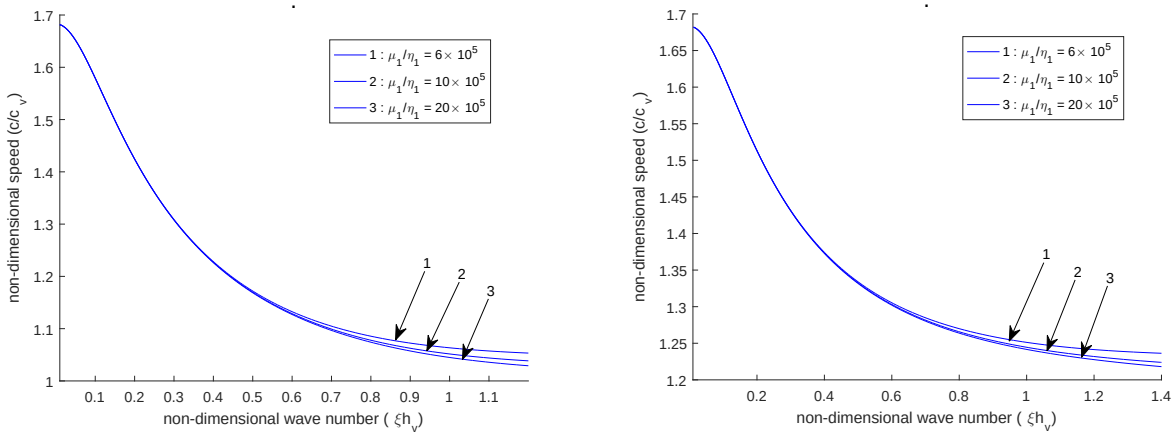

(a) For $PZT-5H$ ceramic (b) For $BaTiO_3$ ceramic

Figure 4.34: Variation of non-dimensional real phase velocity against non-dimensional wave number for different values of internal friction parameter $\frac{\mu_1}{\eta_1} = 6\times10^5$, 10×10^5, 20×10^5, when h_v=0.02m, h_p=0.02m, $l = 0.0001m$ in case of electrical open conditions.

velocity of the Love wave decreases with the increase in the internal friction parameter for both the cases of electrically open and short conditions. The characteristic profiles for electrically open conditions are displayed in figures-4.34 and 4.35 and the characteristic profiles for an electrical short conditions are displayed in figures-4.36 and 4.37.

4.3.11 Effects of a piezoelectric layer material

The effects of piezoelectric layer on Love wave propagation in double-layered structure with the semi-infinite micropolar substrate are illustrated in figures 4.38 and 4.39 for both the cases of electrically open and short conditions respectively. For this, two piezoelectric material, i.e., $PZT-5H$ and $BaTiO_3$ are considered. Here, the characteristic length is taken as $l = 0.0001m$; the thicknesses of the piezoelectric layer and the viscoelastic layer as $h_p = 0.02m$ and $h_v = 0.02m$ respectively. It is observed that the real and damping phase velocity of the Love wave decreases with the increase in wave number. Moreover, it can be seen from the figures that real and damping phase velocity for $BaTiO_3$ piezoelectric material is more as compared to $PZT-5H$ material. The real phase velocity profiles are delineated in figures-4.38(a), 4.39(a)

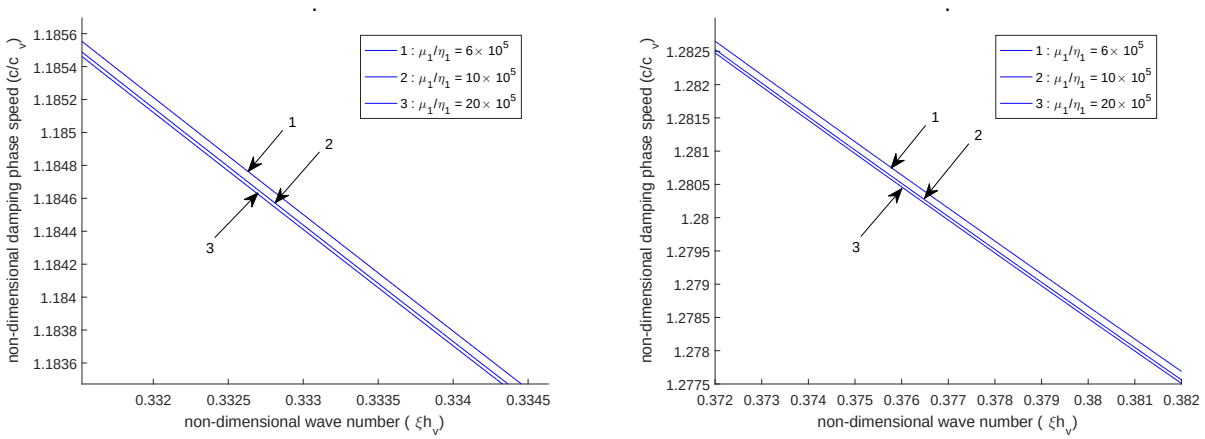

(a) For $PZT-5H$ ceramic (b) For $BaTiO_3$ ceramic

Figure 4.35: Variation of non-dimensional damping phase velocity against non-dimensional wave number for different values of internal friction parameter $\frac{\mu_1}{\eta_1} = 6 \times 10^5$, 10×10^5, 20×10^5, when h_v=0.02m, h_p=0.02m, $l = 0.0001m$ in case of electrical open conditions.

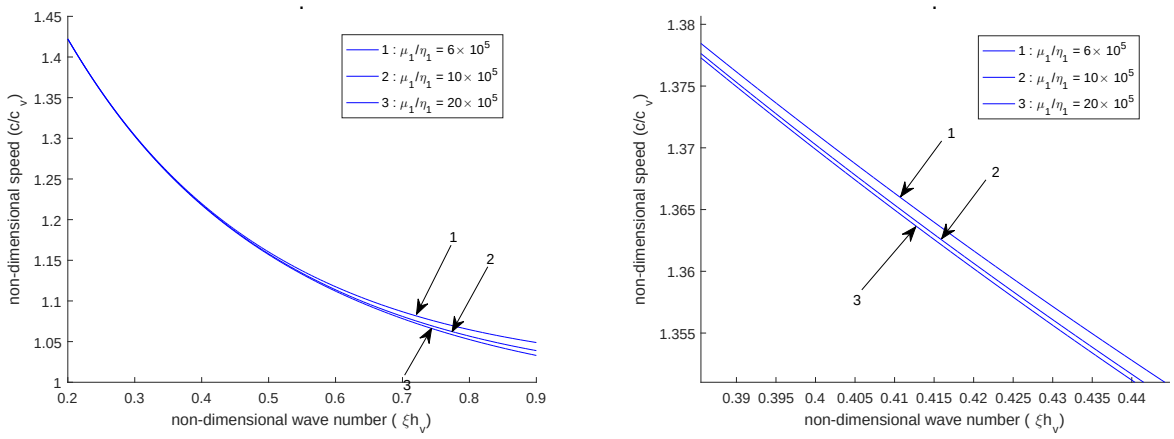

(a) For $PZT-5H$ ceramic (b) For $BaTiO_3$ ceramic

Figure 4.36: Variation of non-dimensional real phase velocity against non-dimensional wave number for different values of internal friction parameter $\frac{\mu_1}{\eta_1} = 6 \times 10^5$, 10×10^5, 20×10^5, when h_v=0.02m, h_p=0.02m, $l = 0.0001m$ in case of electrical short conditions.

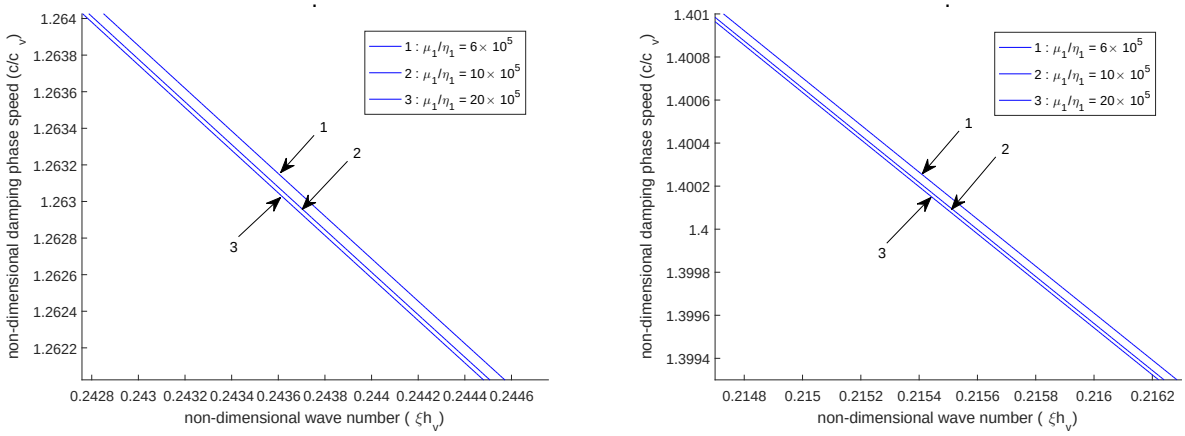

(a) For $PZT-5H$ ceramic

(b) For $BaTiO_3$ ceramic

Figure 4.37: Variation of non-dimensional damping phase velocity against non-dimensional wave number for different values of internal friction parameter $\frac{\mu_1}{\eta_1} = 6 \times 10^5,\ 10 \times 10^5,\ 20 \times 10^5$, when h_v=0.02m, h_p=0.02m, $l = 0.0001m$ in case of electrical short conditions.

and the damping phase velocity profiles are delineated in figures-4.38(b), 4.39(b) for both the considered materials of a piezoelectric layer.

Effects of Piezoelectric constant (e_{15})

The effects of piezoelectric constant e_{15} are shown by considering different values of piezoelectric parameter $e_{15} = 17C/m^2,\ 21C/m^2,\ 25C/m^2$ for piezoelectric material $PZT-5H$ and $e_{15} = 11C/m^2,\ 15C/m^2,\ 19C/m^2$ for piezoelectric material $BaTiO_3$. Here, the characteristic length is taken as $l = 0.0001m$; the thicknesses of the piezoelectric layer and the viscoelastic layer as $h_p = 0.02m$ and $h_v = 0.02m$ respectively. From figures 4.40 and 4.41, it is observed that with the increase in piezoelectric constant, the real phase velocity profiles decreases for both the considered material of piezoelectric material under both cases of electrically open and short conditions.

Effects of Dielectric constant (ϵ_{11})

Figures 4.42 and 4.43 show the effects of dielectric constant on the real phase velocity profiles of Love wave propagation in double-layered structure. The character-

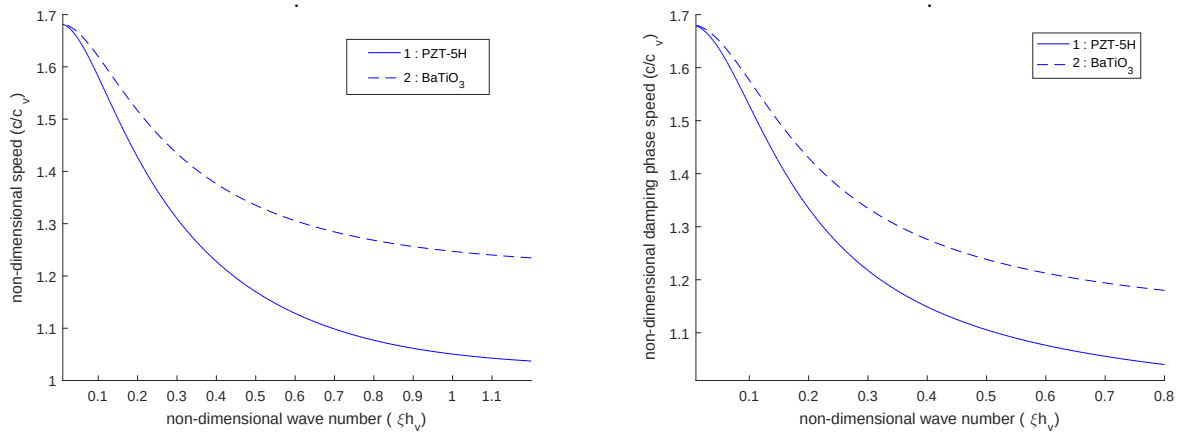

(a) For real phase velocity (b) For damped phase velocity

Figure 4.38: Variation of non-dimensional real and damped phase velocity against non-dimensional wave number when h_v=0.02m, h_p=0.02m, $l = 0.0001m$ in case of electrical open conditions.

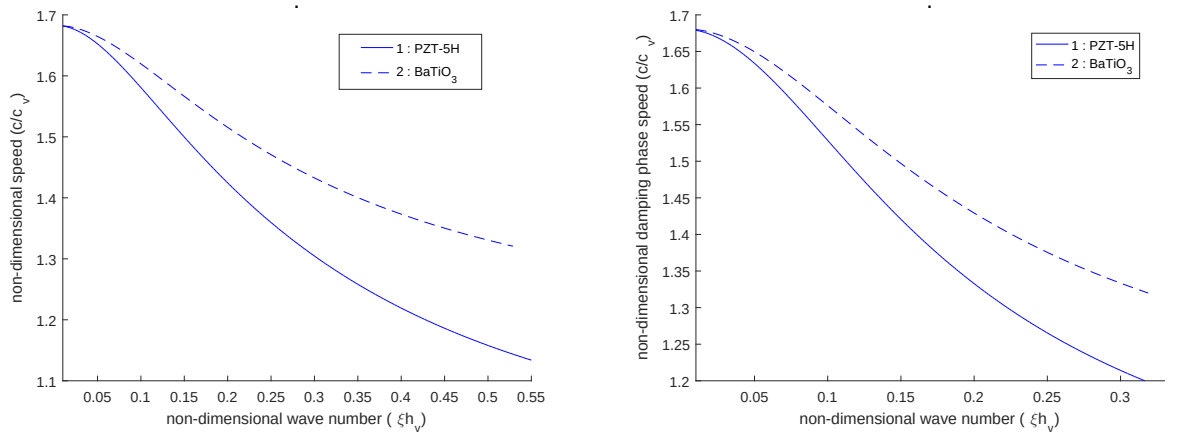

(a) For real phase velocity (b) For damped phase velocity

Figure 4.39: Variation of non-dimensional real and damped phase velocity against non-dimensional wave number when h_v=0.02m, h_p=0.02m, $l = 0.0001m$ in case of electrical short conditions.

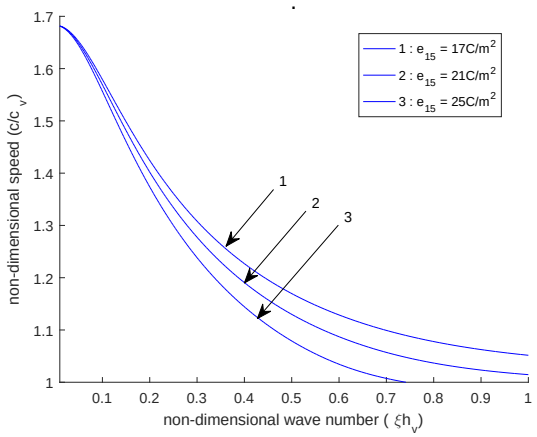

(a) For $PZT-5H$ ceramic

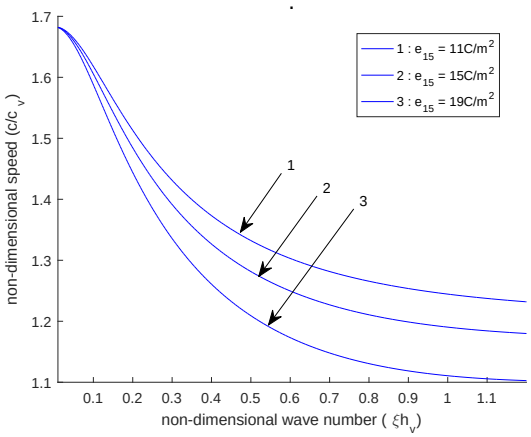

(b) For $BaTiO_3$ ceramic

Figure 4.40: Variation of non-dimensional real phase velocity against non-dimensional wave number for different values of piezoelectric constant $e_{15} = 17C/m^2$, $21C/m^2$, $25C/m^2$ in (a) and $e_{15} = 11C/m^2$, $15C/m^2$, $19C/m^2$ in (b), when h_v=0.02m, h_p=0.02m, $l = 0.0001m$ in case of electrical open conditions.

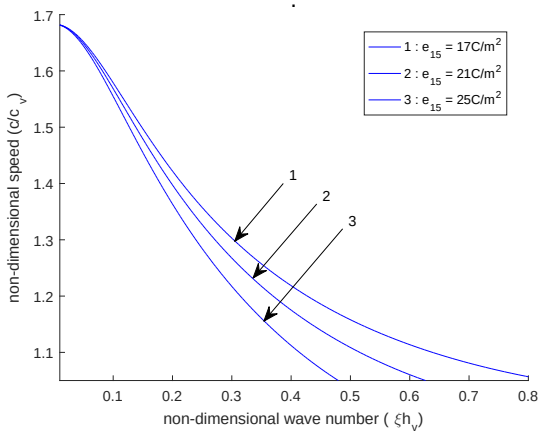

(a) For $PZT-5H$ ceramic

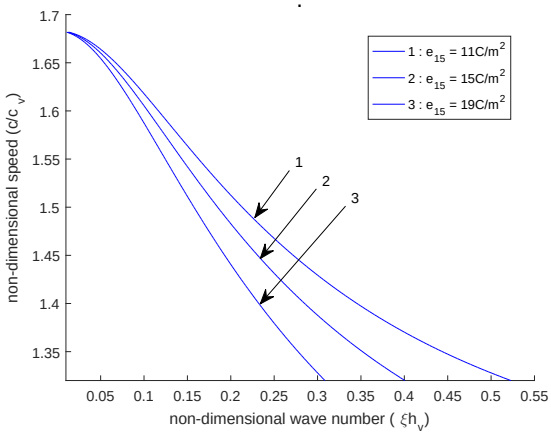

(b) For $BaTiO_3$ ceramic

Figure 4.41: Variation of non-dimensional real phase velocity against non-dimensional wave number for different values of piezoelectric constant $e_{15} = 17C/m^2$, $21C/m^2$, $25C/m^2$ in (a) and $e_{15} = 11C/m^2$, $15C/m^2$, $19C/m^2$ in (b), when h_v=0.02m, h_p=0.02m, $l = 0.0001m$ in case of electrical short conditions.

istic profiles are plotted by considering different values of dielectric constant $\epsilon_{11} = 237 \times 10^{-10} C^2/Nm^2$, $277 \times 10^{-10} C^2/Nm^2$, $317 \times 10^{-10} C^2/Nm^2$ for $PZT - 5H$ material and $\epsilon_{11} = 98 \times 10^{-10} C^2/Nm^2$, $128 \times 10^{-10} C^2/Nm^2$, $158 \times 10^{-10} C^2/Nm^2$ for $BaTiO_3$ material. Here, the value of characteristic length is taken as $l = 0.0001m$; the thicknesses of the piezoelectric layer and the viscoelastic layer as $h_p = 0.02m$ and $h_v = 0.02m$ respectively. It is observed that the real phase velocity profiles increases with the increase in dielectric constant under both the cases of electrically open and short conditions.

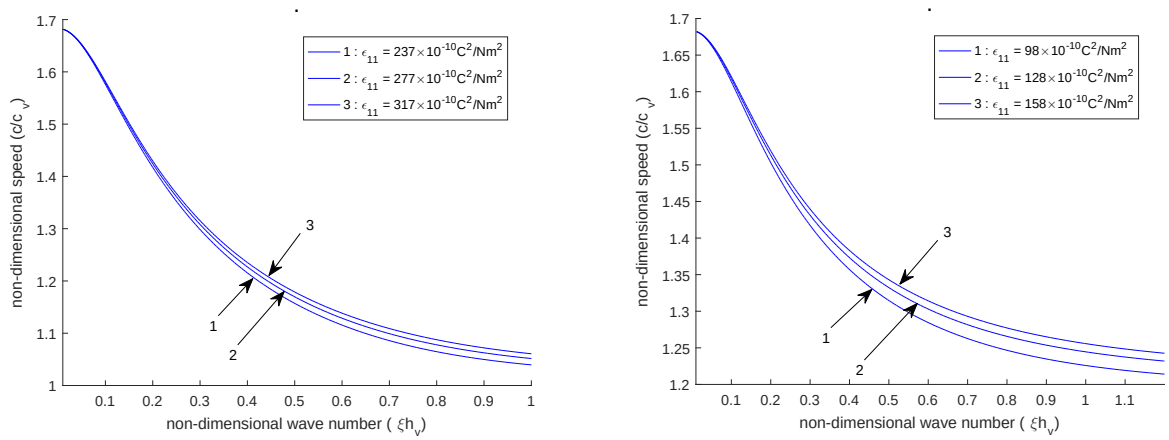

(a) For $PZT - 5H$ ceramic

(b) For $BaTiO_3$ ceramic

Figure 4.42: Variation of non-dimensional real phase velocity against non-dimensional wave number for different values of dielectric constant $\epsilon_{11} = 237 \times 10^{-10} C^2/Nm^2$, $277 \times 10^{-10} C^2/Nm^2$, $317 \times 10^{-10} C^2/Nm^2$ in (a) and $\epsilon_{11} = 98 \times 10^{-10} C^2/Nm^2$, $128 \times 10^{-10} C^2/Nm^2$, $158 \times 10^{-10} C^2/Nm^2$ in (b), when h_v=0.02m, h_p=0.02m, $l = 0.0001m$ in case of electrical open conditions.

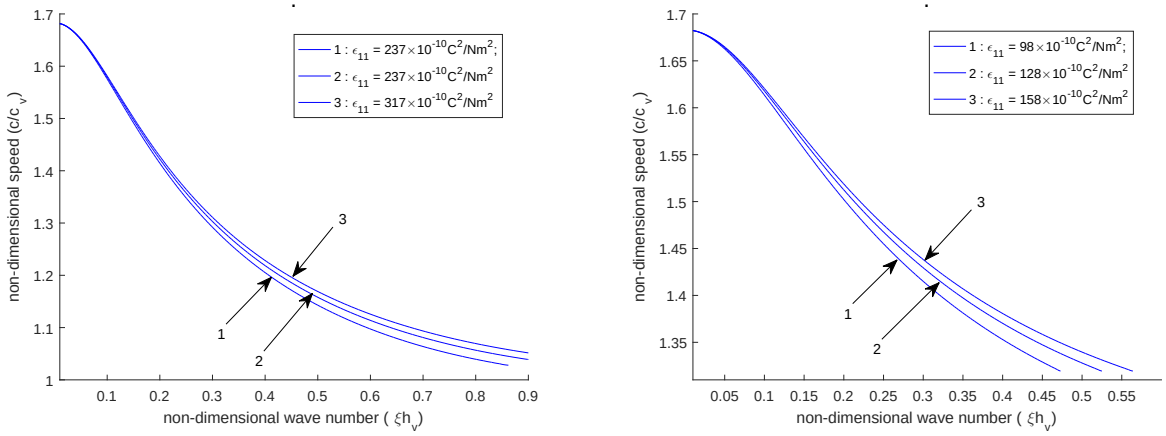

(a) For $PZT-5H$ ceramic

(b) For $BaTiO_3$ ceramic

Figure 4.43: Variation of non-dimensional real phase velocity against non-dimensional wave number for different values of dielectric constant $\epsilon_{11} = 237 \times 10^{-10}C^2/Nm^2$, $277 \times 10^{-10}C^2/Nm^2$, $317 \times 10^{-10}C^2/Nm^2$ in (a) and $\epsilon_{11} = 98 \times 10^{-10}C^2/Nm^2$, $128 \times 10^{-10}C^2/Nm^2$, $158 \times 10^{-10}C^2/Nm^2$ in (b), when h_v=0.02m, h_p=0.02m, $l = 0.0001m$ in case of electrical short conditions.

4.4 Conclusion

The effects of the microstructure of the substrate and other various material parameters have been studied on the propagation of Love wave in a double-layered structure with semi-infinite couple stress substrate and micropolar substrate in section 4.2 and 4.3 respectively. Analytical expressions for the dispersion equations have been obtained and results are displayed graphically. It is observed that the real and damping phase velocity profiles are affected significantly with the variation in associated parameters of the considered double-layered structure. The consideration of microstructural effects of the substrate in this realistic model enhances the domain of Love waves. The following major conclusions are highlighted on the basis of obtaining results.

- The real and damping phase velocity profiles of Love waves are affected significantly in a double-layered structure with wave number. It is observed graphically that the real and damping phase velocity profiles decrease with the increase in non-dimensional wave number in each case of electrically open and

short conditions for both the considered materials of a piezoelectric layer.

- The internal microstructural parameters have prominent effects on both the real and damping phase velocity profiles of the Love wave. Size effects are interpreted in the context of the micropolar theory of elasticity in terms of the parameters "coupling factor (N) and characteristic length (l)" whereas, in couple stress theory, the size effects are interpreted through a single parameter, i.e., "characteristic length". Both coupling factor and the material characteristic length parameter exhibit the favoring effect on the real and damping phase velocity profiles of the Love-type wave. It is observed that with the increase in the magnitude of the coupling parameter and the scaling parameter, the phase velocity profiles of the Love-type wave also increase. The influence of size-dependency on the phase velocity profiles of the Love wave has been shown by plotting the characteristic curves for micropolar elasticity with couple stress theory.

- Heterogeneity parameter associated with viscoelastic layer shows the adverse effect on phase velocity profiles of the Love wave. It is observed that the increase in heterogeneity parameter (αh_v) leads to a decrease in phase velocity profiles of the Love wave for both the considered material of the piezoelectric layer.

- Internal friction parameter associated with viscoelastic layer affects both the real and damping phase velocity profiles of the Love wave substantially. It is observed that the real and damping phase velocity of the Love wave decreases with an increase in the internal friction parameter.

- The effects of the piezoelectric layer are shown by considering two different materials of the piezoelectric layer, i.e., $PZT-5H$ and $BaTiO_3$. It is observed that the real and damping phase velocity for $BaTiO_3$ piezoelectric material is more as compared to $PZT-5H$ material in both the cases of electrically open and short conditions.

- Piezoelectric parameter associated with the piezoelectric layer shows the adverse

effects on the phase velocity profiles of the Love wave. It is observed that the increase in piezoelectric parameters leads to a decrease in the phase velocity of the Love wave in a double-layered structure.

- The phase velocity profiles of the Love wave are affected significantly with the change in the dielectric parameters. It is observed that with an increase in dielectric parameter the phase velocity of Love wave propagation in double-layered structure also increases.

In the years to come, MEMS devices are expected to grow rapidly and develop wider research. Because of the microstructural considerations through length scale parameters, the findings obtained in the present paper could help in the development of more efficient and high-performance Love-wave-based devices. Also, the results obtained from the above-solved models may be useful for the fabrication of Love-wave based sensors and in structural utilization. Since another kind of surface wave-like Rayleigh wave has a wide range of applications in seismology, geophysics, material science, etc. [156]. A possible extension of the considered model could be to study the viscoelastic, piezoelectricity, and microstructural effects on Rayleigh wave propagation.

Chapter 5

The effects of imperfect bonding at the interface of layer and substrate on Love wave

5.1 Introduction

While working on size-dependent models, piezoelectric models, and other different material layers, it was observed that the size-dependent substrate can also be considered with another different material layer like orthotropic medium and many more. In Chapter 2, 3 and 4, the problems on Love-type surface wave propagation considering the perfect interface between the substrate and distinct material layers in single or double-layered structure using the size-dependent model have been successfully solved. In these chapters, almost similar trends of different influencing parameters associated with different material layers have been observed. Though the problems considering the perfect bonding between the substrate and material layer have been solved but it is difficult to achieve this condition in reality. Keeping this aspect in

The content of this chapter is published in the journal *'Mechanics of Materials'*, 155:103772, 2021, *(SCI, Impact factor:2.993)*

view, the present chapter deals with the investigation of the propagation of Love-type waves in the functionally graded orthotropic medium (FGOM) under the influence of initial stress bonded imperfectly over the size-dependent micropolar medium. The strength of many engineering layered models is well known to rely critically on the bonding between the structural components. Therefore, the considerations of imperfectness at the interface of two materials play an important role in the design and modification of various Love-wave-based devices. The earth is indeed a complex system where its layers are not always perfectly bonded. Due to material degradation, interface distortion, cracks, interfaces can be inherently imperfect [103]. The imperfections are very often limited to a very fine layer as an interface that is difficult to characterize [104]. Displacement components are not continuous at the surface of two dissimilar materials in case of an imperfect interface. Significant research has been conducted by numerous investigators to define the physical conditions at the interface by specific mechanical limits [50, 28]. Many researchers demonstrated the effect of the interfacial adhesion on the wave propagation characteristics with different interfacial properties [60, 135, 171]. In addition, the initial stress in an elastic medium is caused due to the overburdened plate, manufacturing processes, temperature fluctuations, magnetic fields, hydrostatic friction, external differential forces, sluggish cracking processes, etc. plays a significant role in the occurrence of earthquakes [176, 22, 136].

Due to the unique thermal and mechanical properties, orthotropic materials having three mutually independent perpendicular directions attracted the attention of many researchers. Certain types of wood, ceramics, sheet metal, as well as bones, exemplify orthotropic medium [12]. These materials are anisotropic in nature. Gupta and Katiyar [64] developed an anisotropic continuum model based upon an improved car-following model by using a series expansion of the headway in terms of the density. In biomechanics, the consideration of the orthotropic material used for the description of the cortical bone yields more realistic displacement results and can be used to simulate implant-bone systems. Schneider et al. [159] outlined a technique for transferring the density distributions gained from clinical computer tomographies to an inhomo-

geneous orthotropic material model for the cortical structure of long bones. Madan et al. [123] and Chugh et al. [30] examined the static deformation of a non-uniform discontinuity in an orthotropic elastic media in a long strike-slip fault. Kundu et al. [100] studied the propagation characteristics of a Love wave in a fiber-reinforced material layer lying over a semi-infinite orthotropic medium under initial stress. Kakar [82] examined the propagation of the Love wave in a homogeneous isotropic layer sandwiched between orthotropic material layer and prestressed inhomogeneous elastic half-space. Vaishnav et al. [196] outlines the influence of the irregular interface on the propagation characteristics of Love-type waves in an initially stressed anisotropic porous medium lying over an initially stressed orthotropic medium having rectangular irregularity. Due to the brittle nature of orthotropic materials, these materials cannot perform well under the influence of high thermal conditions. In order to address this limitation, many researchers studied wave propagation phenomena in the non-homogenous (or functionally graded) orthotropic medium. Abd-Alla and Ahmed [2] studied the propagation of Love waves in a non-homogeneous orthotropic medium having changeable initial compressive stress. Saha et al. [154] investigated Love wave propagation in the heterogeneous orthotropic material layer under the influence of initial stress lying over a gravitating porous half-space. Prasad and Kundu [149] examined Love wave propagation in a prestressed heterogeneous orthotropic material layer overlying a semi-infinite elastic substrate with rectangular irregularity. Wang et al. [202] analytically obtained the dispersion relation for Love wave propagation in a non-homogeneous orthotropic material layer over orthotropic half-space obeying exponential and generalized power-law model. Mandi et al. [124] discussed the impact of corrugation on the Love wave generation in fiber-reinforced layer resting on inhomogeneous orthotropic media. The influence of shear deformations and material gradient on the linear parametric instability of laminated orthotropic conical shells was studied by Sofiyev [186].

In this chapter, the harmonic form of heterogeneity has been employed in orthotropic materials to solve the problem. The dispersion relations are obtained analytically in compact form by employing admissible boundary conditions for the layer and the sub-

strate. The dispersion curves are plotted to illustrate the influence of imperfectness of interface, microstructure of the substrate as well as heterogeneity involved in FGOM layer on the phase velocity profiles of Love-type wave. Moreover, the FGOM layer is considered under an initially stressed state to extend the applicability of the obtained results in geophysical engineering. Relevant particular cases are also obtained to validate the present study.

5.2 Formulation of the problem

On taking into account the model comprising of FGOM layer (L_1) under initially stressed state having finite thickness H bonded imperfectly over a size-dependent substratum (L_2). Here, micropolar material is supposed to capture the microscopic behavior of the material at the microscale. The physical model of the perceived problem is depicted in Figure 5.1. A rectangular coordinate system is chosen in which

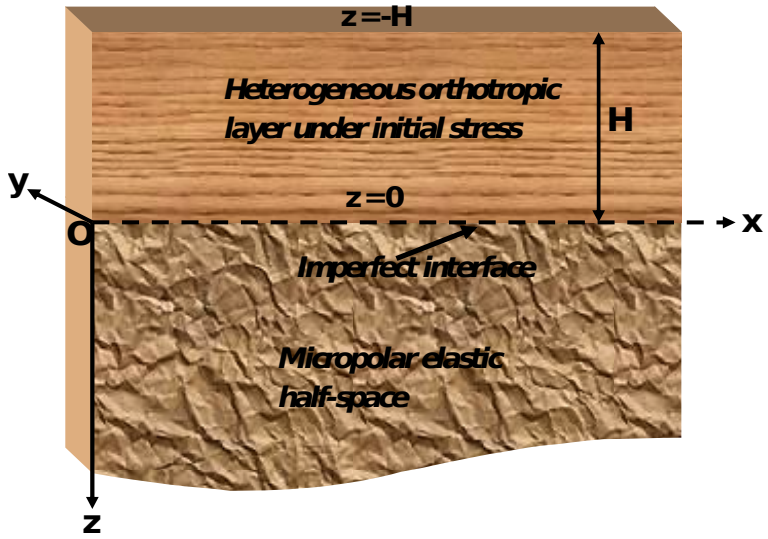

Figure 5.1: Physical model of the problem.

origin O lies at the common interface of FGOM medium and micropolar elastic substrate, which is imperfectly bonded with each other. The propagation of Love-type wave is assumed in x-direction, i.e., in xz-plane where the z-axis acts in the vertically downward direction and no variation is assumed along the y-axis (i.e., $\partial/\partial y \equiv 0$). The mechanical displacement components for Love-type wave in the upper medium

and lower size-dependent half-space were supposed to be $\overrightarrow{u_i^{(o)}} = (u_o, v_o, w_o)$ and $\overrightarrow{u_i^{(m)}} = (u_m, v_m, w_m)$, respectively. As the Love wave is propagating along the direction of the x-axis, it causes displacement in the y-direction only. One may suppose that

$$\begin{aligned} u_o = 0,\ v_o = v_o(x,z,t),\ w_o = 0, \\ u_m = 0,\ v_m = v_m(x,z,t),\ w_m = 0. \end{aligned} \tag{5.1}$$

5.2.1 Governing equations and solutions for FGOM L_1

The Governing equations for FGOM in the absence of body forces under the influence of the initial stress are:

$$\begin{cases} \frac{\partial \sigma_{11}^o}{\partial x} + \frac{\partial \sigma_{12}^o}{\partial y} + \frac{\partial \sigma_{13}^o}{\partial z} - P^{'}\left(\frac{\partial \omega_z^o}{\partial y} - \frac{\partial \omega_y^o}{\partial z}\right) = \rho_o \frac{\partial^2 u_o}{\partial t^2}, \\ \frac{\partial \sigma_{21}^o}{\partial x} + \frac{\partial \sigma_{22}^o}{\partial y} + \frac{\partial \sigma_{23}^o}{\partial z} - P^{'}\left(\frac{\partial \omega_z^o}{\partial x}\right) = \rho_o \frac{\partial^2 v_o}{\partial t^2}, \\ \frac{\partial \sigma_{31}^o}{\partial x} + \frac{\partial \sigma_{32}^o}{\partial y} + \frac{\partial \sigma_{33}^o}{\partial z} - P^{'}\left(\frac{\partial \omega_y^o}{\partial x}\right) = \rho_o \frac{\partial^2 w_o}{\partial t^2}, \end{cases} \tag{5.2}$$

where σ_{ij}^o denotes the stress tensor for FGOM medium; $i, j = (1, 2, 3)$; ρ_o is the density of FGOM; $P^{'}$ indicates the initial stress in orthotropic medium; ω_x^o, ω_y^o and ω_z^o represents the rotational components along x, y and z directions, respectively. The constitutive relations for FGOM can be expressed as:

$$\begin{aligned} \sigma_{11}^o &= M_{11}^{'}(z)e_{11} + M_{12}^{'}(z)e_{22} + M_{13}^{'}(z)e_{33}, \\ \sigma_{22}^o &= M_{21}^{'}(z)e_{11} + M_{22}^{'}(z)e_{22} + M_{23}^{'}(z)e_{33}, \\ \sigma_{33}^o &= M_{31}^{'}(z)e_{11} + M_{32}^{'}(z)e_{22} + M_{33}^{'}(z)e_{33}, \\ \sigma_{23}^o &= 2N_1^{'}(z)e_{23}, \\ \sigma_{31}^o &= 2N_2^{'}(z)e_{31}, \\ \sigma_{12}^o &= 2N_3^{'}(z)e_{12}, \end{aligned} \tag{5.3}$$

where

$$e_{ij} = \frac{u_{i,j}^o + u_{j,i}^o}{2}.$$

Here, $M_{ij}^{'}$ and $N_{i}^{'}$ symbolize the normal and shear elastic coefficients; e_{ij} is the strain tensors; $i, j = (1, 2, 3)$; superscript "o" indicates the term associated with orthotropic medium L_1.

Invoking equations (5.1) and (5.3), equation (5.2) reduces to

$$N_1^{'}\frac{\partial^2 v_o}{\partial z^2} + \left(N_3^{'} - \frac{P^{'}}{2}\right)\frac{\partial^2 v_o}{\partial x^2} + \frac{\partial N_3^{'}}{\partial x}\frac{\partial v_o}{\partial x} + \frac{\partial N_1^{'}}{\partial z}\frac{\partial v_o}{\partial z} = \rho_o \frac{\partial^2 v_o}{\partial t^2}. \tag{5.4}$$

On considering heterogeneity in the elastic coefficients, the initial stress, the density of FGOM medium, the material properties are taken as:

$$\begin{aligned} P^{'} &= P_o(1 - \sin\alpha z), \\ \rho_o &= \rho_0(1 - \sin\alpha z), \\ N_i^{'} &= a_i(1 - \sin\alpha z), \end{aligned} \tag{5.5}$$

where P_o, ρ_0, a_i are values of $P^{'}$, ρ_o and $N_i^{'}$, respectively at $z = 0$; α is the heterogeneity parameter with dimension as inverse of length.

Consider the solution for the upper medium L_1 as:

$$v_o(x, z, t) = V(z)e^{\iota\xi(x-ct)}, \tag{5.6}$$

where ξ is the wave number and c is the phase velocity.

Employing equation (5.6) together with equation (5.5), equation (5.4) reduces to

$$\frac{d^2V}{dz^2} - \left(\frac{\alpha\cos(\alpha z)}{1 - \sin(\alpha z)}\right)\frac{dV}{dz} + \xi^2\left(\frac{c^2}{c_o^2} + \frac{P_o - 2a_3}{2a_1}\right)V(z) = 0, \tag{5.7}$$

where

$$c_o = \sqrt{\frac{a_1}{\rho_0}}.$$

Here c_o is the shear wave velocity in FGOM medium.

In order to solve equation (5.7), one can use the following transformation:

$$V(z) = \frac{f(z)}{\sqrt{(1 - \sin(\alpha z))}}. \tag{5.8}$$

Using equation (5.8) into (5.7), one may obtain the following differential equation:

$$\frac{d^2f}{dz^2} + b^2 f(z) = 0, \tag{5.9}$$

where

$$b^2 = \xi^2\left(\frac{\alpha^2}{4\xi^2} + \frac{c^2}{c_o^2} + \frac{P_o - 2a_3}{2a_1}\right) \quad and \quad I = \frac{P_o}{2a_1}.$$

I indicates the initial stress parameter.

On solving equation (5.9) along with equations (5.8) and (5.6), the mechanical displacement component for FGOM layer L_1 is obtained as:

$$v_o(x,z,t) = \left(\frac{\cos(bz)B_1^{'} + \sin(bz)B_2^{'}}{\sqrt{(1-\sin(\alpha z))}}\right)e^{\iota\xi(x-ct)}, \tag{5.10}$$

where $B_1^{'}$ and $B_2^{'}$ are the arbitrary constants.

5.2.2 Solutions for semi-infinite size-dependent medium L_2

Employing Helmoltz decomposition provided in equation (3.4) of Chapter 3, the components of microrotation vector are

$$\phi_1^{(m)} = \frac{\partial\varphi_m}{\partial x} + \frac{\partial\psi_m}{\partial z},\ \phi_2^{(m)} = 0,\ and\ \phi_3^{(m)} = \frac{\partial\varphi_m}{\partial z} - \frac{\partial\psi_m}{\partial x}, \tag{5.11}$$

where $\overrightarrow{\psi_m} = (0, -\psi_m, 0)$.

Using equation (5.1) and (5.11) in equations (1.15)–(1.16), one may have

$$\nabla^2 v_m + \theta_1^2\nabla^2\psi_m = \frac{1}{\theta_2^2}\frac{\partial^2 v_m}{\partial t^2}, \tag{5.12}$$

$$\nabla^2\varphi_m - \frac{2\theta_5^2}{\theta_3^2+\theta_4^2}\varphi_m = \frac{1}{\theta_3^2+\theta_4^2}\frac{\partial^2\varphi_m}{\partial t^2}, \tag{5.13}$$

$$\nabla^2\psi_m - \frac{2\theta_5^2}{\theta_3^2}\psi - \frac{\theta_5^2}{\theta_3^2}v_m = \frac{1}{\theta_3^2}\frac{\partial^2\psi_m}{\partial t^2}. \tag{5.14}$$

$$\begin{cases} \theta_1 = \sqrt{\frac{\kappa_m}{\mu_m+\kappa_m}},\ \theta_2 = \sqrt{\frac{\mu_m+\kappa_m}{\rho_m}},\ \theta_3 = \sqrt{\frac{\gamma_m}{j\rho_m}}, \\ \theta_4 = \sqrt{\frac{\alpha_m+\beta_m}{j\rho_m}},\ \theta_5 = \sqrt{\frac{\kappa_m}{j\rho_m}}. \end{cases}$$

Assume the solution of equations (5.12)–(5.14) of the form

$$(\varphi_m, \psi_m, v_m)(x, z, t) = (\Phi_m, \Psi_m, V_m)(z)e^{\iota\xi(x-ct)}, \tag{5.15}$$

where ξ is the wave number and c is the phase velocity.

Substitute the solution given in equation (5.15) into the equations (5.12)–(5.14), one may obtain the following differential equations:

$$(D^2 - r^2)\Phi_m = 0, \tag{5.16}$$

where $D \equiv \frac{d}{dz}$,

$$r = \sqrt{\left(\xi^2 - \frac{\xi^2 c^2}{\theta_3^2 + \theta_4^2} + \frac{2\theta_5^2}{\theta_3^2 + \theta_4^2}\right)},$$

$$\left(\frac{d^4}{dz^4} - S\frac{d}{dz^2} + T\right)(\Psi_m, V_m) = 0, \tag{5.17}$$

where

$$S = 2\xi^2 - \frac{\theta_5^2}{\theta_3^2}(\theta_1^2 - 2) - \xi^2 c^2\left(\frac{1}{\theta_2^2} + \frac{1}{\theta_3^2}\right),$$

$$T = \left(\frac{\xi^2 c^2}{\theta_3^2} - \frac{2\theta_5^2}{\theta_3^2} - \xi^2\right)\left(\frac{\xi^2 c^2}{\theta_2^2} - \xi^2\right) - \frac{\theta_1^2\theta_5^2\xi^2}{\theta_3^2}.$$

The equation (5.17) can be rewritten as:

$$(D^2 - s^2)(D^2 - t^2)(\Psi_m, V_m) = 0, \tag{5.18}$$

where

$$s^2, t^2 = \frac{S \pm \sqrt{S^2 - 4T}}{2}.$$

On solving equations (5.16) and (5.18) along with equation (5.11) and using the feasible conditions that $\Phi_m(z), \Psi_m(z), V_m(z) \to 0$ as $z \to \infty$ in the general solution

of the differential equations, one may obtain

$$v_m(x,z,t) = (\wp_1 e^{-sz} B_2 + \wp_2 e^{-tz} B_3) e^{\iota\xi(x-ct)}, \tag{5.19}$$

$$\phi_1^{(m)}(x,z,t) = (-re^{-rz} B_1 - \iota\xi e^{-sz} B_2 - \iota\xi e^{-tz} B_3) e^{\iota\xi(x-ct)}, \tag{5.20}$$

$$\phi_2^{(m)}(x,z,t) = (\iota\xi e^{-rz} B_1 - se^{-sz} B_2 - te^{-tz} B_3) e^{\iota\xi(x-ct)}, \tag{5.21}$$

where

$$\wp_1 = \frac{\theta_3^2}{\theta_5^2}\left(s^2 + \frac{\xi^2 c^2}{\theta_3^2} - \frac{2\theta_5^2}{\theta_3^2} - \xi^2\right),$$

$$\wp_2 = \frac{\theta_3^2}{\theta_5^2}\left(t^2 + \frac{\xi^2 c^2}{\theta_3^2} - \frac{2\theta_5^2}{\theta_3^2} - \xi^2\right).$$

5.3 Boundary conditions and Secular equations

For the propagation of the Love wave in the FGOM medium overlying elastic micropolar half-space, the following limiting conditions must be fulfilled.

(i) Shear stress must vanish at the free-surface of layered structure:

$$\sigma_{yz}^o = 0 \quad at \quad z = -H. \tag{5.22}$$

(ii) At common imperfect interface of FGOM layer and a micropolar half-space, displacement components can be written in terms of stress as:

$$\sigma_{yz}^o = R(v_m - v_o) \quad at \quad z = 0. \tag{5.23}$$

where the parameter R is inversely proportional to the imperfectness. $R = 0$ implies slippage condition, i.e., no bonding between two materials, and $R \to \infty$ corresponds to the perfect interface.

(iii) Stresses must be continuous at the common interface:

$$\sigma_{yz}^o = \sigma_{yz}^m \quad at \quad z = 0. \tag{5.24}$$

(iv) Couple stress vector must vanish at the common interface:

$$\begin{aligned} m_{zz} &= 0 \quad at \quad z = 0, \\ m_{zx} &= 0 \quad at \quad z = 0. \end{aligned} \tag{5.25}$$

Using equation (5.10) into equation (5.3) along with equation (5.5), the following component of the stresses in functionally graded orthotropic medium is obtained as:

$$\sigma^{o}_{yz} = a_1\sqrt{(1-sin\alpha z)}\Bigg(\Bigg[-b\sin bz + \frac{\alpha\cos\alpha z\cos bz}{2(1-\sin\alpha z)}\Bigg]B_1^{'} + \Bigg[b\cos bz + \frac{\alpha\cos\alpha z\sin bz}{2(1-\sin\alpha z)}\Bigg]B_2^{'}\Bigg)e^{\iota\xi(x-ct)}. \tag{5.26}$$

Using equations (5.19)–(5.21) into equations (1.13)–(1.14) of the constitutive relations, one can obtain the following components of the stresses in micropolar medium.

$$\sigma^{(m)}_{yz} = (-\iota\xi\kappa_m e^{-rz}B_1 - \wp_3 e^{-sz}B_2 - \wp_4 e^{-tz}B_3)e^{\iota\xi(x-ct)}, \tag{5.27}$$

$$m^{(m)}_{zx} = (-\iota\wp_5 e^{-rz}B_1 + \wp_6 e^{-sz}B_2 + \wp_7 e^{-tz}B_3)e^{\iota\xi(x-ct)}, \tag{5.28}$$

$$m^{(m)}_{zz} = (\wp_8 e^{-rz}B_1 + \iota\wp_9 e^{-sz}B_2 + \iota\wp_{10} e^{-tz}B_3)e^{\iota\xi(x-ct)}, \tag{5.29}$$

where

$\wp_3 = s(\mu_m\wp_1 - \kappa_m)$, $\quad \wp_4 = t(\mu_m\wp_2 - \kappa_m)$, $\quad \wp_5 = -\xi r(\beta_m + \gamma_m)$,

$\wp_6 = (\beta_m\xi^2 + \gamma_m s^2)$, $\quad \wp_7 = (\beta_m\xi^2 + \gamma_m t^2)$, $\quad \wp_8 = r^2(\alpha_m + \beta_m + \gamma_m) - \alpha_m\xi^2$,

$\wp_9 = \xi s(\beta_m + \gamma_m)$, $\quad \wp_{10} = \xi t(\beta_m + \gamma_m)$.

Using equations (5.10), (5.26), (5.19)–(5.21) and (5.27)–(5.29) into the boundary conditions mentioned in equations (5.22)–(5.25), one can obtain the following algebraic equations with regard to unknown coefficients $B_1^{'}$, $B_2^{'}$, B_1, B_2, and B_3.

$$q_1B_1^{'} + q_2B_2^{'} = 0, \tag{5.30}$$

$$q_3B_1^{'} + \frac{ba_1}{R}B_2^{'} - \wp_1B_2 - \wp_2B_3 = 0, \tag{5.31}$$

$$\frac{a_1\alpha}{2}B_1^{'} + ba_1B_2^{'} + \iota\xi\kappa_mB_1 + \wp_3B_2 + \wp_4B_3 = 0, \tag{5.32}$$

$$\iota\wp_5 B_1 + \wp_6 B_2 + \wp_7 B_3 = 0, \tag{5.33}$$

$$\wp_8 B_1 + \iota\wp_9 B_2 + \iota\wp_{10} B_3 = 0, \tag{5.34}$$

where

$q_1 = b\sin(bH) + \left(\frac{\alpha\cos(\alpha H)\cos(bH)}{2(1+\sin(\alpha H))}\right)$,

$q_2 = b\cos(bH) - \left(\frac{\alpha\cos(\alpha H)\sin(bH)}{2(1+\sin(\alpha H))}\right)$, $\quad q_3 = \frac{\alpha a_1}{2R} + 1.$

The equations (5.30)–(5.34) constitute five boundary conditions. To obtain the non-trivial solution, the determinant of the unknown coefficients $B_1^{'}$, $B_2^{'}$, B_1, B_2, and B_3 of the system must vanish.

$$\wp_{14} p_{16} + \wp_{15} p_{17} = 0, \tag{5.35}$$

where

$\wp_{11} = \wp_6\wp_{10} - \wp_7\wp_9$, $\quad \wp_{12} = \wp_5\wp_{10} + \wp_7\wp_8$, $\quad \wp_{13} = \wp_5\wp_9 + \wp_6\wp_8$,

$\wp_{14} = \xi\kappa_m\wp_{11} - \wp_3\wp_{12} + \wp_4\wp_{13}$, $\quad \wp_{15} = \wp_1\wp_{12} - \wp_2\wp_{13}$,

$p_{16} = \frac{ba_1q_1}{R} - q_2q_3$, $\quad p_{17} = \frac{\alpha a_1 q_2}{2} - ba_1q_1$.

Equation (5.35) represents the dispersion relation for Love-type wave propagation in FGOM medium which is imperfectly bonded with the micropolar substratum.

5.4 Particular cases and Validation of results

5.4.1 Case-1

In the absence of initial stress associated with FGOM medium, i.e., $P_o = 0$, b reduces to $\overline{b} = \xi\sqrt{\frac{\alpha^2}{4\xi^2} + \frac{c^2}{c_o^2} - \frac{a_3}{a_1}}$, equation (5.35) reduces to Love-type wave in FGOM without the initial stress bonded imperfectly over micropolar elastic substrate.

$$\wp_{14}\overline{p_{16}} + \wp_{15}\overline{p_{17}} = 0, \tag{5.36}$$

where

$$\overline{q_1} = \overline{b}\sin(\overline{b}H) + \left(\frac{\alpha\cos(\alpha H)\cos(\overline{b}H)}{2(1+\sin(\alpha H))}\right), \quad \overline{q_2} = \overline{b}\cos(\overline{b}H) - \left(\frac{\alpha\cos(\alpha H)\sin(\overline{b}H)}{2(1+\sin(\alpha H))}\right).$$

$$\overline{p_{16}} = \frac{\overline{b}a_1\overline{q_1}}{R} - \overline{q_2}q_3, \quad \overline{p_{17}} = \frac{\alpha a_1\overline{q_2}}{2} - \overline{b}a_1\overline{q_1}.$$

5.4.2 Case-2

In the absence of heterogeneity parameter, i.e., $\alpha = 0$ and pondering this condition into the previous case, $\overline{b}$ becomes $\widetilde{b} = \xi\sqrt{\frac{c^2}{c_o^2} - \frac{a_3}{a_1}}$, the equation (5.36) reduces to Love-type wave propagating in an orthotropic medium which is imperfectly bonded to micropolar elastic substrate.

$$\wp_{14}\widetilde{p_{16}} + \wp_{15}\widetilde{p_{17}} = 0, \tag{5.37}$$

where

$$\widetilde{q_1} = \widetilde{b}\sin(\widetilde{b}H), \quad \widetilde{q_2} = \widetilde{b}\cos(\widetilde{b}H), \quad \widetilde{q_3} = 1, \widetilde{p_{16}} = \frac{\widetilde{b}a_1\widetilde{q_1}}{R} - \widetilde{q_2}, \quad \widetilde{p_{17}} = -\widetilde{b}a_1\widetilde{q_1}.$$

5.4.3 Case-3

On considering the perfect interface between the layer and the substrate, i.e., $R \to \infty$ and pondering this into case-2, $\widetilde{p_{16}} = \frac{\widetilde{b}a_1\widetilde{q_1}}{R} - \widetilde{q_2}$ changes to $\widetilde{p_{16}} = -\widetilde{q_2}$, the dispersion equation (5.37) reduces to

$$a_1\xi\sqrt{\frac{c^2}{c_o^2} - \frac{a_3}{a_1}}\tan\left(\xi H\sqrt{\frac{c^2}{c_o^2} - \frac{a_3}{a_1}}\right) = -\frac{\wp_{14}}{\wp_{15}}. \tag{5.38}$$

Equation (5.38) represents the dispersion relation for Love-type wave propagation in orthotropic medium bonded perfectly over the micropolar elastic half-space.

5.4.4 Case-4

On considering a homogeneous isotropic medium, i.e., a_1=a_3=μ_o and pondering this condition into the previous case, the dispersion equation (5.38) reduces to

$$\mu_o\xi\sqrt{\frac{c^2}{c_0^2} - 1}\tan\left(\xi H\sqrt{\frac{c^2}{c_0^2} - 1}\right) = -\frac{\wp_{14}}{\wp_{15}}, \tag{5.39}$$

where $c_0 = \sqrt{\mu_o/\rho_0}$.

Equation (5.39) represents the dispersion relation for Love-type wave propagation in the elastic medium which is perfectly bonded over the elastic micropolar half-space.

5.4.5 Case-5

On considering perfect interface between the layer and substrate, i.e., $R \to \infty$ and in the absence of micropolarity, i.e., α_m, β_m, γ_m and $\kappa_m \to 0$, i.e., $\theta_2 \to c_m$ and $\frac{\wp_{14}}{\wp_{15}} \to -\xi\mu_m\sqrt{1-\frac{c^2}{c_m^2}}$; equation (5.35) reduces to

$$\tan\left(\xi H\sqrt{\left(\frac{\alpha}{2\xi}\right)^2+\frac{c^2}{c_o^2}+\frac{P_o-2a_3}{2a_1}}\right) = \frac{\left[-\left(\frac{\alpha}{2\xi}\right)\frac{\cos\alpha H}{1+\sin\alpha H}+\left(\frac{\mu_m}{a_1}\sqrt{1-\frac{c^2}{c_m^2}}+\frac{\alpha}{2\xi}\right)\right]\sqrt{\left(\frac{\alpha}{2\xi}\right)^2+\frac{c^2}{c_o^2}+\frac{P_o-2a_3}{2a_1}}}{\left(\frac{\alpha}{2\xi}\right)^2+\frac{c^2}{c_o^2}+\frac{P_o-2a_3}{2a_1}+\left(\frac{\alpha}{2\xi}\right)\frac{\cos\alpha H}{1+\sin\alpha H}\left(\frac{\mu_m}{a_1}\sqrt{1-\frac{c^2}{c_m^2}}+\frac{\alpha}{2\xi}\right)}. \tag{5.40}$$

Equation (5.40) represents the dispersion relation for Love-type wave propagation in FGOM medium under initial stress which is perfectly bonded over the isotropic elastic half-space which matches with the special case of [154].

5.4.6 Case-6

On pondering the previous case-5 and in the absence of initial stress, i.e., $P_o = 0$; equation (5.40) reduces to

$$\tan\left(\xi H\sqrt{\left(\frac{\alpha}{2\xi}\right)^2+\frac{c^2}{c_o^2}-\frac{a_3}{a_1}}\right) = \frac{\left[-\left(\frac{\alpha}{2\xi}\right)\frac{\cos\alpha H}{1+\sin\alpha H}+\left(\frac{\mu_m}{a_1}\sqrt{1-\frac{c^2}{c_m^2}}+\frac{\alpha}{2\xi}\right)\right]\sqrt{\left(\frac{\alpha}{2\xi}\right)^2+\frac{c^2}{c_o^2}-\frac{a_3}{a_1}}}{\left(\frac{\alpha}{2\xi}\right)^2+\frac{c^2}{c_o^2}-\frac{a_3}{a_1}+\left(\frac{\alpha}{2\xi}\right)\frac{\cos\alpha H}{1+\sin\alpha H}\left(\frac{\mu_m}{a_1}\sqrt{1-\frac{c^2}{\beta_2^2}}+\frac{\alpha}{2\xi}\right)}. \tag{5.41}$$

Equation (5.41) represents the dispersion relation for Love-type wave propagation in FGOM medium without initial stress which is perfectly bonded over the isotropic elastic half-space.

5.4.7 Case-7

On pondering previous case-6 and in the absence of heterogeneity parameter, i.e., $\alpha = 0$; equation (5.41) reduces to

$$\tan\left(\xi H\sqrt{\frac{c^2}{c_o^2}-\frac{a_3}{a_1}}\right)=\frac{\mu_m\sqrt{1-\frac{c^2}{c_m^2}}}{a_1\sqrt{\frac{c^2}{c_o^2}-\frac{a_3}{a_1}}}. \tag{5.42}$$

Equation (5.42) represents the dispersion relation for Love-type wave propagation in the orthotropic medium which is bonded perfectly over the isotropic elastic half-space.

5.4.8 Case-8

On pondering previous case-7 and considering isotropic medium, i.e., a_1=a_3=μ_o; equation (5.42) reduces to

$$\tan\left(\xi H\sqrt{\frac{c^2}{\beta_1^2}-1}\right)=\frac{\mu_m\sqrt{1-\frac{c^2}{c_m^2}}}{\mu_o\sqrt{\frac{c^2}{c_0^2}-1}}. \tag{5.43}$$

Equation (5.43) represents the dispersion relation for Love-type wave propagation in isotropic elastic layer lying over the isotropic elastic substrate which matches with the well-known Classical Love wave [122] equation which validates the outcome of the present problem.

5.5 Numerical results

This section aims to show the impact of imperfect bonding (at the substratum-substrate cross-section), the effects of the initial stress and heterogeneity parameter (gradient factor) associated with the FGOM medium, together with the coupling

and scaling dimensions of the substrate that shows size-dependence properties on the Love-type wave propagation in the composite structure. The characteristic curves are drawn in order to graphically illustrate these results, i.e., the curves that elucidate the variations in the phase speed $\frac{c}{c_o}$ against the wave number ξH. The material properties of the semi-infinite micropolar elastic medium are considered the same as provided in Table 3.1 of Chapter 3 and the material properties of FGOM medium are listed as in Table 5.1. Figures 5.2–5.6 are plotted to illustrate the influence of micropolarity, material length scale parameter, initial stress, gradedness, the imperfectness of interface, on the phase velocity profiles of Love-type wave in the considered model. Significant effects have been observed from the dispersion curves for affecting parameters. It is observed from dispersive curves that with the increase in wave number, the phase velocity of the Love-type wave decreases in the considered model.

Table 5.1: Material constants for FGOM medium [63]

a_1	5.65×10^{10}	$\mathrm{N/m^2}$
a_3	2.46×10^{10}	$\mathrm{N/m^2}$
ρ_o	7800	$\mathrm{kg/m^3}$

5.5.1 Effect of the imperfectness of stratum-substrate interface

Scrutinizing the impact of imperfectness on Love-type wave propagation is necessary due to degradation of materials, distortion of the interface, or some kind of cracks present at the interface of complex structures like earth where its layers are not always perfectly bonded. As the value of imperfect parameter $R \to \infty$, one can get the continuity condition for displacement field components, which means the perfect bonding between the layer and the substrate. Furthermore, $R = 0$ indicates slippage condition at the interface, i.e., no bonding at the surface of two dissimilar materials. To elucidate this effect, the variation in the value of imperfectness is considered, i.e, $R = 0.35 * 10^{10}, 2 * 0.35 * 10^{10}, 10 * 0.35 * 10^{10}$. The dispersion curves reveal that the presence of imperfectness leads to a decrease in phase velocity of the considered

wave, which means phase velocity for perfectly bonded media is more in comparison to imperfectly bonded ones which is shown in figure 5.2.

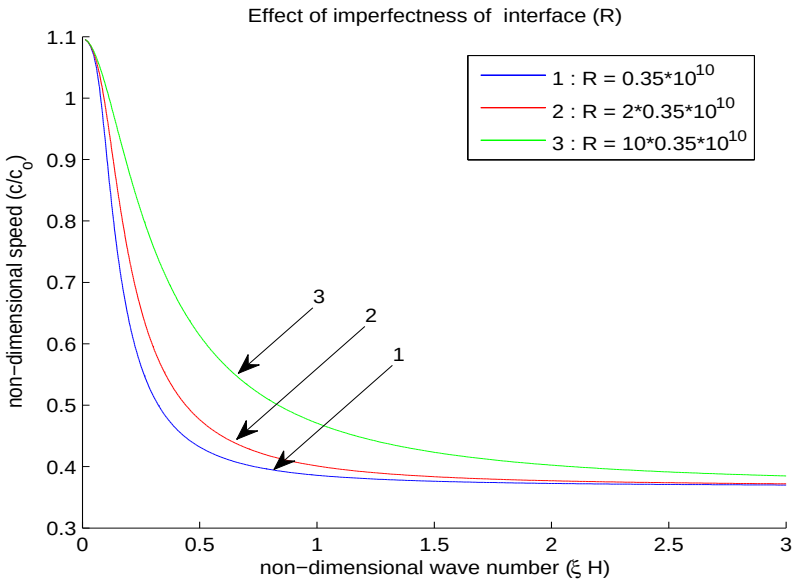

Figure 5.2: Characteristic curves ($\frac{c}{c_o}$ versus ξH) for variation of imperfectness of the interface on the Love-wave phase velocity.

5.5.2 Effect of FGOM stratum

Influence of initial stress parameter (I)**:**

Due to the overburdening of layers, temperature fluctuation, sluggish cracking process, scrutinizing the influence of initial stress in the phase velocity of the Love wave is essential. Figure 5.3 delineates the impact of initial stress when the FGOM layer and size-dependent substrate are imperfectly bonded. To elucidate this effect, the different values of initial stress parameter are considered as $I = 0, 0.1, 0.2, 0.3$. The curve $I = 0$ indicates no initial stress in the considered structure. This figure manifests that initial stress associated with FGOM has disfavoring effects on the phase velocity of the Love-type wave, i.e, with the growing value of this parameter, the phase velocity of the Love-type wave decreases. Another important effect that can be seen from the profile is that the phase velocity is higher in the case of the absence of initial stress, that is, the presence of initial stress reduces the phase velocity of the

Love wave which shows its significance practically.

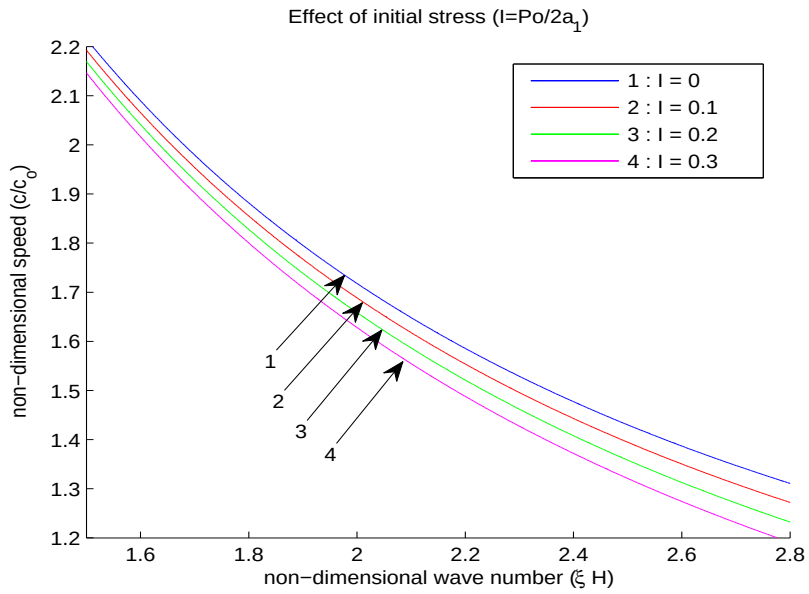

Figure 5.3: Variation of $\frac{c}{c_o}$ versus ξH for different values of initial stress ($I = Po/2a_1$) on the Love-wave phase velocity.

Influence of gradedness or heterogeneity parameter:

The presence of heterogeneity or gradedness of the FGOM media has a significant effect on the phase velocity of Love-type wave propagation in the considered structure. To study this effect, different values of heterogeneity parameters are considered as $\alpha H = 0.6, 1.2, 1.6$. It is observed from the figure 5.4 that the heterogeneity parameter has favoring effect on the phase velocity, i.e., as the values of this parameter increases, the phase velocity of the Love-type wave increases.

5.5.3 Effect of micropolar elastic substrate

Influence of characteristic length:

In order to assess the size effect of structurally sensitive materials incorporating cellular solids, microporosity, granular media, bones, platelets, microcracking, it is important to investigate the effect of the microstructure on the phase velocity of wave propagation in the considered structure. To address this size-effect, the dispersion curves are plotted by considering different values of characteristic length parameter which is

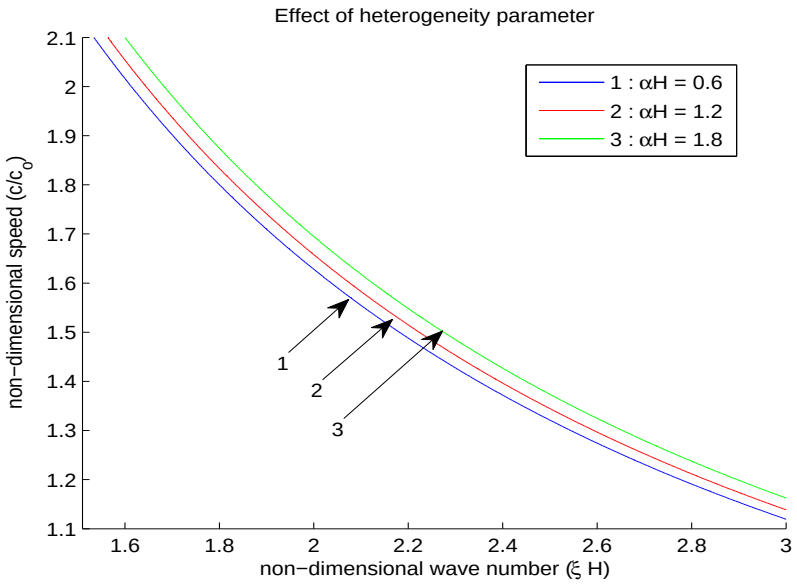

Figure 5.4: Variation of $\frac{c}{c_o}$ versus ξH for different values of heterogeneity parameter (αH) on the Love-wave phase velocity.

the order of average cell size of the microstructure, i.e., $l = 0.001m, 0.002m, 0.003m$. It can be observed from figure 5.5 that material length scale parameter (l) exhibits an encouraging impact on the phase velocity profiles of a Love-type wave.

Influence of coupling factor:

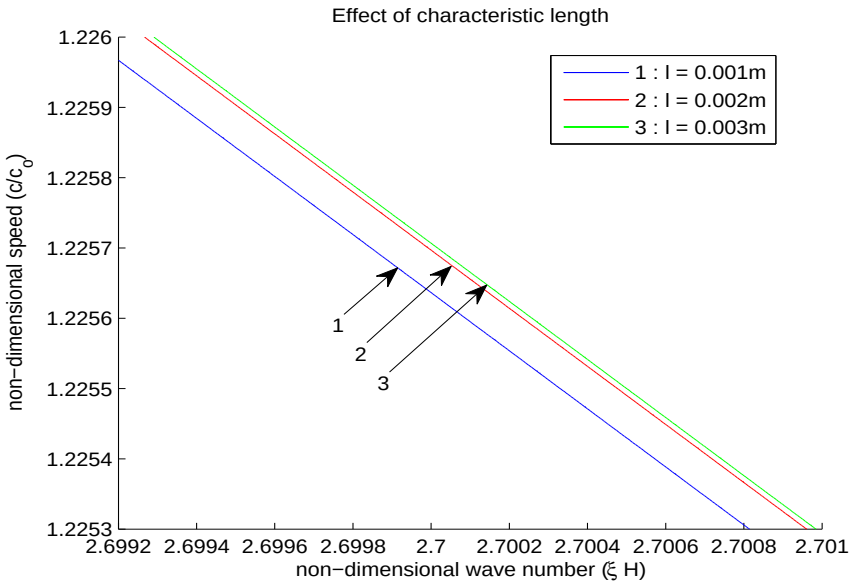

Figure 5.5: Variation of $\frac{c}{c_o}$ versus ξH for different values of length scale parameter on the Love-wave phase velocity.

The coupling factor (N) quantifies the degree of micropolarity of the size-dependent substrate. To acquaint the effect of micropolarity on the phase velocity of Love-type waves, the characteristic curves are plotted by taking different values of coupling factor, i.e., $N = 0.1, 0.6, 0.9$. Figure 5.6 reflects the influence of the coupling factor and shows the prominent effects of micropolarity on the phase velocity profiles of the Love-type wave. It can be seen that the coupling factor exhibits a positive correlation on the phase velocity of wave propagation in the considered structure. This effect justifies the consideration of microstructural properties of the semi-infinite size-dependent substrate.

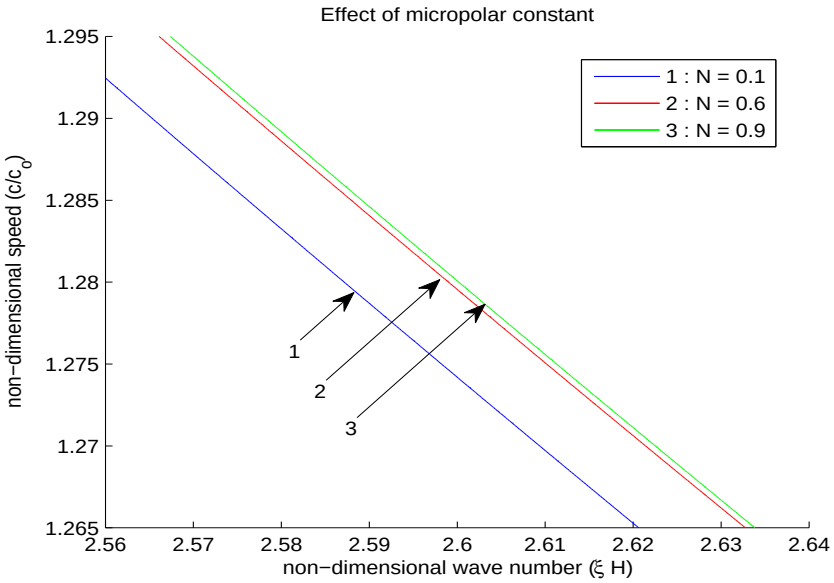

Figure 5.6: Variation of $\frac{c}{c_o}$ versus ξH for different values of coupling factor on the Love-wave phase velocity.

5.6 Conclusion

The present chapter scrutinizes the influence of imperfect bonding at the common interface of FGOM media overlying micropolar elastic substrate to gain a better understanding of the role of layer bonding in considered structures. The closed expression of dispersion relations is accomplished to study Love-type wave propagation in a composite layered system. Numerical computations are performed and the dispersion

expressions are plotted to study the influence of the micropolarity and characteristic length of the substratum exhibiting size-dependency properties; the influence of gradient factor, initial stress of the substratum as well as to study the influence of imperfect parameters, on the phase velocity of Love-type wave propagation in the considered model. The following are the outcomes of the present study:

(i) In the considered problem, the phase velocity of the Love-type wave decreases with an increase in wave number.

(ii) The coupling factor (N) exhibits a substantial effect on the phase velocity of Love-type waves. As the magnitude of the coupling factor increases, the phase velocity also increases.

(iii) The length scale parameter also affects the phase velocity profiles significantly. The phase velocity of the Love-type wave increases with the increment in the characteristic length parameter.

(iv) The gradedness of the substratum has an encouraging effect on the phase velocity of the Love-type wave. As the magnitude of the graded parameter increases, the phase velocity also increases.

(v) Initial stress associated with FGOM does not exhibit favoring effects on the phase velocity characteristics of Love-type wave, i.e, as the value of this parameter increases, the phase velocity of Love-type wave decreases.

(vi) The joint efficiency is diminished substantially by imperfections in the bond line, such as cracks, porosity, etc.

(vii) The Classical Love wave equation is also derived for the sake of validation of results.

The obtained results in some cases depict the negligible effects due to the considered authentic range of material constants. These considerations of microstructure and imperfectness may play an important role in the design and modification of various Love-wave based devices.

Chapter 6

Size-dependent investigation on Rayleigh-type wave in fibre-reinforced layered medium

6.1 Introduction

Scrutinizing the Rayleigh wave propagation phenomena with different boundary conditions plays an important role in examining the dynamics of the earth's structure under different environmental conditions. The magnitude of amplitude of such waves decreases with the distance from the surface resulting in a larger amount of volatile energy that is the main cause of earthquake damage. Many researchers have studied Rayleigh-type seismic wave propagation in various media and have been able to collect a vast amount of information about the earth's interior [45, 17, 3, 4, 63, 62, 195]. In addition, Rayleigh-type waves are used to locate cracks and imperfections in the ultrasonic frequency range [199, 120] and to identify the material's superficial defects [152]. Various researchers have outlined many useful facts in order to illustrate the characteristic of Rayleigh-type wave propagation considering different media [146, 26, 1, 85].

The content of this chapter is communicated in SCI journal

Advances in material sciences have motivated reinforced materials which are superior to many traditional metal materials. These materials are preferred due to their various desirable characteristics such as firmness, low thickness, high strength, resistance to corrosion, and vitality preservation, in many styles of buildings for dams, bridges, buildings, and floor foundations. The literature offers ample evidence that the earth medium might have hard/soft rocks or material with self-reinforcing features. Characteristically, as long as the components of such material remain in the elastic state, the material function together as one anisotropic entity so that they are not relatively displaced. Such features are useful in reducing damage caused by earthquake or vibration effects. Moreover, the study of seismic wave propagation in self-fiber reinforced medium (SFR) plays an important role in several contexts because of their various attractive applications in the construction sector, architecture, and civil engineering. Due to intense temperature and pressure, fiber materials are transformed into SFR materials. Initially, the continuous self-reinforcement model proposed by Belfield et al. [14] which was used by several authors in different fields [24, 23, 89, 171].

In understanding and predicting seismic behavior on the different margins of the earth, a good amount of research has been done to understand the microstructural characteristics of the material. The earth's interior consists of a series of dense shells and damage to the inelastic strain produced inside the earth's crust results from the release of energy from the micro-crack field. In this chapter, the propagation characteristics of the Rayleigh-type wave in the composite structure utilizing the microcontinuum hypothesis are studied. To make the model more pertinent and application-oriented, a layer-based structure is assumed containing a size-dependent couple stress substrate, coated with a thin finite layer of self-fiber reinforced material. Using adequate boundary conditions, the closed-form of the secular equation is obtained analytically. The graphical demonstration is accomplished, featuring the impacts of layer thickness along with size-dependence effects related to the substrate. In addition, the reinforcement effects on phase velocity profiles of Rayleigh-type waves are also shown by comparing the effect of the self-fiber reinforced medium and reinforced-free medium. The particular cases are also deduced that are closely consistent with the existing

findings.

6.2 Problem formulation and Solutions

Consider a model comprising of a semi-infinite size-dependent couple stress elastic medium (M_1) covered with a homogeneous self-fiber reinforced medium (M_0) of thickness H. A stress-free surface is assumed on the reinforced medium. The Cartesian coordinate system is considered in such a way that the wave is propagating along the direction of the x-axis and the z-axis acts in the vertically downward direction. Furthermore, the propagation of surface waves is analyzed in a two-dimensional framework and assuming no particle variation along the y-direction, in light of the fact that the particles are believed to be displaced evenly along the y-axis so that $\frac{\partial}{\partial y} \equiv 0$. The geometry of the considered model is depicted in figure 6.1.

Let $u_i^{(f)} = (u_f, v_f, w_f)$ and $u_i^{(c)} = (u_c, v_c, w_c)$ be the displacement components in

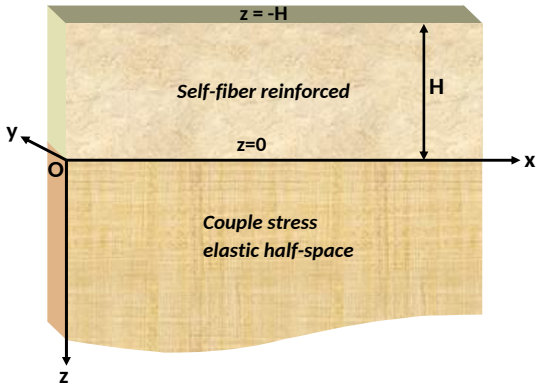

Figure 6.1: Physical model of the problem

the upper self-fiber reinforced layer and lower couple stress substrate, respectively, for surface wave propagation in considered model.

For Rayleigh-type wave propagation, one may have

$$\begin{aligned} u_f = u_f(x,z,t),\ v_f = 0,\ w_f = w_f(x,z,t), \\ u_c = u_c(x,z,t),\ v_c = 0,\ w_c = w_c(x,z,t). \end{aligned} \tag{6.1}$$

6.2.1 For self-fiber reinforced layer at $-H < z < 0$

The equation of motion for the self-fiber reinforced medium layer (M_0) in the absence of the body forces is

$$\sigma_{ji,j} = \rho_f \ddot{u}_i, \tag{6.2}$$

where i, $j = 1, 2, 3$; ρ_f is the density of reinforced medium (M_0).
The constitutive equation for the self-fiber reinforced medium is:

$$\begin{aligned}\sigma_{ij}^{(f)} = \lambda_f e_{rr}\delta_{ij} + 2\mu_T e_{ij} + \alpha_f(a_r a_m e_{rm}\delta_{ij} + a_i a_j e_{rr}) + \\ 2(\mu_L - \mu_T)(a_i a_r e_{rj} + a_j a_r e_{ri}) + \beta_f(a_r a_m e_{rm} a_i a_j),\end{aligned} \tag{6.3}$$

and

$$e_{ij} = \frac{u_{i,j} + u_{j,i}}{2},$$

where λ_f, α_f, β_f, μ_L, μ_T are the elastic constants having dimension same as of the stress; $\sigma_{ij}^{(f)}$ and e_{ij} represent the stress tensor and the strain tensor respectively; the direction of the reinforcement is considered along $\overrightarrow{a} = (a_1, a_2, a_3)$ such that $a_1^2 + a_2^2 + a_3^2 = 1$; "$f$" as subscript and superscript represent the quantity related to the reinforced medium.
The components of $\overrightarrow{a}$ is chosen as $(1, 0, 0)$, i.e., the reinforcement direction is assumed along the x-axis.
By utilizing equation (6.1) and (6.3) into (6.2), the equation of motion for the reinforced medium becomes

$$\begin{aligned}L_1\frac{\partial^2 u_f}{\partial x^2} + L_2\frac{\partial^2 w_f}{\partial x \partial z} + \mu_L\frac{\partial^2 u_f}{\partial z^2} = \rho_f\frac{\partial^2 u_f}{\partial t^2}, \\ \mu_L\frac{\partial^2 w_f}{\partial x^2} + L_2\frac{\partial^2 u_f}{\partial x \partial z} + L_3\frac{\partial^2 w_f}{\partial z^2} = \rho_f\frac{\partial^2 w_f}{\partial t^2},\end{aligned} \tag{6.4}$$

where
$L_1 = (\lambda_f + 2\alpha_f + 4\mu_L - 2\mu_T + \beta_f)$,
$L_2 = (\lambda_f + \alpha_f + \mu_L)$,
$L_3 = \lambda_f + 2\mu_T$.

Assume the solution of equation (6.4) as:

$$\begin{aligned} u_f &= A_1 e^{-p\xi z} e^{\iota\xi(x-ct)}, \\ w_f &= A_2 e^{-p\xi z} e^{\iota\xi(x-ct)}. \end{aligned} \tag{6.5}$$

Substituting equation (6.5) into (6.4), one may obtain

$$\begin{aligned} (p^2\mu_L + \rho_f c^2 - L_1)A_1 - \iota p L_2 A_2 = 0, \\ -\iota p L_2 A_1 + (p^2 L_3 + \rho_f c^2 - \mu_L)A_2 = 0. \end{aligned} \tag{6.6}$$

On solving equation (6.6), the non-trivial solution becomes

$$\left(\frac{L_3}{\mu_L}\right)p^4 + M_1 p^2 + N_1 = 0, \tag{6.7}$$

where

$p_j^2 = \dfrac{-M_1 \pm \sqrt{M_1^2 - 4N_1\left(\frac{L_3}{\mu_L}\right)}}{2\left(\frac{L_3}{\mu_L}\right)}$, $j = 1, 2$, $\quad c_f = \sqrt{\frac{\mu_L}{\rho_f}}$,

$M_1 = \left(\frac{c^2}{c_f^2} - 1\right) + \left(\frac{L_3}{\mu_L}\right)\left(\frac{c^2}{c_f^2} - \frac{L_1}{\mu_L}\right) + \left(\frac{L_2^2}{\mu_L^2}\right)$, $N_1 = \left(\frac{c^2}{c_f^2} - \frac{L_1}{\mu_L}\right)\left(\frac{c^2}{c_f^2} - 1\right)$.

Using equations (6.5)–(6.7), the resulting mechanical displacement components for the reinforced medium are:

$$\begin{aligned} u_f(x,z,t) &= [\Re_1 e^{-p_1\xi z} + \Re_2 e^{-p_2\xi z} + \Re_3 e^{p_1\xi z} + \Re_4 e^{p_2\xi z}]e^{\iota\xi(x-ct)}, \\ w_f(x,z,t) &= [\zeta_1(\Re_1 e^{-p_1\xi z} - \Re_3 e^{p_1\xi z}) + \zeta_2(\Re_2 e^{-p_2\xi z} - \Re_4 e^{p_2\xi z})]e^{\iota\xi(x-ct)}, \end{aligned} \tag{6.8}$$

where

$$\zeta_j = \frac{p_j^2 + \frac{c^2}{c_f^2} - \frac{L_1}{\mu_L}}{\iota\left(p_j \frac{L_2}{\mu_L}\right)}, \quad j = 1, 2.$$

Here, $\Re_1$, $\Re_2$, $\Re_3$, and $\Re_4$ are the arbitrary unknown coefficients.

6.2.2 For couple stress substrate at $z > 0$

To solve equation (1.19), the displacement potential function ϕ_c and ψ_c are introduced which are defined as

$$\vec{u} = \nabla\phi_c + \nabla \times \vec{\psi_c}, \quad \nabla.\vec{\psi_c} = 0, \tag{6.9}$$

where $\overrightarrow{\psi_c} = (0, \psi_c, 0)$.

The component form of the displacement vector in couple stress elastic half-space is:

$$u_f = \frac{\partial\phi_c}{\partial x} - \frac{\partial\psi_c}{\partial z}, \qquad v_f = 0, \qquad w_f = \frac{\partial\phi_c}{\partial z} + \frac{\partial\psi_c}{\partial x}. \tag{6.10}$$

Using equation (6.10), the equation of motion for the propagation of Rayleigh-type surface wave in the couple stress medium in terms of the displacement potential functions ϕ_c and ψ_c can be written as:

$$\begin{aligned} \frac{\partial^2\phi_c}{\partial x^2} + \frac{\partial^2\phi_c}{\partial z^2} &= \frac{1}{c_{c1}^2}\frac{\partial^2\phi_c}{\partial t^2}, \\ (1 - l^2\nabla^2)\left(\frac{\partial^2\psi_c}{\partial x^2} + \frac{\partial^2\psi_c}{\partial z^2}\right) &= \frac{1}{c_{c2}^2}\frac{\partial^2\psi_c}{\partial t^2}, \end{aligned} \tag{6.11}$$

where

$c_{c1} = \sqrt{\frac{\lambda_c + 2\mu_c}{\rho_c}}, \quad c_{c2} = \sqrt{\frac{\mu_c}{\rho_c}}$.

Here, c_{c1} and c_{c2} are the dilatational and the shear wave propagation speed in the considered composite structure.

Assuming the solution of equation (6.11) as:

$$\begin{aligned} \phi_c(x, z, t) &= F(z)e^{\iota\xi(x-ct)}, \\ \psi_c(x, z, t) &= G(z)e^{\iota\xi(x-ct)}. \end{aligned} \tag{6.12}$$

On substituting equation (6.12) into (6.11), one may get the following differential equations

$$\begin{aligned} \frac{d^2F}{dz^2} - r^2F(z) &= 0, \\ \frac{d^4G}{dz^4} - M_2\frac{d^2G}{dz^2} + N_2G(z) &= 0. \end{aligned} \tag{6.13}$$

On solving equation (6.13) and by applying feasible conditions for the substrate, i.e., $\{F(z), G(z)\} \to 0$ as $z \to \infty$ in the general solution of the differential equations, one may obtain

$$\begin{aligned} \phi_c(x,z,t) &= \Re_5 e^{-rz} e^{\iota\xi(x-ct)}, \\ \psi_c(x,z,t) &= [\Re_6 e^{-sz} + \Re_7 e^{-tz}] e^{\iota\xi(x-ct)}, \end{aligned} \tag{6.14}$$

where $\omega = \xi c$, c is the phase speed and ξ is the wave number.

$$\begin{aligned} r^2 = \xi^2\left(1 - \frac{c^2}{c_{c1}^2}\right), \qquad s^2, t^2 = \frac{M_2 \pm \sqrt{M_2^2 - 4N_2}}{2}, \\ M_2 = \left(2\xi^2 + \frac{1}{l^2}\right), \qquad N_2 = \left(\xi^4 + \frac{\xi^2}{l^2} - \frac{\omega^2}{l^2 c_{c2}^2}\right). \end{aligned}$$

By substituting equation (6.14) into (6.10), the resulting mechanical displacement components for the couple stress substrate are obtained as

$$\begin{aligned} u_c(x,z,t) &= [\iota\xi e^{-rz}\Re_5 + s e^{-sz}\Re_6 + t e^{-tz}\Re_7] e^{\iota\xi(x-ct)}, \\ w_c(x,z,t) &= [-r e^{-rz}\Re_5 + \iota\xi e^{-sz}\Re_6 + \iota\xi e^{-tz}\Re_7] e^{\iota\xi(x-ct)}, \end{aligned} \tag{6.15}$$

where $\Re_5$, $\Re_6$, and $\Re_7$ are the arbitrary unknown coefficients.

6.3 Boundary Conditions and Dispersion relations

The boundary conditions for Rayleigh-type wave propagation in a considered composite structure are:

(A) At the traction-free surface of upper medium, i.e., at $z = -H$:

$$\sigma_{zz}^f = 0, \qquad \sigma_{zx}^f = 0. \tag{6.16}$$

(B) At the common interface of layer and substrate, i.e., at $z = 0$:

$$\sigma_{zz}^f = \sigma_{zz}^c, \qquad \sigma_{zx}^f = \sigma_{zx}^c, \qquad u_f = u_c, \qquad w_f = w_c, \qquad \mu_{zy}^c = 0. \tag{6.17}$$

Using equation (6.1) into equation (6.3), the constitutive equations in term of the displacement components are obtained as:

$$\begin{aligned}\sigma_{zz}^{(f)} &= (\lambda_f + \alpha_f)\frac{\partial u_f}{\partial x} + (\lambda_f + 2\mu_T)\frac{\partial w_f}{\partial z},\\ \sigma_{zx}^{(f)} &= \mu_L\left(\frac{\partial u_f}{\partial z} + \frac{\partial w_f}{\partial x}\right).\end{aligned} \tag{6.18}$$

Using equation (6.8), equation (6.18) reduces to

$$\begin{aligned}\sigma_{zz}^{(f)} &= \iota\xi[m_1\Re_1 e^{-p_1\xi z} + m_2\Re_2 e^{-p_2\xi z} + m_1\Re_3 e^{p_1\xi z} + m_2\Re_4 e^{p_2\xi z}]e^{\iota\xi(x-ct)},\\ \sigma_{zx}^{(f)} &= \iota\mu_L[-m_3\Re_1 e^{-p_1\xi z} - m_4\Re_2 e^{-p_2\xi z} + m_3\Re_3 e^{p_1\xi z} + m_4\Re_4 e^{p_2\xi z}]e^{\iota\xi(x-ct)},\end{aligned} \tag{6.19}$$

where

$m_1 = (\lambda_f + \alpha_f) - p_1\zeta_1(\lambda_f + 2\mu_T), \quad m_2 = (\lambda_f + \alpha_f) - p_2\zeta_2(\lambda_f + 2\mu_T),$

$m_3 = (p_1 + \zeta_1), \quad m_4 = (p_2 + \zeta_2).$

Using equation (6.1) into (1.17) and (1.18), one may obtain the following constitutive relations in terms of the displacement components as

$$\begin{aligned}\sigma_{zz}^{(c)} &= \lambda_c\frac{\partial u_c}{\partial x} + (\lambda_c + 2\mu_c)\frac{\partial w_c}{\partial z},\\ \sigma_{zx}^{(c)} &= \mu_c\left(\frac{\partial u_c}{\partial z} + \frac{\partial w_c}{\partial x}\right) - \mu_c l^2\left(\frac{\partial^3 u_c}{\partial x^2\partial z} - \frac{\partial^3 w_c}{\partial x^3} + \frac{\partial^3 u_c}{\partial z^3} - \frac{\partial^3 w_c}{\partial x\partial z^2}\right),\\ \mu_{zy}^{(c)} &= -2\mu_c l^2\left(\frac{\partial^2 u_c}{\partial z^2} - \frac{\partial^2 w_c}{\partial x\partial z}\right).\end{aligned} \tag{6.20}$$

On substituting equation (6.15) into equation (6.20), one may obtain

$$\begin{aligned}\sigma_{zz}^{(c)} &= [\xi_1 e^{-rz}\Re_5 - \iota\xi\xi_2 e^{-sz}\Re_6 - \iota\xi\xi_3 e^{-tz}\Re_7]e^{\iota\xi(x-ct)},\\ \sigma_{zx}^{(c)} &= -[\iota\xi\xi_4 e^{-rz}\Re_5 + \xi_5 e^{-sz}\Re_6 + \xi_6 e^{-tz}\Re_7]e^{\iota\xi(x-ct)},\\ \mu_{zy}^{(c)} &= 2\mu_c l^2[\xi_7 e^{-sz}\Re_6 + \xi_8 e^{-tz}\Re_7]e^{\iota\xi(x-ct)},\end{aligned} \tag{6.21}$$

where

$\xi_1 = \mu_c\left[\frac{c_1^2}{c_2^2}(r^2 - \xi^2) + 2\xi^2\right], \quad \xi_2 = 2\mu_c s, \quad \xi_3 = 2\mu_c t,$

$\xi_4 = 2\mu_c r, \quad \xi_5 = \mu_c[(s^2 + \xi^2) - l^2(s^2 - \xi^2)^2], \quad \xi_6 = \mu_c[(t^2 + \xi^2) - l^2(t^2 - \xi^2)^2],$

$\xi_7 = s(s^2 - \xi^2), \quad \xi_8 = t(t^2 - \xi^2).$

Using equations (6.8), (6.19), (6.15) and (6.21) into the boundary conditions (6.16)–(6.17), one may obtain the following algebraic equations with regards to unknown coefficients $\Re_1$, $\Re_2$, $\Re_3$, $\Re_4$, $\Re_5$, $\Re_6$, $\Re_7$.

$$m_1\Re_1 e^{p_1\xi H} + m_2\Re_2 e^{p_2\xi H} + m_1\Re_3 e^{-p_1\xi H} + m_2\Re_4 e^{-p_2\xi H} = 0, \tag{6.22}$$

$$m_3\Re_1 e^{p_1\xi H} + m_4\Re_2 e^{p_2\xi H} - m_3\Re_3 e^{-p_1\xi H} - m_4\Re_4 e^{-p_2\xi H} = 0, \tag{6.23}$$

$$\iota\xi[m_1\Re_1 + m_2\Re_2 + m_1\Re_3 + m_2\Re_4] - \xi_1\Re_5 + \iota\xi\xi_2\Re_6 + \iota\xi\xi_3\Re_7 = 0, \tag{6.24}$$

$$\iota\mu_L[-m_3\Re_1 - m_4\Re_2 + m_3\Re_3 + m_4\Re_4] + \iota\xi\xi_4\Re_5 + \xi_5\Re_6 + \xi_6\Re_7 = 0, \tag{6.25}$$

$$\Re_1 + \Re_2 + \Re_3 + \Re_4 - \iota\xi\Re_5 - s\Re_6 - t\Re_7 = 0, \tag{6.26}$$

$$\iota\zeta_1(\Re_1 - \Re_3) + \iota\zeta_2(\Re_2 - \Re_4) + r\Re_5 - \iota\xi\Re_6 - \iota\xi\Re_7 = 0, \tag{6.27}$$

$$\xi_7\Re_6 + \xi_8\Re_7 = 0. \tag{6.28}$$

The equations (6.22)–(6.28) constitute seven boundary conditions. To obtain the non-trivial solution, the determinant of the unknown coefficients $\Re_1$, $\Re_2$, $\Re_3$, $\Re_4$, $\Re_5$, $\Re_6$, $\Re_7$ of the system must vanish.

$$\begin{aligned} &\chi_3(S_1 + S_2)e^{(p_1+p_2)\xi H} + \chi_3(-S_1 + S_2)e^{-(p_1+p_2)\xi H} \\ &+\chi_4(S_3 + S_4)e^{(p_1-p_2)\xi H} + \chi_4(S_3 - S_4)e^{-(p_1-p_2)\xi H} + S_5 = 0, \end{aligned} \tag{6.29}$$

where

$S_1 = t_5\chi_2 - t_6\chi_5 - t_9\chi_{10}, \quad S_2 = -t_7\chi_7 - t_8\chi_8 + t_{10}\chi_3, \quad S_3 = t_5\chi_1 + t_7\chi_6 + t_8\chi_9 - t_{10}\chi_4,$
$S_4 = -t_6\chi_5 + t_9\chi_{10}, \quad S_5 = -4m_1m_2\zeta_2t_5 - 4m_2m_4\zeta_1t_5 - 4m_1m_3m_4t_7 - 4m_2m_3m_4t_7 -$
$4m_1m_2m_3\zeta_2t_8 - 4m_1m_2m_4\zeta_1t_8 + 8m_1m_2m_3m_4t_{10},$
$t_1 = \xi_3\xi_7 - \xi_2\xi_8, \quad t_2 = \xi_5\xi_8 - \xi_6\xi_7, \quad t_3 = s\xi_8 - t\xi_7, \quad t_4 = \xi_7 - \xi_8,$
$t_5 = -(\xi^2\xi_4t_1 + t_2\xi_1), \quad t_6 = -\xi\mu_L(\xi^2t_1 + t_3\xi_1), \quad t_7 = \xi^2\mu_L(rt_1 - t_4\xi_1),$
$t_8 = \xi^2(t_3\xi_4 - t_2), \quad t_9 = \xi(rt_2 + \xi^2t_4\xi_4), \quad t_{10} = \xi^2\mu_L(rt_3 + \xi^2t_4),$
$\chi_1 = \zeta_1 + \zeta_2, \quad \chi_2 = \zeta_1 - \zeta_2, \quad \chi_3 = m_2m_3 - m_1m_4, \quad \chi_4 = m_2m_3 + m_1m_4,$

$\chi_5 = m_4\zeta_1 - m_3\zeta_2, \quad \chi_6 = m_3 + m_4, \quad \chi_7 = m_3 - m_4, \quad \chi_8 = -m_1\zeta_2 + m_2\zeta_1,$
$\chi_9 = m_1\zeta_2 + m_2\zeta_1, \quad \chi_{10} = m_1 - m_2.$

6.4 Particular Cases

6.4.1 Case-1:

When $\mu_L = \mu_T = \mu_f$, $\alpha_f = 0$, $\beta_f = 0$, i.e., reinforced free medium.

$$\overline{\chi_3}(\overline{S_1} + \overline{S_2})e^{(\overline{p_1}+\overline{p_2})\xi H} + \overline{\chi_3}(-\overline{S_1} + \overline{S_2})e^{-(\overline{p_1}+\overline{p_2})\xi H} + \overline{\chi_4}(\overline{S_3} + \overline{S_4})e^{(\overline{p_1}-\overline{p_2})\xi H} + \overline{\chi_4}(\overline{S_3} - \overline{S_4})e^{-(\overline{p_1}-\overline{p_2})\xi H} + \overline{S_5} = 0, \tag{6.30}$$

where $\overline{S_1} = t_5\overline{\chi_2} - \overline{t_6}\overline{\chi_5} - t_9\overline{\chi_{10}}, \quad \overline{S_2} = -\overline{t_7}\overline{\chi_7} - t_8\overline{\chi_8} + \overline{t_{10}}\overline{\chi_3},$
$\overline{S_3} = t_5\overline{\chi_1} + \overline{t_7}\overline{\chi_6} + t_8\overline{\chi_9} - \overline{t_{10}}\overline{\chi_4}, \quad \overline{S_4} = -\overline{t_6}\overline{\chi_5} + t_9\overline{\chi_{10}},$
$\overline{S_5} = -4\overline{m_1m_2}\overline{\zeta_2}t_5 - 4\overline{m_2m_4}\overline{\zeta_1}t_5 - 4\overline{m_1m_3m_4}\overline{t_7} - 4\overline{m_2m_3m_4}\overline{t_7} - 4\overline{m_1m_2m_3}\overline{\zeta_2}t_8 - 4\overline{m_1m_2m_4}\overline{\zeta_1}t_8 + 8\overline{m_1m_2m_3m_4}\overline{t_{10}},$
$\overline{L_1} = (\lambda_f + 2\mu_f) = \overline{L_3}, \quad \overline{L_2} = (\lambda_f + \mu_f), \quad \overline{c_f} = \sqrt{\frac{\mu_f}{\rho_f}},$
$\overline{p_j^2} = \frac{-\overline{M_1} \pm \sqrt{\overline{M_1}^2 - 4\overline{N_1}\left(\frac{\overline{L_1}}{\mu_f}\right)}}{2\left(\frac{\overline{L_1}}{\mu_f}\right)}; \; j = 1, 2, \quad \overline{\zeta_j} = \frac{\overline{p_j}^2 + \frac{c^2}{\overline{c_f}^2} - \frac{\overline{L_1}}{\mu_f}}{\iota\left(\overline{p_j}\frac{\overline{L_2}}{\mu_f}\right)}, \quad j = 1, 2,$
$\overline{M_1} = \left(\frac{c^2}{\overline{c_f}^2} - 1\right) + \left(\frac{\overline{L_1}}{\mu_f}\right)\left(\frac{c^2}{\overline{c_f}^2} - \frac{\overline{L_1}}{\mu_f}\right) + \left(\frac{\overline{L_2}}{\mu_f}\right)^2, \quad \overline{N_1} = \left(\frac{c^2}{\overline{c_f}^2} - \frac{\overline{L_1}}{\mu_f}\right)\left(\frac{c^2}{\overline{c_f}^2} - 1\right),$
$\overline{m_j} = \lambda_f - \overline{p_j}\overline{\zeta_j}\overline{L_1}, \quad j = 1, 2, \quad \overline{m_j} = (\overline{p_j} + \overline{\zeta_j}), \quad j = 3, 4$
$\overline{t_6} = -\xi\mu_f(\xi^2 t_1 + t_3\xi_1), \quad \overline{t_7} = \xi^2\mu_f(rt_1 - t_4\xi_1), \quad \overline{t_{10}} = \xi^2\mu_f(rt_3 + \xi^2 t_4),$
$\overline{\chi_1} = \overline{\zeta_1} + \overline{\zeta_2}, \quad \overline{\chi_2} = \overline{\zeta_1} - \overline{\zeta_2}, \quad \overline{\chi_3} = \overline{m_2m_3} - \overline{m_1m_4}, \quad \overline{\chi_4} = \overline{m_2m_3} + \overline{m_1m_4},$
$\overline{\chi_5} = \overline{m_4}\overline{\zeta_1} - \overline{m_3}\overline{\zeta_2}, \quad \overline{\chi_6} = \overline{m_3} + \overline{m_4}, \quad \overline{\chi_7} = \overline{m_3} - \overline{m_4}, \quad \overline{\chi_8} = -\overline{m_1}\overline{\zeta_2} + \overline{m_2}\overline{\zeta_1},$
$\overline{\chi_9} = \overline{m_1}\overline{\zeta_2} + \overline{m_2}\overline{\zeta_1}, \quad \overline{\chi_{10}} = \overline{m_1} - \overline{m_2}.$

Equation (6.30) represents the dispersion relation for Rayleigh wave in reinforced free medium lying over the couple stress substrate.

6.4.2 Case-2:

Using case-1 and considering no layer thickness, i.e., $H = 0$, one may have

$$\xi_1[tK_t(l^2K_s^2 - S_s) - sK_s(l^2K_t^2 - S_t)] - 4rst(K_s - K_t)\xi^2 = 0, \tag{6.31}$$

where $K_s = (\xi^2 - s^2)$, $K_t = (\xi^2 - t^2)$, $S_s = (\xi^2 + s^2)$, $S_t = (\xi^2 + t^2)$.
Equation (6.31) represents the dispersion relation for Rayleigh wave in semi-infinite couple stress substrate [169].

6.4.3 Case-3:

Taking $l \to 0$ and pondering previous cases, one may obtain

$$\left(2 - \frac{c^2}{c_2^2}\right)^2 = 4\sqrt{1 - \frac{c^2}{c_1^2}}\sqrt{1 - \frac{c^2}{c_2^2}}. \tag{6.32}$$

Equation (6.32) represents the dispersion relation for Rayleigh wave in isotropic elastic half-space [151].

6.5 Numerical Discussion

The dispersion relations are determined analytically in the considered model to analyze the effect of the various parameters on the phase velocity profiles of Rayleigh-type wave propagation in the size-dependent layered structure. The following details were taken into account to unravel the effects of various parameters affecting the characteristic profiles of the Rayleigh-type wave.
(1) Self-fiber reinforced medium constants shown in Table 6.1.
(2) The size-dependent couple stress medium constants shown in Table 6.2.
(3) The reinforced-free medium, i.e., $\alpha_f = 0$, $\beta_f = 0$ and $\mu_L = \mu_T = \mu_f$ constants shown in Table 6.3.
The graphs are plotted for secular equation (6.29) to study the influence of reinforcement parameter, layer thickness together with a microstructural parameter associated

Table 6.1: Material constants for self-fibre reinforced medium [125]

ρ_f	7.8×10^3	Kg/m^3
λ_f	5.65×10^9	N/m^2
μ_L	5.66×10^9	N/m^2
μ_T	2.46×10^9	N/m^2
α_f	-1.28×10^9	N/m^2
β_f	220.9×10^9	N/m^2

Table 6.2: Material constants for couple stress medium [198]

ρ_c	1.5×10^3	kg/m^3
λ_c	1.452×10^{10}	N/m^2
μ_c	5.11×10^9	N/m^2
c_{c1}	4063	m/s
c_{c2}	1846	m/s

with the substrate. The phase velocity profiles are shown by considering the variation in phase velocity $\left(\frac{c}{c_f}\right)$ of Rayleigh-type wave propagation against wave number (ξH). There is one common phenomenon observed in all plots, i.e., with the increase in wave number, the phase velocity decreases.

6.5.1 Influence of self-fiber reinforced layer thickness H

Curves in figures 6.2 and 6.3 elucidate the impact of layer thickness on the phase velocity profiles of Rayleigh-type waves in the considered model. Distinct values of layer thickness $H = 0.01m, 0.02m, 0.03m$ are considered to document this effect. Particularly, Figure 6.2 is plotted for the self-fiber reinforced medium whereas Figure 6.3 is plotted for the reinforced-free medium. The variation in layer thickness shows an encouraging effect on the characteristic profiles of the Rayleigh-type wave, i.e., with the increment in the magnitude of layer thickness, the phase speed also increases for both the reinforced and reinforced-free medium.

6.5.2 Influence of microstructural parameter l

The influence of size-dependent parameters on the phase velocity profiles of Rayleigh-type wave has been shown in Figures 6.4 and 6.5. To document this size-effect, the

Table 6.3: Material constants for reinforced-free medium [63]

ρ_f	4705	Kg/m^3
λ_f	2.510×10^9	N/m^2
μ_f	1.987×10^9	N/m^2

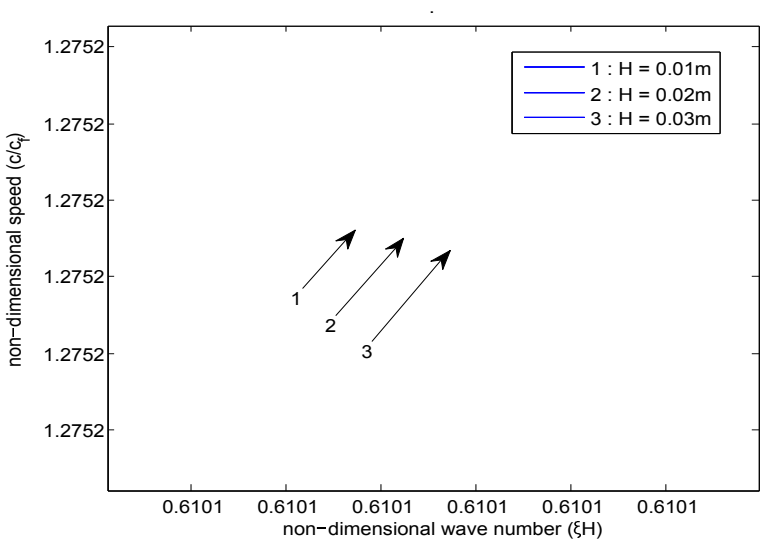

Figure 6.2: Variation of phase velocity c/c_f verses wave number ξH for different values of layer thickness under reinforced medium.

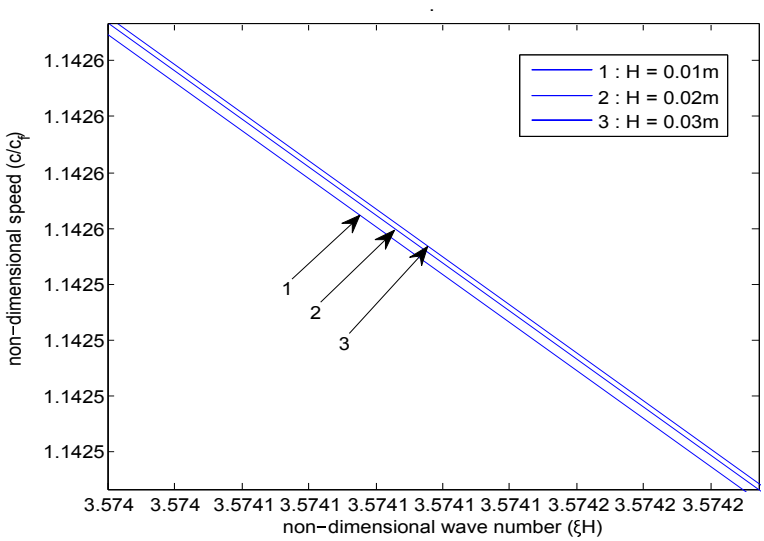

Figure 6.3: Variation of phase velocity c/c_f verses wave number ξH for different values of layer thickness under reinforced-free medium.

dispersive curves are plotted by taking distinct values of characteristic length $l = 0.001m, 0.003m, 0.005m$. Prominent effects have been traced out from both figures. Figure 6.4 reflects the presence of size-effect under reinforced medium and Figure 6.5

reflect the same effect under reinforced-free medium. It can be perceived from both the figures that the material length parameter has a discouraging impact on the phase velocity profiles of the Rayleigh-type wave.

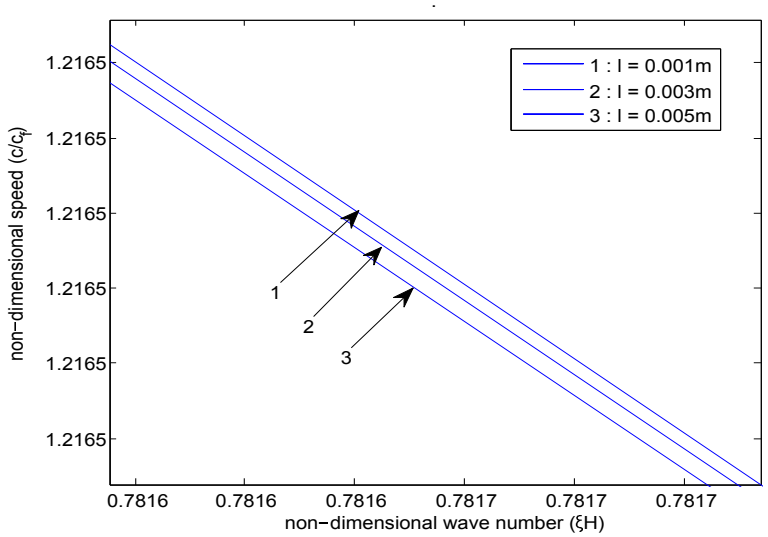

Figure 6.4: Variation of phase velocity c/c_f verses wave number ξH for different values of intrinsic characteristic length parameter under reinforced medium.

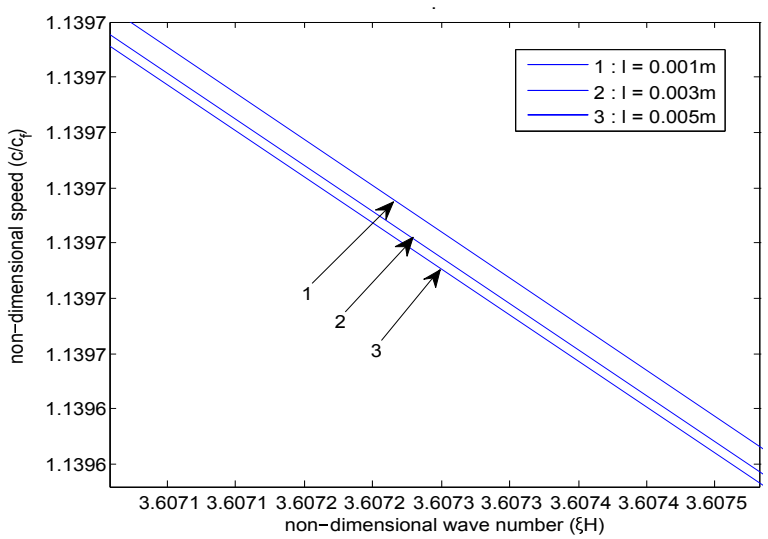

Figure 6.5: Variation of phase velocity c/c_f verses wave number ξH for different values of intrinsic characteristic length parameter under reinforced-free medium.

6.5.3 Influence of reinforcement parameter

The graphical representation featuring the impact of the reinforced parameter on the phase speed of the Rayleigh-type wave for the considered model is shown in figure 6.6. In this figure, curve 1 represents the reinforced medium whereas curve 2 represents the reinforced-free medium. It may be observed that the increase in reinforcement leads to an increase in the phase velocity profiles of the Rayleigh wave in the considered layered structure.

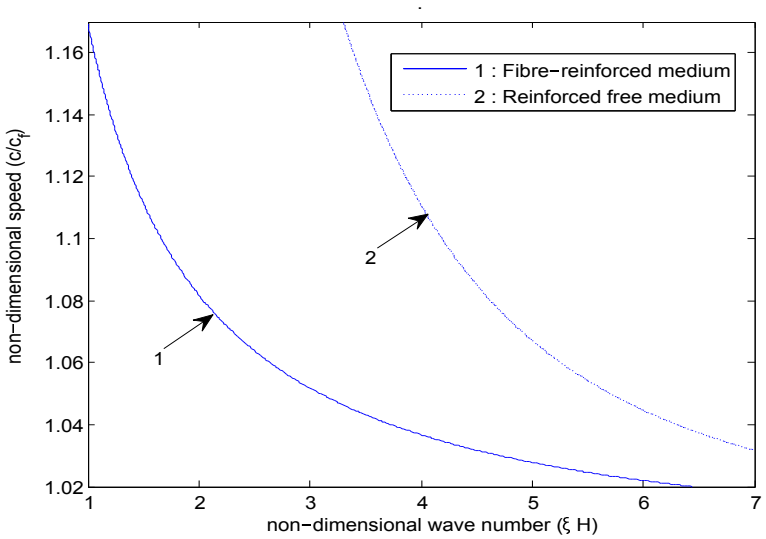

Figure 6.6: Variation of phase velocity c/c_f verses wave number ξH for reinforced and reinforced free medium.

6.6 Conclusions

A quantitative procedure has been scrutinized to analyze the Rayleigh-type surface wave propagation in the layered structure consisting of a finite thickness self-fiber reinforced medium layer over the size-dependent couple stress half-space. The compact form of the secular equation is achieved by employing suitable boundary conditions for the proposed model. The structure proposed is intended for the characterization of curves to establish the effect of a Rayleigh-type wave with different affected parameters on its phase velocity, namely the varying reinforced medium thickness,

the parameter of material length representing the microstructural behavior of the substratum. The results achieved in this study can be summarized as:

(i) Significant effects have been observed on the phase velocity of the Rayleigh wave with wave number in the proposed structure. It may be noted that the phase velocity for short wave numbers is dispersive and non-dispersive for higher wave numbers.

(ii) The microstructural characteristic length parameter l shows a disfavoring impact on the phase velocity profiles of Rayleigh-type waves in layered media. As the extent of the material characteristic length increases, the phase speed of the Rayleigh wave decreases. Since the Classical hypothesis is inadequate to catch the size impact, the considered model portrays the size impact that is explained by the profile variety alongside the variety of the material length.

(iii) The variation in the layer thickness of the reinforced medium shows the significant effects on the phase velocity profiles of the Rayleigh-type wave. It is observed that the phase velocity shows a favoring effect with the layer thickness, i.e., the increase in the thickness of the reinforced medium leads to an increase in phase velocity of the Rayleigh-type wave.

(iv) The influence of reinforcement on the phase velocity profiles of the Rayleigh wave is shown by comparing the effect of the reinforced medium and reinforced-free medium.

(v) The secular equation is also obtained by excluding the surface layer to validate the result, which is well in accordance with the established result.

In the context of size-dependent theory, the study of Rayleigh-type surface wave propagation must be a topic of continued concern since it is extremely important to understand the inner environment and the earth's structure. The dispersion relations have a wide range of uses in the field of seismology, geology, and terrestrial sciences to understand and estimate earthquake damage.

Summary and Suggestion for future work

Through the rigorous study of existing elastic models, two size-dependent models have been selected namely the couple stress model and micropolar elastic model, and the propagation of Love-type surface wave in piezoelectric ceramic overlying the size-dependent half-spaces have been investigated by considering two sets of piezoelectric material, i.e., $PZT-5H$ and $BaTiO_3$. Upon applying the appropriate boundary conditions, the closed-form expressions of the dispersion equation for both the cases of electrically open and electrically short conditions have been obtained analytically. Numerical computations have been performed for studying the effect of the underlying microstructure of the substrate, the thickness of the layer, piezoelectric and dielectric constants on the phase velocity profiles of the Love wave.

Moreover, the study is also extended to the double-layered model by considering another layer between the finite layer of piezoelectric material and size-dependent substrate. The consideration of another layer is more fruitful in the design process to accomplish an explicit objective. Seeing the merits of hybrid structure, the two-layered structure has been considered in which a heterogeneous viscoelastic layer is sandwiched between a finite layer of piezoelectric medium and semi-infinite size-dependent elastic substrate to improve the performance of Love wave-based devices. The dispersion equations have been obtained analytically in closed-form expression for the real and the damping case under the conditions of electrically open and short circuits. Numerical calculations have been done to examine the impact of different parameters by taking two distinct piezoelectric materials, i.e., $PZT-5H$ and $BaTiO_3$.

The results obtained from the above-solved model may be useful for the fabrication of Love-wave-based sensors and in structural utilization.

While working on the different layered models, it has been observed that along with the piezoelectricity model, the size-dependent substrate can be considered with another different material like orthotropic medium and many more. Though, the problems have been done considering the perfect bonding between the substrate and material layer. But the strength of many engineering materials is well known to rely on the bonding between the structural components. Keeping this aspect in view, a Love-type surface wave has been investigated in the functionally graded orthotropic medium under initial stress bonded imperfectly over the size-dependent micropolar medium.

In addition to Love-type surface waves, the mathematical modeling for Rayleigh-type surface waves has been done by utilizing a microstructural model along with self-fiber reinforced, and the dispersions relations have been obtained in this context.

The considered size-dependency in these models shows a prominent effect on the phase velocity characteristics of the Love-type wave. These variations in profiles describe the consideration of size-effect in the context of classical theory.

Following suggestions have been made for the extension and further use of the present research work:

- The present work can be extended to study the reflection and refraction phenomena at the interface of size-dependent couple stress and micropolar elasticity along with the consideration of thermoelasticity into account.

- There is a scope to extend the study in rods and beams by utilizing the different microstructural models, particularly, size-dependent piezoelectric theory.

- The study can be explored further in the problem involving the propagation of Stoneley waves and torsional waves to analyze the impact of internal character-

istic length associated with the microstructural model.

- There is a scope to extend the present models to investigate the effects of non-linearity considering different microcontinuum theories.

- The present models can be further extended to investigate the effects of different materials with or without voids.

The study of material microstructural effects on the solution of these problems may suggest some amendments to the literature based on classical elasticity theory and the results of the solution of the aforementioned problems may enhance the domain of applicability of surface wave-based devices using size-dependent models of elasticity.

Bibliography

[1] Abd-Alla, A., Abo-Dahab, S. and Hammad, H.: 2011, Propagation of Rayleigh waves in generalized magneto-thermoelastic orthotropic material under initial stress and gravity field, *Applied Mathematical Modelling* **35**(6), 2981–3000.

[2] Abd-Alla, A. M. and Ahmed, S. M.: 1999, Propagation of Love waves in a non-homogeneous orthotropic elastic layer under initial stress overlying semi-infinite medium, *Applied Mathematics and Computation* **106**, 265–275.

[3] Achenbach, J. D.: 1976, *Wave propagation in elastic solids*, North Holland Publication Company, New York.

[4] Aki, K. and Richards, P. G.: 1980, Quantitative seismology, *Theory and Methods* **1**, 557.

[5] Alavi, S. E., Sadighi, M., Danesh Pazhooh, M. and Ganghoffer, J.-F.: 2019, Development of size-dependent consistent couple stress theory of timoshenko beams, *Applied Mathematical Modelling* **79**.

[6] Alinaghizadeh, F. and Shariati, M.: 2020, Nonlinear analysis of size-dependent annular sector and rectangular microplates under transverse loading and resting on foundations based on the modified couple stress theory, *Thin-Walled Structures* **149**, 106583.

[7] Amirinezhad, H., Amirinezhad, A. and Talebitooti, R.: 2020, Acoustic wave transmission through a polymeric foam plate using the mathematical model

of functionally graded viscoelastic (FGV) material, *Thin-Walled Structures* **148**, 106466.

[8] Arani, A. G., Kolahchi, R. and Mortazavi, S. A.: 2014, Nonlocal piezoelasticity based wave propagation of bonded double-piezoelectric nanobeam-systems, *International Journal of Mechanics and Materials in Design* **10**(2), 179–191.

[9] Argyros, I., Kansal, M. and Kanwar, V.: 2016, On the local convergence of an eighth-order method for solving nonlinear equations, *Annals of West University of Timisoara - Mathematics* **1**, 3–16.

[10] Auffray, N., Quang, H. L. and He, Q. C.: 2013, Matrix representations for 3D strain-gradient elasticity, *Journal of the Mechanics and Physics of Solids* **61**(5), 1202–1223.

[11] Auld, B. A.: 1981, Wave propagation and resonance in piezoelectric materials, *The Journal of the Acoustical Society of America* **70**(6), 1577.

[12] Bader, T. K., Dastoorian, F., Ebrahimi, G., Unger, G., Lahayne, O., Hellmich, C. and Pichler, B.: 2016, Combined ultrasonic-mechanical characterization of orthotropic elastic properties of an unrefined bagasse fiber-polypropylene composite, *Composites Part B: Engineering* **95**, 96–104.

[13] Baroi, J., Sahu, S. A. and Singh, M. K.: 2018, Dispersion of polarized shear waves in viscous liquid over a porous piezoelectric substrate, *Journal of Intelligent Material Systems and Structures* .

[14] Belfield, A. J., Rogers, T. G. and Spencer, A. J. M.: 1983, Stress in elastic plates reinforced by fibres lying in concentric circles, *Journal of the Mechanics and Physics of Solids* **31**(1), 25–54.

[15] Borcherdt, R. D.: 1973, Rayleigh-type surface wave on a linear viscoelastic half-space, *The Journal of the Acoustical Society of America* **55**(1), 13–15.

[16] Borges, M. F., Antunes, F. V., Prates, P. A. and Branco, R.: 2020, A numerical study of the effect of isotropic hardening parameters on mode I fatigue crack growth, *Metals* **10**(2), 177.

[17] Brekhovskikh, L.: 1960, *Waves in Layered Media*, Academic Press, New York.

[18] Cady, W. G.: 1922, The Piezoelectric Resonator, *Proceedings of the Institute of Radio Engineers* **10**, 83–114.

[19] Cao, X., Hu, S., Liu, J. and Shi, J.: 2019, Generalized Rayleigh surface waves in a piezoelectric semiconductor half-space, *Meccanica* **54**.

[20] Cao, X., Jin, F., Jeon, I. and Lu, T. J.: 2009, Propagation of Love waves in a functionally graded piezoelectric material (FGPM) layered composite system, *International Journal of Solids and Structures* **46**, 4123–4132.

[21] Cerveny, V. and Psencik, I.: 2005, Plane waves in viscoelastic anisotropic media-i, *Geophysical Journal International banner* **161**(1), 197–212.

[22] Chatterjee, M., Chattopadhyay, A. and Dhua, S.: 2017, Shear wave propagation in viscoelastic heterogeneous layers lying over an initially stressed half-space, *Mechanics of Advanced Materials and Structures* **24**(15), 1247–1256.

[23] Chattopadhyay, A., Gupta, S., Sahu, S. A. and Singh, A. K.: 2012, Dispersion of horizontally polarized shear waves in an irregular non-homogeneous self-reinforced crustal layer over a semi-innite self-reinforced medium, *Journal of Vibration and Control* **19**(1), 109–119.

[24] Chaudhary, S., Kaushik, V. P. and Tomar, S. K.: 2005, Transmission of shear waves through a self-reinforced layer sandwiched between two inhomogeneous viscoelastic half-spaces, *International Journal of Mechanical Sciences* **47**(9), 1455–1472.

[25] Chaudhary, S., Sahu, S. A., Dewangan, N. and Singhal, A.: 2019, Stresses produced due to moving load in a prestressed piezoelectric substrate, *Mechanics of Advanced Materials and Structures* **26**(12), 1028–1041.

[26] Chaudhary, S., Sahu, S. A. and Singhal, A.: 2017, Analytic model for Rayleigh wave propagation in piezoelectric layer overlaid orthotropic substratum, *Acta Mechanica* **228**(2), 495–529.

[27] Chaudhary, S., Sahu, S. A. and Singhal, A.: 2018, On secular equation of SH waves propagating in pre-stressed and rotating piezo-composite structure with imperfect interface, *Journal of Intelligent Material Systems and Structures* **29**(10), 1–13.

[28] Chaudhary, S., Singhal, A. and Sahu, S. A.: 2019, Influence of the imperfect interface on Love-type mechanical wave in a FGPM layer, *Journal of Solid Mechanics* **11**(1), 201–209.

[29] Chiriţă, S. and Ghiba, I.-D.: 2011, Rayleigh waves in cosserat elastic materials, *International Journal of Engineering Science* .

[30] Chugh, S., Madan, D. K. and Singh, K.: 2011, Static deformation of an orthotropic elastic layered medium due to a non uniform discontinuity along a very long strike-slip fault, *International Journal of Engineering Science and Technology* **3**(1), 69–86.

[31] Cooper, H. F.: 1967, Reflection and transmission of oblique plane waves at a plane interface between viscoelastic media, *The Journal of the Acoustical Society of America* **42**, 1064–.

[32] Cosserat, E. and Cosserat, F.: 1909, Theorie des corps deformables (Theory of deformable bodies), *A Hermann et Fils, Paris* .

[33] Cui, J., Du, J. and Wang, J.: 2013, Study on SH waves in piezoelectric structure with an imperfectly bonded viscoelastic layer, IEEE.

[34] Curie, J. and Curie, P.: 1880, Développement par compression de l'électricité polaire dans les cristaux hémièdres à faces inclinées, *Comptes Rendus* **91**, 294–295.

[35] Curtis, R. G. and Redwood, M.: 1973, Transverse surface waves on a piezoelectric material carrying a metal layer of finite thickness, *Journal of Applied Physics* **44**(5), 2002–2007.

[36] dell'Isola, F., Sciarra, G. and Vidoli, S.: 2009, Generalized Hooke's law for isotropic second gradient materials, *Proceedings of The Royal Society A* **465**(2107), 2177–2196.

[37] Du, J., Harding, G. L., Ogilvy, J. A., Dcnchcr, P. R. and Lake, M.: 1996, A study of Love-wave acoustic sensors, *Sensors and Actuators A* **56**(3), 211–219.

[38] Erbay, H. A.: 2000, Asymptotic theory of thin micropolar plates, *International Journal of Engineering Science* **38**, 1497–1516.

[39] Erbay, S., Erbay, H. A. and Dost, S.: 1992, Nonlinear wave interactions in a micropolar elastic medium, *Wave Motion* **16**(2), 163–172.

[40] Eremeyev, V. A., Skrzat, A. and Vinakurava, A.: 2016, Application of the micropolar theory to the strength analysis of bioceramic materials for bone reconstruction, *Strength of Materials* **48**(4), 1–10.

[41] Eringen, A. C.: 1966, Linear theory of micropolar elasticity, *Journal of Mathematics and Mechanics* **15**, 909–923.

[42] Eringen, A. C.: 1968a, Mechanics of micromorphic continua, in E. Kroner, ed., *Mechanics of Generalized Continua. IUTAM Symposia (International Union of Theoretical and Applied Mechanics)*, Springer, Berlin, Heidelberg, pp. 18–35.

[43] Eringen, A. C.: 1968b, Theory of micropolar elasticity, *Fracture ed H Liebowitz Academic Press New York* **2**, 662–729.

[44] Eringen, A. C.: 1990, Theory of thermo-microstretch elastic solids, *International Journal of Engineering Science* **28**(12), 1291–1301.

[45] Ewing, W. M., Jardetzky, W. S. and Press, F.: 1957, *Elastic waves in layered media*, McGraw-Hill, New York.

[46] Ezzin, H., Amor, M. B. and Ghozlen, M. H. B.: 2016, Love waves propagation in a transversely isotropic piezoelectric layer on a piezomagnetic half-space, *Ultrasonics* **69**, 83–89.

[47] Ezzin, H., Amor, M. B. and Ghozlen, M. H. B.: 2017, Propagation behavior of SH waves in layered piezoelectric/piezomagnetic plates, *Acta Mechanica* **228**(3), 1071–1081.

[48] Fakhrabadi, M. M. S.: 2014, Size effects on nanomechanical behaviors of nanoelectronics devices based on consistent couple-stress theory, *International Journal of Mechanical Sciences* **92**.

[49] Fan, H. and Xu, L.: 2018, Love wave in a classical linear elastic half-space covered by a surface layer described by the couple stress theory, *Acta Mechanica* **229**(12), 5121–5132.

[50] Fan, H., Yang, J. and Xu, L.: 2006, Antiplane Piezoelectric Surface Waves over a Ceramic Half-Space with an Imperfectly Bonded Layer, *IEEE Transactions on Ultrasonics, Ferroelectrics, and Frequency Control* **53**(9), 1695–1698.

[51] Fantuzzi, N., Trovalusci, P. and Dharasura, S.: 2019, Mechanical behavior of anisotropic composite materials as micropolar continua, *Frontiers in Materials* **6**(59), 1–11.

[52] Farokhi, H. and Ghayesh, M. H.: 2016, Size-dependent behaviour of electrically actuated microcantilever-based MEMS, *International Journal of Mechanics and Materials in Design* **12**(3), 301–315.

[53] Fatemi, J., Keulen, F. V. and Onck, P. R.: 2002, Generalized Continuum Theories: Application to Stress Analysis in Bone, *Meccanica* **37**(4-5), 385–396.

[54] Fathalilou, M. and Rezazadeh, G.: 2016, Effects of the length scale parameter on the thermoelastic damping of a microbeam considering the couple stress theory, *International Journal of Applied Mechanics* **08**.

[55] Gaur, A. M.: 2018, Influence of stress on propagation of shear wave in piezoelectric-piezoelectric (PE-PE) composite layered structure, *Latin American Journal of Solids and Structures* **15**(1).

[56] Gaur, A. M. and Rana, D. S.: 2015, Dispersion relations for SH waves propagation in a porous piezoelectric (PZT-PVDF) composite structure, *Acta Mechanica* **226**(12), 4017–4029.

[57] Gauthier, R. D.: 1982, Experimental investigation on micropolar media., *Mechanics of micropolar media. World Scientific, Singapore* pp. 395–463.

[58] Georgiadis, H. G. and Velgaki, E. G.: 2003, High-frequency Rayleigh waves in materials with micro-structure and couple-stress effects, *International Journal of Solids and Structures* **40**(10), 2501–2520.

[59] Ghodrati, B., Yaghootian, A., Zadeh, A. G. and Mohammad-Sedighi, H.: 2018, Lamb wave extraction of dispersion curves in Micro/Nano plates using couple stress theories, *Waves in Random and Complex Media* **28**(1), 15–34.

[60] Golub, M. V. and Doroshenko, O. V.: 2019, Effective spring boundary conditions for modelling wave transmission through a composite with a random distribution of interface circular cracks, *International Journal of Solids and Structures* **165**, 115–126.

[61] Gourgiotis, P. A. and Georgiadis, H. G.: 2015, Torsional and SH surface waves in an isotropic and homogenous elastic half-space characterized by the Toupin-Mindlin gradient theory, *International Journal of Solids and Structures* **62**(1), 217–228.

[62] Graff, K. F.: 1991, *Wave motion in elastic solids*, Dover Publications, New edition, New York.

[63] Gubbins, D.: 1990, *Seismology and Plate Tectonics*, Cambridge University Press, Cambridge.

[64] Gupta, A. K. and Katiyar, V. K.: 2006, A new anisotropic continuum model for traffic flow, *Physica A: Statistical Mechanics and its Applications* **368**(2), 551–559.

[65] Gupta, S., Ahmed, M. and Misra, J. C.: 2019, Effects of periodic corrugated boundary surfaces on plane SH-waves in fiber-reinforced medium over a semi-infinite micropolar solid under the action of magnetic field, *Mechanics Research Communications* **95**, 35–41.

[66] Gupta, V. and Vashishth, A. K.: 2016, Effects of piezoelectricity on bulk waves in monoclinic poro-elastic materials, *Journal of Theoretical and Applied Mechanics* **54**(2), 571–577.

[67] Hadjesfandiari, A. R. and Dargush, G. F.: 2011, Couple stress theory for solids, *International Journal of Solids and Structures* **48**, 2496–2510.

[68] Hadjesfandiari, A. R. and Dargush, G. F.: 2013, Fundamental solutions for isotropic size-dependent couple stress elasticity, *International Journal of Solids and Structures* **50**(9), 1253–1265.

[69] He, Z., Zhu, H., Wang, X. and Ma, S.: 2020, Experimental investigation on scale effect of mechanical properties of heterogeneous micropolar medium materials, *Composite Structures* **251**, 112667.

[70] Heydarpour, Y., Malekzadeh, P., Dimitri, R. and Tornabene, F.: 2020, Thermoelastic analysis of functionally graded cylindrical panels with piezoelectric layers, *Applied Science* **10**(4), 1397.

[71] Hilal, M. I. M., Tantawi, R. and Othman, M.: 2018, The gravity impact in a rotating micropolar thermoelastic medium with microtemperatures, *Journal of Ocean Engineering and Science* .

[72] Honein, B., Braga, A. M. B., Barbone, P. and Herrmann, G.: 1991, Wave propagation in piezoelectric layered media with some applications, *Journal of Intelligent Material Systems and Structures* **2**(4), 542–557.

[73] Huang, Y. and Li, X.-F.: 2011, Interfacial waves in dissimilar piezoelectric cubic crystals with an imperfect bonding, *IEEE Transactions on Ultrasonics, Ferroelectrics and Frequency Control* **58**(6), 1261–1265.

[74] Iesan, D.: 1981, Some applications of micropolar mechanics to earthquake problems, *International Journal of Engineering Science* **19**(6), 855–864.

[75] Iesan, D.: 1987, Plane strain problems in piezoelectricity, *International Journal of Engineering Science* **25**(11-12), 1511–1523.

[76] Irino, T. and Shimizu, Y.: 1985, Theoretical analysis of stoneley waves propagating along an interface between piezoelectric material and isotropic material, *Electronics and Communications in Japan (Part II: Electronics)* **68**(3), 727–732.

[77] Jakoby, B. and Vellekoop, M. J.: 1997, Properties of Love waves : Applications in sensors, *Smart Materials and Structures* **6**(6), 668–679.

[78] Jam, M. T. and Shodja, H. M.: 2020, Interface effects on the electromagnetic radiation emanating from an embedded piezoelectric nano-fiber incident upon by SH-waves, *Wave Motion* **94**, 102513.

[79] Jiaoa, F., Weia, P., Zhoua, Y. and Zhou, X.: 2019, Wave propagation through a piezoelectric semiconductor slab sandwiched by two piezoelectric half-spaces, *European Journal of Mechanics - A/Solids* **75**, 70–81.

[80] Jin, F., Qian, Z., Wang, Z. and Kishimoto, K.: 2005, Propagation behavior of Love waves in a piezoelectric layered structure with inhomogeneous initial stress, *Smart Materials and Structures* **14**(4), 515–523.

[81] Jouneghani, F. Z., Dashtaki, P. M., Dimitri, R., Bacciocchi, M. and Tornabene, F.: 2018, First-order shear deformation theory for orthotropic doubly-curved shells based on a modified couple stress elasticity, *Aerospace Science and Technology* **73**, 129–147.

[82] Kakar, R.: 2015, Dispersion of Love wave in an isotropic layer sandwiched between orthotropic and prestressed inhomogeneous half-spaces, *Latin American Journal of Solids and Structures* **12**(10), 1934–1949.

[83] Kakar, R. and Kakar, S.: 2017, Love wave in a Voigt-type viscoelastic heterogeneous layer overlying heterogeneous viscoelastic half-space, *International Journal of Geomechanics* **17**(1), 06016009 (10pp).

[84] Kansal, M., Kanwar, V. and Bhatia, S.: 2015, On some optimal multiple root-finding methods and their dynamics, *Applications and Applied Mathematics: An International Journal* **10**(1), 349–367.

[85] Kaur, I. and Lata, P.: 2019, Rayleigh wave propagation in transversely isotropic magneto-thermoelastic medium with three-phase-lag heat transfer and diffusion, *International Journal of Mechanical and Materials Engineering* **14**(12).

[86] Kaur, J., Tomar, S. K. and Kaushik, V. P.: 2005, Reflection and refraction of SH-waves at a corrugated interface between two laterally and vertically heterogeneous viscoelastic solid half-spaces, *International Journal of Solids and Structures* **42**(13), 3621–3643.

[87] Kaur, S. P., Mittal, A. K., Kukreja, V. K., Parumasur, N. and Singh, P.: 2018, An efficient technique for solution of linear and nonlinear diffusion-dispersion models, *AIP Conference Proceedings* **1975**(1).

[88] Kaur, T., Kumar, S. and Singh, A. K.: 2018, Love wave propagation in vertical heterogeneous fiber-reinforced stratum imperfectly bonded to a micropolar elastic substrate, *International Journal of Geomechanics* **18**(2), 04017146.

[89] Kaur, T., Sharma, S. K. and Singh, A. K.: 2016a, Effect of reinforcement, gravity and liquid loading on Rayleigh-type wave propagation, *Meccanica* **51**(10), 2449–2458.

[90] Kaur, T., Sharma, S. K. and Singh, A. K.: 2016b, Influence of imperfectly bonded micropolar elastic half-space with non-homogeneous viscoelastic layer

on propagation behavior of shear wave, *Waves in Random and Complex Media* **26**(4), 650–670.

[91] Kaur, T., Sharma, S. K. and Singh, A. K.: 2017, Shear wave propagation in vertically heterogeneous viscoelastic layer over a micropolar elastic half-space, *Mechanics of Advanced Materials and Structures* **24**(2), 149–156.

[92] Kazemi, A., Vatankhah, R. and Farid, M.: 2019, Vibration analysis of size-dependent functionally graded micro-plates subjected to electrostatic and piezoelectric excitations, *European Journal of Mechanics - A/Solids* **76**.

[93] Kennedy, T. C. and Kim, J. B.: 1992, Dynamic stress concentrations in micropolar elastic materials, *Computers & Structures* **45**(1), 53–60.

[94] Koiter, W. T.: 1964, Couple stresses in the theory of elasticity- I and II., *Proceedings of the Koninklijke Nederlandse Akademie Van Wetenschappen* **67**, 17–44.

[95] Kong, Y., Liu, J. and Nie, G.: 2015, Propagation characteristics of SH wave in an mm2 piezoelectric layer on an elastic substrate, *AIP Advances* **5**(9).

[96] Kumar, J. and Kukreja, V. K.: 2019, Analytic solution of a diffusion dispersion model of packed bed of finite thickness, *Journal of Interdisciplinary Mathematics* **22**(1), 1–16.

[97] Kumar, R., Abo-Dahab, S. M. and Devi, S.: 2018, Rayleigh waves at the boundary surface of modified couple stress generalized thermoelastic with mass diffusion, *Advanced Composite Materials* **27**(3), 309–329.

[98] Kumar, R. and Gupta, R.: 2010, Propagation of waves in transversely isotropic micropolar generalized thermoelastic half space, *International Communications in Heat and Mass Transfer* **37**, 1452–1458.

[99] Kumar, S., Sharma, J. N. and Sharma, Y. D.: 2011, Generalized thermoelastic waves in microstretch plates loaded with fluid of varying temperature, *International Journal of Applied Mechanics* **3**(3), 563–586.

[100] Kundu, S., Gupta, S. and Manna, S.: 2014, Propagation of Love wave in fiber-reinforced medium lying over an initially stressed orthotropic half-space, *International Journal for Numerical and Analytical Methods in Geomechanics* **38**(11), 1172–1182.

[101] Kundu, S., Kumari, A., Pandit, D. K. and Gupta, S.: 2017, Love wave propagation in heterogeneous micropolar media, *Mechanics Research Communications* **83**, 6–11.

[102] Lakhtakia, A.: 1995, Wave propagation in a piezoelectric, continuously twisted, structurally chiral medium along the axis of spirality, *Applied Acoustics* **44**(1).

[103] Lavrentyev, A. I. and Rokhlin, S. I.: 1994, Models for ultrasonic characterization of environmental degradation of interfaces in adhesive joints, *Journal of Applied Physics* **76**(8), 4643.

[104] Lavrentyev, A. I. and Rokhlin, S. I.: 1998, Ultrasonic spectroscopy of imperfect contact interfaces between a layer and two solids, *Journal of Acoustical Society of America* **103**(2), 657–664.

[105] Lee, J. C., Shin, S. W., Kim, W. J. and Lee, C. J.: 2016, Electro-mechanical impedance based monitoring for the setting of cement paste using piezoelectricity sensor, *Smart Structures and Systems* **17**(1), 123–134.

[106] Leonetti, L., Fantuzzi, N., Trovalusci, P. and Tornabene, F.: 2019, Scale effects in orthotropic composite assemblies as micropolar continua: A comparison between weakand strong-form finite element solutions, *Materials* **12**(5), 758.

[107] Lesan, D.: 1990, Reciprocity, uniqueness and minimum principles in the linear theory of piezoelectricity, *International Journal of Engineering Science* **28**(11), 1139–1149.

[108] Li, P. and Jin, F.: 2015, Excitation and propagation of shear horizontal waves in a piezoelectric layer imperfectly bonded to a metal or elastic substrate, *Acta Mechanica* **226**(2), 267–284.

[109] Li, Y., Wei, P. and Wang, C.: 2019, Propagation of thermoelastic waves across an interface with consideration of couple stress and second sound, *Mathematics and Mechanics of Solids* **24**, 235–257.

[110] Lianngenga, R. and Singh, S. S.: 2019, Symmetric and anti-symmetric vibrations in micropolar thermoelastic materials plate with voids, *Applied Mathematical Modelling* **76**.

[111] Liao, W.: 2011, A computational method to estimate the unknown coefficient in a wave equation using boundary measurements, *Inverse Problems in Science and Engineering* **19**(6), 855–877.

[112] Liao, W., Yong, P., Dastour, H. and Huang, J.: 2018, Efficient and accurate numerical simulation of acoustic wave propagation in a 2D heterogeneous media, *Applied Mathematics and Computation* **321**, 385–400.

[113] Lippmann, G.: 1881, Principle of the conservation of electricity, *Annales de chimie et de physique* **24**, 145–178.

[114] Liu, C.: 2011, *Foundations of MEMS*, second edition edn, Pearson.

[115] Liu, H., Wang, Z. K. and Wang, T. J.: 2001, Effect of initial stress on the propagation behavior of Love waves in a layered piezoelectric structure, *International Journal of Solids and Structures* **38**(1), 37–51.

[116] Liu, J.: 2014, A theoretical study on Love wave sensors in a structure with multiple viscoelastic layers on a piezoelectric substrate, *Smart Materials and Structures* **23**(7), 075015 (8pp).

[117] Liu, J. and He, S.: 2010, Theoretical analysis on Love waves in a layered structure with a piezoelectric substrate and multiple elastic layers, *Journal of Applied Physics* **107**(7), 073511 (8pp).

[118] Liu, J., Wang, L., Lu, Y. and He, S.: 2013, Properties of Love waves in a piezoelectric layered structure with a viscoelastic guiding layer, *Smart Materials and Structures* **22**(12), 1–8.

[119] Liu, X., Chen, J., Zhao, Z., Lan, H. and Liu, F.: 2018, Simulating seismic wave propagation in viscoelastic media with an irregular free surface, *Pure and Applied Geophysics* **175**.

[120] Liu, X. and Fan, Y.: 2012, On the characteristics of high-frequency Rayleigh waves in stratified half-space, *Geophysical Journal International* **190**(2), 1041–1057.

[121] Love, A. E. H.: 1911, *Some problems of Geodynamics*, Cambridge University Press, London.

[122] Love, A. E. H.: 1920, *Mathematical Theory of Elasticity*, Cambridge University Press.

[123] Madan, D. K., Singh, K., Aggarwal, R. and Gupta, A.: 2005, Displacements and stresses in an anisotropic medium due to non-uniform slip along a very long strike-slip fault, *ISET Journal of Earthquake Technology* **42**(1), 1–11.

[124] Mandi, A., Kundu, S., Pati, P. and Pal, P. C.: 2019, Love wave propagation in a fiber-reinforced layer with corrugated boundaries overlying heterogeneous half-space, *Journal of Applied and Computational Mechanics* **5**(5), 926–934.

[125] Markham, M. F.: 1969, Measurement of the elastic constants of fibre composites by ultrasonics, *Composites* **1**(2), 145–149.

[126] Mawassy, N., Reda, H., Ganghoffer, J.-F., Eremeyev, V. A. and Lakiss, H.: 2021, A variational approach of homogenization of piezoelectric composites towards piezoelectric and flexoelectric effective media, *International Journal of Engineering Science* **158**, 103410.

[127] McGregor, M. and Wheel, M. A.: 2014, On the coupling number and characteristic length of micropolar media of differing topology, *Proceedings of the Royal Society A* **470**(2169).

[128] Merkel, A. and Luding, S.: 2016, Enhanced micropolar model for wave propagation in ordered granular materials, *International Journal of Solids and Structures* **106**.

[129] Meschke, G., Pichler, B. and Rots, J. G.: 2018, *Computational Modelling of Concrete Structures: Proceedings of the Conference on Computational Modelling of Concrete and Concrete Structures (EURO-C 2018)*, Bad Hofgastein, Austria.

[130] Midya, G.: 2004, On Love-type surface waves in homogeneous micropolar elastic media, *International Journal of Engineering Science* **42**, 1275–1288.

[131] Midya, G., Layek, G. C. and De, T.: 2008, On diffraction of normally incident SH-waves by a line crack in micropolar elastic medium, *International Journal of Solids and Structures* **45**, 2706–2722.

[132] Mindlin, R. D.: 1965, Second gradient of strain and surface-tension in linear elasticity, *International Journal of Solids and Structures* **1**(4), 417–438.

[133] Mindlin, R. D. and Eshel, N. N.: 1968, On first strain-gradient theories in linear elasticity, *International Journal of Solids and Structures* **4**(1), 109–124.

[134] Mindlin, R. D. and Tiersten, H. F.: 1962, Effects of couple-stresses in linear elasticity, *Archive for Rational Mechanics and Analysis* **11**, 415–448.

[135] Mori, N., Matsuda, N. and Kusaka, T.: 2019, Effect of interfacial adhesion on the ultrasonic interaction with adhesive joints: A theoretical study using spring-type interfaces, *The Journal of the Acoustical Society of America* **145**(6), 3541.

[136] Mseddi, S., Tekeli, F., Njeh, A., Donner, W. and Ghozlen, M. H. B.: 2016, Effect of initial stress on the propagation behavior of SAW in a layered piezoelectric structure of ZnO/Al2O3, *Mechanics Research Communications* **76**(c), 24–31.

[137] Nath, S., Sengupta, P. R. and Debnath, L.: 1998, Magneto-thermoelastic surface waves in micropolar elastic media, *Computers & Mathematics with Applications* **35**(3), 47–55.

[138] Negin, M. and Yahnioglu, N.: 2019, On attenuation of the seismic Rayleigh waves propagating in an elastic crustal layer over viscoelastic mantle, *Journal of Earth System Science* **128**.

[139] Nie, G., Liu, J. and Liu, X.: 2017, Propagation behavior of two transverse surface waves in a three-layer piezoelectric/piezomagnetic structure, *Waves in Random and Complex Media* **27**(4), 637–663.

[140] Ninh, D. and Bich, D.: 2018, Characteristics of nonlinear vibration of nanocomposite cylindrical shells with piezoelectric actuators under thermo-mechanical loads, *Aerospace Science and Technology* **77**.

[141] Nirwal, S., Sahu, S. A., Baroi, J. and Singh, A.: 2019, Analysis of different boundary types on wave velocity in bedded piezo-structure with flexoelectric effect, *Composites Part B Engineering* **167**, 434–447.

[142] Othman, M. I. A. and Abd-Elaziz, E. M.: 2017, Effect of rotation on a micropolar magneto-thermoelastic solid in dual-phase-lag model under the gravitational field, *Microsystem Technologies* **23**(10), 4979–4987.

[143] Ottosen, N. S., Ristinmaa, M. and Ljung, C.: 2000, Rayleigh waves obtained by the indeterminate couple-stress theory, *European Journal of Mechanics - A/Solids* **19**(6), 929–947.

[144] Pabst, W.: 2005, Micropolar materials, *Ceramics - Silikaty* **90**(3), 170–180.

[145] Pak, Y. E.: 1990, Crack extension force in a piezoelectric material, *Journal of Applied Mechanics-transactions of The Asme* **57**.

[146] Pang, Yu Liu, J.-X., Wang, Y.-S. and Zhao, X.-F.: 2008, Propagation of Rayleigh-type surface waves in a transversely isotropic piezoelectric layer on a piezomagnetic half-space, *Journal of Applied Physics* **103**(7).

[147] Park, H. C. and Lakes, R. S.: 1986, Cosserat micromechanics of human bone: Strain redistribution by a hydration sensitive constituent, *Journal of Biomechanics* **19**(5), 385–397.

[148] Pichler, B., Hellmich, C., Eberhardsteiner, J., Wasserbauer, J., Termkhajornkit, P., Barbarulo, R. and Chanvillard, G.: 2013, Effect of gel-space ratio and microstructure on strength of hydrating cementitious materials: An engineering micromechanics approach, *Cement and Concrete Research* **45**, 55–68.

[149] Prasad, R. M. and Kundu, S.: 2017, Dispersion of Love wave in a heterogeneous orthotropic layer under compressive pre-stress lying over an isotropic elastic half-space with rectangular irregularity, *Procedia Computer Science* **115**, 22–29.

[150] Ravindra, R.: 1968, Usual assumptions in the treatment of wave propagation in heterogeneous elastic media, *Pure and Applied Geophysics* **70**(1), 12–17.

[151] Rayleigh, L.: 1885, On waves propagated along the plane surface of an elastic solid, *Proceedings of the London Mathematical Society* **17**(1), 4–11.

[152] Reinhardt, H. W. and Dally, J. W.: 1970, Some characteristics of Rayleigh wave interaction with surface flaws, *Materials Evaluation* **28**, 213–220.

[153] Romeo, M.: 2003, Interfacial viscoelastic SH waves, *International Journal of Solids and Structures* **40**(9), 2057–2068.

[154] Saha, A., Kundu, S., Gupta, S. and Vaishnav, P. K.: 2015, Love waves in a heterogeneous orthotropic layer under initial stress overlying a gravitating porous half-space, *Proceedings of the Indian National Science Academy* **81**(5), 1193.

[155] Sahu, S. A., Saroj, P. K. and Dewangan, N.: 2014, SH-waves in viscoelastic heterogeneous layer over half-space with self-weight, *Archive of Applied Mechanics* **84**(2), 235–245.

[156] Sahu, S. A., Singhal, A. and Chaudhary, S.: 2017a, Influence of heterogeneity on Rayleigh wave propagation in an incompressible medium bonded between two half-spaces, *Journal of Solid Mechanics* **9**(3), 555–567.

[157] Sahu, S. A., Singhal, A. and Chaudhary, S.: 2017b, Surface wave propagation in functionally graded piezoelectric material: An analytical solution, *Journal of Intelligent Material Systems and Structures* **29**(3), 1–15.

[158] Salah, I. B., Amor, M. B. and Ghozlen, M. H. B.: 2015, Effect of a functionally graded soft middle layer on Love waves propagating in layered piezoelectric systems, *Ultrasonics* **61**(1), 45–50.

[159] Schneider, R., Faust, G., Hindenlang, U. and Helwig, P.: 2009, Inhomogeneous, orthotropic material model for the cortical structure of long bones modelled on the basis of clinical CT or density data, *Computer Methods in Applied Mechanics and Engineering* **198**(27-29), 2167–2174.

[160] Schoenberg, M.: 1971, Transmission and reflection of plane waves at an elastic-viscoelastic interface, *Geophysical Journal International* **25**(1-3), 35–47.

[161] Sengupta, P. R. and Ghosh, B.: 1974, Effects of couple stresses on the propagation of waves in an elastic layer, *Pure and Applied geophysics* **112**(2), 331–338.

[162] Sharma, A. and Sharma, J N andSharma, Y. D.: 2012, Modelling reflection and transmission of acoustic waves at a semiconductor: fluid interface, *Advances in Acoustics and Vibration* .

[163] Sharma, J. N. and Kumar, S.: 2009, Lamb waves in micropolar thermoelastic solid plates immersed in liquid with varying temperature, *Meccanica* **44**, 305–319.

[164] Sharma, J. N., Kumar, S. and Sharma, Y. D.: 2007, Propagation of Rayleigh surface waves in microstretch thermoelastic continua under inviscid fluid loadings, *Journal of Thermal Stresses* **31**(1), 18–39.

[165] Sharma, V. and Kumar, S.: 2014, Velocity dispersion in an elastic plate with microstructure: effects of characteristic length in a couple stress model, *Meccanica* **49**(5), 1083–1090.

[166] Sharma, V. and Kumar, S.: 2016, Influence of microstructure, heterogeneity and internal friction on SH waves propagation in a viscoelastic layer overlying a couple stress substrate, *Structural Engineering and Mechanics* **57**(4), 703–716.

[167] Sharma, V. and Kumar, S.: 2017, Dispersion of SH waves in a viscoelastic layer imperfectly bonded with a couple stress substrate, *Journal of Theoretical and Applied Mechanics* **55**(2), 535–546.

[168] Sharma, V. and Kumar, S.: 2018a, Dispersion of Rayleigh waves in a microstructural couple stress substrate loaded with liquid layer under the effects of gravity, *Archives of Acoustics* **43**(1), 11–20.

[169] Sharma, V. and Kumar, S.: 2018b, Effects of microstructure and liquid loading on velocity dispersion of leaky Rayleigh waves at liquid-solid interface, *Canadian Journal of Physics* **96**(1), 11–17.

[170] Sharma, V. and Kumar, S.: 2019, Microstructural and viscous liquid loading effects on the propagation of Love waves in a piezomagnetic layered structure, *Mechanics of Advanced Materials and Structures* pp. 1–11.

[171] Sharma, V. and Sharma, V.: 2020, Love waves in fiber-reinforced layer imperfectly bonded to microstructural couple stress substrate, *Journal of Theoretical and Applied Mechanics* **58**(1), 221–232.

[172] Shaw, R. P. and Bugl, P.: 1969, Transmission of plane waves through layered linear viscoelastic media, *The Journal of the Acoustical Society of America* **46**(3), 649–654.

[173] Shodja, H. M. and Ghazisaeidi, M.: 2007, Effects of couple stresses on antiplane problems of piezoelectric media with inhomogeneities, *European Journal of Mechanics - A/Solids* **26**(4), 647–658.

[174] Simonetti, F. and Peter Cawley, P.: 2004, On the nature of shear horizontal wave propagation in elastic plates coated with viscoelastic materials, *Proceedings of the Royal Society A* **460**(2048), 2197–2221.

[175] Singh, A., Chaki, M. and Chattopadhyay, A.: 2017, Remarks on impact of irregularity on SH-type wave propagation in micropolar elastic composite structure, *International Journal of Mechanical Sciences* **135**.

[176] Singh, A. K., Das, A., Lakshman, A., Negi, A. and Chattopadhyay, A.: 2017, Effects of irregularity and initial stresses on the dynamic response of viscoelastic half-space due to a moving load, *Acta Mechanica Solida Sinica* **30**(3), 306–317.

[177] Singh, A. K., Kumar, S. and Chattopadhyay, A.: 2015, Love-type wave propagation in a piezoelectric structure with irregularity, *International Journal of Engineering Science* **89**, 35–60.

[178] Singh, A. K., Kumar, S., Dharmender and Mahto, S.: 2017, Influence of rectangular and parabolic irregularities on the propagation behavior of transverse wave in a piezoelectric layer: A comparative approach, *Multidiscipline Modeling in Materials and Structures* **13**(2), 188–216.

[179] Singh, A., Ray, A. and Chattopadhyay, A.: 2019, Analytical study on propagation of G-type waves in a transversely isotropic substrate beneath a stratum considering couple stress, *International Journal of Geomechanics* **19**.

[180] Singh, B.: 2012, Reflection and transmission of plane harmonic waves at an interface between liquid and micropolar viscoelastic solid with stretch, *Sadhana* **25**, 589–600.

[181] Singh, B., Sangwan, A. and Singh, J.: 2019, Reflection and transmission of elastic waves at an interface between two micropolar piezoelectric half-spaces, *Journal of Ocean Engineering and Science* **4**.

[182] Singh, M. K., Sahu, S. A., Singhal, A. and Chaudhary, S.: 2018, Approximation of surface wave velocity in smart composite structure using Wentzel-Kramers-Brillouin method, *Journal of Intelligent Material Systems and Structures* **29**(18), 1–16.

[183] Singhal, A., Sahu, S. A. and Chaudhary, S.: 2018a, Approximation of surface wave frequency in piezo-composite structure, *Composites Part B: Engineering* **144**, 19–28.

[184] Singhal, A., Sahu, S. A. and Chaudhary, S.: 2018b, Liouville-Green Approximation: An analytical approach to study the elastic waves vibrations in composite structure of piezo material, *Composite Structures* **184**, 714–727.

[185] Singhal, A., Sahu, S. A., Chaudhary, S. and Baroi, J.: 2019, Initial and couple stress influence on the surface waves transmission in material layers with imperfect interface, *Materials Research Express* **6**, 1–10.

[186] Sofiyev, A. H.: 2019, Influences of shear deformations and material gradient on the linear parametric instability of laminated orthotropic conical shells, *Composite Structures* **225**, 111156.

[187] Sokolnikoff, I. S.: 1956, *Mathematical theory of elasticity*, Mc Graw Hill, New York.

[188] Song, Y., Zhang, Y., Xu, H. and Lu, B.: 2006, Magneto-thermoviscoelastic wave propagation at the interface between two micropolar viscoelastic media, *Applied Mathematics and Computation* **176**, 785–802.

[189] Spencer, A. J. M.: 2004, *Continuum Mechanics*, Dover books on physics, Dover Publications.

[190] Szabo, T. L. and Wu, J.: 2000, A model for longitudinal and shear wave propagation in viscoelastic media, *The Journal of the Acoustical Society of America* **107**(7), 2437.

[191] Tomar, S. K. and Kaur, J.: 2007, Shear waves at a corrugated interface between anisotropic elastic and visco-elastic solid half-spaces, *Journal of Seismology* **11**(3), 235–258.

[192] Tomar, S. K. and Kumar, R.: 1995, Reflection and refraction of longitudinal displacement wave at a liquid-micropolar solid interface, *International Journal of Engineering Science* **33**(10), 1507–1515.

[193] Toupin, R. A.: 1962, Elastic materials with couple-stresses, *Archive for Rational Mechanics and Analysis* **11**, 385–414.

[194] Toupin, R. A.: 1964, Theories of elasticity with couple-stress, *Archive for Rational Mechanics and Analysis* **17**, 85–112.

[195] Udias, A.: 1999, *Principles of Seismology*, Cambridge University Press, Cambridge, England.

[196] Vaishnav, P. K., Kundu, S., Gupta, S. and Saha, A.: 2016, Propagation of Love-type wave in porous medium over anorthotropic semi-infinite medium with rectangular irregularity, *Mathematical Problems in Engineering* **2016**, 1–9.

[197] Vardoulakis, I. and Georgiadis, H. G.: 1997, SH surface waves in a homogeneous Gradient-Elastic half-space with surface energy, *Journal of Elasticity* **47**(2), 147–165.

[198] Vavva, M. G., Protopappas, V. C., Gergidis, L. N., Charalambopoulos, A., Fotiadis, D. I. and Polyzos, D.: 2009, Velocity dispersion of guided waves propagating in a free gradient elastic plate: Application to cortical bone, *The Journal of the Acoustical Society of America* **125**(5), 3414–3427.

[199] Viktorov, I. A.: 1967, *Rayleigh and Lamb waves: Physical theory and applications*, Plenum Press, New York.

[200] Voigt, W.: 1887, Theoretische Studien über die Elastizitätsverhältnisse der Kristalle (Theoretical studies on the elasticity relationships of crystals), *Abhandlungen der Gesellschaft der Wissenschaften zu Göttingen* **34**, 3–51.

[201] Wang, C., Chen, X., Wei, P. and Li, Y.: 2017, Reflection and transmission of elastic waves through a couple-stress elastic slab sandwiched between two half-spaces, *Acta Mechanica Sinica* **33**(6), 1022–1039.

[202] Wang, C.-D., Chou, H.-T. and Peng, D.-H.: 2017, Love-wave propagation in an inhomogeneous orthotropic medium obeying the exponential and generalized power law models, *International Journal of Geomechanics* **17**(7), 04017003.

[203] Wang, H. M. and Zhao, Z. C.: 2013, Love waves in a two-layered piezoelectric/elastic composite plate with an imperfect interface, *Archive of Applied Mechanics* **83**(1), 43–51.

[204] Wang, H. and Qin, Q. H.: 2019, *Methods of Fundamental Solutions in Solid Mechanics*, Elsevier, pp. 53 – 90.

[205] Wang, Q.: 2002, Wave propagation in a piezoelectric coupled solid medium, *Journal of Applied Mechanics* **69**(6), 819–824.

[206] Wang, Y., Wang, M. and Liu, J.: 2012, Propagation behaviors of SH waves in piezoelectric layer/elastic cylinder with an imperfect interface, *Applied Mechanics and Materials* **151**, 130–134.

[207] Wei, W., Liu, J. and Fang, D.: 2009, Shear horizontal surface waves in a Piezoelectric-Piezomagnetic coupled layered half-space, *International Journal of Nonlinear Sciences and Numerical Simulation* **10**(6), 767–778.

[208] Wong, E. W., Sheehan, P. E. and Lieber, C. M.: 1997, Nanobeam Mechanics: Elasticity, Strength, and Toughness of Nanorods and Nanotubes, *Science* **277**(5334), 1971–1975.

[209] Yan, W., Li, B., Yan, S., Wuc, W. and Lia, Y.: 2019, Experiment and simulation analysis on noise reduction of cylindrical shells with viscoelastic material, *Results in Physics* **14**, 102385.

[210] Yang, J. F. C. and Lakes, R. S.: 1982, Experimental study of micropolar and couple stress elasticity in compact bone in bending, *Journal of Biomechanics* **15**(2), 91–98.

[211] Yang, W., Liang, X. and Shen, S.: 2017, Love waves in layered flexoelectric structures, *Philosophical Magazine* **97**(33), 3186–3209.

[212] Yu, H., Sumigawa, T. and Kitamura, T.: 2014, A domain-independent interaction integral for linear elastic fracture analysis of micropolar materials, *Mechanics of Materials* **74**, 1–13.

[213] Zakharenko, A. A.: 2005, Love-type waves in layered systems consisting of two cubic piezoelectric crystals, *Journal of Sound and Vibration* **285**(4-5), 877–886.

[214] Zhou, Y., Wei, P. and Jiao, F.: 2020, Dispersion of elastic waves in a micropolar metamaterial plate with periodical arranged resonators, *Applied Mathematical Modelling* **87**.